UNIVERSITÀ DEGLI STUDI DI PALERMO
DIPARTIMENTO DI SCIENZE DELLA TERRA E DEL MARE

Dottorato in Scienze della Terra e del Mare

CHARACTERIZATION OF SHIP AND WILDFIRE EMISSION TRANSPORT EVENTS IN SOUTHERN SICILY, BASED ON BLACK CARBON OBSERVATIONS ANALYSIS DURING 2015 – 2016 AT THE CAPO GRANITOLA BASELINE SITE

Settore scientifico disciplinare GEO / 08

Borsa di studio finanziata dal Consiglio Nazionale delle Ricerche

TESI DI
DARIO FILARDO

RELATORE
PROF. ANTONIO MAZZOLA

CORRELATORI
DOTT. MARIO SPROVIERI
DOTT. PAOLO BONASONI

XXIX CICLO ANNO ACCADEMICO 2016 - 2017

DOTTORATO

ABSTRACT

The Mediterranean basin can be considered a vulnerable climate and air quality hotspot, being seriously impacted by manifold atmospere pollution phenomena and climate change - linked processes resulting from the concentration of economic activities in its coastal areas.
The probable strong regional-scale impact of this situation on natural systems and productive sectors requires the adoption of effective mitigation countermeasures, which can only be promoted on the basis of continuous, appropriate and representative monitoring activity of Mediterranean atmosphere state of health.
The goal of this thesis has been exploring time variability in atmospheric aerosols and particulate matter properties and composition recorded in the Mediterranean baseline conditions – representative station of Capo Granitola (37°34'31'' N; 12°39'34'' E, 5 m a.s.l., Campobello di Mazara, Italy).

Since this WMO / GAW Regional Station is considered representative of average western Sicily / central Mediterranean basin regional background atmospheric conditions, it hosts continuous near real time (NRT) measuring activities of parameters indicative of atmospheric chemistry and properties, contributing to i - AMICA network with continuous (24/24 and 7/7) atmospheric composition measurements programmes, providing useful hints to investigate the influence of specific atmospheric processes (e.g. long-range air-mass transport) on the variability of trace gases- and aerosol- related parameters.

The final aim of this thesis has been to identify wildfire / biomass burning and ship - traffic -related events and to try to localize their potential sources; for this purpose, data mining procedures have been applied on raw data from instrumental atmospheric monitoring and subsequently intersected with data from Automatic Information System (AIS) ship position tracking register and Moderate Resolution Imaging Spectroradiometer (MODIS) satellite remote sensing observation systems, in order to trace back and investigate the most remarkable case studies.

Particular attention has been paid to black carbon (BC), particulate matter and trace - gases, considered as tracers of combustion processes, to discriminate events of wildfire and ship exhaust – polluted atmospheric transport.

BC is short - lived climate pollutant (SLCP) and a greenhouse agent originating from incomplete combustion processes; this notoriously dangerous air pollutant, prevalently classified as $PM_{2.5}$, plays

a key role in regional and global climate system for its tendency to undergo regional and intercontinental transport, thus exerting an undisputed impact on climate.

Starting from a raw data dataset of 17544 hourly records of 22 parameters for biennium 2015 / 2016, R – statistical software analysis has been carried out and salient episodes have been isolated within black carbon time series, on which the analysis of all other available datasets was deepened: 64 BC – polluted days (9,0 % of biennium dataset), seasonally concentrated in spring and late – summer season, have been identified, whose mean daily values increased by 125 to 275 % with respect to the biennium – based one (0,4 μg / m^3), on average.

Among polluted days, 35 BC pollution events have been identified on the biennium basis, 1 to 9 days long, whose occurrence resulted to be concentrated on 2015 (25 out of 35 events), with prevailing wind direction WNW / ESE.

Afterwards, long – lasting events have been splitted, thus obtaining a subset of 18 most polluted elementary events, concentrated in summer; in correspondence of this most polluted event subset, backtrajectories have been elaborated through the computational approach HYSPLIT, to determine the origin of air masses responsible for measures, in the intent to track air mass history and behavior and establish source-receptor relationships for the evaluation of ship and wildfire contribution to chemical composition measured in the remote site.

Backtrajectories have been intersected with ship traffic data, MODIS data product “Thermal Anomalies & Fire Daily L3 Global 1km Level 3 Daily” (MOD14A2 and MYD14A2) and 2015 land cover data from Land Cover CCI Project, highlighting 12 case studies, 6 linked to ship traffic and 6 to wildfire occurrence, by an integrated approach, in which fire occurrence, atmospheric composition and backtrajectories inspection have been mixed together.

Case studies analysis allowed to confirm the environmental burden of marine transport and wildfire occurrence on mediterranean coastal atmosphere, at the same time supporting the validity of such an integrated approach for characterization of BC – pollution phenomena at mediterranean scale.

1. THE MEDITERRANEAN BASIN: A VULNERABLE CLIMATE AND AIR QUALITY HOTSPOT

1.1. Introduction

The Mediterranean basin area extends 2.51 million km^2 and represents the largest semi - closed sea in the world, with 3 continents, 22 countries and about 1600 coastal cities bordering 46000 km of coastline and an overall population of more than 150 million people (CNR - ISAC / IAMC, 2016).

At present, central Mediterranean Sea region has one of the most polluted atmosphere in the world, after an unbridled development season (Kanakidou et al., 2011; Becagli et al., 2011).

There is agreement in the scientific community in recognizing the role of hotspot for climate and air quality of this area, whose extraordinary biodiversity (8% of known marine species) reflects the extreme variety of its bio-geographical conditions but, at the same time, accounts for its extreme vulnerability to repercussions triggered by global climate change (UNEP / MAP, 2009), primarily as concerns desertification, increased incidence of river and coastal floods, increase of temperature and incidence of extreme heat events and wildfires, reduced drinking water availability (CNR, 2014; IPCC, 2014; Cristofanelli et al., 2013; Hill et al., 2008).

In more detail, today the Mediterranean basin has gained the status of target of a manifold and heterogeneous ensemble of climate change - linked processes, reasonably interrelated (EEA, 2015; CNR, 2014; IPCC, 2014; EEA, 2012a; UNEP / MAP, 2009; see also http://climate.nasa.gov/evidence):

- temperature increase above european average values, furtherly estimated to increase 2.2 ° C to 5.1 ° C by 2100;
- reduction of annual rainfall and river flow - rate, with an outlook increase in drought frequency and severity in the near future;
- increase of forest fires / wildfires and biomass burning occurrence;
- rise of average sea level, with consequences on coastal natural processes and morphology: on a global scale, sea level rose about 17 centimeters in the last century, while, looking even back in time, the rate of sea level rise since the mid-19th century has been larger than the mean rate during the previous two millennia;

- increased risk of water scarcity episodes occurrence, desertification and related decrease in resilience capacity and agricultural productivity after disturbance;
- increased risk of biodiversity loss, resulting in depletion commercially valuable fish stock and, definitively, in food production capacity;
- increased frequency of extreme weather events;
- habitat loss and degradation determined by shoreline erosion or destabilization and overfishing; this undermines the delivery of valuable ecosystem services by coastal and marine habitats to all inhabitants of the Mediterranean;
- disturbance and contamination of sediments and biota caused by pollution, primarily from urbanization and industry, but also from atmospheric inputs of hazardous compounds and antifoulants paints; on the other hand, nutrient over - enrichment can occasionally lead to ecological imbalances, eutrophication and hypoxia episodes, with reduced water quality and growth of algae;
- invasive species spread, substituting autoctonous fauna and flora: it has been estimated that 19 % of known Mediterranean species are threatened both locally and worldwide;
- degradation of transitional or estuarine areas, acting as biodiversity hotspot as they represent critical nursery areas for commercial fisheries.

This set of deep derangements is mirroring, over a continental scale, on physical systems (glaciers, snow, ice extension, rivers and lakes health), terrestrial and marine ecosystems, as well as human and managed ecosystems, where global change and its regional - scale effects can have also meaningful repercussions on the productive world (food production, livelihood, economics) and, eventually, on human health (CNR, 2014; IPCC, 2014).

This condition is further worsened by the the main features of the Mediterranean climate, characterized by hot and dry summers with high solar radiation and moderately rainy winters, with frequent clear sky conditions and numerous extensive water shortage phenomena, as a consequence of its intense evaporation regime (Kanakidou et al., 2011).

In past decades, European Mediterranean has undergone widespread land use transformations, mainly resulting from modifications of socio-economic conditions; this new situation had strong

repercussions on land utilization practices and triggered and extensive desertification process as a result of a remarkable alteration of regional hydrological cycle following to the amount of transformations occurred in human–nature interactions, mainly in the direction of abandonment of rural areas, conversion to intensive agriculture and industrialization (Hill et al., 2008).

Present - day deep demographic, socio - cultural, economic and environmental transformations that the Mediterranean region is undergoing are making it particularly responsive to atmospheric pollution and climate change, furtherly worsened by its geographical position as a natural crossroads for numerous air mass streams from Europe, Asia and Africa, as well as by its reliance on climate - sensitive agriculture (Kanakidou et al., 2011; UNEP / MAP, 2009).

In addition, Mediterranean basin is exposed to multiple stressors, such as massive release of natural and anthropogenic polluting compounds and greenhouse gases resulting from the concentration of economic activities in coastal areas, intense ship traffic, wildfires, and mineral dust from north Africa, as well as from the crowding of many megacities near the coast line and the relentless industrial development of coastal States (Cesari et al., 2016; Becagli et al., 2011; Kanakidou et al., 2011; Chen et al., 2008).

Moreover, anthropogenic pollutants emitted in continental Europe are reported to be easily transported towards the south continental portion and the Mediterranean, during summer (Cristofanelli et al., 2013), adding to to the high population density and intense ship traffic linking Atlantic and Indian Oceans (Kanakidou et al., 2011) to make the atmosphere of Central Mediterranean Sea one the most polluted in the world.

On the whole, the coexistence of such an amount of impact sources is considered likely to have strong regional-scale impact on natural systems and productive sectors (agricultural practises, forestry, fishery, aquaculture, commerce, tourism, energy), posing a serious risk for food production, threatening its populations' ability of adaptation and reducing mitigation strategies' successful margins at tolerable costs, and, ultimately, exerting severe repercussions on air quality, public health and, ultimately, on welfare (IPCC, 2014).This condition is even more harshened when considering the increasing influence of desertification and land degradation / misuse for Mediterranean area deriving from its intense exposition to mineral dust outbreaks: Africa accounts for about half global emissions of mineral dust aerosol from north african Sahara and Sahel deserts, which are the main contributor to coarse - mode aerosols (Bonasoni et al., 2004).

In this regard, Sahara dust is considered as a major natural source of mineral aerosols for

Mediterranean, potentially transportable across the Mediterranean basin towards Southern, and occasionally Central and Northern, Europe, playing an important role on climatic system (Marenco et al., 2006) and determining direct and indirect effects on atmospheric transparency and visibility, aerosol composition, air quality and radiative budget (Forster et al., 2007; Penner et al., 2001; Dickerson et al., 1997; Andreae, 1995). During dust transport events short - term chemistry interactions can occur into the dust plume and trigger even strong modifications in the atmospheric composition, as well as in the ecosystem trophic structure and productivity, as a consequence of a significant addition of nutrient elements (Chen et al., 2008; Bonasoni et al., 2004; Hansen and Nazarenko, 2003).

The relevance of such a situation is evident when considering that it dramatically reverberates on vital economies of mediterranean countries, too, putting at risk a large volume of business (EEA, 2015; IPCC, 2014): for all these reasons, pursuing the goal of an effective preservation of the "natural capital" of this climatic hot - spot is undeferrable to ensure structural and functional integrity of its local ecosystems, which human health, economy, society and quality of life for its local population are based on (EEA, 2015).

As a matter of fact, since **a thorough knowledge of regional - scale mediterranean climatic features will reveal an indispensable key issue in future strategic policies for competitiveness strengthening**, every scientific investigation effort to conduct a **continuous, appropriate and representative monitoring activity of Mediterranean atmosphere state of health** represents today a precious aid to implement mitigation responses and natural resilience processes support, with the purpose of counteracting the environmental impacts of climate change on production and economic system.

In this direction, the **goal** of this thesis has been **exploring time variability in atmospheric aerosol and particulate matter properties and composition** recorded in the **Mediterranean baseline conditions – representative station of Capo Granitola (Campobello di Mazara, Italy)**: thanks to its instrumentantion, this WMO / GAW Regional Station hosts **continuous near real time recording of environmental parameters dataset** directly responsible for influencing atmospheric chemistry and properties.

This thesis reports the outcomes of analysis conducted on this dataset: **the final aim has been that to identify wildfire and ship - traffic -related events** and to try to localize the potential **sources**; in this perspective, particular attention has been paid to **black carbon, particulate matter and**

trace gases from ship traffic and wildfire / biomass burning in uncultivated areas and landfills, since these activities are highly accounted for release of such substances, ascertained to worsen air quality over the Mediterranean basin and to play a crucial role in Earth's climate system (Bond et al., 2013) with strong repercussions on the earth system (CIMAC, 2012; Becagli et al., 2012).

With this intent, **subsets that were expressive of episodes of relevant interest have been isolated within black carbon time series, on which the analysis of all other available datasets was deepened**; the next step has been **identifying sources** through an integrated approach based on **data mining procedures**, in which **data from near real time (NRT) instrumental monitoring of chemical and physical parameters, as well as from satellite remote sensing observation systems, are compared**.
Data processing techniques were conducted by **OPENAIR**, the software R - based open - source tool package for air pollution data analysis, and allowed the exploration of the large amounts of structured data produced in the Observatory of Capo Granitola with the intent to highlight any correlation between variables and to extract any hidden information, in order to enable pattern recognition to trace back relevant events (case studies) from the monitored raw data.

Broadly considering, the activities carried on were specifically intended to investigate the interactions taking place between the studied mediterranean coastal ecosystem and atmosphere, with particular concern to coast line / atmosphere / hydrosphere interface, in order to qualitatively and quantitatively describe the ship traffic and fire - related atmospheric phenomena directly affecting climate in this context: the innovative nature of the project relies in its contribution to bridge the gap coming from the unavailability of such an observational structure on the sicilian territory, to date.

1.2. Main atmospheric compounds affecting air quality and climate

Air quality and climate are closely linked; this Project intends to characterize emissions reaching CGR that can contribute to increase the anthropogenic contribution to air pollution.

According to the coastal setting of the observational station and the local absence of industrial activities and away from densely populated cities, most contributions are expected from natural sources (e.g. dust desert advection, forest fires plumes, sea spray), even if anthropogenic contribution cannot be neglected (e.g. ship traffic exhausts); hence, main parameters worthy of being investigated are discussed in detail below.

Firstly, **atmospheric aerosol** was investigated: this term generally refers to every suspension of microscopically dispersed solid particles or insoluble liquid droplets into a surrounding gaseous medium; in more details, an aerosol is a colloidal two - phase system composed of a continuous phase, being the medium of suspension, and a dispersed phase unable to settle over a long time appreciably, being generically a mixture of substances different as concerns nature, geometry and dimension, aggregated into approximately 1 to 1000 nm - clusters.

Atmospheric aerosols are characterized by relevant day-to-day variability as refers to origin, composition, size distribution and global distribution, being produced and released both from local and regional sources or being conveyed by long - range transport episodes (Marinoni et al., 2013; Marenco et al., 2006; Bonasoni et al., 2004).

A huge diversity of commonly known natural phenomena can be described as aerosol examples: mist, fog, haze, airborne particles from volcanic eruptions, dust advection or resuspended particulate matter from soil, salt particles formed from ocean spray, atmospheric cloud droplets.

When dealing with atmospheric aerosol it is common to refer to as **particulate matter (PM),** by this way referring to a mixture of solid particles and liquid droplets suspended in the air; these particles are released in many sizes and shapes and can be made up of hundreds of different chemicals, mainly sulfate, nitrate, black carbon, organic carbon, and mineral dust. Such an heterogeneous nature requires to adopt a size criteria, in terms of dimensional threshold, to distinguish PM member particles: acronyms PM_{10}, $PM_{2.5}$ and PM_1 refer to particulate matter with an aerodynamic diameter lower than 10 (coarse fraction), 2.5 and 1 (fine fraction) μm, respectively.

Large surface area of aerosol particles is able to **actively promote heterogeneous - phase chemical reactions** which can be responsible for decomposition / catalytic destruction of many airborne

compounds (including ozone) or their absorption on mineral oxides (Bonasoni et al., 2004); these conditions are favored every time coarser particles are ground up into ultrafines (diameter below 1 micron).

PM is an intensively studied atmospheric pollutant owing to its undisputed **influence on local and regional deterioration of air quality, visibility reduction, and global climate system change**; this justifies worldwide scientific efforts to detect sources and reconstruct travel patterns influencing local PM chemical composition and concentration, in order to develop air quality applications and pollution mitigation strategies, as well as to elucidate relationships between air quality and climate (Cesari et al., 2016; Putero et al., 2014).

Primary and **secondary** PM must be distinguished: the first one refers to particles emitted as they are directly from a source, regardless of its natural or artificial nature, while the second one to particles forming in the atmosphere.

Mineral dust lifting and long - distance advection in the free troposphere by weather conditions is responsible for about 37 % of the total production of atmospheric primary aerosols by both natural and anthropogenic sources (Penner et al., 2001).

Secondary aerosols result from a chain reaction of volatile organic compounds, mainly emitted from power plants, industries and transport sector (EEA, 2012b; Lack et al., 2009; Di Natale and Carotenuto, 2015), leading to their transformation into liquid or solid state: by this way fine aerosol (< 1 μm) particles are mostly produced (Bonasoni et al., 2004).

Primary and secondary PM can be furtherly distinguished between **natural** and **anthropogenic** PM: usually the latter are composed of coarser particles (> 1 μm) (Marenco et al., 2006).

Main **natural PM sources** are:

- wind - blown desert dust, composed of resuspended and transported particles from dry regions;
- sea spray aerosol, formed by the action of the wind on the sea;
- volcanogenic particulate matter, emitted by volcanic eruptions and seismic activities;
- wild - land fires particulate matter, released by burning non - managed and managed vegetation, triggered by a natural cause.

Noteworthy **anthropogenic PM sources** are triggered fires, road dust, industrial processes, waste disposal and energy-related sources, including electricity generation, residential wood combustion and and fossil fuel combustion.

Genetic mechanisms of PM is obviously as much diversified as the wide range of existing natural aerosols; however, in general, an aerosol is formed by the conversion of gases to particles or by the disintegration of liquids or solids into finer parts. As a rule of thumb, crustal dust and sea salt aerosols are coarser - sized (Marenco et al., 2006), while anthopogenic ones usually fall into the fine particle fraction (Chen et al., 2008).

Even if much air pollution results from human activities, natural sources emitt air pollutants, too, contributing to the exposure of European citizens and ecosystems to bad air quality from natural air pollution (EEA, 2012b): under this respect, the Directive 2008/50/EC on Ambient Air Quality and Cleaner Air for Europe clearly allows that, every time PM10 daily and annual limit values are exceeded, contributions from natural sources may be subtracted before member States compare ambient air pollutant concentrations with relevant legally binding limit values. It must be considered that, if the pollution is imported from another country, then it becomes even more difficult to justify natural contributions to exceedances of limit values, and, however, this eventuality proved to be scarcely determining for italian stations reporting exceedances of the daily PM_{10} limit value (EEA, 2012b).

According to Whitby Model, size distribution of particles in air shows a characteristic trimodal fashion centered around the following sizes:

* 30 nm (**Aitken mode**, size range 5 to 10 nm): numerically prevailing, these electrically charged transient particles (**Aitken nuclei**) result from condensation of gases into solid particles or from the coagulation of non volatile particles released from eruptions or combustion processes. As a consequence of their tendency to aggregate to coarser aerosol particles, they rapidly grow into the following accumulation mode, acting as **condensation nuclei** for rain triggering. Average lifetime is therefore short;

- 400 nm (**accumulation mode**, size range 100 to 2000 nm): particles produced by the condensation of low volatile vapors or by coagulation of inner particles, prevalently removed by washout processes;

- 10 μm (**coarse mode**, size greater than 2000 nm): particles produced by mechanical processes (sea spray, sand, spores, pollens, volcanic ashes, desert dust), prevalently removed by sedimentation processes; however, beyond 1 μm deposition rate is controlled by gravity, thus growing with growing particles dimensions.

Ambient particle size distributions typically have a minimum concentration at about 2 μm, between the accumulation and coarse modes; for this reason two main fractions can be distinguished, with diameters < 2 μm and > 2 μm, respectively; these two fractions have major differences both in origin and in physical / chemical characteristics, the first fraction including the nuclei mode and deriving mainly from combustion, whereas the coarse fraction being principally generated by mechanical processes.

According to Whitby, the accumulation mode also contains droplets formed by the chemical conversion of gases to vapors which condense. The coarse particle fraction contains windblown dust, sea spray, and plant particles.

Basically, methods involved in atmosphere cleaning out from aerosols are subdivided in pollutants deposition on the earth surface and conversion.

Differently from conversion, deposition is the process according to which aerosol particles, potentially containing pollutants, collect and settle down on solid surfaces or water table as they are, decreasing their concentration in the air. The rate of deposition shows a typically trimodal behavior, with the intermediate size particles taking most time, very large size ones quickly depositing through gravitational sedimentation and very small ones undergoing Brownian diffusion leading to their coagulation in few hours until they reach a critical size of 0.3 micron. Deposition can be furtherly distinguished into dry deposition, being the result of concurring phenomena of collision, gravitational sedimentation and turbulence, and wet deposition, namely atmospheric water droplets - mediated scavenge of aerosol particles.

Dry deposition velocity changes in dependence on aerosol particle size: it was noted that, for particles with aerodynamic diameter greater than 5 μm, deposition velocities increase dramatically with size; dry deposition velocity depends also on local meteorological conditions (wind speed, air column stability, humidity) (Chen et al., 2008).

Health risk linked to PM depends on the nature of particles, their dimension, their chemical composition and the time of exposition; it is unquestioned that ischaemic heart disease, heart stroke

and chronic obstructive pulmonary disease are due to $PM_{2.5}$ air pollution, and a relationship with low birth weight (Corbett et al., 2007) has been reported, too.

Several studies clearly point out that ultra fine particles (diameter below 1 micron) can reach lungs, blood and brain, with a toxicity significantly rising with their surface area, thus improving reaction ability with human target tissues (Kaiser, 2005).

Atmospheric aerosols exert a **negative contribution on global climate** (Penner t al., 2001) in the measure they modify the radiative energy balance through scattering and light absorption (Forster et al., 2007; Bonasoni et al., 2004; Dickerson et al., 1997; Andreae, 1995; Crutzen and Andreae, 1990): the magnitude of aerosol alone forcing is assessed to be –0.45 on average (– 0.95 to + 0.05) Wm^{-2} (WMO / GAW, 2016), even if, presently, scientific community agree on the fact that, despite substantial progress has been made to understand climate - relevant aerosol processes and aerosol source attribution, aerosols still contribute to the largest uncertainty in estimates and interpretations of the Earth's climate forcing.

Larger surface area fraction of atmospheric aerosol deserves a separate discussion, since it can powerfully promote light scattering and absorption of the short - wave solar radiation, thus influencing the radiative forcing of climate and modifying the balance of energy (Dickerson et al., 1997) and atmospheric trace gases: this consequence is particularly meaningful in the lower atmosphere (Bonasoni et al., 2004).

Radiative forcing mechanisms linked to main aerosols types are illustrated on fig.1.

Source	Lifetime (days)	Forcing (direct) ($W\ m^{-2}$)
Natural		
Primary		
Soil dust (mineral aerosol)	4	–0.75
Sea-salt	1	–0.09
Volcanic dust	4	–0.05
Biological debris	4	–0.07
Secondary		
Sulphates from biogenic gases	5	–0.68
Sulphates from volcanic SO_2	5	–0.09
Organic matter from biogenic NMHC[a]	7	–0.55
Nitrates from NO_X	4	–0.03
Total natural		–2.3
Anthropogenic		
Primary		
Industrial dust, etc.	4	–0.14
Black carbon (soot and charcoal)	6	–0.21
Secondary		
Sulphates from SO_2	5	–1.06
Biomass burning (w/o black carbon)	8	–0.91
Nitrates from NO_X	4	–0.05
Organics from anthropogenic NMHC[a]	7	–0.10
Total anthropogenic		–2.5
Total		–4.8
Anthropogenic fraction (%)		52

[a]NMHC, non-methane hydrocarbons.

Fig. 1 - Direct radiative forcing due to the various types of aerosols (adapted from Andreae, 1995)

The need to execute measures of aerosols has greatly increased over the last few decades in various sectors, such as air pollution, public health, job security and atmospheric science.

In particular, scientific study of aerosols is aimed to understand and describe their influence on the Earth's climate, with the purpose to support regulation demand for mitigating particulate matter pollution; such a scope requires the punctual, reliable and timely measurement of physical and chemical characteristics of aerosols, thus calling for a time- and resource-intensive descriptive approach.

Aerosol most intensively monitored properties include black carbon content, fine and coarse particle volumes, scattering coefficient, chemical composition and enhancement ratios (ER).

Current air quality standards for PM refer to PM mass concentration, both in terms of its fraction with aerodynamic diameters ≤ 10 μm (PM_{10}) and the aliquot with aerodynamic diameters ≤ 2.5 μm ($PM_{2.5}$) (Janssen et al., 2011).

Reference method for PM_{10} sampling and measurement is described in **UNI EN 12341:1999 standard** "Air quality. Determination of suspended particulate PM_{10}. Reference method and procedure for field trials to demonstrate the equivalence of measurement methods than the reference method", while the reference method for $PM_{2.5}$ sampling and measurement is described in **UNI EN 14907:2005 standard** "Ambient air quality. Normalized measuring gravimetric method for the determination of suspended $PM_{2.5}$ particulate maximum fraction".

Together with several hazardous gaseous compounds, aerosols are considered responsible for the increase of greenhouse effect and related global warming (Forster et al., 2007).

On a global scale, anthropogenic **greenhouse gases (GHG)** emissions have increased since the pre-industrial era (see fig. 2), driven primarily by economic and population growth (see fig. 3), and are now higher than ever, suggesting as likely that continued emission of such substances could sustain further warming and long-lasting changes in all components of the climate system and irreversible impacts for people and ecosystems (Forster et al., 2007); currently, atmospheric concentrations of carbon dioxide, methane and nitrous oxide are unprecedented in at least the last 800,000 years (IPCC, 2014).

In the direction to allow a comparison in terms of impact on climate alteration, **global warming potential (GWP)** has been introduced by IPCC to overcome the difficulties in comparing components with differing physical properties by expressing a given compound's relative potency in heating atmosphere through an index measuring the cumulative radiative forcing following an emission of a unit mass, accumulated over a a 100 - year timespan, compared to CO_2, as reference substance.

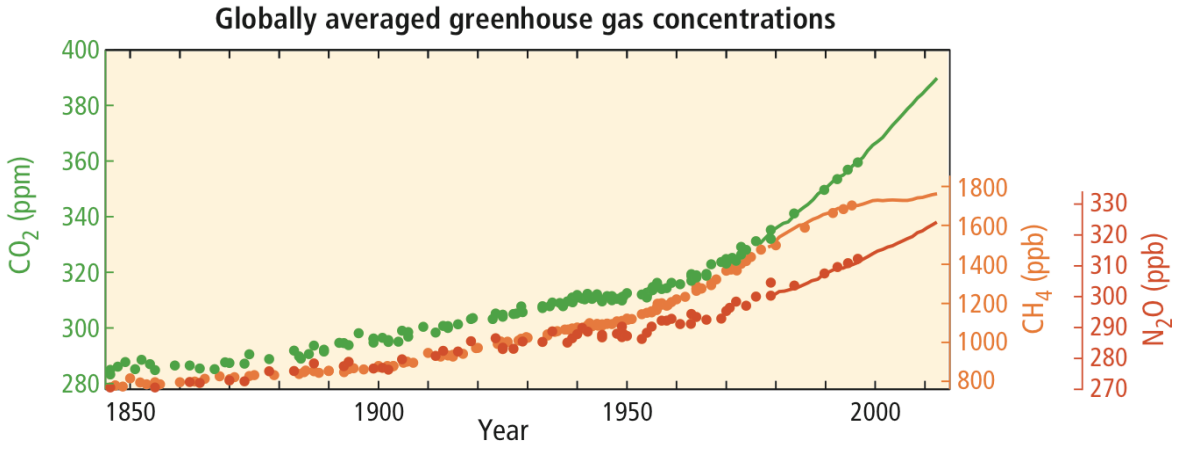

Fig. 2 – Globally averaged GHG concentrations (source: IPPC, 2014)

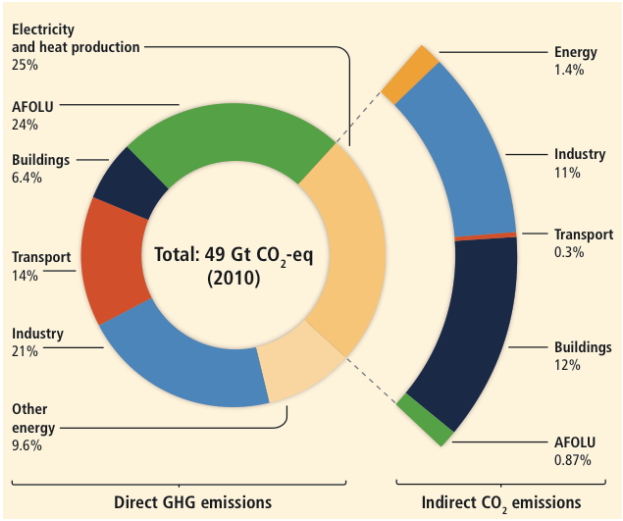

Fig. 3 - Greenhouse gas emissions by economic sectors

(AFOLU: agriculture, forestry and other land use) (IPCC, 2014)

Particular attention in monitoring activities has been paid to the **short - lived climate pollutants (SLCPs)**, agents with a powerful warming influence on climate and relatively short lifetime in the atmosphere, days to weeks, notably less than residence time of longer - lived climate pollutants (CO_2, CH_4, …).

Despite atmosphere residence time is notoriously inversely related to chemical reactivity, SLCPs are reported to be highly contributing to the human enhancement of global greenhouse effect over

the short term, gaining the alternative denomination of **short - lived climate forcers (SLCFs)**; they have been considered as a major development issue after various linked detrimental impacts were reported on human health (in terms of premature death from outdoor air pollution), agriculture (crop losses) and ecosystems (sea level rise, extreme weather events), with evident repercussions on food and water supply security of large populations (IPCC 2014; EEA, 2012a).

Main investigated SLCP / Fs are greenhouse agents, such as black carbon, tropospheric ozone and methane.

Black Carbon (BC) is one of the important warming SLCP/Fs, consisting of a fine - particulate carbonaceous - material aerosol consisting of pure carbon in several linked forms with a unique combination of physical properties, produced prevalently in flames from anthropogenic sources and directly emitted to the atmosphere, where it mostly falls into the finer aerosol fraction (CIMAC, 2012). This term is commonly adopted when optical properties such as light adsorption of atmospheric aerosols is discussed, together with its general synonym "absorbing aerosols".

In addition to the CO_2, as being the most important greenhouse gas, many reports published by the Intergovernmental Panel on Climate Change (IPCC) have elucidated aerosols potential for affecting the climate in the direction of cooling, due to their ability to reflect light back to space before reaching the surface of earth.

BC, however, absorbs light effectively, thus having an **opposite, warming contribution**: the heating power absorbed by black carbon particles in the atmosphere reduces the radiation reaching the earth surface, with a net heating power depending on the underlying surface. In consideration of its direct impact on solar an thermal radiation, BC is widely recognized as a contributing factor in global warming (Bond et al., 2013)

Discussions have started up among regulators, including International Maritime Organization (IMO), about the need and potential for restricting black carbon emissions as a measure for abating global warming (CIMAC, 2012).

BC originates from incomplete combustion (CIMAC, 2012) linked to industrial pollution, traffic, indoor activities like resident biofuel and coal cooking and heating, incomplete combustion of fossil carbon - based fuels, particularly from older diesel engines of ships and trucks, wood and biomass / biomass fuels burning, particularly coal burning and forest fires (Bond et al., 2013; Marinoni et al.,

2013; EPA, 2012; EEA, 2012a; Andreae et al., 1995).

These sources include **both natural and anthropogenic sources**; since combustion is never complete, every burning of organic matter always releases BC, together with gaseous compounds like carbon monoxide, methane, non-methane volatile organic compounds: total global BC emissions were estimated in 7500 Gg yr^{-1} in 2000, compared to an estimate of background preindustrial emissions of 1400 Gg per year (Bond et al., 2013); it is suggested that particles from combustion sources may be more relevant to human health than those from other sources (Janssen et al., 2011).

Past excessively generic use of this term frequently rose unsolvable ambiguities in BC characterization and a lack of comparability among results; just recently salient physical properties of BC have been elucidated: according to Bond et al. (2013), they include the strong capacity of absorbing visible light at all visible wavelengths, the refractory nature at very high temperatures (vaporization temperature of about 4000 K), insolubility in water, organic solvents and other components of atmospheric aerosol and its small spherules aggregate nature.

BC exerts an undisputed impact on climate (IPPC, 2014; EPA, 2012; Lack et al., 2009); the best quantified climate impact of BC is its atmospheric direct positive radiative forcing effect on the energy budget of the atmosphere (Marinoni et al., 2013; Bond et al., 2013) exerted through a number of different processes, ultimately giving reason of its dangerous interference with the climate system (Cristofanelli et al., 2013; Hansen and Nazarenko, 2003): it was estimated that 37% of arctic BC comes from biomass burning (CIMAC, 2012), while, according to Bond et al. (2013), BC is second to carbon dioxide as the largest contributor to human induced climate warming.

Firstly, since atmospheric BC particles are dark and fall into fine aerosol dimensional range, when located above a reflective surface, such as clouds, ice or snow, they are highly efficient in accelerating absorption of solar radiation and converting it to heat, decreasing the reflectivity of surfaces (albedo), increasing atmosphere instability and determining atmospheric warming and increase of ice cover melting rate and sea level rise (CIMAC, 2012; Andreae, 1991); it was estimated that the “soot effect” on snow albedo may be responsible for a quarter of GHG - related global warming (Hansen and Nazarenko, 2003; Kaufman et al., 1998).

Secondly, BC influences microphysics of clouds and their formation processes, modifying regional circulation, local radiative fluxes, temperature profiles, cloud properties and rainfall distribution patterns (Putero et al., 2014), playing a negative effect on photosynthesis and plants growth rate

(EPA, 2012).

Thirdly, atmosphere heating can deeply modify the hydrological cycle through changes in latent heating and convection and large-scale circulation patterns (EPA, 2012).

Main BC emission sources and processes controlling its distribution are outlined in fig. 4.

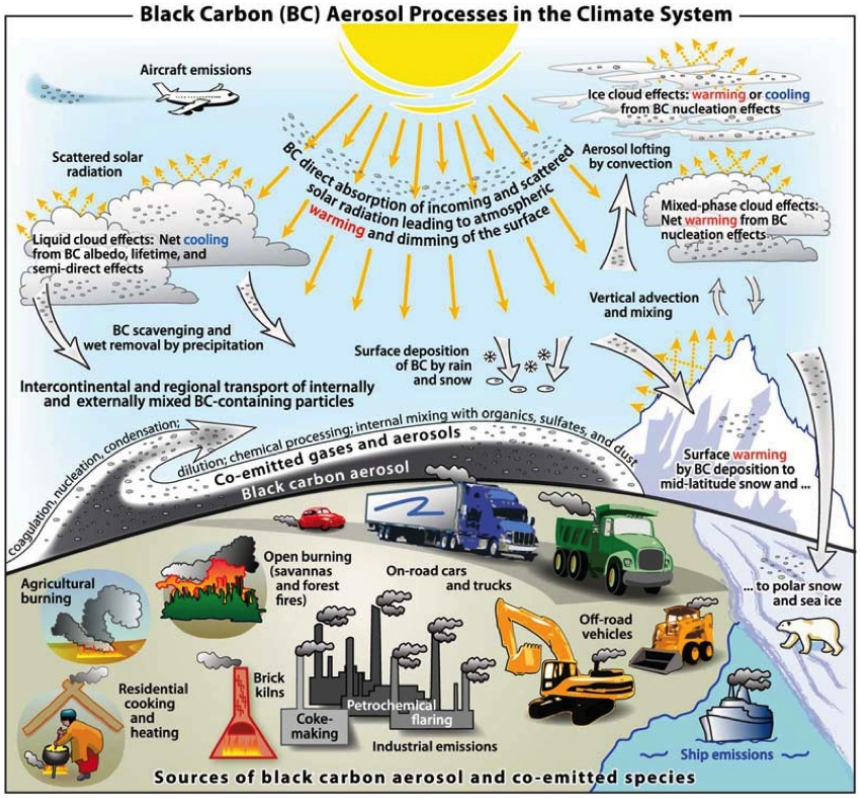

Fig. 4 - Schematic overview of the primary BC emission sources and processes controlling the distribution of black carbon in the atmosphere and determine its role in the climate system (from Bond et al., 2013)

A common operational definition of BC is the absorbing component of carbonaceous aerosols due to its positive radiative forcing (Marenco et al., 2006), being about twice as effective as CO_2 in altering global surface air temperature (Hansen and Nazarenko, 2003); its GWP is estimated among 460 and 1500 (IPCC, 1996), whereas the global climate forcing by fossil fuel BC aerosols is estimated about 0.2 W / m^2 (Hansen and Nazarenko, 2003).

Indeed, BC plays a key role in regional and global climate system (Marinoni et al., 2013), acting as

a Short - Lived Climate Forcer / Pollutant (Putero et al., 2014) with residence time in atmosphere of days to weeks, locally and seasonally variable; additionally, since sources typically emitting BC also release other short-lived species and co-pollutant particles, that may either cool or warm climate, with a variable ratio responsible for a net warming or cooling effect on climate that must therefore be estimated time to time. Unfortunately, present - day limited level of detailed knowledge gives reason for a high degree of uncertainty in the estimation of overall global warming effect of co - emitted species (EEA, 2012a).

Being a substantial component of fine particulate matter in air pollution, BC is notoriously a dangerous local air pollutant, prevalently classified as $PM_{2.5}$ (Bond et al., 2013); for its tendency to undergo regional and intercontinental transport (Marinoni et al., 2013) during its short atmospheric lifetime (a few days to weeks), BC is nowadays considered a leading environmental risk factor relating to the incidence of human health issues such as lung cancer, respiratory illness, and cardiopulmonary disease, as well as premature death globally (Johnson et al., 2016; Bond et al., 2013); in 2010, outdoor $PM_{2.5}$ air pollution was estimated to have caused over 3.2 million premature deaths (source: Climate and Clean Air Coalition, http://www.ccacoalition.org/en/slcps/black-carbon).

Janssen et al. (2011) report that health effect estimates from mortality and morbidity time - series studies are higher when looking at BC particles than PM_{10} or $PM_{2.5}$, as well as cohort studies.

Its health-damaging impact is due to both outdoor and indoor exposure and affects the respiratory and cardiovascular systems; as concerns intervention strategies, even if the most common regulatory approaches are based on overall reduction in fine particulate matter, reductions of $PM_{2.5}$ are not considered necessarily sufficient to reduce BC exposition levels.

Additionally, current economic recovery, increasing traffic and exchanged volumes and the related growing use of diesel-powered vehicles concur in determining a tendential increase in atmospheric release of BC, even if its atmospheric concentrations quickly respond to reductions in emissions, because its removal from atmosphere by deposition processes is quick.

Despite the existence of many potential methodologies and instruments to effectively measure marine BC emissions, measurement approach exerts a substantial impact on BC emissions estimation.

Two properties related to light absorption and heat resistance reveal particularly useful for BC

measurement purposes: BC strongly absorbs visible light with a mass absorption coefficient (MAC) value above 5 m^2 g^{-1} at λ = 550 nm for freshly produced particles, hence determination is prevalently carried out by light absorbing capability of BC resulting in black colour; the absorption properties of BC are the reason it is considered a short lived climate forcer, and thus photometry - based absorption methods based on filter darkening measurement are usually viewed as more relevant for climate impact assessment because they delivers results in real time with a high time resolution; alternatively, BC is thermally refractory, with a volatilization temperature near 4000 K (Johnson et al., 2016).

Tropospheric Ozone (O_3): this reactive gas exists both in the stratosphere and the troposphere; in particular, tropospheric ozone is considered as a significant anthropogenic greenhouse gas (Forster et al., 2007), a short - lived climate forcer and a dangerous atmospheric pollutant for its harmful effects on human health and agriculture.

It is a secondary pollutant that is formed in the troposphere by complex solar radiation - driven photochemical oxidation processes of ozone natural and anthropogenic precursors, mainly methane, carbon monoxide, nitrogen oxides (NO_X) and non - methane hydrocarbons (NMHCs), arising from both natural sources and a broad range of human activities (Marinoni et al., 2013; Dickerson et al., 1997).

Taking into account only the direct effect of ozone change, IPCC estimates tropospheric ozone to provide the third largest anthropic contribution to positive radiative forcing, and therefore global greenhouse effect, since the preindustrial era, after carbon dioxide and methane, with a threefold increase in ozone concentrations in the northern hemisphere during the past 100 years (Gauss et al., 2003).

Due to its high chemical reactivity, ozone has a brief lifetime of a few days to a few weeks, being involved in photochemical reactions responsible for strongly influencing on overall oxidative capacity of troposphere and impacting on climate (Putero et al., 2014; Marinoni et al., 2013).

Moreover, locally frequent clear sky meteorological conditions agevolate the formation of photochemical ozone from its precursors, emitted in great quantity from continental Europe; ozone destroys plant cell structural integrity, thus reducing plant ability to absorb CO_2 and playing a detrimental effect on quality and nutritive value of food and feed: it has been estimated that present

day global relative yield losses due to tropospheric ozone exposure range between 7-12% for wheat, 6-16% for soybean, 3-4% for rice, and 3-5% for maize (source: Climate and Clean Air Coalition, http://www.ccacoalition.org/en/science-resources). Additionally, it exhibits not negligible impacts on diversity and growth of plant communities, as well as on ecosystem structure and function.

As a powerful oxidizing gas, tropospheric ozone exerts a negative impact on human health, too: human diseases due to ozone include breath problems following to airway inflammation and oxidative - stress induced reduction of lung function.

Mediterranean basin is recognized as a hotspot for short - term variations of tropospheric ozone concentration.

Carbon dioxide (CO_2): despite its relatively short residence time in atmosphere, about 15 years, air levels of this powerful greenhouse gas are at their highest in 650000 years, at present (October 2016) reaching 404 ppb; exerting a positive radiative forcing, carbon dioxide is highly responsible for global temperature increase, globally estimated in about 3°C since 1880, with nine of the ten warmest years on record having occurred since 2000: this is provoking thinning in arctic ice minimum of 13.3 % per decade and sea level increase of 3.4 mm per year (source: http://climate.nasa.gov).

Carbon dioxide is released from fossil fuel combustion, energetic and industrial activities, as well as transport sector; cumulative emissions of CO_2 largely determine global mean surface warming by the late 21st century and beyond (IPCC, 2014), as outlined in fig. 5.

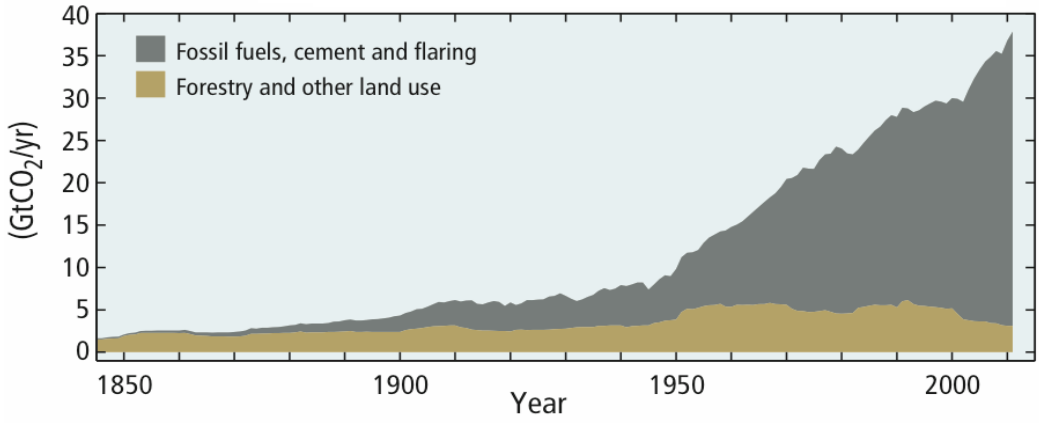

Fig. 5 - Global anthropogenic CO2 emissions from forestry and other land use as well as from burning of fossil fuel, cement production and flaring (from IPCC, 2014)

Carbon monoxide (CO) is a short-lived highly toxic GHG, with a residence time in atmosphere of about 2 months (Bond et al., 2013), resulting from incomplete combustion of carbon - based compounds; its main natural sources are volcanic emissions, wildfires and photochemical oxidation of methane; an interesting body of studies on aerosol chemical composition (Becagli et a., 2011; Lack et al., 2009) reported the presence of CO into the chemical composition of ship - emitted plumes from marine engines fed with heavy fuel oil, in different engines load condition.

Additionally, CO exerts a serious impacts on the large - scale troposphere functioning in terms of its capacity of pollutants photochemical oxidation to carbon dioxide: being this process promoted by hydroxyl radical and tropospheric ozone, that are actively consumed by the CO produced, their reduction and unavailability for tropospheric self - cleaning processes may trigger a feedback accumulation of pollutants and carbon monoxide (Andreae, 1991).

Human impacts of exposition to CO affect primarily central nervous system, respiratory and cardiovascular systems.

Interestingly, since carbon monoxide release into the atmosphere is reported from biomass burning, it can be considered as a tracer of combustion processes related to biomass burning or anthropogenic pollution: the cause is probably linked to a non optimal mixing between carbon fuel and oxygen; however, considering that, even in conditions of high oxygen availability the reaction rate of the oxidation of carbon to CO is about ten times higher than the reaction rate of further oxidation of CO to CO_2, it necessarily follows that CO is always present as a by-product during combustion events.

Methane (CH_4) is a potent greenhouse gas at the same time (GWP = 21), one of the most important precursors of tropospheric ozone and thus highly contributing to background ozone levels in the troposphere and air pollution; its lifetime in atmosphere is about 10 years.

Moreover, considering its largest radiative forcing by any greenhouse gas after carbon dioxide, the accumulation of methane in the atmosphere up to levels unprecedented in at least the last 800000 years determined a direct influence on the climate system, too, in terms of energy uptaking.

Methane is the principal component of natural gas and its atmospheric concentrations have grown as a result of natural processes like decomposition of plant and animal waste, but also from human activities related to coal mining, natural oil and gas extraction and distribution, biomass burning and

waste treatment process and landfills, as well as agriculture, including rice cultivation and zootechnical ruminant livestock.

Methane is clearly associated to a great deal of indirect effects on human health and ecosystems, including its role as an important precursor to the formation of dangerous tropospheric ozone in the lower atmosphere.

Nitrogen oxides (NO_X): besides its bimolecular form, constituting almost 80 % of earth atmosphere, nitrogen is present in the air as oxidized species N_2O, NO, NO_2 and HNO_3, too, and as reduced species NH_3.

NO is produced from endothermic reaction between N_2 and O_2 during combustion processes in presence of air, at temperatures higher than 700°C; a further oxidation of NO determines its conversion into NO_2, in a proportion of 10 %.

A remaining quantity of NO_2 derives from the interaction between UV solar radiation and ozone, during the so - called **photocatalytic cycle**: UV solar radiation at wavelength ranging from 280 to 430 nm promotes the photodissociation of NO_2 in NO and O radical, which easily reacts with atmospheric O_2 turning into tropospheric ozone, which in turns is consumed by reacting with NO to give NO_2 and O_2. Every time the concurrent emission of NO_x and hydrocarbons from the same source takes place, O radical coming from photolysis of NO_2 can attack volatile hydrocarbons giving free radicals.

The most dangerous free radical is the peroxide radical RO_2, that again can react with NO to give back NO_2 without ozone consumption, thus determining the depletion of NO and the accumulation of NO_2 and O_3 in the troposphere, and consequently quenching the normal ozone clean out process: together with ozone, the levels of secondary pollutants from UV - mediated hydrocarbon oxidation rises, too.

The mix resulting from hydrocarbon - deriving interference globally on the photolytic cycle of NO_2 and the accumulation of free radicals generated by the UV - mediated ozone decomposition is globally known as **photochemical smog**.

NO_X are indirect climate - altering substances, that can have both positive and negative radiative forcing as a result of ozone formation and enhancement in methane loss, respectively.

Sulphur dioxide (SO_2): this primary pollutant is climate - altering with a negative radiative forcing.

Its residence time in atmosphere of about 40 days, the fundamental scavenging process being the humidity - triggered conversion into particles of sulphate and following wet deposition; a further oxidation may produce SO_3 in unappreciable quantity, since SO_2 does not show great reactivity with O_2 for kinetic reasons.

It is capable to determine irritation of respiratory system.

Offshore traffic ship emissions accounts for a determining share of atmospheric SO_2 release in central Mediterranean basin (Becagli et al., 2012; EEA, 2013).

In response to this situation, Directive 2005 / 33 / EC limited the maximum sulphur content in ship fuels in SECAs to 1.5% by mass.

2. THE CLIMATIC OBSERVATORY OF CAPO GRANITOLA

2.1. Site description

Generally, coastal marine ecosystems' peculiarity relies on their extreme vulnerability together with the possibility of privileged observation for the study of their characterizing phenomena.

The Climate - Environmental Observatory of Capo Granitola (37°34'31'' N; 12°39'34'' E, 5 m a.s.l.) has been started at the Torretta Granitola coastal site in the municipality of Campobello di Mazara (12000 inhabitants), in December 2014.

The observatory is placed along the southern Sicily coastline facing the Strait of Sicily, 12 Km from the municipality of Mazara del Vallo (52000 inhabitants) in NO direction.

The realization has been carried out by the the Institute for Atmosphere and Climate Sciences of italian National Research Council (ISAC - CNR), inside the scientific campus of the Institute for Marine - Coastal Environment of italian National Research Council (IAMC - CNR), afferent to the CNR Departmet of Earth System Sciences and Environmental Technologies (DTA) and in the framework of the I-AMICA PON Project (see Appendix 2). Near-real-time data can be seen at the web page http://www.i-amica.it/i-amica/?page_id=1125.

This remote site is considered representative of average western Sicily / central Mediterranean basin regional background atmospheric conditions since it is the first observational system located at the interface between earth and sea, with limited impacts from local or regional emissions under land breeze circulation (Marinoni et al., 2016).

This scientific structure provides in continuous data representative of atmospheric physical and

optical properties and composition in the facing coastal area, including the main reactive and GHG gases; these data are exploited to improve scientific knowledge about the influence of a wide spectrum of phenomena, such as ship traffic emissions, land-based pollutants emission and marine spray, on variations in atmospheric composition and to investigate the variability of climate - changing and pollutant agent (trace gases and aerosol), as well as their relationships to phenomena not necessarily taking place in the immediate vicinity, particularly long-range air mass transport processes, especially Saharan dust advection episodes (CNR - ISAC / IAMC, 2016; Marenco et al., 2006). In addition, the comprehension of the dynamics of coastal processes is of key importance as it ultimately proved to strongly influence air quality and environmental resources - centered economy of even the most inner areas of the territory (UNEP / MAP, 2009).

Acquired data proved to well depict the background conditions of the Mediterranean basin, at the same time providing useful hints to investigate the influence of specific atmospheric processes (e.g. long-range air-mass transport, mineral dust emitted from northern Africa, anthropogenic ship emissions) on the variability of trace gases- and aerosol- related parameters (CNR - ISAC / IAMC, 2016); a 36 - days sampling campaign conducted in this Climate - Environmental Observatory in 2015 recorded an average PM_{10} concentration in CGR of 23.1 ug m^{-3}, whereas $PM_{2.5}$ accounts for 45 % of PM_{10}, signaling a significant contribution from sea spray, together with a remarkable crustal fraction as consequence of desert dust transport events (Marinoni et al., 2016).

The Observatory of Capo Granitola is part of i - AMICA network, to which it contributes with continuous (24/24 and 7/7) atmospheric composition measurements programmes facing the Channel of Sicily in the fields of meteo parameters and solar radiation, surface ozone and sulphur dioxide, carbon monoxide, carbon dioxide, methane and nitrogen oxides, aerosol number size distribution (size range from 280 nm to 10 μm), aerosol mass ($PM_{2.5}$ and PM_{10}), equivalent black carbon concentration and aerosol absorption coefficient, aerosol scattering coefficient at various wavelengths, integrated aerosol particle counting (limited to particles with 4 μm - lowest diameter).

See the following table for a complete illustration of measured parameter.

Parameter	Relevance	Measurement principle
Surface O_3	Short life time climate forcer, greenhouse gas, secondary pollutant	UV - Absorption
CO	Primary pollutant, ozone precursor, combustion tracer	Cavity Ring Down Spectroscopy
NO_x	Primary (NO) / secondary (NO_2) pollutants, ozone precursors, combustion tracers	Chemiluminescence
SO_2	Primary pollutant, secondary aerosol and acid rain precursor	Fluorescence
Black carbon concentration	Short life time climate forcer, primary pollutant, combustion tracer, concurring to PM_1	Multi-Angle Absorption Photometry
Fine particulate matter numeric concentration	Short life time climate forcer, primary and secondary aerosol, pollution tracer, concurring to PM_1	Optical Particle Counting
Coarse particulate matter numeric concentration	Short life time climate forcer, primary aerosol, mineral dust and sea spray tracer, concurring to PM_{10}	Optical Particle Counting
Particulate matter total numeric concentration	Short life time climate forcer, primary aerosol	Condensation Particle Counting
Particulate matter mass concentration (PM_{10} - $PM_{2.5}$)	Short life time climate forcer / pollutant, primary and secondary aerosol	ß attenuation - based airborne particulate matter mass measure on filtering membrane
CO_2	Main long life time climate forcer, primary, combustion tracer, biogenic activity	Cavity Ring Down Spectroscopy
CH_4	Short life time climate forcer, primary, greenhouse gas, tropospheric ozone precursor	Cavity Ring Down Spectroscopy
Aerosol scattering coefficient	Particulate matter concentration index, PM optical behavior, climate forcing through interaction with sunlight	Nephelometry
Rain load	Meteorology and interpretation of data	Piezoelectrical measurement

Temperature and relative humidity	Meteorology and interpretation of data	Capacitive measurement
Atmopheric pressure	Meteorology and interpretation of data	Capacitive measurement
Wind intensity and direction	Meteorology and interpretation of data	Ultrasound transit time measurement

The Observatory of Capo Granitola is now entering many continental- and planetary- scale observational networks; in 2015 it entered the **World Meteorological Observatory (WMO) Global Atmospheric Watch (GAW) Program**, to which it contributes in quality of "Regional Station" (GAW ID: CGR).

WMO is a specialized agency of the United Nations dedicated to international cooperation and coordination on atmosphere present conditions, influences on climate and weathering and interactions with terrestrial and marine ecosystems.

In an effort of a timely provision of updated informations about interactions between atmosphere, oceans and biosphere, GAW network was established by a partnership agreement among WMO members to set up an interconnected array of global and regional measurement station, operated by their host countries, to promote global - scale activities of long-term observations of air chemical composition and selected physical characteristics in order to generate reliable scientific data on chemical composition of the atmosphere, as well as its naturally- and anthropogenically-driven modifications, through standardized monitoring practices and procedures; consequently, GAW can be considered the atmospheric chemistry component of the Global Climate Observing System (GCOS).

GAW provides a comprehensive set of observations of atmospheric composition in support of the Intergovernmental Panel on Climate Change (IPCC) process and supports United Nations Framework Convention on Climate Change (UNFCCC), especially by contributing to the implementation plan for the **Global Climate Observing System (GCOS)**, as well as the **Convention on Long-Range Transboundary Air Pollution (CLRTAP)**.

The ultimate goal of GAW program is to detect trends in global distributions of chemical constituents in air, understand and control the increasing influence of human activity on the global atmosphere, prevent changes in the weather and climate related to human influence on atmospheric composition, particularly as concerns greenhouse gases, ozone and aerosols, as well as to contribute

to scientific assessments in support of environmental policy, since long-range transport and deposition of air pollution is ultimately finalized to risk reduction of air pollution on human health; (WMO / GAW, 2016).

In particular, aerosol issue is one of the 6 GAW focal areas of socio - economic relevance rising from deep relationship linking weather, climate, human and ecosystem health, water supply and quality, and agricultural production: under this respect, the objective of GAW is to determine the spatio - temporal distribution of aerosol properties related to climate forcing and air quality on multi-decadal time scales and on regional and global spatial scales; for this reason emphasis was given to benefits coming from improved satellites and ground-based monitoring capabilities (WMO / GAW, 2016).

GAW's Scientific Advisory Group (SAG) on Aerosols recommended the implementation of a global aerosol observing system compounded of a network of ground-based stations taking part to inter calibration activities, to produce an integrated set of global aerosol observations according to strictly specified methodologies and procedures to guarantee the traceability to the original raw observational data and improve data quality, as well as to enhance their extended use by the scientific community.

Currently GAW backbone is constituted by 31 global stations, more than 400 regional stations and around 100 contributing stations; CGR is considered a background regional station whose measurements are mainly referable to long-range transport; for this reason data obtained from this serving station are particularly indicative in order to minimize the interference of non-long-range transport sources when defining the typical regional background conditions.

CGR is also inserted in the network AQICN (Air Quality and Pollution Measurement, http://aqicn.org/city/italy/capo-granitola/cnr-isac/), providing near-real-time (NRT) data about air quality.

The geographical position of the site along the south - western coast - line of Sicily and in proximity to coastline, together with the substantial ecological integrity and the absence of industrial activities and urban settlements nearby, the peculiar meteorological conditions and distance from city centers, justify Capo Granitola's election to Site of Community Importance (ITA010011) under the **Habitat Directive 92 / 43 / EEC** .

Additionally, CGR observatory is directly interested by a **systematically occurring sea - land**

breeze regime, with a prevailing gentle wind breezes from inland (NW - SE) during night - time and winds from the sea (W - SE) during day - time; together with PBL dynamics and photochemistry reactions, such a sea / land breeze regime determines a well - defined diurnal cycle of reactive gases (O_3, NO, NO_2, CO, SO_2) variability, giving account for its representativeness of the regional Mediterranean background when marine air masses affect the station.

The site is strongly interested by air masses coming from central Mediterranean Basin (Tyrrenian Sea), thus suggesting a prevailing **north - westerly circulation pattern**; furthermore, from a **synoptic scale perspective**, referring to the scale adopted for large - scale weather system description of the state of the atmosphere over a wide area, circulation over the station is often related to northern Africa.

2.2. Instrumental set-up

The climate - environment observatory of Capo Granitola is accommodated in a shelter located near the sea, about 5 m above sea level.

The inlets for sampling air consist of 2 teflon columns (height: 2600 mm, inner diameter: 50 mm, sampling height: 1500 mm above station roof):

- **gas column** for reactive gases and greenhouse gases sampling, with a teflon - coated upper hood so as to prevent rain penetration and to ensure chemical inertia;

- **aerosol column** for particulate matter, whose hood is capable to select particulate matter with aerodynamic diameter < 10 μm. equipped with an outdoor inlet head to prevent rain droplets from sampling and, at the same time, to act as an impactor for aerodynamic size cut-off at PM10 with an operating laminar sampling flow rate of 100 L / min, under ambient conditions. This value is high enough to ensure that even smallest particles are properly sampled and conveyed: the Reynolds number is lower than 2000. Inlet position is vertical, omni - directional and high enough above ground level to minimize local influences and obstacles, so as to maintain high aerosol transmission efficiency independently on wind direction or speed. An electrically conductive sampling head is intended to minimize electrostatic phenomena responsible for particles loss and their underestimation, together with any chemical alteration of particulate

matter. These features respect WMO / GAW recommendations (2016), according to which an eligible aerosol sampling system must be capable to provide a representative ambient aerosol sample, namely as much undisturbed as possible and with minimal diffusional and inertial losses, by minimizing the evaporation of volatile particulate species, excluding precipitation from the sampled aerosol and providing aerosol particles at low relative humidity (< 40%): this precaution is reasonable because of the strong influence of relative humidity on the size of most airborne particles. The lower section of sampling line includes a dilution chamber and a smart aerosol conditioner, and hosts a flow meter and a temperature and relative humidity sensor. Aerosol instrumentation should optimally be housed in a closed shelter providing a clean laboratory environment and indoor temperatures between 20 and 25 °C.

Both columns are equipped with AISI316 stainless steel sampling head, whose geometry is compliant with international standards (WHO / GAW, 2016), a pump with flow rate of 250 l / min and an output to avoid wind - related mechanical resistance, a volumetric counter to measure the volume of air crossing the filtering membrane, and temperature and pressure detectors for continue correction of volume measures in the environmental conditions.

A brief overview of instrumental setup, including salient device features and a schematic description of the principles of measure, follows.

Multichannel OPC Monitor (FAI INSTRUMENTS s.r.l., Italy): an Optical Particle Counter (OPC) executes automatic and sequential sampling of airborne particulate matter for its size distribution description, in terms of optical diameter, by means of a laser source (laser diode, 35 mW) coupled with an electro - optical detection system and embedded electronics to specifically amplify the signal.

The device installed in CGR observation station is set up in its standalone configuration and is equipped with a sampling head and line (sampling rate 1 L / min, accuracy ± 2 %), a T & RH sensor external to cabinet and a sensor unit, installed inside the control unit. The air sampling system is coupled with a dilution system (dilution flow tunable 1 to 5 L / min), fed with particles - free air by absolute filters with the purpose to avoid the bias due to coincidence of particles.

Finally, air sampling system hosts a smart heater and a silica gel desiccator cartridge to prevent humidity oscillations in incoming air: values lower than 60 % are recommended by the

manufacturer.

The instrument principle of measure is based on the **phenomenon of light scattering from suspended particles in aerosol**: the measurement principle relies on the detection of laser light scattering on a wide - angle elliptical mirror, highly sensitive to refraction index of particles; a semiconductor photodetector performs the detection of the amount of light that is redirected by a particle crossing the detection area by performing signals counting (particle number concentration) and generating an electronic signal proportional to light amount scattered by the particle, enabling a **size - based classification of particles**.

Atmospheric aerosol is characterized both in terms of **particle number concentration (PNC)**, expressed as particles / l with a concentration range up to 2000000 particles / l, and of **particle mass concentration (PMC)**, expressed as μg/m^3, through the real-time estimate of mass concentration PM_x of suspended particulate matter, providing data for coarse (PM_{10} and $PM_{2.5}$) and fine (PM_1) fractions.

PNC is provided for 8 optical channels with contiguous size classes (thresholds at 0.28, 0.4, 0.5, 0.7, 1.1, 2.0, 3.0, 5.0 μm), in terms of counts per minute (cpm) for each channel: this parameter can provide useful hints on correlation with pollution sources and typology.

Unlike canon two - phase methods involving aerosol collection followed by laboratory analysis, this device operates in continuous and real - time mode, showing in situ, short - time measurement capability of airborne particle concentration.

Dimensional sensibility is 0.28 μm (50 ± 10 % count efficiency) in terms of optical diameter., whereas dimensional resolution is 0.05 μm. Typical detection sensitivity of the light scattering

method is 0.05 μm or larger; sampling time is 1 min.

Ultrafine Condensation Particle Counter 3776 (TSI Incorporated, USA): this instrument specifically suited for atmospheric and climate research detects and counts airborne particles greater than 3 μm down to 2.5 nm in diameter, with extended single particle counting up to 300000 particles/cm^3. This is of crucial importance because particles smaller than 50 nm are generally undetectable with conventional optical techniques.

In a UCPC particles are exploited as nucleation centers to create droplets in a supersaturated gas; by this way their enlargement is promoted, thus facilitating their detection.

The technique adopted to produce nucleation is the most efficient **thermal diffusion**: by promoting its cooling inside a condensation chamber, a working fluid (n - butanol) is forced to reach supersaturation conditions; this triggers its heterogeneous nucleation and droplet growth on surface of a suspended solid particle.

Operationally, in a laminar-flow, alcohol-based diffusional thermal cooling CPC, a stable volumetric inlet aerosol sample flow is continuously aspired by a built - in high vacuum pump through a heated hollow block of porous material (saturator) in contact with the working liquid (reagent - grade n - butyl alcohol), to ensure high vapour content and consequently its uniform vaporization and diffusion into the sample stream. Subsequently, the sheath - air - flow of the humidified mixture enters a cooled condenser, confining the aerosol flow path near its centerline, where alcohol vapor surrounding particles reaches a certain degree of supersaturation and starts condensing onto the particles, enlarging them into easily detectable droplets, where sample particles act as effective condensation nuclei (Kaufman et al., 1998; Crutzen and Andreae, 1990). By this

way heterogeneous nucleation starts occurring, during which particles grow up and so become conveniently detectable.

Aerosol inlet flows of 0.3 or 1.5 l / min can be tuned as needed: high inlet sample flow mode is suited for smaller particles, which are transported more quickly through sampling lines reducing particle diffusion losses; inversely, to measure size distributions for wider particle size range the low flow mode is chosen.

Besides, it should be pointed out that, on the microscopic scale, vapor pressure over a convex surface is less than over a plane one: this justifies the greater content of vapor in air required to reach actual working fluid's supersaturation criteria; additionally, since vapor pressure furtherly decreases along with decrease in particle size, the lowest diameter for which condensation can happen at a certain saturation level parallel decreases; this critical value is called **Kelvin diameter**.

On the other hand, supersaturation level can't be excessive as to prevent homogeneous nucleation between liquid molecules, which would produce false counts: tuning of operating temperature is therefore required to allow heterogeneous condensation to take place.

Temperature difference between the heater and the cooler determines the supersaturation, which in its turn inversely determines the minimal size of particles that will be detected and counted. The more uniform is obtained supersaturation, the sharper is particle minimal size cutoff.

Particles with a diameter exceeding Kelvin diameter threshold quickly grow into larger droplets in the supersaturated atmosphere of butanol and are revealed and counted by a diode photodetector optical detector coupled to a laser-diode light source, via particles - scattered light collection.

The device operated in continuous, executing live - time coincidence correction to improve accuracy and sharpness in lower - size - detection limit, with minimal ultrafine and nanoparticles diffusion losses.

Particle concentration is presented as particles per cubic centimeter (p / cc), determined from the count rate (particles counted per tenth of a second) and the actual aerosol flow rate measured.

SWAM 5A Dual Channel Monitor (FAI Instruments s.r.l., Italy): this atmospheric PM_x monitor is aimed to support studies on air PMx pollution and air quality, by automatic and sequential 24 hours - long sampling of airborne suspended particulate matter on ø 47mm collection filter membranes, exploitable for further analysis.

The device operates with two independent sample lines, equipped with a size fractionator sampling head, to monitor two size fractions of particulate matter; in the adopted configuration, it works with PM_{10} and $PM_{2.5}$ sampling inlets with a flow rate of 1 m^3/h: optimal operating flow rate depends on the features of sampling head and on size cut, the programmable operating flow rate range 0.8 ÷ 2.5 m^3/h and can be independently set by regulating the two pumping units located downstream the sampling unit.

The calculation of the sample particulate mass stored on the filtering medium in the previous 24 hours is provided, for both fractions, with an uncertainty in the order of 10 µg, using the **ß attenuation** method from a ^{14}C radioactive source with nominal activity of 3.7 MBq (100 µCi).

Mass concentration measurement precision is ± 0.3 µg / m^3, whereas mass concentration measurement detection limit is 1 µg / m^3, referred to 24 hours cycle and 2.3 m^3/h operating flow rate.

Reference technical standard for PM_{10} and $PM_{2.5}$ measurement is UNI EN 12341:2014 “Ambient air - Standard gravimetric measurement method for the determination of the PM_{10} or $PM_{2.5}$ mass concentration of suspended particulate matter”: it considers beta radiation assorbance measurement on the particulate matter sampled on a filter as an equivalent method of the standard reference gravimetric method.

Multi-Angle Absorption Photometer black carbon monitor 5012 (Thermo Fisher Scientific, USA): this continuous instrument is devoted to survey the elemental suspended BC loading in the ambient atmosphere, as well as aerosol light absorption properties.

In general, BC optical measurement implies the assessment of light transmission through a glass fiber collection filter on which particles have been sampled.

Since unfortunately this measurement is unavoidably affected by light reflection and multidirectional scattering, as a function of particle size and shape, the assay of aerosol black carbon content is likely to be unreliable; this obstable is overcome by simultaneously and continuously measuring the optical absorption and scattering of light by the particles collected on a glass fiber filter tape, type GF 10.

The **principle of BC detection of MAAP** is based on the direct relationship between aerosol - related light absorption and the corresponding atmospheric BC mass concentration; light absorption methods are **filter - based** because they rely for quantification on light absorption by particles through a filter previously loaded with them followed by calculation using factors that link light absorption to mass concentration.

In more details, a multi angle absorption photometer is capable to analyze the modification of radiation fields in the forward (transmission) and backward (scattering) hemisphere of a glass-fiber filter on which particles were deposited; typically, this approach allows to isolate and remove scattering effects potentially interfering with traditional optical absorption methods.

The sample is drawn into the device through the inlet and flows until it deposits onto the glass fiber filter tape: it stores an aerosol sample on a dust collecting spot f 2.0 cm^2 up to a threshold accumulation value, whereupon the filter tape will automatically advance prior to reaching saturation. Once sample accumulation has finished, a 670 nm visible light source is directed

towards the deposited aerosol and filter tape matrix, inside the detection chamber; meanwhile, an array of photo - detectors (measuring head, a forward hemisphere one and several back hemisphere ones) measures the light transmitted into the forward hemisphere and the one reflected into the back hemisphere. The reduction of light transmission and multiple reflection intensities are continuously integrated over the sample run period to provide a real- time data output of black carbon concentration measurements; data inversion algorithm is based on a radiative transfer method to take multiple scattering processes inside the deposited aerosol and between the aerosol layer and the filter matrix into account.

MAAP device incorporates a volumetric flow rate meter based on the pressure drop as measured at the orifice plate just downstream the filter tape, as well as a pressure and temperature probe compensated for air flow rate, to express volumetric air flow referenced to standard temperature and pressure conditions: this is crucial as a correct sample volume determination is strictly required for turning BC mass into BC concentration data.

Post - collected data may be converted to the aerosol light absorption coefficient by applying the specific attenuation factor (sigma) used in the Calibration menu.

BC measurement range is 0 - 180 $\mu g/m^3$ @ 10, averaging, respectively (95 % confidence level), at a flow rate of 1000 lh^{-1}. Minimum detection is < 100 ng/m^3, on 2 - minute average.

Integrated nephelometer 3563 (TSI Incorporated, USA): designed for long-term monitoring of visual range and air quality in ground-based and airborne studies, this instrument continuously and accurately monitors light-scattering coefficient of air molecules and airborne particles present in the sample chamber, by measuring the light scattered by atmospheric aerosol particles and subtracting light scattered by the gas.

This analytical device is targeted for both short- and long-term measurements of aerosol optical properties related to climate and air quality, it is designed specifically for studies of direct radiative forcing of the Earth's climate by aerosol particles.

Nephelometry is an optical analytical technique aimed to appreciating the quantity of a dispersed substance by measuring the scattered radiation; the measurement principle relies on the **effect Tyndall**, consisting in the omnidirectional diffusion of an electromagnetic wave inside a colloidal two - phase system composed of suspended particles of the same order of magnitude in size than the radiation wavelength, following to multiple reflections and refractions. This effect is mostly influenced by the radiation wavelength, the average size of dispersed particles and the difference between refraction indexes of dispersing and dispersed phase.

For sufficiently dispersed systems, the concentration of dispersed phase, in terms of number of suspended particles, is proportional to the intensity of scattered light, according to the **law of Rayleigh**: this relationship can be profitably exploited for extremely fine dispersed phases sensible detection and, additionally, it allows measure standardization and high levels of precision, whereas beyond a threshold of concentration the increase of absorption by particles determines a linearity and sensibility loss.

The device is endowed with an internal turbine blower to draw an aerosol sample through the inlet port and to push it into the measurement volume, where the sample is illuminated by a halogen light source directed through an optical pipe and opal glass diffuser. The light scattered by the aerosol is split into three wavelengths (450 nm, blue, 550 nm, green, and 700 nm, red) using high-pass and band-pass color filters in front of three photomultiplier tubes (PMTs), which accurately measure both total and backscatter signals with a wide angular integration from 7 to 170°, through a series of apertures set placed along the axis of the instrument body.

The parameter of interest is the **aerosol scattering coefficient**, being the light scattering by particles expressed in units of inverse meters. Aerosol scattering is viewed against the dark backdrop of a very efficient light trap, that, combined with a highly light - absorbing coating on all internal surfaces, gives very low baseline scattering from the walls of the instrument.

Particle scattering is measured by taking the total scattering value of the sample and then subtracting contributions of scattering from air molecules (Rayleigh scattering or elastic scattering) and the instrument background; Rayleigh scattering results always quantifiable because, being elastic, this portion shows the same frequency and wavelength of incoming radiation.

Since aerosol scattering coefficients represents a highly variable aerosol property, integrating nephelometer measure the angular integral of light scattering over an angle of 7 to 170° that yields the quantity called the **scattering coefficient,** which is used in the **Beer - Lambert Law** to

calculate total light extinction coefficient (sigma), given as the sum of scattering coefficient and absorption coefficient

A constantly rotating, reference chopper provides three modes of signal detection: the first one is a measure of the aerosol light - scattering signal, the second one blocks all light from detection and gives a measurement of the PMT dark current, which will be afterwards subtracted from the measured signal, lastly the third one consists in inserting a translucent surface into the direct path of the light to provide a measure of the light - source signal: in this way, the instrument compensates for changes in the light source.

Periodically, an automated ball - valve built into the inlet can be activated to divert all of the aerosol sample through a high - efficiency filter and provide a measure of the clean - air signal for the local environment: afterwards, this signal is subtracted, along with the PMT dark - current signal, from the aerosol - scatter signal to give only that portion of the scatter signal provided by the sample aerosol.

The photodetector is placed at 90° respect to the direction of the incoming radiation, as to collect the most of energy, thus optimizing sensibility.

Upper detection limit of the device is 2.0×10^{-2} / m, while its highest sensitivity is guaranteed to light - scattering coefficients as low as 1.0×10^{-7} / m, at 60 - sec averaging time.

Cavity Ring - Down Spectroscopy G2401 (Picarro Inc, USA): this spectral absorption - based automatic analyzer continuously collects data on the concentration of main GHGs, namely CO_2 (v/v), CO (v/v), CH_4 (v/v) and water vapor (%) down to parts - per - billion (ppb) sensitivity.

In the instrument, sample air is aspired by a pump, filtered and pushed through a capillary, as to control the flow.

Analytical principle is the patented **Cavity Ring - Down Spectroscopy (CRDS) technology**, enabling time - based measurement relying on a laser to quantify spectral features of gas phase molecules in an optical cavity.

In brief, nearly every small gas - phase molecule has a unique near - infrared absorption spectrum, consisting in a series of narrow, well - resolved lines with a well - known wavelength; the concentration of any species can be therefore determined by measuring the height of a specific absorption peak; unfortunately, this is impossible when dealing with trace gases (sub - ppm concentration), whose absorption is too little to measure.

CRDS allows to bypass this obstacle, resulting in exceptional precision and sensitivity: a laser beam, from a single - frequency laser diode and circulating into a craft configuration of a three - high - reflectivity - mirror cavity, determines a continuous traveling light wave whose intensity is measured by a photodetector as it passes through one mirror.

When the photodetector signal reaches a threshold level the laser is abruptly turned off, thus leaving the light already inside the cavity continuing to be reflected in the inter - mirrors space and to reach an effective path length of many kilometers; this doesn't impede the **exponential decay ("ring down") of light intensity inside the cavity** to zero, that can be measured in real - time by the photodetector.

For an empty cavity, the amount of **ring down time** depends exclusively on the reflectivity of the mirrors: the 25 cm - long cavity embedded in the device can generate an effective measurement path length of over 20 kilometers; instead, if the cavity is filled with a laser light absorbing gas species, a second light extinction mechanism within the cavity must be taken into account, that is able to accelerate the ring down time in a fashion strictly dependent on the gas species: by continuously measuring and comparing the ring down time of the cavity with and without gas - related absorption, intra-cavity loss pattern of temporal variation can be evaluated in a precise, quantitative and robust manner, thus leading to concentration of target gas species data in a way that is independent from unavoidable laser intensity fluctuations.

In practical terms, comparison is done between different wavelengths radiations, where the target gas species absorbs and does not absorb the light emitted by a tunable laser, instead of between full

and empty cavity condition.

More precisely, the laser is tuned to several locations across the target gas's spectral absorption line, and in each point ring down measurements are performed; then, a mathematical fit to the shape of that absorption line enables to calculate the actual gas concentration: this method provides a good signal to noise ratio and sensitivity levels of parts per billion or, in some cases, per trillion.

The cavity incorporates temperature and pressure control to ensure measurement fidelity over long periods of time, even in the harshest environments.

High - precision wavelength monitor helps to maintain absolute spectral position and the most accurate peak quantification, as well as to guarantee that only the spectral features of interest are being monitored, which greatly reduces the analyzer's sensitivity to interfering species.

Routine monthly calibration is carried out using couples of working standards obtained from 3 primary standards containing CH_4, CO_2 and CO, each one according to mixing ratios close to upper and lower ones expected in the ambient.

Operating range of 0 – 1000 ppm, 0 – 5 ppm, 0 – 20 ppm and 0 - 7 %v are guaranteed for CO_2, CO, CH_4 and H_2O, respectively. Two - point calibration (**zero - span calibration**) is periodically requested with standard gases for each species, as to span a representative range of values over which the analyzer will typically be operated; once a **calibration offset** (slope and intercept) has been found for each species, a third intermediate point can be used for verification of the linear best-fit equation calculated from data.

Furthermore, this device provides the level of precision needed to meet WMO requirements standards on the precision of GHGs and CO measurements made at its GAW stations.

NO - NO_2 - NO_x chemiluminescence analyzer Tei42i - TL (Thermo Fisher Scientific, USA): this gas analyzer measures the atmospheric amount of nitrogen oxides from sub - ppb levels up to 100 ppm. Analytical principle relies on the **chemiluminescence phenomenon**, according to which a molecule typically emits electromagnetic radiation in visible or near visible field as a result of the extinction of the exceeding energy of its electrons and their return to the fundamental energetic state.

In more detail, in this case chemiluminescence consists in the emission of a characteristic IR radiation (≈ 700 nm) when electronically excited NO2 molecules, produced by exergonic gas - phase chemical reaction between nitric oxide (NO) and ozone (O_3), decay to lower energy states, according to the following reaction sequence:

$$O_3 + NO \rightarrow NO_2^* + O_2$$
$$NO_2^* \rightarrow NO_2 + h\nu$$

This instrument comprises single chamber with a flow switch, hosting a flow of both sample air, conveyed by dry air at a flow rate of about 0.6 – 0.8 LPM, and ozone, from an embedded discharge ozonator; in the reaction chamber ozone supplied quantitatively reacts with the NO in the sample to produce excited NO_2 molecules and generate the radiation emission from the chemiluminescence reaction, whose intensity is detected and measured by a single photomultiplier tube housed in a thermoelectric cooler; ultimately, intensity is correlated to the concentration of NO, as it results linearly proportional.

The instrument can be operated continuously in either the **NO or NO_x modes**, the first expressed above, since this chemiluminescent reaction - based measurement principle is able to appreciate just NO; on the other hand, NO_2 measurement is possible just after its complete conversion into NO, by sending sample air to a **molybdenum - based catalytic converter** able to promote the complete reduction of NO_2 to NO at the operating temperature of about 325 °C, before pushing the sample in the reaction chamber (NO_x mode).

By this way the global NO_x concentration can be appreciated, while NO_2 concentration is calculated as the difference between concentrations.

By continuously alternating the two instrumental configurations (via converter and not) via a mode solenoid valve routing the sample either straight to the reaction chamber (NO mode) or through the NO_2 - to - NO converter and then to the reaction chamber (NO_x mode), both measures are given,

and the difference expresses NO_2 concentration value.

Once analyzed, the exhaust is forced through an ozone converter and an active - carbon filter to remove any residue of ozone, and finally released through the vent.

Since the detector is the same, its measure needs to be accompanied by the configuration of the mode valve, to assign it either to NO or NO_x concentration.

The instrument performance is verified monthly with zero / span checks using an external zero air generator Thermo 1160 and gas dilution / GPT systems (Thermo 160i) equipped with a 5 ppm NO standard in N_2.

Lower detectable limit is about 0.05 ppb, at 60 second averaging time, while precision is +/-0.4 ppb in the 500 ppb range.

Response time is 40 seconds, operating at 10 second average time.

Reference technical standard is UNI EN 14211:2012 “Ambient air. Standard method for the measurement of the concentration of nitrogen dioxide and nitrogen monoxide by chemiluminescence”.

Sulphur Dioxide Fluorescence Analyzer Tei43i - TLE (Thermo Fisher Scientific, USA): this pulsed fluorescence gas analyzer allows to measure the amount of SO_2 in the air in the range 0.05 to 100 ppm.

The instrument operates on the principle that SO_2 molecules can absorb quantitatively opportune -wavelength ultraviolet radiation, reaching an energetic transition to an excited state, then decay to a lower energy state by emitting UV light at a higher wavelength, with an intensity that is proportional to the SO_2 concentration, according to the following scheme:

$$SO_2 + h\nu_1 \ (\lambda_1 = 214 \text{ nm}) \rightarrow SO_2^*$$

$$SO_2^* \rightarrow SO_2 + h\nu_2 \ (\lambda_2 = 330 \text{ nm})$$

The phenomenon of **fluorescence** can be described as a particular type of luminescence commonly taking place in gaseous systems in response to an excitement exerted by an electromagnetic radiation of different and well characteristic wavelength, impacting a body, in a time span of no more than 10^{-8} s after the incidence of excitement radiation.

Fluorescence radiation can be revealed by enlighting the system with opportune wavelength radiations at their highest intensity possible, and observing the response radiation by side.

Operationally, the air sample enters the instrument at the standard flow rate of about 0.5 L / min, then it flows through a "hydrocarbon kicker" specifically devised to exclude hydrocarbons from the sample by forcing their permeation outside. Following that, the sample flows into the **fluorescence chamber**, where **pulsating UV radiation** at 214 nm excites SO_2 molecules: the pulsing of the UV source lamp serves to increase the optical intensity and UV energy throughput, meaning lower detectable SO_2 concentrations; after a fraction of second, an aliquot of the population of excited molecules comes back to its fundamental energetic state, emitting a **fluorescence radiation**, whose intensity is collected by a detector located at the back of the fluorescence chamber and continuously compared to the one registered in absence of excitement radiation, to compensate for fluctuations in the UV light. Ultimately, the intensity of fluorescence radiation is converted in SO_2 concentration.

Condensing lenses are inserted to focus the pulsating UV light into the **mirror assembly**, consisting of four selective mirrors isolating only the opportune wavelengths for SO_2 molecules excitement.

It is crucial to observe that, as stated by the **Stokes law**, the wavelength of the reemitted radiation the fluorescence intensity is by far lower than the exciting radiation's one: in this instrument, this demands for a physical protection of the detector from the UV source, by interposing filters between the system under observation and the detector; additionally, a reflective bandpass filter allowing only the wavelengths emitted by the excited SO_2 molecules to reach the photomultiplier tube improves resistance to photochemical degradation of detector and an increase in selectivity in terms of wavelength isolation, thus resulting in both increased detection specificity and long term stability.

Once the sample leaves the optical chamber, it passes through a flow sensor and then flows to the pump and is exhausted out.

The instrument is equipped with an internal span source (permeation tube) and external zero source (activated charcoal filled cartridge) for daily zero / span verifications, whereas a dilution system Environics 4000 allows a multi - point calibration in the range 0.5 - 10 ppb starting from a 5 ppm SO_2 standard, to avoid any possible drifts.

Lower detectable limit is 0.17 ppb and response time 110 sec, at 60 second averaging time, while precision is 1 ppb.

Reference technical standard is UNI EN 14212:2012 "Ambient Air - Standard Method For The Measurement Of The Concentration Of Sulphur Dioxide By Ultraviolet Fluorescence".

Ozone UV - Absorption Analyzer 49*i* (Thermo Fisher Scientific, USA): this dual - cell UV photometric gas analyzer enables to measure the amount of ozone in the surface air from ppb levels up to 200 ppm.

The instrument operates according to the principle that ozone molecules absorb UV light at a wavelength of 254 nm, at a degree directly dependent on the ozone concentration.

Once the sample is drawn into the instrument, at a customizable flow rate in the range of 1 - 3 LPM, it is split into two gas streams, one flowing through an ozone scrubber to become the reference gas, the other flowing directly; two devoted solenoid valves alternate reference and sample gas streams between two cells every 10 seconds.

An UV lamp emits a radiation that is partially absorbed in presence of ozone, while light extinction is detected and measured inside a **sample cell** with a well established optical path and the value of concentration is calculated afterwards, on the basis of the **law of Lambert - Beer**, through a previous multi - point calibration:

$$\frac{I}{I_o} = e^{-KLC}$$

where:

I = UV light intensity of sample with ozone (sample gas);

I_o = UV light intensity of sample without ozone (reference gas);

K = ozone molecular absorption coefficient, 308 cm^{-1} (at 0°C and 1 atmosphere);

L = length of cell, 38 cm;

C = ozone concentration, in ppm.

UV light intensities in each cell are measured by two detectors, with a pause in measures for several seconds in correspondence to every cell switching, to allow the cells to be completely flushed, and intensity of radiation is led back to the concentration of ozone; finally, the instrument calculates the ozone concentration for each cell and outputs the average concentration.

The instrument is equipped with an internal span sure (ozonator) and external zero source (purafill filled cartridge) for daily zero / span checks; furthermore, it is calibrated every year in situ against a traveling calibrator (Thermo 49iPS), hosted at the i - AMICA Observatory in Lecce, which is compared against the standard reference SRP15 hosted at GAW WCC at EMPA.

Instrumental operational range is 50 ppb to 200 ppm, whereas lower detectable limit is about 1 ppb, so as precision; moreover, since the instrument has both sample and reference flowing at the same time, a response time of 20 seconds can be achieved, with 10 second lag time.

Reference technical norma is UNI EN 14625:2012 “Ambient Air - Standard Method For The Measurement Of The Concentration Of Ozone By Ultraviolet Photometry”.

Weather Transmitter WXT520 (Vaisala Oyj, Finland): this small and lightweight real - time instrument can measure the 6 most essential weather parameters (barometric pressure, humidity, precipitation, temperature, wind horizontal speed and direction).

Barometric pressure, temperature, and humidity measurements are combined in the **PTU module** using capacitive measurement for each parameter, while precipitation measurement is based on the **RAINCAP® sensor**, detecting the impact of individual rain drops and producing signals

proportional to the volume of the drops, in response, that can be integrated over time to totalize the accumulated rainfall, besides rain intensity and duration. Finally, wind data are made available by the ultrasounds based **WINDCAP® sensor**.

Detected parameters are reported in the scheme below.

Parameter	Range	Response time	Accuracy
Barometric pressure	600 to 1100 hPa	—	±0.5 hPa, at 0 to +30 °C
Relative humidity	0% to 100 %RH	—	±3 %, at 0% to 90% RH
Rainfall	0 to 200 mm/h	10 s	5%
Temperature	-52° C to +60° C	—	±0.3 °C, at 20° C
Wind speed	0 to 60 m / s	250 ms	±3%, at 10 m/s
Wind direction	0 to 360°	250 ms	±3°

The **WINDCAP® sensor technology** relies on measuring the time it takes ultrasounds to travel from each item of an array of three equally spaced ultrasonic transducers, on a horizontal plane, in both directions: wind speed and wind directions are determined through the evaluation of difference between forward and reverse transit times in the considered direction, directly depending on the wind speed along the sound path.

The **RAINCAP® sensor technology** relies on detecting the impact of individual raindrops by means of a precipitation sensor composed of a steel cover and a piezoelectrical sensor mounted on

its bottom surface; produced signals following each impact are proportional to the volume of the drops. Measured parameters are: accumulated rainfall, rain current and peak intensity and the duration of a rain event; furthermore, it is also possible distinguishing hails from raindrops.

In addition, PTU module contains separate sensors for pressure (**BAROCAP®** capacitive silicon sensor), temperature (**THERMOCAP®** capacitive ceramic sensor), and humidity (**HUMICAP® 180** capacitive thin film polymer sensor) measurement; for each of them, measurement principle is based on a RC oscillator and two reference capacitors against which the capacitance of the sensors is continuously measured.

The device is resistant to flooding, clogging, wetting, and evaporation losses in the rain measurement.

2.3. Time variability of atmospheric parameters

Validated particulate and gaseous / meteorological datasets were elaborated by the openair package of R open source software, as to represent distribution, annual trends, daily variability and seasonality of monitored parameters values, as well as wind roses to detect the sectors mostly responsible for pollutant provision in the measurement site.
Results are reported following.

Overview on instrumental dataset parameters

A validated dataset of 17544 records exploring 22 parameters for each hour of biennium 2015 / 2016 has been analysed; parameters are:

- Temperature (°C)
- Relative humidity (%)
- Atmospheric pressure (hPa)
- Wind speed (m s^{-1})
- Wind direction (°)
- Rain (mm)

- O_3 concentration (ppb)
- NO concentration (ppb)
- NO_2 concentration (ppb)
- SO_2 concentration (ppb)
- CO concentration (ppb)
- CO_2 concentration (ppm)
- CH_4 concentration (ppb)
- PM_{10} mass concentration (ug m^{-3})
- $PM_{2.5}$ mass concentration (ug m^{-3})
- Coarse particles (diameter >1 um) numeric concentration (n cm^{-3})
- Fine particles (diameter <1 um) numeric concentration (n cm^{-3})
- Total particles numeric concentration (n cm^{-3})
- BC mass concentration (µg m^{-3})
- Scattering coefficient at 450 nm (Mm^{-1})
- Scattering coefficient at 550 nm (Mm^{-1})
- Scattering coefficient at 700 nm (Mm^{-1})

Instrumental dataset parameters sum – up info are reported in Appendix 3.

Data analysis produced a wide set of graphs, which are extensively reported in Appendix 3 and that now will be briefly illustrated, together with main results obtained.

Summary plots shows the effective data availability, whose interruptions (red sectors) result from occasional instrument faults, together with their frequency distibution illustration.

Even if 2016 was more affected by data leakage (33,5 % of missing data, against 5% for 2015, on average), it is possible to notice a general diminution in mean temperature, passing from 18°C to 16,3°C (-9,4 %), paralleled by relative humidity (from 75,4 to 72,7, equivalent to -3,6 %).

For each year, rain occurrencies are concentrated on the semester autumn / winter; this feature doesn't impede, even if the extensive data leakage occurred on summer 2016, to consider 2015 as

more rainy than 2016, on the whole, with cumulated rain values of about 487 mm against 159 mm (+206 %).

Wind was just slighlty more intense on 2016 (4,5 ms^{-1} vs 4,1 ms^{-1}, namely -8,9 %, on average).

CO_2 average concentration values passed from 405,1 ppm to 406,6 ppm with a meaningful increment of almost 0,37 % in just one year time span; at the opposite, CO diminuished from the average value of 131,1 ppb to 127 ppb on 2016 (- 3,1 %); however, roughly 40% data leakage for both gases in 2015 must ba taken into consideration.

Average CH_4 concentration values passed from 1923,7 ppb on 2015 to 1960,9 ppb on 2016 (+ 1,9 %), while NO_2 concentration increased of approximately 70 % (from 1 to 1,7 ppb), unparalleled by NO concentration which remains almost constant in the biennium (0,1 ppb).

Average SO_2 concentration doubled on 2016, passing from 0,1 ppb to 0,2 ppb, while average O_3 concentration values decreased from 41,6 ppb to 40,9 ppb (- 1,7 %).

On average, BC concentration values diminuished on 2016 of about 25 %, passing from 0,4 μg / m^3 to 0,3 μg / m^3.

2016 is characterized by a minor impact from aerosol: total particles numeric concentration passed from 6133,4 (2015) to 2960 particles / cm^2, namely – 51,7 %; this feature is just partly explicable with the greater data leakage for this parameter on 2015 (62,3 %, against 56,9 % on 2016), spanning on the more rainy winter period.

Despite of a substantial invariance in coarse particles numerical concentration (about 1,5 / cm^3 on both years), fine particles fraction (aerodynamic diameter less than 1 μm) falls from 50,5 particles / cm^3 to 33,4 particles / cm^3, in correspondence of a 25 % lower data coverage).

$PM_{2.5}$ mass concentration remain stable on the biennium, at 9 μg / m^3, while PM_{10} decreases from 16,6 μg / m^3 (2015) to 15,1 μg / m^3 (2016).

Daily average parameters time series were calculated with the mean value, by shadening the 95 % confidence interval area.

Daily average temperature pattern in the biennium remains approximately stable: values are constant on January and February (12° C to 14 °C), starting to increase on March and reaching the

peak on August (26 °C), then decreasing until December; data leakage on 2016 doesn't allow to properly appreciate the peaking trend.

Daily average relative humidity pattern in centered in the range from 64 % to 75 %, for both years, with a more pronounced oscillation in the period march - june 2015, in repect of the same period of 2016.

Daily average atmospheric pressure shows a minimum on the period february – april on both years; data leakage on 2016 impairs any inter – year comparison in the second semester.

Daily average rain reaches two peaks on February and October 2015, with maximum daily values around 2,5 mm, while less rainy 2016 reaches just one peak around 1 mm, on October.

Daily average wind speed general pattern decreases from February to September, and increases from October to February; on absolutely terms, 2015 proved more windy than 2016, notwithstanding extensive data unavailability on 2016.

Daily average wind pattern on 2015 shows a prevalence from SSW on hot semester and from S on cold semester, even if great inter – day variability must be signalled; on 2016 this variability exasperates.

Daily average O_3 concentration values shows a common increase pattern starting on January and ending on May, then slowly decreasing up to December; on absolute terms, 2015 registered the higher O_3 concentration values, more than 50 ppb, on May, together with the lower values, less than 30 ppb, on January.

Daily average SO_2 concentration values show are sharply higher and more oscillating on 2016, with peak almost doubled in value, even if peaks locate at the same period, January and June / July.

Daily average NO concentration peak values are centered on the summer period and are slightly higher on 2015; while daily average NO_2 concentration values are maximum on July / August, however with a remarkable increase pattern on October / December period, expecially on 2015.

Daily average CO concentration values were higher on the the first quarter of year, even if data absence for 2015; as a whole, as concerns the first semester 2015, values appear higher on 2015, while during the second semester 2016 values overcome 2015 ones. A particularly strong concentration peak (almost 400 ppb) must be highlighted on January 2016.

Daily average CO_2 concentration values were higher on winter / spring semester for the prevalence of biological release as a by-product of aerobic methabolism, then declining up to August.

Daily average CH_4 concentration values remained quite steady on 2015, around 2100 ppb; on the contrary, values very highly oscillated on 2016, with relevant peaks on February, March, September, December, globally overcoming 2015 values.

Daily average PM_{10} mass concentration values were on average slightly lower on 2016, but exhibit 8 peaks overcoming 40 μg / m^3 threshold; on 2015 these value is passed just 5 times.

Daily average $PM_{2.5}$ mass concentration values were higher on 2016, globally considering; but appear much more oscillating on 2015, especially in the first semester, with 7 peaks overcoming 20 μg / m^3 threshold.

Daily average total particles numeric concentration values are clearly higher on 2015, up to 3 times more, with an increasing trend from april to may, subsequently affected by data leakage. As regards 2016, values are centered around about 4000 particles / cm^3.

Daily average fine particles numeric concentration values are generally higher on 2015, with an increasing trend from March to July; on the other hand, the absolutely most remarkable peak is signalled on late January 2016.

Daily average coarse particles numeric concentration values are centered around a baseline of about 1 particle / cm^3, peaking on the first semester; from comparison, 2015 showed an higher number of peaks on the first semester and a lower number on the final year portion.

Back carbon mass concentration values are reported on hourly basis and on daily - averaged basis: what stands out is the impulse – like nature of peaks, visible just on a hourly sampling time scale; as regards daily average values, 2015 is clearly more affected by BC - pollution phenomena, with daily peaks overcoming 1 μg / m^3 threshold on July; on the other hand, it must be specified that the same period of 2016 is not covered in the dataset.

During the observation period, daily averaged scattering coefficients values at 450, 550 and 700 nm were notably higher and more diversified on July 2015, while difference on 2016 was higher in September but on about - a - half values.

Time series of hourly and daily averaged black carbon concentration are reported on the next page;

all remaining daily averaged parameters time series graphs are reported on Appendix 3.

Time series of hourly and daily averaged black carbon concentration (µg/m^3)
(thick line: average / shaded area: 95 % confidence level)

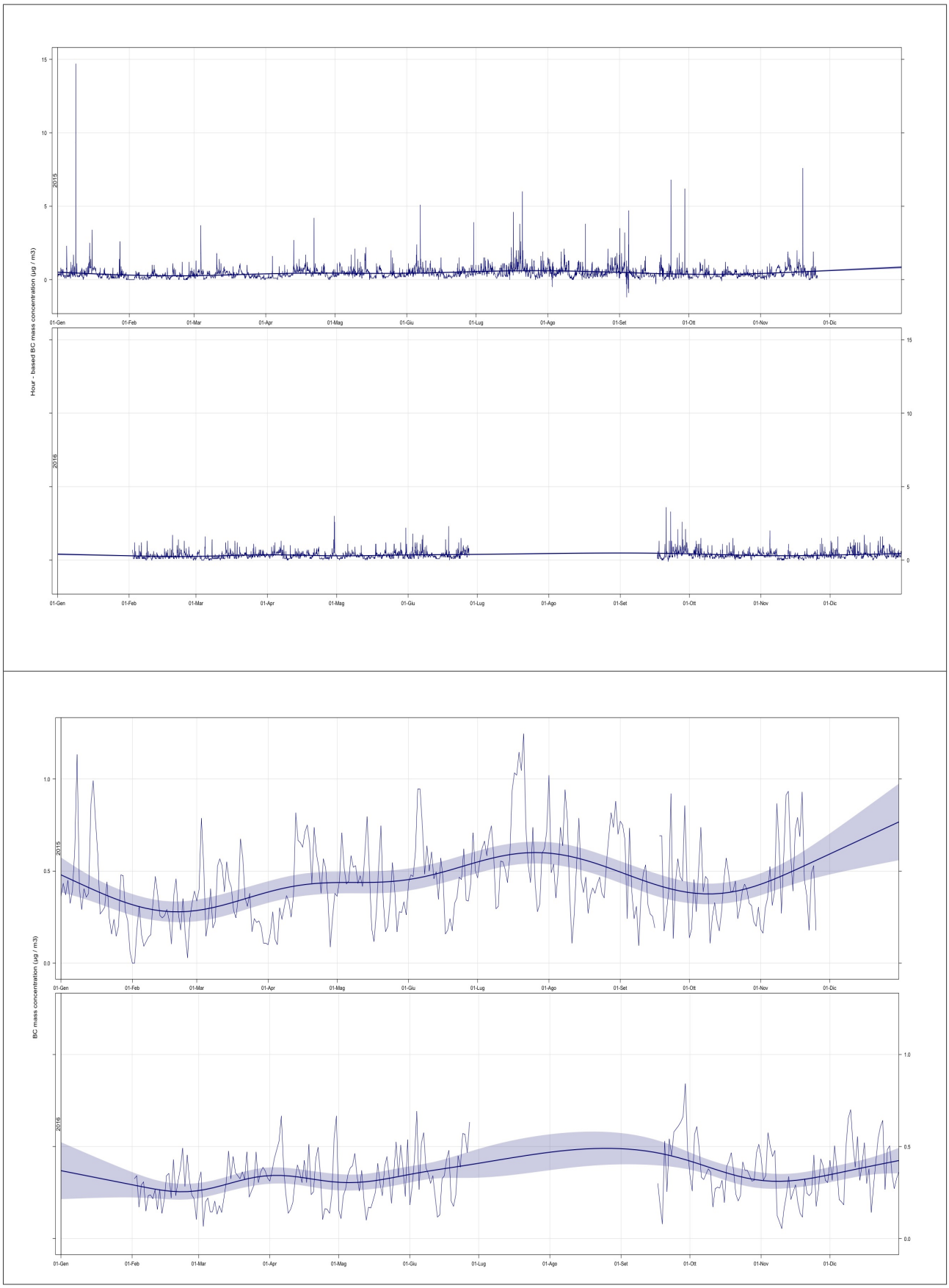

Daily and monthly average charts of the biennium period allow to compare the temporal patterns in the evolution weather parameters.

What stands out clearly is that an atmospheric pressure peak occurred on December 2015 is responsible for the absence of rain in this usually rainy month and determines a minimum in wind speed during the same period, as well as the interruption of the October – to – February rain period.

Reative humidity shows significantly higher values on 2015, with an evolution paralleling the temperature's one.

PM_{10} and $PM_{2.5}$ shows a maximum on March 2016, accompanied by a maximum in the coarse particle fraction numeric concentration but, strangely, not by a parallel peak in fine particle concentration; conversely, $PM_{2.5}$ and fine particles agree well on July 2015 peaks and on November 2016 minima.

Scattering coefficients peaks on July 2015 and minima on February 2015 and November precisely mate.

O_3 concentration values are higher on both spring 2015 and 2016, while SO_2 on March 2016, corresponding to CO concentration pattern.

During the considered period, CH_4 concentration values remain far below 2 ppm, except on September 2016, almost in conjunction with the August 2016 peak of NO and NO_2.

Finally, the absence of a correspondence in NO_x concentration patterns must be reported for July 2015.

Daily and monthly average charts are reported in Appendix 3.

Frequency distribution by wind direction ("wind rose") charts show the relative occurrence of wind phenomena from the different sectors.

In general terms, over the observational site air masses mainly coming from WNW and ESE arrive on both 2015 and 2016; this is particularly evident on the period from March to October, while the situation on December, January and February is rather fickle.

On a seasonal perspective, spring and autumn are the most windy periods, while winter and summer showe an higher occurrence of north – easternly wind, especially on 2016.

Inter – year and season – based wind rose comparison are reported on the next pages.

Inter – year wind rose comparison

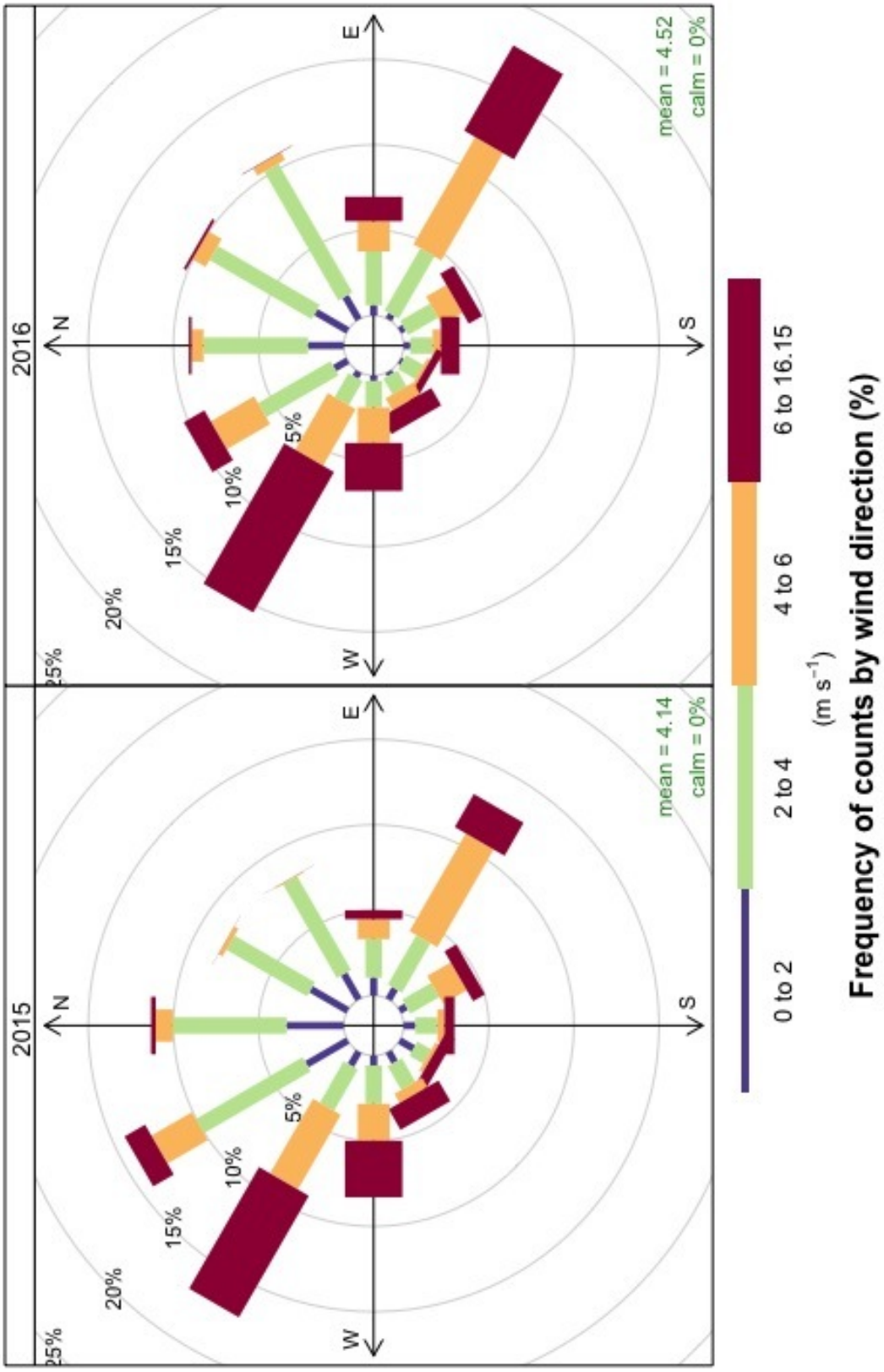

Seasonal wind direction in 2015

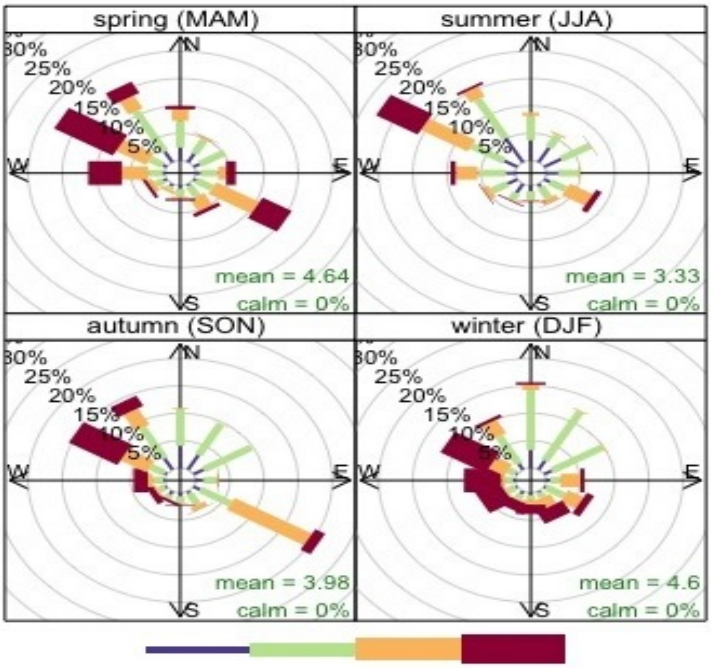

Frequency of counts by wind direction (%)

Seasonal wind direction in 2016

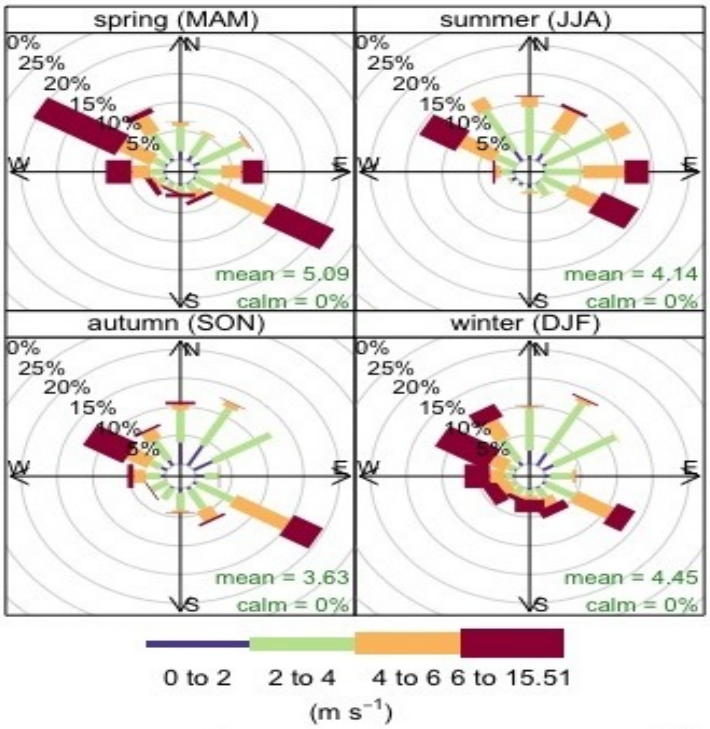

Frequency of counts by wind direction (%)

Seasonal variation of parameters v/s wind direction

Seasonal parameters variation according to wind direction distribution is a precious instrument to elucidate lower troposphere circulation pattern and, as a matter of fact, the sectors most responsible for an eventual peak detected by instrumental setting; additionally, inter – year comparison allows to throw light on yearly oscillations or events taking place in a particular moment, that the observational station is able to indirectly detect.

The great majority of parameters clearly show a maximum in correspondence to prevailing WNW and ESE spring, summer and autumn wind direction distribution.

CO makes an exception on both 2015 and 2016, as well as PM_{10} on autumn 2016 (no data on summer 2016) and $PM_{2.5}$ on autumn 2016 (no data on summer 2015).

BC clearly agrees with wind distribution, as showed by the following graph; charts of seasonal variation v/s wind direction for all remaining measured parameters are reported in Appendix 3.

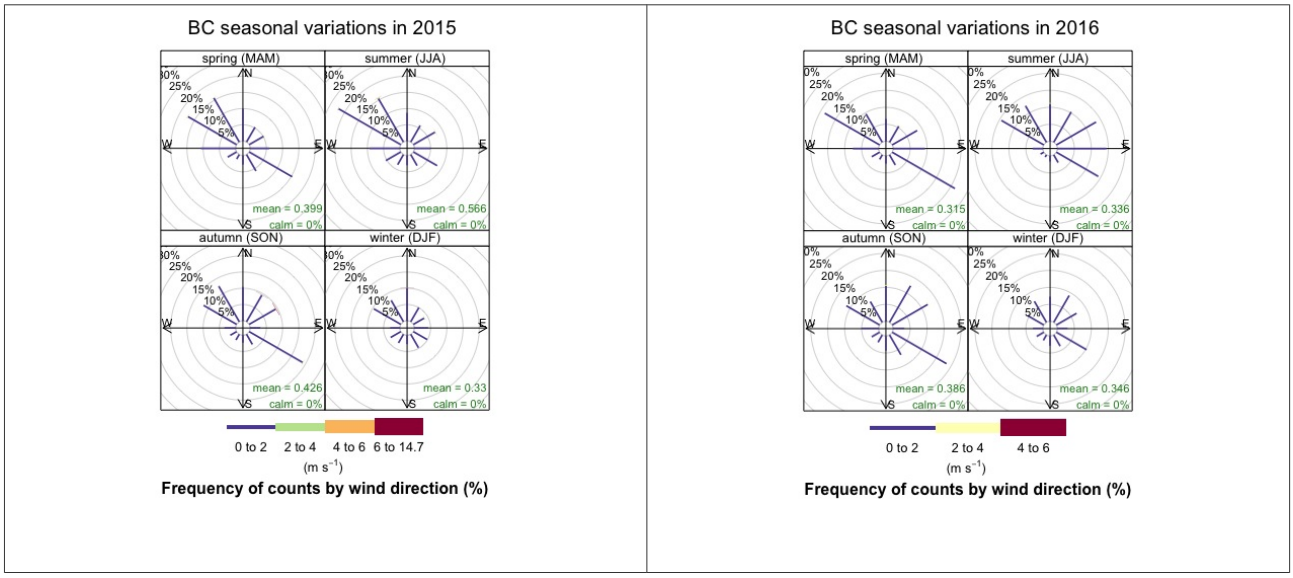

Calendar plots

Calendar plot can be considered as an ingenious expedient to have an "ensemble overview" over data time variation pattern; the adoption of a chromatic scale furtherly facilitate data interpretation, at such an extent that it needs no additionally comment.

Calendar plots for all measured parameters are reported in Appendix 3.

Yearly weekday trends

Yearly weekday trends support in detecting inter – year pattern variation in parameters trends.

Weather parameters doesn't show any unexpected behaviour, while some features in gas parameters trends can be highlighted.

Tropospheric O_3 concentration reaches a maximum on Spring at afternoon, slightly higher on 2015, and decade on the cold semester, as a result of lower sunlight irradiation.

Despite substantial numeric inter – year invariance, NO_x trend peak is at about 8 a.m. for NO and 6 a.m / 9 p.m. for NO_2 but the two years shows different trend: on 2015, while NO concentration level reaches its most during summer, NO_2 grows up during all the year, till its most on Dicember; on the contrary on 2006, NO concentration level remains higher than 0,07 ppb during spring and summer and drops just on September, whereas NO_2 peaks on August, then falls down until November. On both year it is possible to distinguish a clear reduction in NO_x concentration levels on weekends, with a decreasing gradient from saturdays to sundays.

SO_2 concentration levels are at most after 6 a.m., but, while on 2015 the peak is located on January and June, on 2016 it is centered on March; further, peak values on 2016 are roughly four times higher; week trend is increasing from monday to saturady, with a marked collapse on Sunday (-18 %, on average).

CO levels yearly peak on the starting the period January – March 2016 can't find a comparison because of missig data on the same period 2015; however on december 2015 it reaches its most, unparalleled on december 2016. On the whole, CO concentration levels are the lowest on day – light hour and the highest on the dark hours.

CO_2 concentrations remain quite stable during the week, and are lower on daylight hours and spring

/ summer semester.

CH_4 concentration values grow up during the night and are globally higher on 2016 (+ 3 % at 6 a.m.) and reach its most on September and the final part of both 2015 and 2016.

Globally speaking, PM_{10} peak values are higher on 2016 and in the first semester of both years, centering on February; as concerns daily pattern, 2015 situation is more complex to describe, with two peaks at 11 a.m. and 10 p.m., while 2016 pattern is quite smooth, peaking at 8 p.m.

$PM_{2.5}$ values are at most after 6 p.m. in both years, globally increasing on 2016. Peaks are located on the first semester on both years, even if they extend more on 2015 (from February to July).

Total particles numeric concentrations result to grow during the first sunlight hours on both yeras, but on 2016 they tend to remain on high values during afternoon, too; peaks are located on spring / summer months, but on may 2015 concentrations reach almost doubled, reaching 10000 particles / cm^3, while on 2016 the threshold of 3500 particles / cm^3 has never been overcome, on a monthly averaged basis.

The two size fractions show opposite behaviour on the considered biennium: fine particles concentrations are higher on 2015, peaking during dark hours on summer, on the contrary, coarse particles concentration reach their most on 2016, peaking on February but don’t exhibit any meaningful daily trend, so as on 2015.

Scattering coefficients daily patterns are similarly peaking on late – spring / late – summer period of both years, increasing during late afternoon and night hours.

Finally, black carbon mass concentration values are at most at 6 a.m. and 10 p.m. on both years, peaking on saturdays of July 2015 and September 2016. Globally considering, BC concentrations on 2015 are higher (+ 28 %, on average).

Yearly weekday trends for all measured parameters are reported in Appendix 3.

2.4. Chemical assay on particulate samples

In order to identify the possible influence of ship emissions and wildfire events on aerosol particles in Mediterranean Sea, chemical data from a previous aerosol chemical characterization campaign, conducted on december 2015 in the investigated area (Marinoni et al., 2016), have been reconsidered.

The sampling campaign had place within the monitoring network i – AMICA, and required the collection of particulate samples: during this, contemporary measurement of all available weather, gas and particulate concentration parameters was combined to measurements of particulate matter chemical composition of daily (0 – 24) PM_{10} and $PM_{2.5}$ samples simultaneously collected through an automated sampler SWAM 5a Dual Channel Monitor (FAI Instruments) on quartz microfiber filters (Whatman Q-grade, diameter 47 mm), pre-fired for 2 hours at 700 °C; typical uncertainty on measured daily mass concentration was 0.5-0.6 mg/m^3.

Adopted analytical methodologies were ionic chromatography (IC) for ionic fraction (Cl^-, NO_3^-, SO_4^{2-}, $C_2O_4^{2-}$, $HCOO^-$, CH_3COO^-, Ca^{2+}, Na+, NH_4^+, K^+, Mg^{2+}), thermo – optical method (TOT) (Lab OC-EC Aerosol Analyzer, FID, EUSAAR II protocol) for elementary and organic carbon fraction, ICP – MS for metal content.

As concerns IC, ions were extracted in 15 ml ultra-pure water using a micro-wave assisted extraction technique; the water-soluble ionic composition (Na+, NH_4^+, K^+, Mg^{2+}, Ca^{2+} , Cl^- , Br^- , SO_4^{2-}, PO_4^{3-} , NO_2^- , NO_3^- and several organic acids) was determined with an ICS-1100 Dionex system, using an injection volume of 25 µl in a Dionex IonPac CS12A column and a cation self-regenerating suppressor CSR-ULTRA II (2 mm) for cations; methanesulfonic acid was used as eluent at a concentration of 20 mM and a flow rate of 0.25 ml/min. For anions, an injection volume of 25 µl in a Dionex IonPac AS14A column and an anion self-regenerating suppressor ASRS-300 (4 mm) was used. Before the analysis, calibration plots were made for 24 anions and cations, using single- and multi- component standard solutions for IC.

As concerns TOT, to ensure the accuracy of OC and EC analysis, the analyser was multipoint calibrated using as external standard a sucrose solution.

Blank filters, from each measurement site, were also analysed for correcting measured concentrations.

The average contamination for OC was 2.3 µg/cm^2 (standard deviation ± 0.8 µg/cm^2), with an uncertainty variable between 5% and 6%; negligible contamination was observed for EC (< 0.1 µg/cm^2), with uncertainties variability of 20%.

Results, drawn from Marinoni et al. (2016), are reported below.

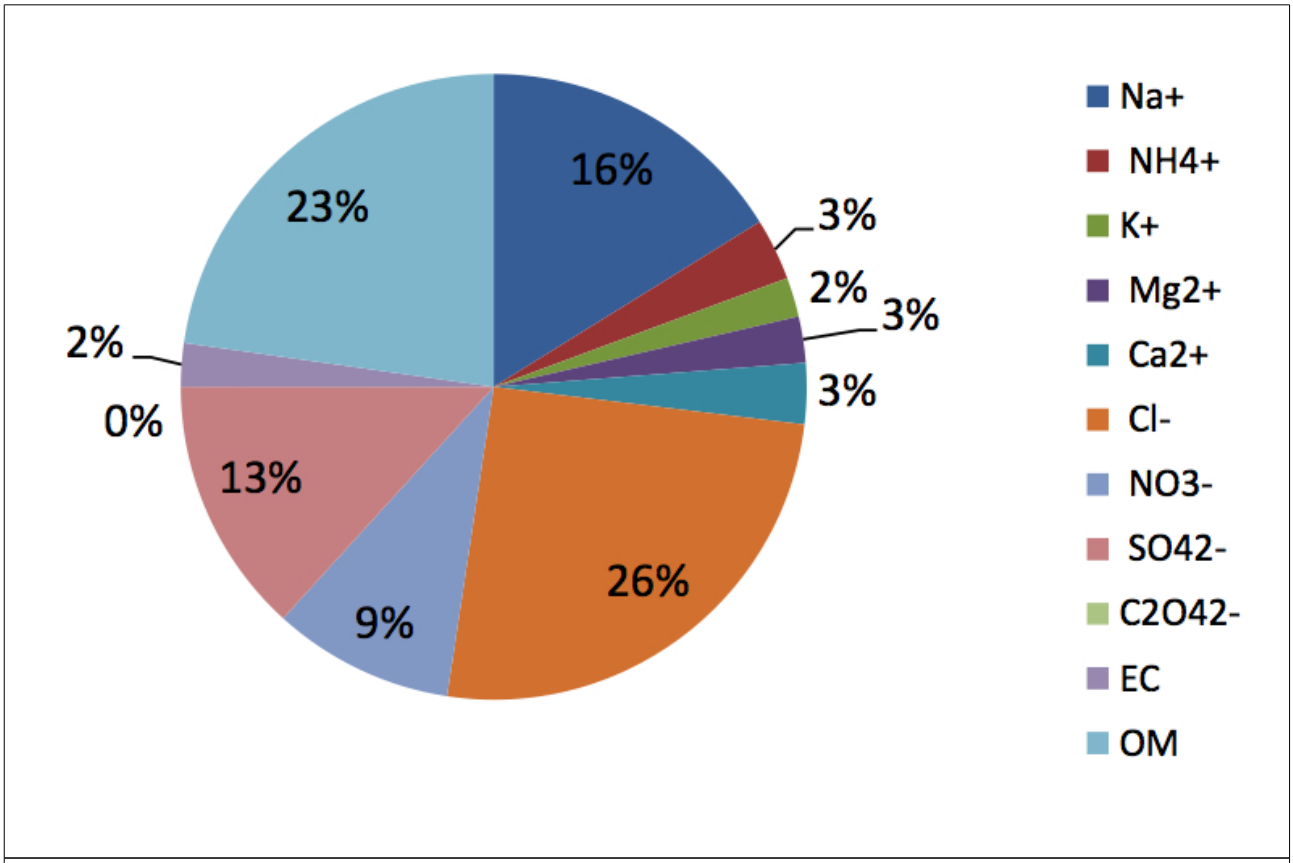

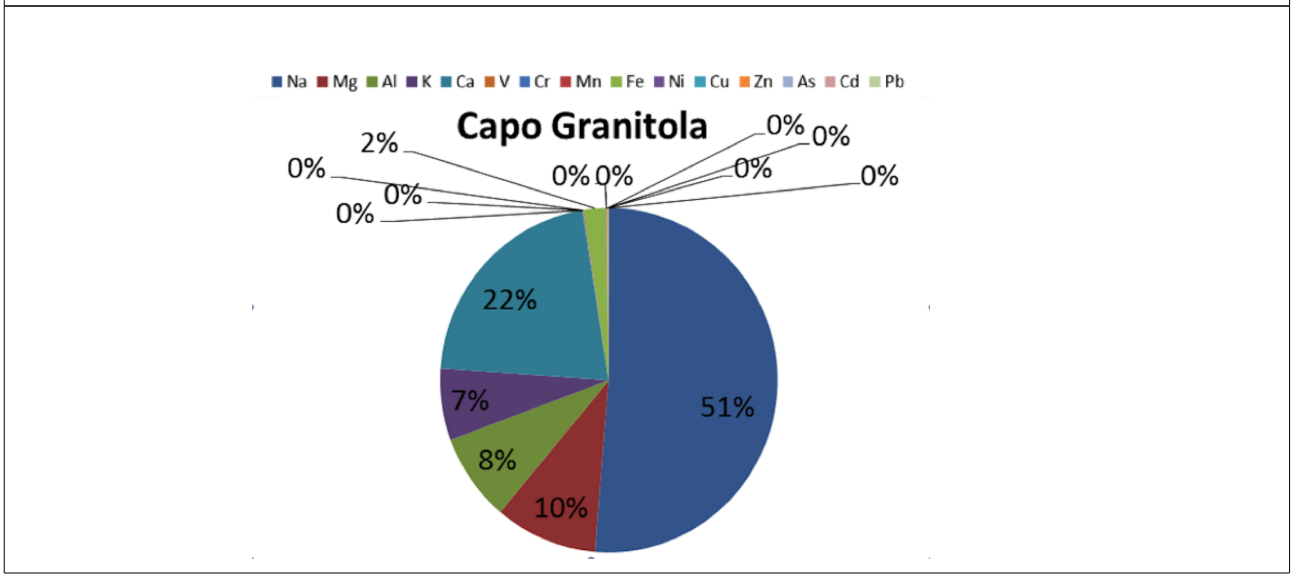

Aerosol chemical composition clearly indicated the proximity of the station site to the sea (Na^+, Mg^{2+}, Cl^- and SO_4^{2-} prevalence), but also a meaningful terrigenous contribution (Al, Ca, Fe), probably direct consequence of exposition to dust transport episodes from north Africa, as confirmed by the extremely low concentrations of Cd and Pb, contrary to what reported for European - derived air masses (Chen et al., 2008).

On the other hand, if a contribution to aerosol chemical composition from secondary aerosol sulphates from oxidation of ship - emitted SO_2 can't be excluded, however, the low concentration of Ni and V, being well - known ship aerosol markers because markers of heavy oil combustion in atmospheric particulate matter (Becagli et al., 2011), must be noticed.

This feature has to be probably linked to campaign time, whose purpose was to characterize background conditions for this station; under this respect, this observation agrees with what the following discussion will demonstrate, that no considerable BC – pollution events have been reported on December 2015.

2.5. Three-dimensional back trajectories analysis

Since particulate matter and gaseous pollutants are dispersed and transported in the atmosphere, meteorological information provides a valid support in understanding the contour conditions responsible of the detection of a punctual pollution event in a well defined instant time (Marenco et al., 2006).

Atmospheric models are extensively used to calculate and predict physical processes influencing the transport within the atmosphere; on the other, they can be adopted to elaborate the atmospheric state in a near past moment, particularly to connect a receptor, signalling pollution at present instant, to a wide range of potential past sources.

Most adopted atmospheric models can be distinguished between Eulerian ones, based on the definition of a fixed gridded system in which atmospheric properties are monitored over time, and Lagrangian ones, being centered on the behavior of a single finite element, namely "air parcel", whose position and properties are calculated over time according to the surrounding condition (wind field, random turbulence).

In this work **air mass 3D back trajectories analysis** has been carried out by **HYSPLIT (HYbrid**

Single Particle Lagrangian Integrated Trajectory) model, elaborated by Air Resources Laboratory's (ARL) of the National Oceanic and Atmospheric Administration (NOAA) for computing simple air parcel trajectories for atmosphere science applications.

This model simulates complex atmospheric transport, dispersion, chemical transformation and deposition processes regarding pollutants, hazardous materials, wildfire smoke, windblown dust, etc.

Essentially, dealing with a certain pollutant mass in a well established position in the time t, the computation of the new position at a time step (t + Δt) due to the mean advection by the wind determines the trajectory that a particle will follow.

$$\mathbf{P}_{\text{mean}}(t+\Delta t) = \mathbf{P}_{\text{mean}}(t) + \frac{1}{2}\Big[\mathbf{V}(\mathbf{P}_{\text{mean}}, t) + \mathbf{V}\Big(\Big\{\mathbf{P}_{\text{mean}}(t) + \big[\mathbf{V}(\mathbf{P}_{\text{mean}}, t)\Delta t\big]\Big\}, t+\Delta t\Big)\Big]\Delta t$$

The previous equation is the basis for the calculation of trajectories in HYSPLIT. It should be specified that only the advection component is considered when running trajectories, while the turbulent dispersion component are considered by adding a turbulent component to the mean velocity obtained from the meteorological data, after the advection computation.

Conceived in 1949 on the basis of dispersion studies, HYSPLIT has evolved to a system accounting for multiple interacting pollutants transported, dispersed, and deposited over local to global scales.

The development of HYSPLIT version 1 dates back to the early 1980s, dealing with modeling of wind shear effects on the dispersion of pollutants during long - range transport (Draxler and Taylor, 1982); nowadays HYSPLIT became one of the most extensively used models in the atmospheric sciences community (Stein et al., 2015).

An extensively adopted application of HYSPLIT is **backtrajectory analysis**, its attractive purpose being to determine the origin of air masses and likely targets for them, thus supporting in **tracking air mass history and behavior and establishing source-receptor relationships, as well as allowing airmass movement forecasting**.

The model's computational approach is a hybrid between the Lagrangian approach and the Eulerian

methodology: the dispersion of a pollutant is calculated by assuming either puff or particle dispersion: in the first approach, puffs expand until they exceed the size of the meteorological grid cell and then arise new puffs, each with its portion of pollutant mass; the second approach, instead, is centered on a fixed number of particles advection by the mean wind field and their spreading by a turbulent component.

As a matter of fact, single trajectory cannot faithfully express the turbulent mixing processes that air parcels undergoes during transport; from here follows that coupling the back-trajectory calculation with a Lagrangian dispersion component determines a more realistic depiction of the link between the concentrations at the receptor and the sources influencing it: backward-in-time advection with dispersion has been included in the HYSPLIT modeling system by simply applying the dispersion equations to the upwind trajectory calculation. In this way, the increasingly wider distribution of particles or puffs released from a receptor undergoing backward-in- time transport and dispersion represents the geographical extent and strength of potential sources influencing the location of interest.

To simplify analysis and interpretation of the depicted trajectories, grouping option applied on those sharing some space and / or time features is promising, also by considering the unavoidable uncertainty in the determination of the atmospheric transport pathways; in this work the average backtrajectory was determined, as to ease the visual evaluation of spatial proximity.

HYSPLIT trajectory and dispersion simulations can be run interactively on the web together with meteorological data, in the Real-Time Environmental Applications and Display System (READY, ready.arl.noaa.gov/), a web-based system developed by ARL and bringing together trajectory and dispersion model, graphical display programs and textual forecast programs.

In order to determine the main source regions for black carbon measured in situ, the path 6 h- and 120 h- long backtrajectories of air-masses reaching the observational station were calculated for the evaluation of ship and wildfire contribution, respectively, in consideration of the different spatial extension of available datasets: infact, the narrow extension of ship traffic dataset considered would have impeded the spatial evaluation of proximity for time points farther in time.

Backtrajectories were calculated on a 0.25° - resolution grid, ending to the measurement site, in correspondence of particularly BC - polluted days as revealed by MAAP instrument, and were computed based on the Global Data Assimilation System (GDAS) meteorological field produced by National Weather Service's National Centers for Environmental Prediction (NCEP), limiting height

to 100 m to consider only the PBL in air mass behaviour modelization and setting zoom factor to 100.

1-hour label interval graphical marks were added.

Together with backtrajectories, trajectory frequency maps have been elaborated in the area surrounding station, as to elucidate the probability of backtrajectory crossing of each cluster, and have been reported in the following ship traffic analysis.

3. INFLUENCE OF POLLUTED AIR MASSES ON THE BACKGROUND CONDITIONS OF CAPO GRANITOLA DUE TO WILDFIRES AND SHIP EMISSIONS

3.1. Capo Granitola: black carbon and carbon monoxide as tracers of wildfire events and ship traffic emissions.

The observational station of Capo Granitola has been explicitly chosen for its position particularly far away from pollution sources; notwithstanding this, local land use patterns, based on extensive agricolture, together with the widespread and well established practice of **wildfire** triggering in the surrounding area and intense **ship traffic** in the facing coastal area determine all together its particular eligibility to observational site for **long – range transport processes**, potentially responsible for air quality alteration even in this expecially unpolluted site, that must be taken into account when dealing with instrumental dataset.

After all, this situation can be exploited to try to trace these 2 classes of phenomena, not necessarily taking place closely nearby, that nowadays are considered as a primary issue for an insufficient sector legislation (CIMAC, 2012, EPA 2012; EEA, 2012a).

As further illustrated, since BC and CO are both well represented in fire and ship engine exhausts as resulting from combustion – related phenomena, in this work they have been chosen as the most indicative tracers to verify in following case studies analysis.

Fires are undoubtedly a fascinating scientific elements for its use as a tool to manipulate environment, but fire products strongly impact climate, weather, human health, visibility, ecology,, transportation by the release of energy, particulate matter (smoke aerosols) and trace gases into atmosphere (Ichoku and Kaufman, 2005; Kaufman et al., 1998).

At the global scale, the duration of annual fire season usually varies between 2 and 6 months, with July, August and September being the peak months of fire occurrence in both hemispheres, while February the minimum one; in tropical areas global patterns of fire seasonality are coupled to the seasonal cycle of precipitation, with an overall duration of the annual fire season of 2 to 6 months, highly constrained by the length of the dry season (Giglio et al., 2006).

As a matter of fact, wildfires are not started and controlled by people but have significant **economic and ecological consequences, especially in the Mediterranean region**, where they harshly

threaten its habitat integrity, agricultural practices and land management / security (San-Miguel-Ayanz et al., 2012); wildfire emissions from north America are reported to be easily transported towards the south continental european portion and the Mediterranean, during summer season (Cristofanelli et al., 2013).

Uncontrolled fires significantly affect Mediterranean since they take place in forested areas and requires drier and warmer climate compared to other parts of Europe, as those usually registered in this area during the summer (San-Miguel-Ayanz et al., 2012), leading to change in pollutant transport patterns over Europe and to a BB increase with the resulting enhanced photochemical ozone production (Cristofanelli et al., 2013).

Independently from year - to - year variability affecting global fire activity and wildfire emissions, a significant increasing trend in fire activity is evident in Europe and Africa in the last decades (San-Miguel-Ayanz et al., 2012) and the probability of a future large - fires increase is considered high (Ichoku and Kaufman, 2005); the European Commission's Joint Research Centre (JRC) estimated that more than 90 % of all fires in the Mediterranean region are actually caused by human activities (JRC, 2007).

In the mediterranean landscape, local patches of abrupt disturbance, mainly resulting from fire occurrence, are inserted into a general widespread increase in vegetation, resulting from the abandonment of rural areas and potentially capable to determine an environmental risk in terms of alterations in local fire regimes and hydrological cycle (Hill et al., 2008); on the other side, apparent increases of accidental wildfires may result from forest management practices, climate change, and the rise in human population density near fire-prone areas (Naeher et al., 2007); focusing on southern Sicily coast, lighter herbaceous vegetation (grassland / pasture) prevails, typically drying out much more quickly and being consumed by hotter flaming combustion.

Wildfires can have a pronounced effect on both local and regional **air quality for an extended period of time**: it is undisputed that wildland fires and intentional agricultural waste fires are nonpoint sources of **smoke aerosols and gases, emitting significant quantities of known health-damaging pollutants and several carcinogenic compounds (Naeher et al., 2007) (e.g. polycyclic aromatic hydrocarbons, benzene, aldehydes, respirable particulate matter, carbon monoxide, nitrogen oxides, and free radicals)**, including primary air pollutants such as particulate matter, CO and NO_X, which are globally responsible for modifying ambient atmospheric PM levels, together with the distribution of main atmospheric constituents, and for attenuating solar radiation by

scattering and absorption processes, as well as for modifying cloud microphysical properties (concentration, size spectrum, etc.) and therefore the way clouds quench solar radiation (indirect aerosol effect) (Lack et al., 2009; Crutzen and Andreae, 1990).

It has been reported that wide wildfires are responsible for the emissions of large amounts of **primary gaseous pollutants** such as greenhouse gases (CO_2, CH_4), NMVOC, NO_x and **aerosol particles** in the atmosphere (Putero et al., 2014; Urbanski et al., 2009), whereas ozone (O_3) and secondary organic aerosol can be produced in the atmosphere when some gaseous components released by fires, such as non-methane volatile organic compounds (NMVOC) and NO_X, undergo photochemical processing (Urbanski et al., 2009).

A further complication issue arises from the fact that ambient combustion particle concentrations is strongly affected by contributions from a great variety of sources: besides motorized road traffic, wood and coal burning, shipping and industrial sources must be taken into account (Janssen et al., 2011).

By this way atmospheric composition get notably modified, at such a point that Novelli et al. (2003) reports the relevance of **impact** exerted by exceptionally widespread boreal forests wildfires - related CO pulse **on variability of tropospheric carbon monoxide and ozone in the northern hemisphere**. In particular, CO exerts an influence on OH radical abundance, triggering cascading reactions involving climate altering compounds (Forster et al., 2007), while O_3 plays a crucial role in photochemical reactions, thus influencing the oxidative capacity of troposphere (Gauss et al., 2003), even if O_3 levels in BB plumes can widely oscillate during the air mass travel because of chemical and photochemical side - processes and mixing with air masses of different origin (Urbanski et al., 2009). Fire emissions can perturb CO levels over regional and global scales, disturbing oxidation / reduction chemistry in the troposphere and determining globally averaged atmospheric CO concentration reflecting annual changes in emissions from biomass burning (Novelli et al. 2003), **giving reason for the adoption of CO concentration as an indirect gaseous tracer to follow the impacts of wild land fires in time and space and for air quality monitoring** purposes in the potentially affected area investigated in the present work**.**

Besides, **wildfires acts as a climate change factor** on a global perspective (Kaufman et al., 2003), because of the significant effect of emissions on atmospheric particulate matter concentrations: in fact, despite the prevalence of coarse particles, only briefly residing in the atmosphere, the smaller particles are much more long - lived and effective in scattering solar radiation (Crutzen and

Andreae, 1990).

There is growing concern about the **potential health impacts of such events, since, even if health impacts of exposures to smoke gases and other constituents (e.g., benzene) are well characterized, fire products may be considered as a special case requiring separate health evaluation (Naeher et al., 2007)**; in addition, global effects of fires and emitted smoke aerosols and trace gases are still poorly understood (Ichoku and Kaufman, 2005).

Smoke from biomass burning contains a wide range of both solid, liquid, and gaseous constituents potentially liable to change, sometimes rapidly, with time, temperature, sunlight, and interaction with other pollutants, water vapor, and surfaces (Naeher et al., 2007), as reported in the following figure 6.

Compound	Examples[a]	Source	Notes	Mode of toxicity
Inorganic gases	*Carbon monoxide (CO)*	Incomplete combustion	Transported over distances	Asphyxiant
	Ozone (O_3)	Secondary reaction product of nitrogen dioxide and hydrocarbons	Only present downwind of fire, transported over long distances	Irritant
	Nitrogen dioxide (NO_2)	High-temperature oxidation of nitrogen in air, some contribution from fuel nitrogen	Reactive	Irritant
Hydrocarbons	Many hundreds	Incomplete combustion	Some transport—also react to form organic aerosols. Species vary with biomass and combustion conditions	
	Unsaturated: 40+, e.g., *1,3-butadiene*			Irritant, carcinogenic, mutagenic
	Saturated: 25+, e.g., n-*hexane*			Irritant, neurotoxicity
	Polycyclic aromatic (PAHs): 20+, e.g., *benzo[a] pyrene*			Mutagenic, carcinogenic
	Monoaromatics: 28+, e.g., *benzene, styrene*			Carcinogenic, mutagenic
Oxygenatated organics	Hundreds	Incomplete combustion	Some transport—also react to form organic aerosols. Species vary with biomass and combustion conditions	
	Aldehydes: 20+, e.g., *acrolein, formaldehyde*			Irritant, carcinogenic, mutagenic
	Organic alcohols and acids: 25+, e.g., *methanol* acetic acid			Irritant, teratogenic
	Phenols: 33+, e.g., *catechol, cresol (methylphenols)*			Irritant, carcinogenic, mutagenic, teratogenic
	Quinones: *hydroquinone,* fluorenone, anthraquinone			Irritant, allergenic, redox active, oxidative stress and inflammation, possibly carcinogenic
Chlorinated organics	*Methylene chloride, methyl chloride, dioxin*	Requires chlorine in the biomass		Central nervous system depressant (methylene chloride), possible carcinogens

Fig.6 - Major health-damaging pollutants from biomass combustion (from Naeher et al., 2007)

[a]Compounds in italics either are criteria air pollutants or are included on the list of hazardous air pollutants specified in Section 112 of the U.S. Clean Air Act. At least 26 hazardous air pollutants are known to be present in woodsmoke.

[b] Coarse particles are defined as those between 2.5 and 10 μm in size.

[c]Particles are created directly during the combustion process and also formed later from emitted gases through condensation and atmospheric chemical reactions.

Biomass burning (BB) represents a phenomenon associated to **human land - use activities**: in agriculture practice, BB serves a wide range of purposes, primarily clearing of forest and brush land for the control of brush, weed and litter accumulation, removal of agriculture wastes (sugar cane, rice straw, etc), forests conversion to agricultural and pastoral lands and nutrient regeneration in crop lands (Andreae, 1991; Crutzen and Andreae, 1990).

Globally, BB is responsible for an estimated annual destruction of 5500 - 9200 Tg of biomass, corresponding to about 3.1 x 10^9 t of biomass carbon (Ichoku and Kaufman, 2005); whereas it is estimated that ~ 40% of BC emissions originate from open biomass burning (CIMAC, 2012).

Open burning of forests and savannas is by far the largest global source of BC (Bond et al., 2013): 0.5 to 1.4 Pg of C are estimated to be exposed to fire, annually (Crutzen and Andreae, 1990), not taking into account the amount of BC emitted from open burning of agricultural waste.

BB constitute a **major source of trace gases and aerosol particles** (Urbanski et al., 2009; Kaufman et al., 1998): this aspect determines several implications linked to atmospheric chemistry, cloud properties, radiation budget and, ultimately, climate (Kaufman et al., 2003; Hao and Liu, 1994; Crutzen and Andreae, 1990). Additionally, forest wildfires exert a noticeable impact on variability of CO, O_3 and BC in the north hemisphere (Cristofanelli et al., 2013): estimates of emissions at the European scale are available, based on the European Union's fire database (San-Miguel-Ayanz et al., 2012).

Atmospheric compounds directly emitted by BB or produced by photochemical processes within BB plumes can travel for long distances, significantly influencing trace gases composition and aerosol properties of both PBL and free troposphere, with **regional - to global - scale effects both on air quality and climate**, strictly depending on large - scale circulation patterns (Cristofanelli et al., 2013; Crutzen and Andreae, 1990): on a **mediterranean scale perspective**, advection of air masses rich in BB products both from inland (illegal landfills fires) and from North Africa can take place and significantly influence radiative properties (in terms of scattering coefficient) and air quality over mediterranean basin, depending on weather conditions (JRC, 2007).

BB events are implicated in **regional and global climate change**, since they are among the major sources of a large variety of **climate altering species** (CO, CH_4, NO, SO_2) contributing to the greenhouse effect (Giglio et al., 2006; Simmonds et al., 2005; Andreae, 1991); additionally they accounts for the alteration of atmospheric composition as a result of the massive tropospheric emission of **atmospheric hazardous pollutants** produced from incomplete combustion of carbon

compounds and biological substances (aminoacids, proteins, etc); additionally, BB emissions contain **particulate matter (aerosol)** in the smoke, composed of organic matter, BC, inorganic substances.

At the same time, biomass consumption induces **modifications affecting nutrient biogeochemical cycles of water and nutrients (carbon, nitrogen, phosphorus) and soil structure** (Andreae, 1991), as well as **atmospheric radiation budget**, on which fire radiative energy exerts an additional energy input (Devasthale et al., 2006; Kaufman et al., 2003).

Together with naturally occurring wildfire, BB has come to be recognized as having a crucial role in numerous **ecological processes**: fires are extensively exploited as an integral part of land use in many tropical areas, too, and play also a relevant role in **tropical and sub - tropical deforestation**, naturally occurring in many temperate biomes on a periodic basis (Kaufman et al., 1998; Crutzen and Andreae, 1990).

Dealing with **fire ecology**, it is important to underline that fire represents a considerable periodic factor acting in the ecology of savannas, boreal forests and tundra: in fact, tropical savannas and brushland are burned every 1 to 4 years during the dry season, at an increasing extent due to growing population pressures and more intensive land use in the developing countries (Crutzen and Andreae, 1990).

How wildfires affect animal and plant populations is a complex ecological issue; however, it is now undisputed that inappropriate fire regimes are potentially threatening to the conservation of landscape and biodiversity, rising many troubling questions about biota ecological responses to fire regimes and limits of tolerance to the regime extremes (Whelan, 2006).

Consequently, **BB emissions need to be carefully monitored** (Wooster et al., 2003): what clearly stands out when looking at BB emission chemical composition is the **dominance of carbon oxides**, reasonable if considering that dry plant biomass consists of about 45 % carbon by weight and content of nutrient elements is lower: 0.3 % to 3.8 % nitrogen, 0.1 % to 0.9 % sulphur, 0.01 % to 0.3 % phosphorus, 0.5 % to 3.4 % potassium (Andreae, 1991).

Bond et al., 2004 reported that BC produced by boreal wildfires accounts for 10 % of the annual anthropogenic BC emissions in the northern hemisphere and, in effects, the **extensive release of BC during wildfires** deserves even more attention when considering its crucial role in triggering global warming (Putero et al., 2014): as a result, **this clearly gives support for the election of BC as an**

indirect indicator of BB events in the present work.

Over time, a consensus has been progressively realized over the role of BC as a meaningful additional air quality indicator to evaluate the health risks of air quality dominated by primary combustion particles (Janssen et al., 2011).

Identifying the causes of wildland fires is difficult, since human activities potentially arising forest fires may include direct ignition, both accidental and intentional, as well as littering of forest areas with flammable materials or the absence of proper forest management strategies, leaving forest areas uncared for and prone to fires (EEA, 2012b).

An **integrated approach** is strictly recommended to assess the contribution of wild - land fires, in which fire occurrence geo – referencing, air quality modelling and back trajectories, satellite and measurements at ground based monitoring sites and chemical analysis of particulate matter intervene (EEA, 2012b); an alternative promising approach is centered on the comparison of air pollutant concentration levels with rural and / or remote stations in non - affected areas or levels assessed in the same site during periods not affected by wildfires: under this perspective the choice of the station of Capo Granitola ensures very indicative data for wildfire impact estimation.

3.2 Satellite data for identification of transboundary fires – MODIS satellite dataset

A valuable option for wildfire tracing is given by **exploration of satellite data** for the analysis of possible plume trajectories using model calculations in terms of back - trajectories and description of the development of plumes from suspected source areas **to demonstrate the relationship between potentially high levels of BC and / or CO and a wildfire event**.

Interest in **monitoring fires and smoke and assessing BB by remote** naturally derives from the awareness that this investigation approach may empower a deeper knowledge of BB effects on health and environment starting from the compilation of an accurate **quantitative inventory of the fire locations, magnitudes, frequencies, amount of biomass consumed and gaseous / particulate / energy released.**

Such an approach led to the inclusion of two fire channels in the **Moderate Resolution Imaging Spectroradiometer (MODIS)** sensor, launched on the National Aeronautics and Space Administration (NASA) aboard its polar orbiting satellites (Earth Observation Systems, EOS) Terra

(december 1999) and Acqua (may 2002), with globally four equator daily crossing times around 10:30 am / pm and 1:30 am / pm (Cristofanelli et al., 2013; Kaufman et al., 2003; Kaufman et al., 1998). The MODIS instrument is operating on both the Terra and Aqua spacecraft: the first MODIS instrument, with a 10:30 a.m. equatorial crossing time, was launched aboard Terra platform in 1999, while in 2002 the second MODIS instrument, with a 1:30 p.m. equatorial crossing time, was launched aboard the Aqua platform. Both Terra and Aqua sweep the entire Earth's surface every 1 to 2 days, acquiring data with a field of view of 110° and a viewing swath width of 2,330 km.

Terra MODIS instrument acquires data twice daily (10:30 AM and PM), similarly to Aqua MODIS instrument (1:30 PM and AM).

Its detectors measure 36 spectral bands between 0.405 and 14.385 μm, and it acquires data at three spatial resolutions: 250 m (bands 1-2), 500 m (bands 3-7), 1000 m (bands 8-36), respectively.

Notably, the twin-MODIS design was specifically tailored to optimize cloud-free imaging while minimizing the optical effects of shadows and glare occurring with morning and afternoon sunlight.

MODIS sensor is endowed with 36 spectral channels with bands ranging in wavelengths from 0.4 μm to 14.4 μm for a wide array of land, ocean atmospheric characterization and studies, as reported in the Appendix 4.

Data products derived from MODIS observations describe features of the land, oceans and the atmosphere that can be used as a starting point for studies of processes and trends on local to global scales; **MODIS data products** preciously support the understanding of global environmental processes and dynamics occurring on the land, in the oceans, and in the lower atmosphere (see Appendix 4).

MODIS is capable of distinguishing different fire intensities based on brightness temperature differences, on the condition comparisons with ground - based observations are conducted (Kaufman et al., 2003). It stands out in supporting fire science because of its unique ability to use the **thermal signature** to discriminate the fire signal from the background signal, thus detecting **fires and fire - related phenomena, smoke and burn scars** and monitoring their spatial and temporal distribution in different ecosystems, as well as their derivative **products**.

This capability is mainly due to its devoted spectral fire detection channels for global fire monitoring with 1 km spatial resolution at about 4 micron (bands 21 and 22, with saturation temperature of 500 K ad 335 K, respectively, being the second one less affected by noise) and 11

micron (with saturation temperature of 400 K). Since these saturation brightness temperature are rarely reachable, MODIS data are used to **monitor in near real time active fires, burn scars and ancillary data, like vegetation type and condition, water vapor and clouds coverage**, and therefore for regional monitoring the occurrence of fire activity and emissions spreading, even in combination to other observing tools.

For this thesis' purposes MODIS land products named "**Thermal Anomalies - Active Fires**" were exploited, **available at the website** https://lpdaac.usgs.gov.

MODIS Thermal Anomalies / Fire products are derived from MODIS 4 μm and 11 μm radiances, with a **fire detection strategy based on absolute detection of a fire when its intensity is enough to detect, and on detection relative to its background otherwise, to account for variability of surface temperature and reflection by sunlight**; this product distinguishes between fire, no fire and no observation.

Since MODIS data on Terra and Aqua are acquired from each platform twice daily at mid-latitudes, four daily MODIS fire observations are typically acquired for global monitoring of active fire processes and their effects on ecosystems, the atmosphere, and climate.

The **active fire product** (see Appendix 4) is released on the so - called **MODIS Climate Modeling Grid (CMG)**, providing useful information about spatial and temporal dynamics of global fire activity distribution within different land coverage types in a summarized way on a daily, weekly and monthly period over the entire globe on a grid of 1° spatial resolution and at 10 km resolution: fire occurrence and location, rate of thermal energy emission, rate of biomass burning, rough estimate of smoldering - to - flaming ratio; by this way, the incorporation of MODIS active fire data into global emissions and chemical transport models is facilitated (Giglio et al., 2006; Justice et al., 2002).

This work was conducted on the MODIS fire product named "**Thermal Anomalies & Fire Daily L3 Global 1km Level 3 Daily**" (MOD14A2 and MYD14A2), whose version 6 is an 8 - day composite product including 8 separate days of data detailing pixels in terms of fire detection, that are located in each 1 kilometer grid cell over the 8-day period, with a temporal extent July 2002 – present. Data files (format .hdf) of this product are produced on a sinusoidal coordinate system at 1-kilometer resolution as a gridded level-3 fire-mask (8-bit integer data type) product in the 8-day period, expressing confidence of fire on a scale ranging 1 to 9. Each dataset has an areal extension of 10° x 10° and is composed of 1200 x 1200 rows / columns, equivalent to a 1200 km x 1200 km

grid (pixel size = 1000 m). This information is highly helpful in monitoring the spatial and temporal distribution of fires in different ecosystems, detecting changes in fire distribution and identifying new fire frontiers, wild fires, and changes in the frequency of the fires or their relative strength. Files .hdf were visualized, merged and processed through the software Panoply netCDF, HDF and GRIB Data Viewer.

In the present work the fire area information was overlapped with land cover information, expressing the physical material at the surface of the earth. Under this respect, the most detailed and up-to-date global land cover map for the period of interest is the one produced by the European Space Agency for the year 2015: this 300-m annual global land cover categorical raster map was released by Land Cover CCI Project promoted in the framework of the Climate Change Inititiave (CCI) funded by ESA (http://maps.elie.ucl.ac.be/CCI/viewer), on the basis of reprocessing and interpretation of 5 different satellite missions providing daily observation of the Earth (NOAA-AVHRR HRPT, SPOT-Vegetation, ENVISAT-MERIS FR and RR, ENVISAT-ASAR, and PROBA-V). Land cover is divided into 22 land cover classes, based on the UN Land Cover Classification System, as reported in Appendix 4.

3.3 Overview on mediterranean marine transport pollution – related critical issues

Marine transport sector is a keystone component of european economy, especially when taking into account goods transport: in 2010 shipping sector was responsible for the movement of some 1400 billion tones - kilometers in the EU-27 and of a significant boost to socioeconomic development, giving a precious contribution to worldwide seaborne trade, where an unrestrainable growth in the volume of merchandise is confirmed and global seaborne shipments have doubled from 1978 to 2010 and increased by 3.4 % in 2014 (Merico et al., 2016; UNCTAD, 2015; EEA, 2013).

Data provided by italian Dipartimento della Protezione Civile clearly report that, on a daily basis, 1200 ferries, 1500 cargoes and 2000 commercial crafts cross Mediterranean; among them 300 tankers are included, representing 30 % of global world seaborne traffic and 20% of oil traffic, equivalent to 8 millions barrel of oil, daily (CNR - ISAC / IAMC, 2016).

On the other hand, this activity represents an **environmental burden**, significantly contributing to air pollution and climate change, besides acidification and eutrophication of water and soil in

coastal regions, and being responsible for local air quality deterioration in Europe because of its **strong dependence on fossil fuel combustion** (Becagli et al., 2011) and the present absence of a specific binding regulation: in particular, emissions of particulate matter, air pollutants (sulphur and nitrogen compounds) and GHGs (CO_2, CO) from maritime transport in European waters account for a significant portion of worldwide ship emissions, up to 20 % (EEA, 2013).

Demand for seaborne transport services and trade volumes continue to be shaped by global economic growth and keep rather **unresponsive to air quality issues** (UNCTAD, 2015); it derives that ship emissions are expected to increase in the next years in response to the expansion of the international trade (Merico et al., 2016). **Shipping emissions** are not quantified in detail, yet, and **remain one of the last regulated anthropogenic source**, and international and european air quality and climate policymaking appear, under this respect, very urgent, in the wake of the European case (EEA, 2013; EEA, 2012a; Becagli et al., 2011), at such a point that there are several areas in Europe where the contribution of shipping reaches 80 % for NO_X and SO_2 concentrations (EEA, 2013).

Both composition of gaseous pollutants and particles size are different in emissions referred to different shipping phases (sailing on open sea, manoeuvring in ports, hotelling) (Merico et al., 2016); emissions quantities from ships depend primarily on the **quantity and quality of the fuel consumed** as well as the **engine type**, and the need for reliable information on the consumption and combustion of bunker fuel is essential to estimate resulting emission of air pollutants, besides to keep operating costs under control, since fuel cost accounts for up to 50 % of total shipment costs (Di Natale and Carotenuto, 2015; EEA, 2013). Secondly, **rate of fuel consumption per distance** also affects emission levels: it is ship - specific, as it depends on a variety of factors such as the condition of the engine and the shape and roughness of the hull. Thirdly, the **type and specifications of the engines** also are able to influence fuel consumption, having repercussions on gaseous and particulate emission levels.

Ship movement is mainly driven through the combustion of fossil fuels, commonly referred to as **marine bunker fuel oil**: in this term are encompassed marine heavy fuel oil (HFO), marine diesel oil (MDO), marine gasoline oil (MGO) and liquefied natural gas (LNG); international shipping exploit mainly HFO (87 %) and MGO / MDO (13 %), while in domestic shipping MGO / MDO prevail (60 %), followed by HFO (31 %) (EEA, 2013). Fuel quality and potential environmental impact are dependent on the refinery process: for this reason international fuel standards are needed, like ISO 8217:2012, defining fuel requirements to ensure safe application of fuels in ship engines (EEA, 2013).

Often marine vessels use bunker fuels with high sulphur content, thus heightening SO_X and PM emissions from shipping: under this respect, it's meaningful that the sulphur content of standard marine fuel (heavy fuel oil) is currently 2 700 times higher than that of conventional diesel for cars. The **impact of gases and particles emitted by ship** is consistently exerted on human health (Merico et al., 2016; Corbett et al., 2007), acidification and eutrofization of water and soil in coastal regions due to deposition of sulphur and nitrogen compounds (Derwent at al., 2005) and on regional - scale climate change triggering through sulphur containing particles (Devasthale et al., 2006), greenhouse gases (IPCC, 2014) and absorbing black carbon aerosols (Lack et al., 2009).

Maritime emissions in Europe increased constantly during the period 1995–2010 due to the rise in transport demand. Even if shipping km activity is currently forecast to grow by almost 90 % by 2050, emissions from ships are expected to decrease in future years as a result of improved fuel quality and improved engine technology, driven by various sector policies (EEA, 2012a); in particular, while SO_2 and $PM_{2.5}$ emissions are expected to diminish from 2020 onwards due to legislation on fuel sulphur content, nitrogen oxides release is projected to increase to the point that they will reach land - based emissions in 2020; several european hotspot areas register a contribution up to 80 % for NO_x and SO_2 levels and 25 % for $PM_{2.5}$ (EEA, 2013).

It was estimated that **nearly 70 % of ship emissions occur within 400 km from land**, while harbour logistics has a relevant role in determining the total impact from shipping on coastal areas air quality, too; the **main pollutants emitted by ships** are NO_X, SO_2 and PM, whose global emissions are 5 - 7, 4.7 - 6.5 and 1.2 - 1.6 Tg / year, respectively, whereas about 3.3 % of global CO_2 emissions and 2 % of global BC emissions are produced by shipping (Merico et al., 2016). In EEA member countries in 2010 ships were globally responsible for around 21 % of SO_2, 19 % of NO_X, 3 % of VOC, 8 % of PM_{10}, 12 % of $PM_{2.5}$ and 2 % of CO international and national emissions: in terms of the shipping sector's performance when compared to other transport modes, **shipping is responsible for the majority of SO_2 emissions, and it also contributes considerably to NO_X and PM emissions**; furtherly, an **impact on global and regional radiative forcing** is undisputed (EEA, 2013; EEA, 2012a).

Contribution of maritime transport sector emissions to atmospheric concentrations of gaseous pollutants (NO, NO_2, SO_2, and O_3) and of particles especially represents a growing concern in **coastal areas**, since they are considered a significant source of air pollution and are particularly vulnerable to ship - related pollution.

Ports and marine vessels are a large source of black carbon (Johnson et al., 2016), whose emissions from ships are of global interest and, widening the view, nowadays the demand for considering the impact of BC emissions from international shipping is gaining strength; notwithstanding this, **BC emission factors** [EFs = g(BC) / Kg(fuel)] for marine engines and fuels are uncertain because of the challenges of measuring BC emissions using a number of measurement approaches and different analytical techniques.

Large diesel engines emit black carbon and aerosols into the atmosphere; under this respect, as reported by the International Council on Combustion Engines (CIMAC) in its report on BC emissions from large marine engines issued in 2012 to evaluate measurement methods, emissions factors and abatement strategies, measurements of ship-related BC emission factors range from 0.1 to 1 g/kg fuel, whereas the contribution of shipping to global BC emissions was estimated well below 1% (CIMAC, 2012).

With the aim to fill this knowledge gap, a comprehensive study to characterize BC emissions from marine engines on test bench conditions and actual ocean-going-vessel (OGV) conditions was undertaken by the International Council on Clean Transportation (ICCT), with the aim to delucidate the impacts of variability in engine operating conditions, marine fuel choice and vessel operations (e.g., vessel speed reduction) on BC EFs and to consider the existing marine BC mitigation strategies including slow-steaming, fuel switching, and scrubbers (Johnson et al., 2016): what was highlighted by this BC marine transportation sector - related emission research is that BC emissions tend to decrease as engine load increases, according to the improved combustion efficiency occurring at higher loads, while the introduction of a scrubber system (exhausted gas cleaning system, EGCS) reduces BC emissions on the order of 30 %; as such, this research has implications for marine BC measurement approaches, emissions inventories, and reduction options, too.

In more details, research informed an updated global marine BC emissions inventory and a database of effective BC emissions reduction technologies and strategies, at the same time showing BC EFs as being a function of (respectively in order of significance):

1) engine cruise speed, with the slow speed two-stroke engines used for the largest oceangoing vessels having lower BC emission factors than medium- and high-speed four-stroke diesel engines, on a mass per unit distance basis, so that to point out that slow-steaming practice / vessel speed reduction (VSR) may profitably reduce BC emissions compared to higher speed operations. Noteworthly, it was discovered that intermediate speeds are just associated with

higher emissions, this clearly implies a demand for engine calibration to abate emissions under typical navigation operations;

2) engine load, with an inverse correlation holding between engine load and BC EFs for larger engines and the reverse relationship for smaller ones;

3) engine displacement, in the terms of an inverse correlation in respect of relative BC emissions, reported across a variety of diesel engine types;

4) engine Tier, suggesting that modern marine engines, endowed with electronic controls and in-cylinder approaches according to control strategies to reduce NOx emissions, may have BC cobenefits, in terms of lower BC emission factors;

5) the adoption of the latest generation of emission control strategies on BC and other emissions: in the direction to evaluate the impacts from the installation of an Exhaust Gas Control System (EGCS) scrubber on an OGV to meet sulphur fuel standards and limits, it was noted this device may contemporarily ensure BC benefits, being capable of promoting ~30% reduction in BC emissions; on the other hands, the drawback not to promote the control of sulphur particles emission stands still;

6) fuel type, where distillate fuels exhibited the lowest BC EFs, thus appearing as the most promising for BC emission shrinkening, followed by conventional high sulphur HFO; on the opposite, desulphurized residual fuels, despite being capable of meeting existing sulphur requirements, produced higher BC emissions; such a point raises concerns about the potential impact of IMO's tightened global sulphur limit of 0.5% for marine fuels in 2020 on BC emissions if pursued mainly through fuel blending.

Many possible black carbon abatement measures have been proposed in various documents to be applied on diesel engines: improvement of the combustion process in terms of thermal efficiency and reduction unburned compounds formation, switch to low sulphur fuel and distillate fuel (LFO), fuel injection valve restyle to prevent fuel oil from evaporating uncontrolled into the combustion chamber and subsequently "escaping" unburned to the exhaust resulting in BC emissions, Exhaust Gas Recirculation (EGR), Diesel Particulate Filter (DPF), De - SOx systems / Scrubbers, not always resulting in reduced BC emissions (CIMAC, 2012).

Central Mediterranean basin can be rightfully considered a hotspot for the impact of ship emission on air chemistry (EEA, 2013); tightening the view to Sicily channel, what stands out clearly is that

it hosts an intense ship traffic (Becagli et al., 2011), especially in oil transport and fishery sectors; the intense impact exerted by these activities deeply influences many processes, such as acidification and eutrofization of water and soil in coastal regions, linked to deposition of sulphur and nitrogen compounds (as reported by IPCC, 2014 and Derwent et al., 2005), and climate change.

High SO_2 emissions currently occur from shipping: the international maritime sector has been estimated to be responsible for 87 % of all SO_X emitted by the transport sector in 2010; additionally, with the present SO_2 and NO_X emissions declining trends from other sectors, shipping will make a larger relative contribution to secondary inorganic aerosols in Europe (EEA, 2012a).

In consideration of the necessity to preserve the relevant and economically valuable local fish stocks, mediterranean air quality and atmospheric composition vulnerability to ship emissions, **international mitigation strategies** to reduce ship emissions have been conceived, but they did not reveal productive till now; in this direction, the **Council directive 1999/30/EC of the European Union** introduces an implicit regulation in the sulphur content of liquid fuels that limits the maximum sulphur content of marine fuels.

Noteworthly, emissions from diesel engines show a high proportion of CO to cooling co-pollutants, whereas emissions from wildfires and open-burning of biomass contain a more balanced ratio (source: Climate and Clean Air Coalition, http://www.ccacoalition.org/en/slcps/black-carbon)

Widening the view, BC is a portion of PM, whose contribution from marine transport to local concentrations has been estimated up to 30 %, particularly for ultrafine size portion which is predominant in anthropogenic emissions (EEA, 2013; Marenco et al., 2006) and in shipping emissions in particular.

Diesel particulate matter emissions are a major source of BC, that is released by ships as a result of the incomplete combustion of diesel fuel; this situation is particularly harsh if considering that no rigorous sector legislation has been issued at present to disciplinate BC ship emissions (EEA, 2013); nowadays, the International Maritime Organization (IMO) regulates emissions from ships with international marine environmental convention MARPOL Annex VI, setting limits on NO_x and SO_x emissions and promoting special SO_x Emission Control Areas (ECA, in Europe being the Baltic Sea, the North Sea and the English Channel), with stricter emission limits. Under this respect, in July 2011 a new chapter to Annex VI was added on Regulations on energy efficiency for ships, with the aim to reduce air pollutants emission through reducing fuel consumption.

Present – day studies on ship aerosol contributions are so far based on maritime emissions inventories and atmospheric-chemistry-models based analyses, concurring in reporting a meaningful and potentially increasing contribution to Mediterranean air pollution from the shipping sector.

Automatic Information System (AIS) provides univoque information about identity, tipology, position, speed and course of in - transit ships for vessel traffic services and allowing maritime authorities to track and monitor vessels movement.

In the framework of Marine Strategy collaboration, a daily – based AIS ship traffic register was aquired by Capitaneria di Porto in the area of Sicily straits, roughly falling into the coordinate system ranging from 37 N to 38.5 N and from 11.5 to 13.5 W; ship traffic daily subdataset were 1 – minuted based, but were integrated on a 10 – minute basis to ease data visualization and processing.

In correspondence of the considered events (BC peak days), minimum distances of on – going ships were elaborated for each our, with respect to the 6-h atmospheric backtrajectory ending to the observational station at the peak hour; every ship was identified by its AIS code by feedback on marinetraffic.com and vesselfinder.com websites.

4. CHARACTERIZATION OF BLACK CARBON POLLUTION EVENTS

4.1. Identification and characterization of black carbon pollution events

For the specific purpose of investigating the occurrence of BC pollution events at Capo Granitola station, **the days characterized by the presence of a significant BC increase with respect to the typical seasonal cycle - dependent background condition were selected on the basis of comparison between triply smoothed 21-day running mobile averages applied on daily average BC values and daily average BC values themselves**, by selecting the days with values beyond the 75th centile of the positively anomalous days distribution

By this way, synoptic time scale (few days) oscillations in BC concentrations were excluded from analysis; the result of such an approach was that one to neglect sudden steep peak days in BC if too restricted in time, and to shed light on events characterized by relatively modest peaks in BC, but sufficiently extended in time, on the contrary.

64 days were identified as affected by remarkable BC pollution (see the following figure), corresponding to 9,0 % of the entire dataset, with mean daily values increasing by 125 to 275 % with respect to the biennium – based one (0,4 μg / m^3), on average.

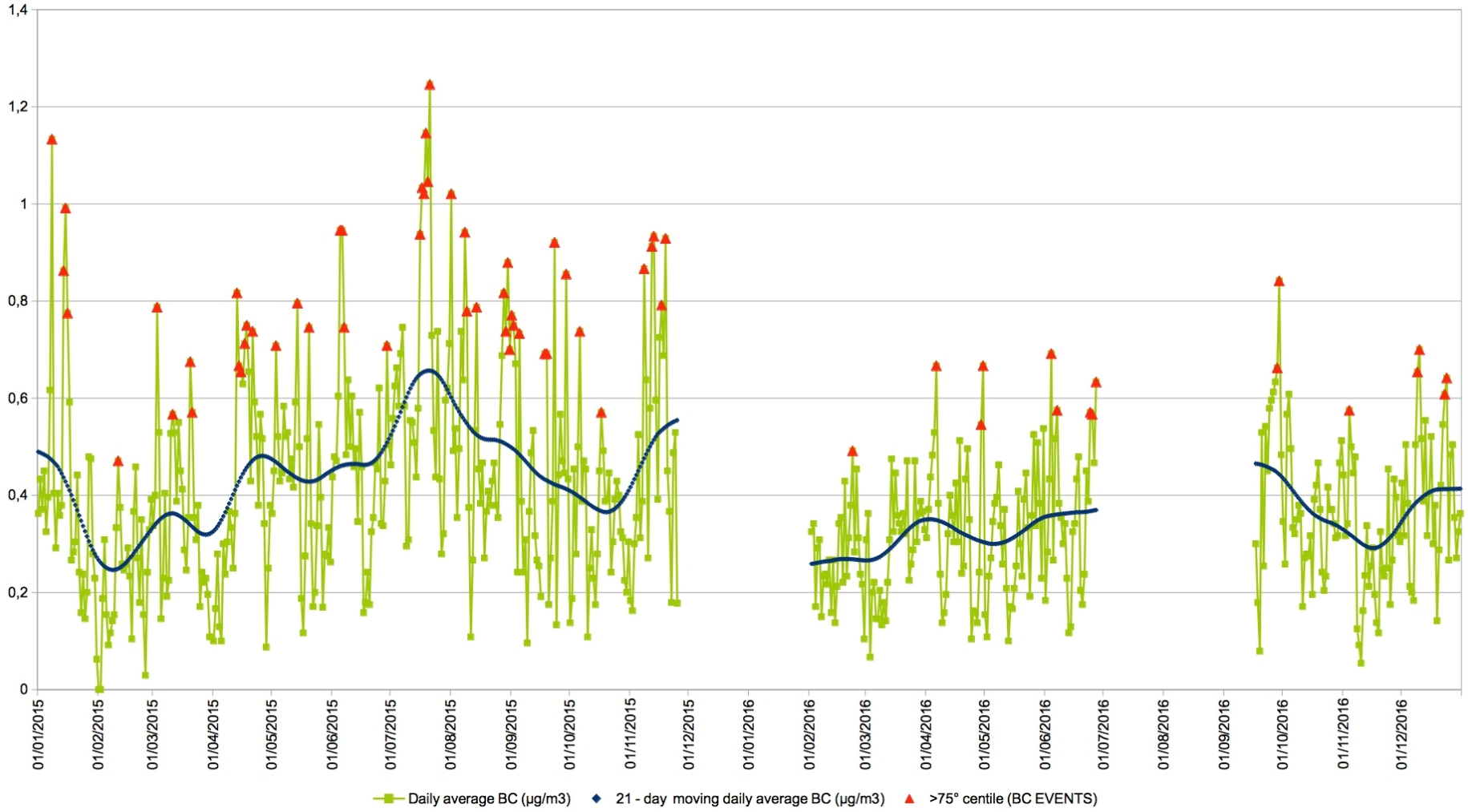
1,4
1,2
1
0,8
0,6
0,4
0,2
0
01/01/2015
01/02/2015
01/03/2015
01/04/2015
01/05/2015
01/06/2015
01/07/2015
01/08/2015
01/09/2015
01/10/2015
01/11/2015
01/12/2015
01/01/2016
01/02/2016
01/03/2016
01/04/2016
01/05/2016
01/06/2016
01/07/2016
01/08/2016
01/09/2016
01/10/2016
01/11/2016
01/12/2016
Daily average BC (µg/m3)
21 - day moving daily average BC (µg/m3)
>75° centile (BC EVENTS)

Days were grouped together into **BC – pollution events** on the basis of their temporal distance: contiguous polluted days have been considered as belonging to a single event every time their distance between contiguous events has been up to 2 days.

Seasonal distribution of BC – pollution days resulted to be concentrated in spring and late – summer season, as represented in the following chart.

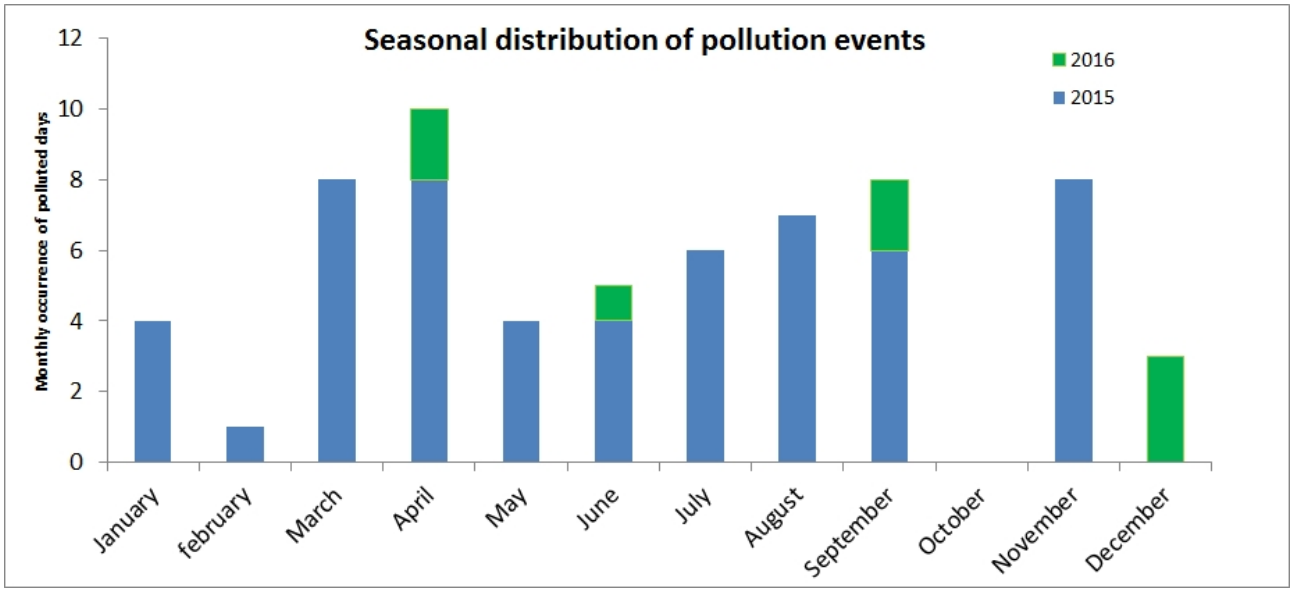

Dealing with a comparison based on triply iterated average values, a following visual verification of time series allowed to refine events time extremes and to highlight **35 BC – pollution events on a biennium basis**, distributed on overall 60 days, 45 in 2015 and 15 in 2016, with length ranging from 1 to 9 days, as represented in the following table.

In the following table the events are classified, indicating starting date and length of the event (in days) besides the related BC average concentration in µg / m^3. The figure in the next page shows the temporal localization of every event highlighted in pink boxes.

EVENT	STARTING EVENT DAY	EVENT LENGTH (DAYS)	EVENT – RELATED BC AVERAGE (µg / m^3)
01	08/01/2015	1	**1,1**
02	14/01/2015	2	**0,9**
03	11/02/2015	1	**0,5**
04	03/03/2015	1	**0,8**
05	11/03/2015	1	**0,6**
06	20/03/2015	1	**0,6**
07	13/04/2015	9	**0,7**
08	03/05/2015	1	**0,7**
09	14/05/2015	1	**0,8**
10	20/05/2015	1	**0,7**
11	05/06/2015	2	**0,9**
12	29/06/2015	1	**0,7**
13	17/07/2015	5	**1,1**
14	01/08/2015	1	**1,0**
15	08/08/2015	2	**0,9**
16	14/08/2015	1	**0,8**
17	01/09/2015	5	**0,7**
18	19/09/2015	1	**0,7**
19	23/09/2015	1	**0,9**
20	29/09/2015	1	**0,9**
21	06/10/2015	1	**0,7**
22	17/10/2015	1	**0,6**
23	08/11/2015	1	**0,9**
24	12/11/2015	2	**0,9**
25	19/11/2015	1	**0,8**
26	23/02/2016	1	**0,5**
27	06/04/2016	1	**0,7**
28	30/04/2016	1	**0,6**
29	04/06/2016	1	**0,7**
30	07/06/2016	1	**0,6**
31	24/06/2016	3	**0,6**
32	28/09/2016	2	**0,8**
33	04/11/2016	1	**0,6**
34	09/12/2016	2	**0,7**
35	23/12/2016	2	**0,6**

BC hourly mass concentration (µg/m3)
2015
2016
01-Gen
01-Feb
01-Mar
01-Apr
01-Mag
01-Giu
01-Lug
01-Ago
01-Set
01-Ott
01-Nov
01-Dic
0
5
10
15

BC pollution events are concentrated on 2015 (25 out of 35, corresponding to 71,4 %), probably as a result of data leakage affecting BC dataset on 2016, too.

In more details, the most affected months were April 2015 (9 days beyond threshold), followed by August and September 2015 (8 days both); however, on absolute terms the most polluted month resulted to be January 2015 (14,7 μg / m^3, event 1), followed by November 2015 (7,6 μg / m^3, event 25) and September 2015 (6,8 and 6,2 μg / m^3, event 19 and 20).

As depicted in previous charts, during these highest BC - pollution events wind prevailing direction is WNW and wind speed overcoming 75th centile for 2015 (5,4 ms^{-1}).

Pinching the visual, event 1 reports a parallel considerable increase in both mass concentration and numeric concentration parameters, while no gas data are available.

Interestingly, events 19 and 20 show a parallel steep increase in CO and SO_2 concentrations and scattering coefficients values (no further aerosol data are available), while event 25 O_3 and SO_2 increase are mentioning worth.

Event 7 (13 – 21 April 2015) is the longer lasting , including 2 microevents (7a and 7b: 2,7 and 4,2 μg / m^3, respectively): during the first microevent NO_x, PM and fine particles are signalled to grow up, while during the second one CO, PM and both fine and coarse particles rise.

CO is reported to grow up during 20 out of 35 events (8, 9, 10, 11, 12, 14, 15, 16, 18, 19, 20, 22, 26, 27, 28, 29, 30, 31, 34, 35), NO_2 during 19 out of 35 events (3, 4, 5, 6, 8, 9, 10, 19, 20, 21, 22, 24, 28, 29, 30, 32, 33, 34, 35), SO_2 during out 8 of 35 events (3, 6, 9, 16, 18, 19, 24, 30), PM_{10} during 13 out of 35 events (1, 2, 6, 9, 10, 23, 24, 25, 27, 28, 29, 30, 33), $PM_{2.5}$ during 15 out of 35 events (1, 2, 5, 6, 9, 10, 11, 23, 24, 25, 27, 28, 29, 30, 33), fine particles during 19 out of 35 events (1, 2, 3, 4, 5, 6, 8, 9, 10, 11, 12, 21, 23, 24, 25, 28, 29, 30, 33), while scattering coefficients during 22 out of 35 events (1, 2, 3, 4, 6, 9, 10, 11, 12, 13, 16, 17, 18, 19, 20, 21, 24, 27, 28, 29, 30, 31).

On the whole, prevailing wind direction during BC - polluted days is WNW, with the addition of ESE direction on spring and winter.

Event 1

(8 / 1 / 2015)

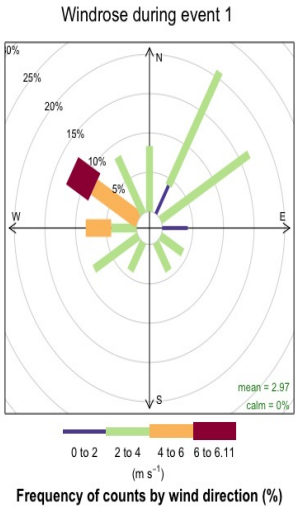

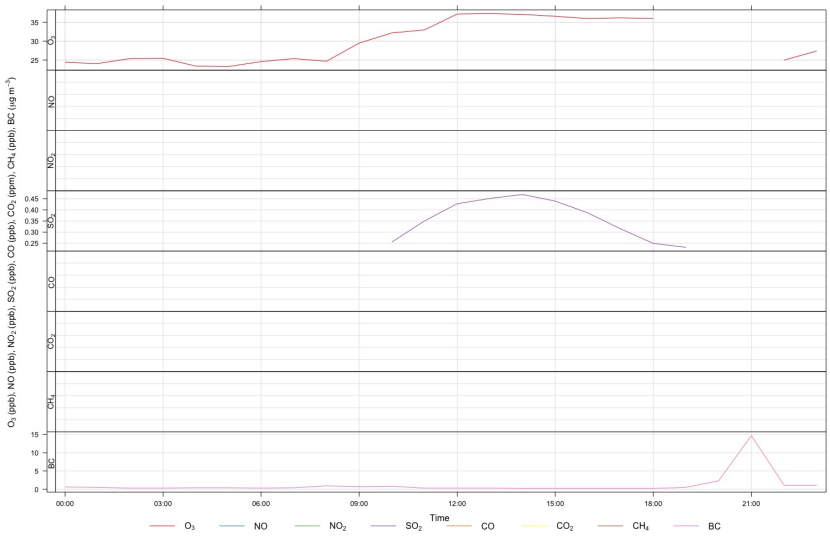

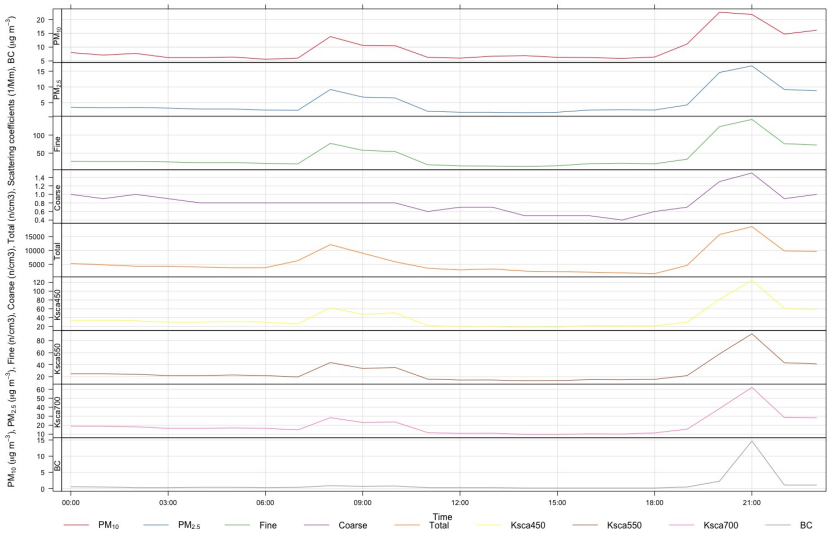

Event 2

(14 - 15 / 1 / 2015)

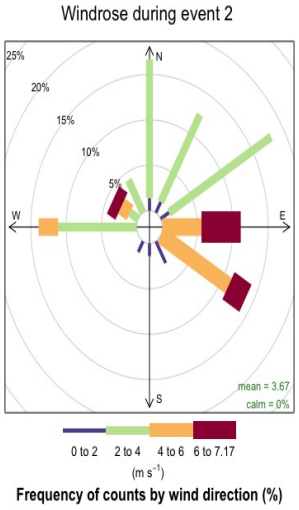

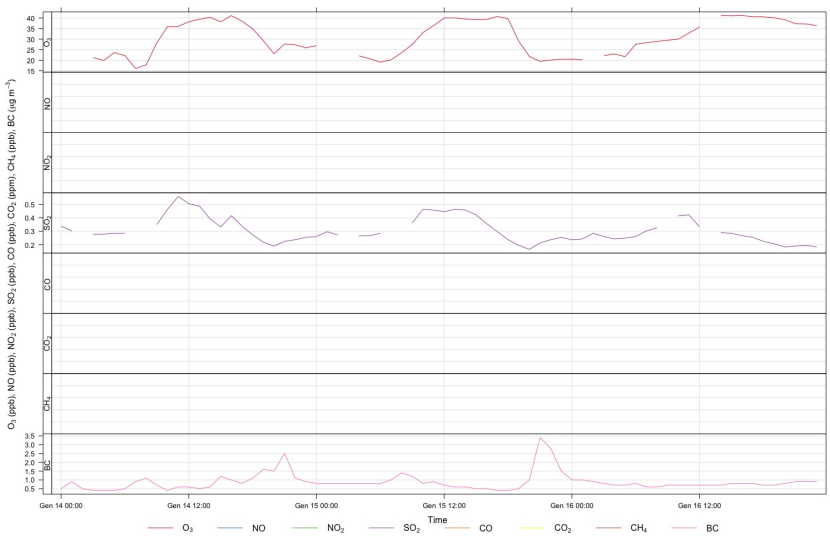

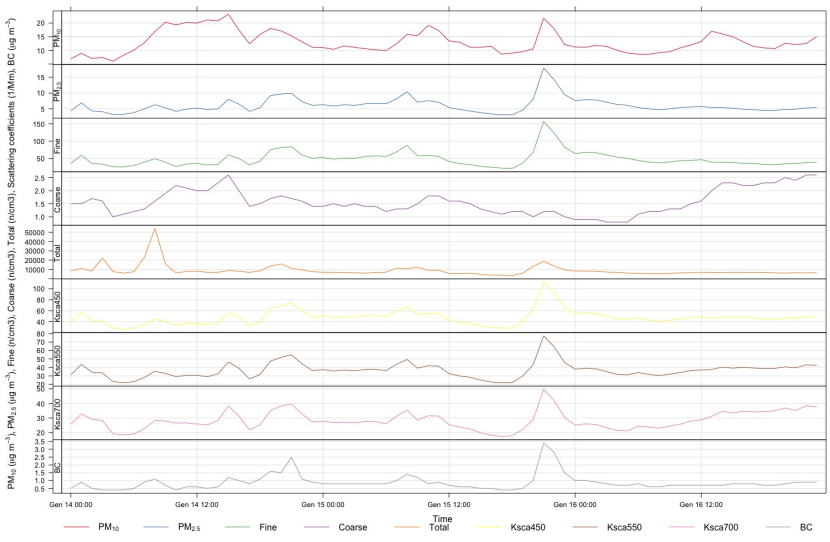

Event 3

(11 / 2 / 2015)

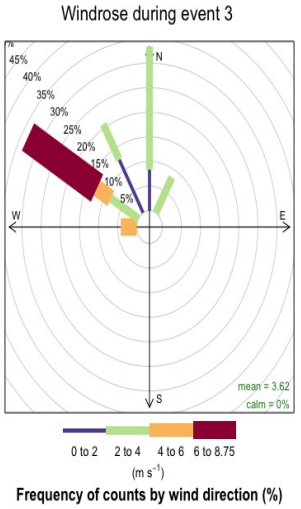

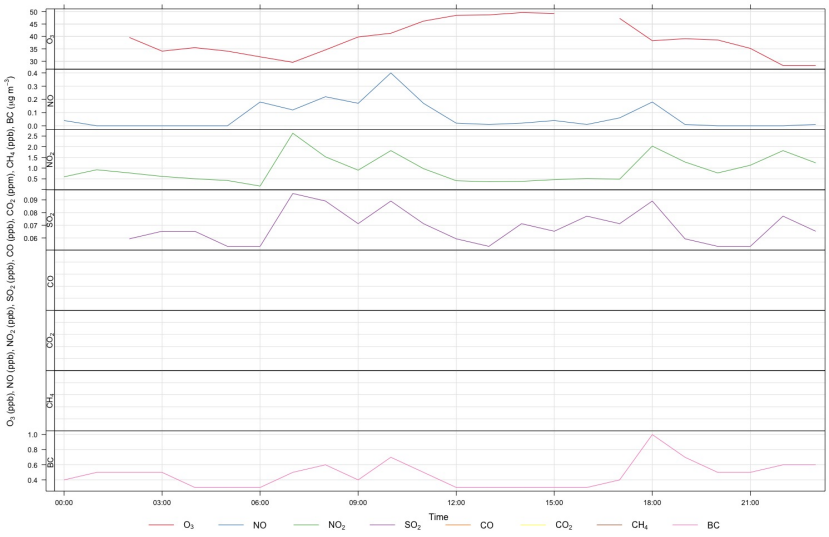

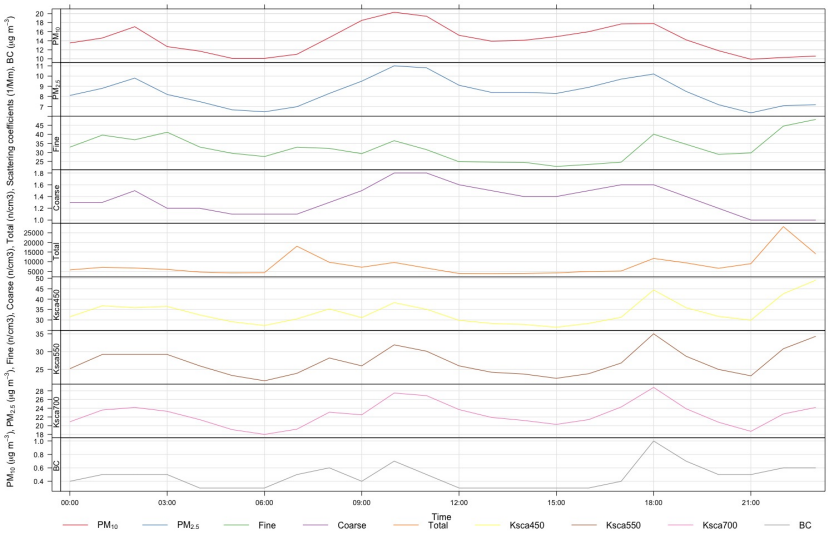

Event 4

(3 / 3 / 2015)

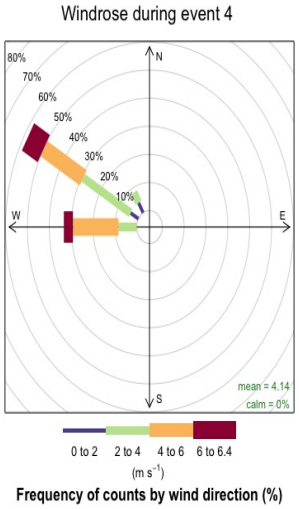

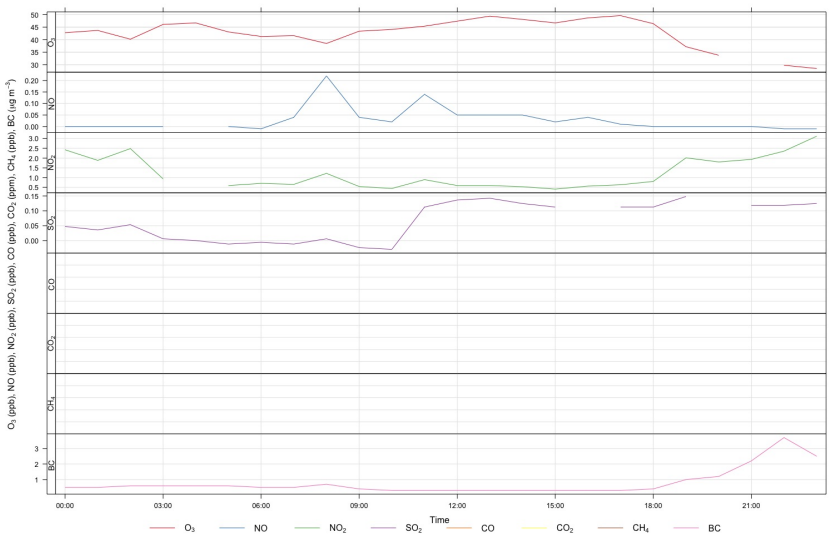

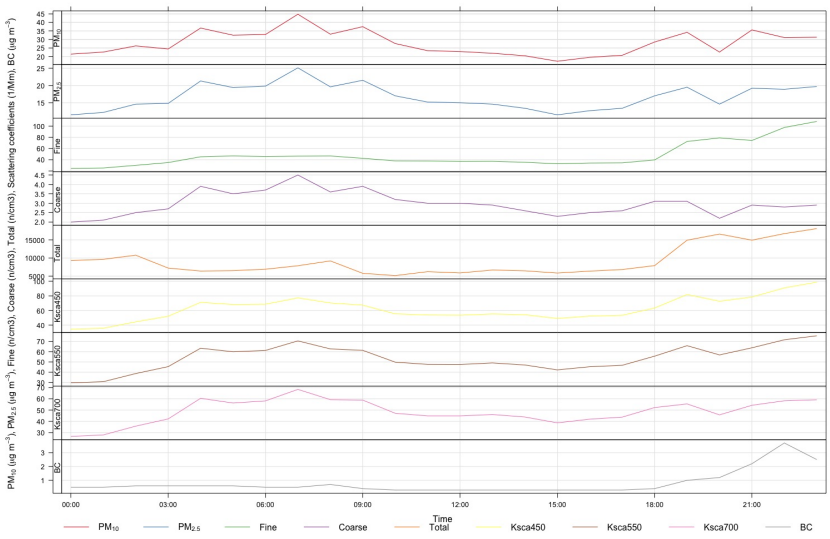

Event 5

(11 / 3 / 2015)

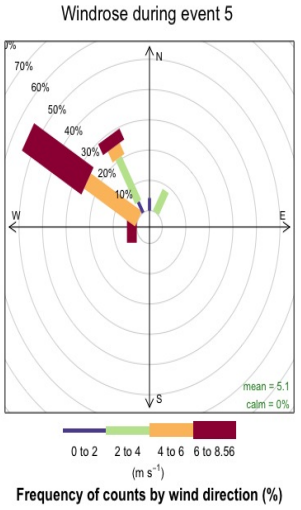

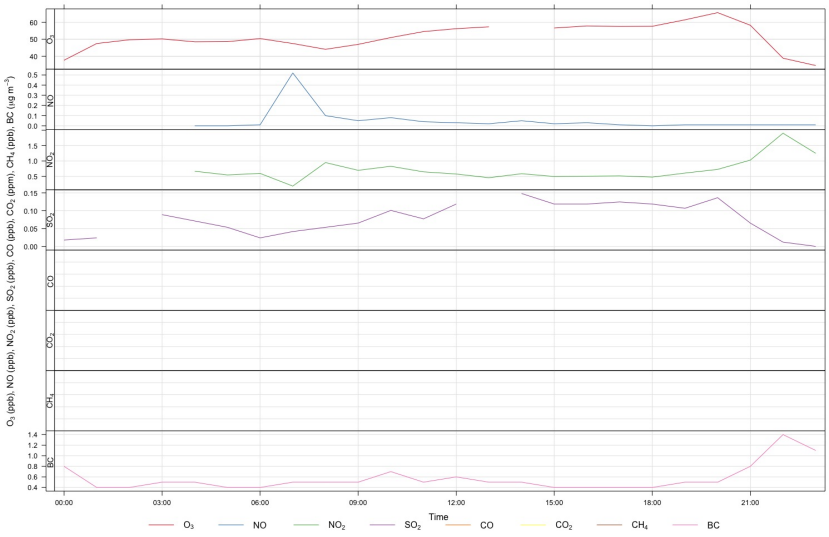

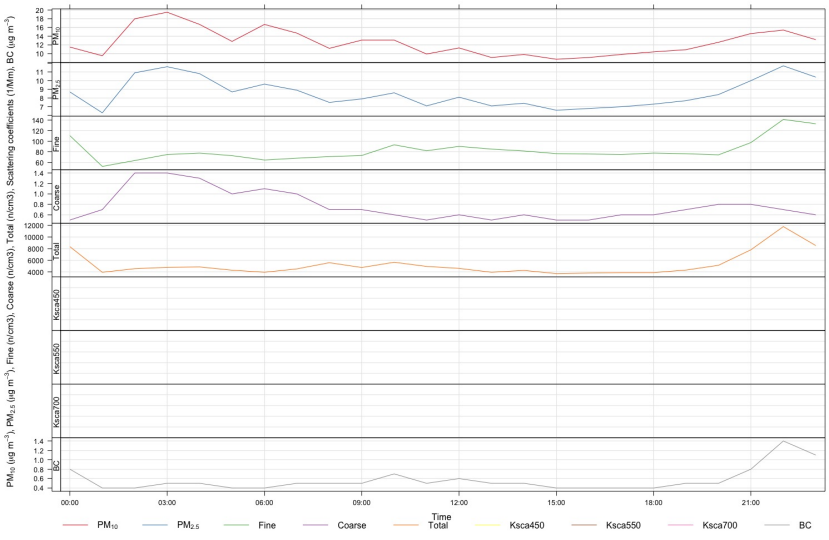

Event 6

(20 / 3 / 2015)

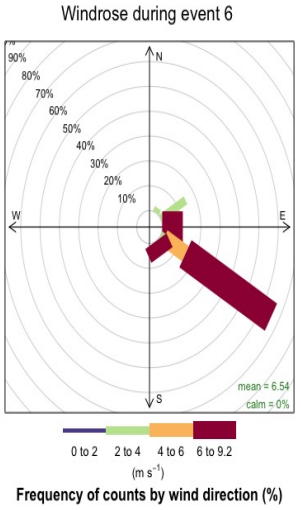

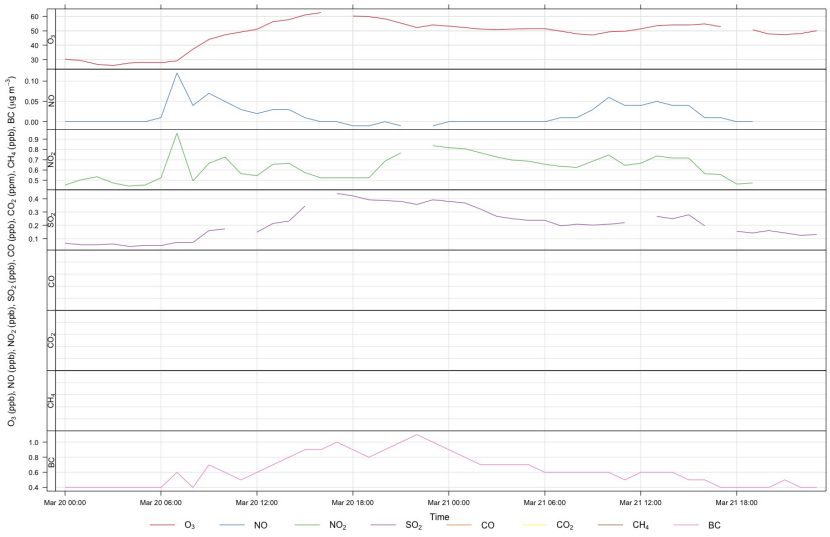

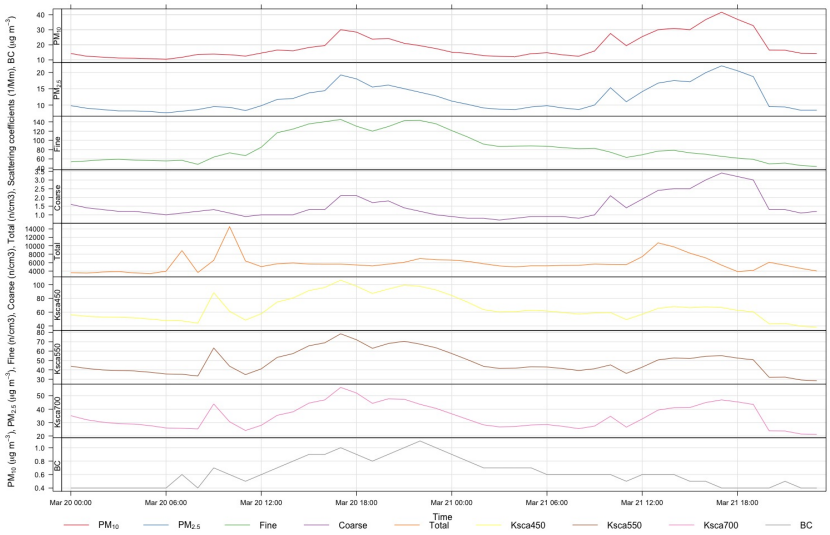

Event 7

(13 - 21 / 4 / 2015)

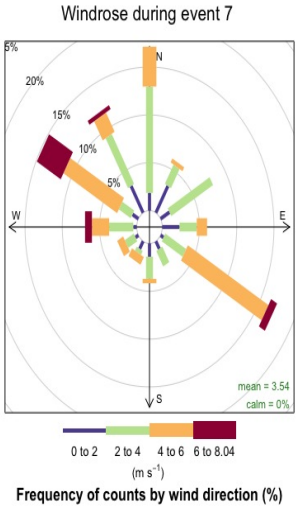

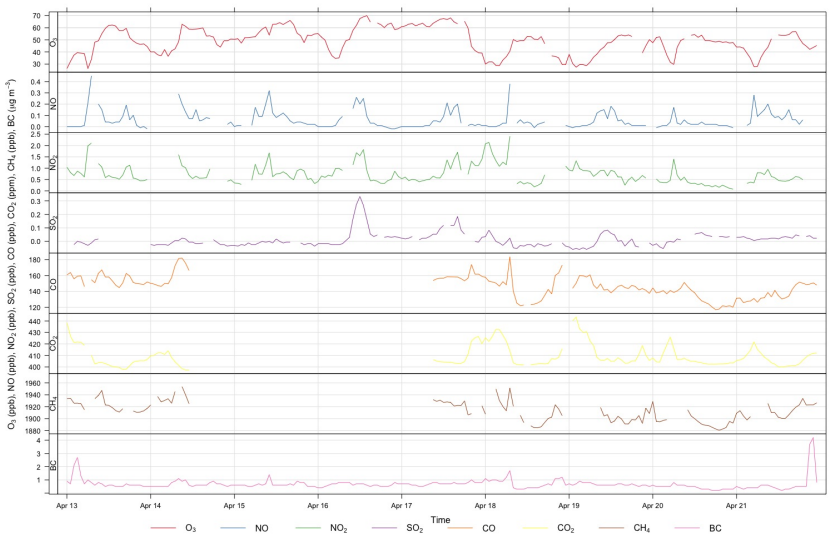

Event 8

(3 / 5 / 2015)

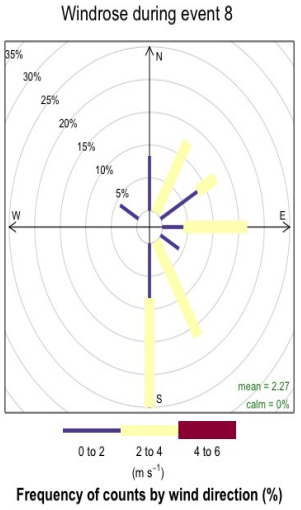

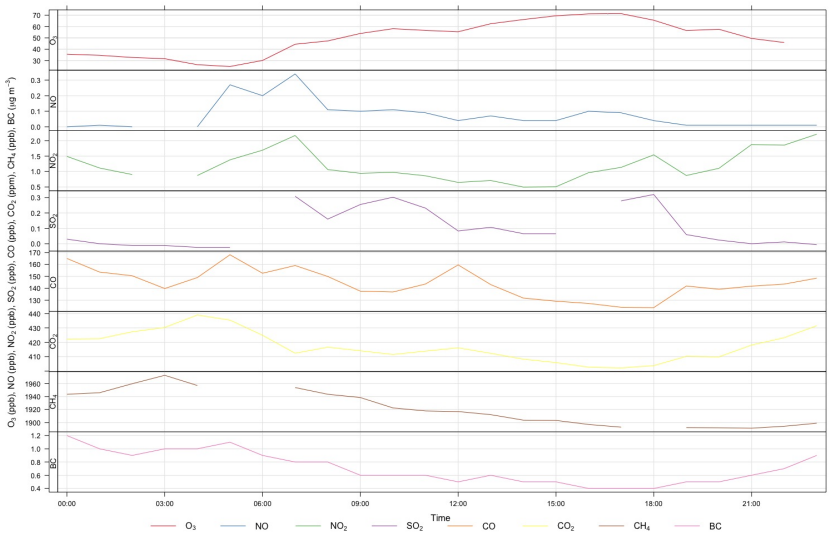

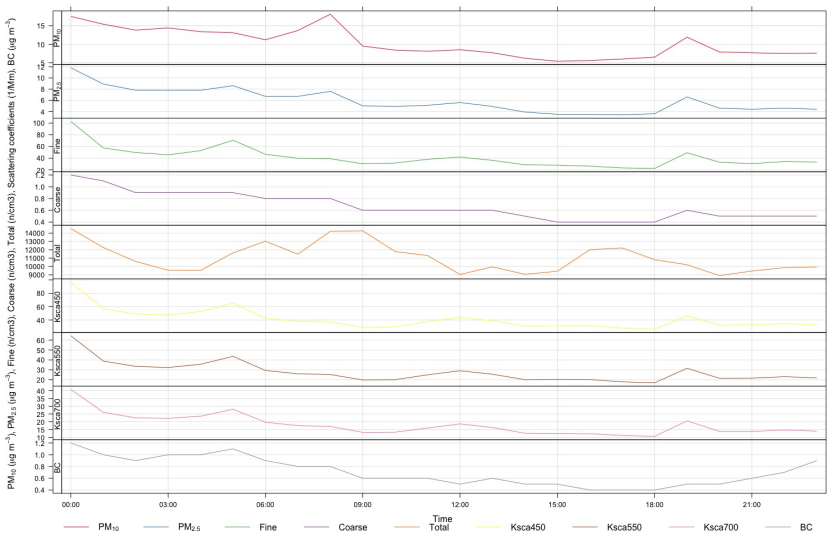

Event 9

(14 / 5 / 2015)

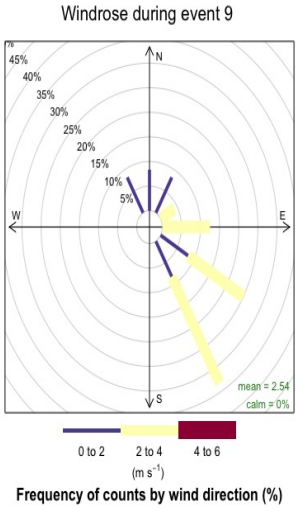

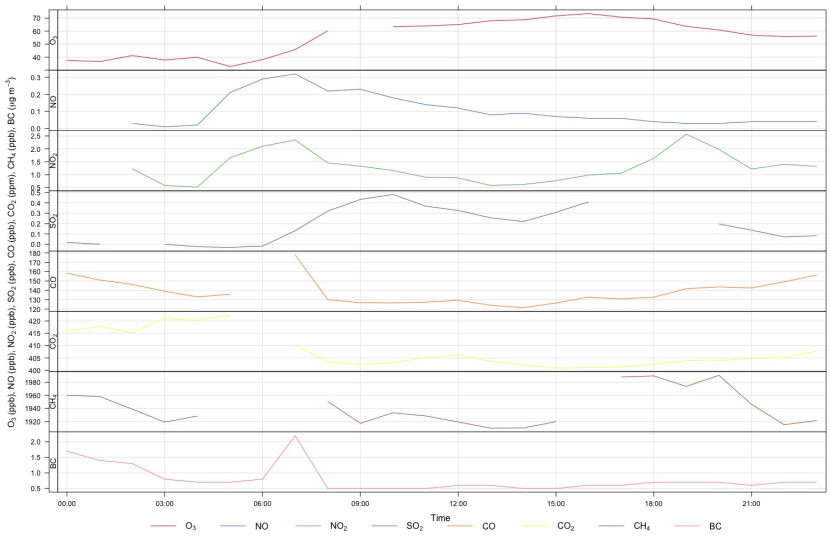

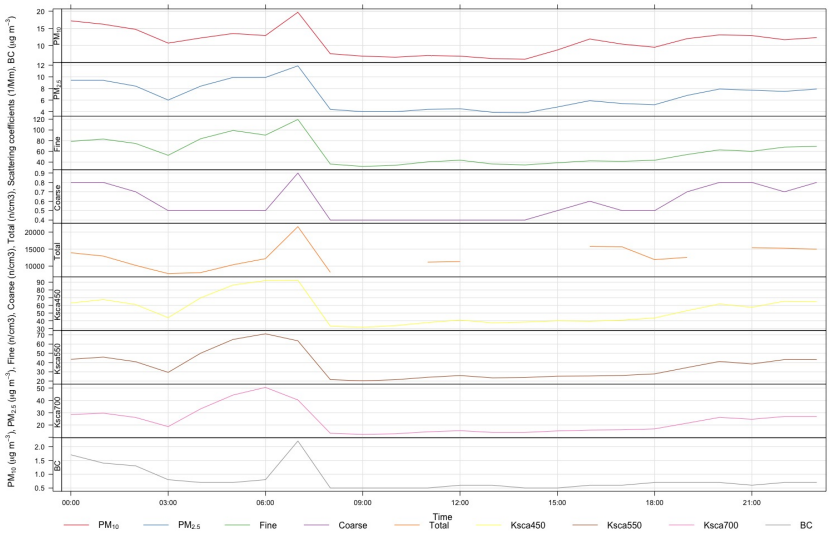

Event 10

(20 / 5 / 2015)

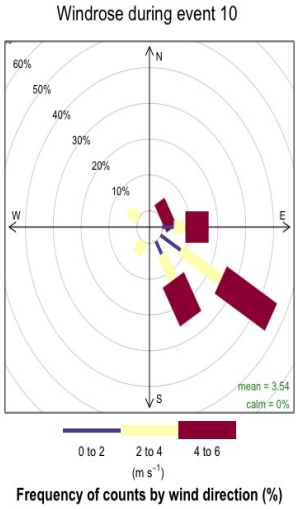

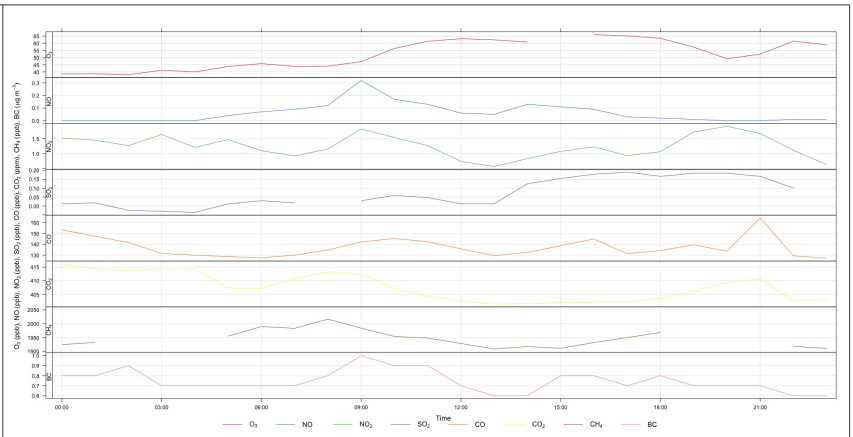

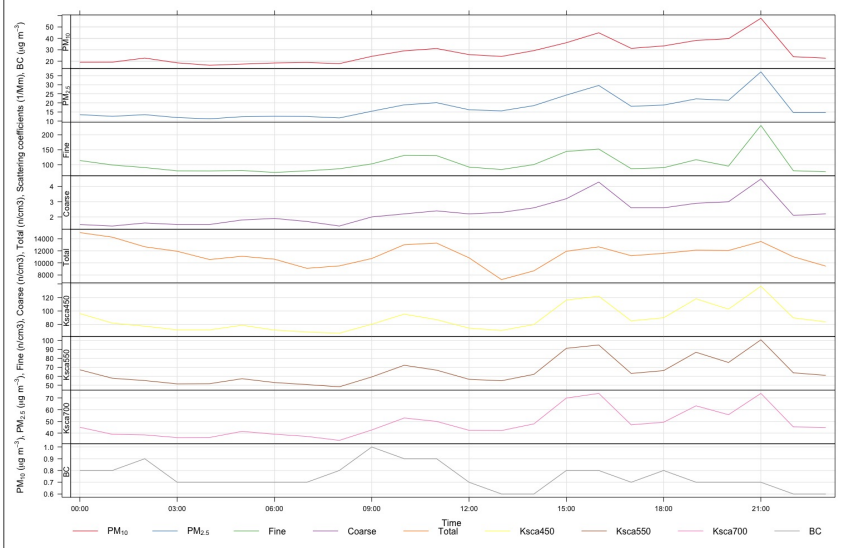

Event 11

(5 - 6 / 6 / 2015)

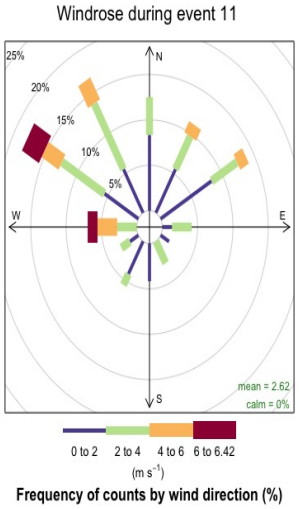

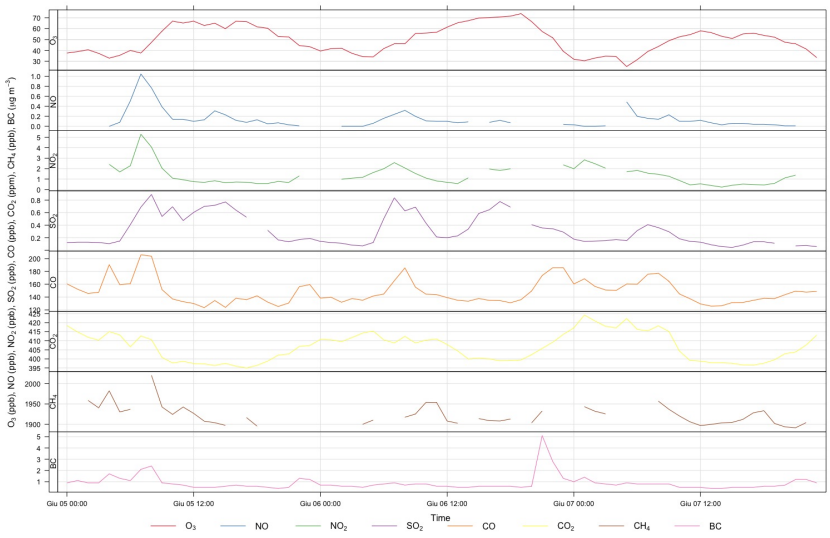

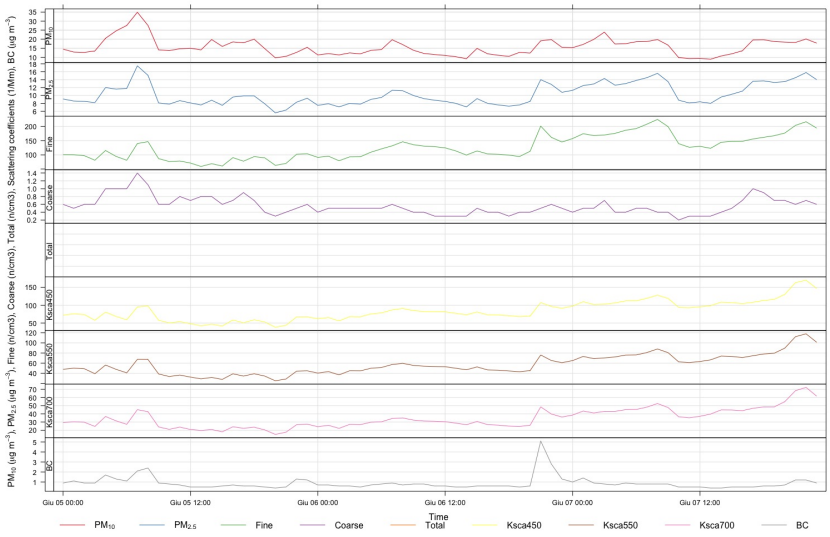

Event 12

(29 / 6 / 2015)

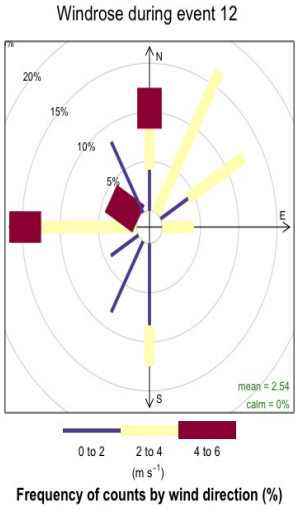

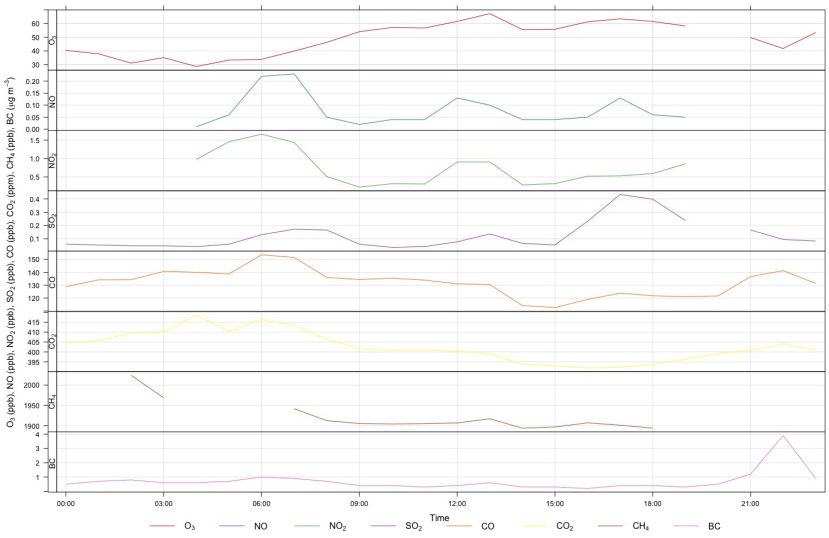

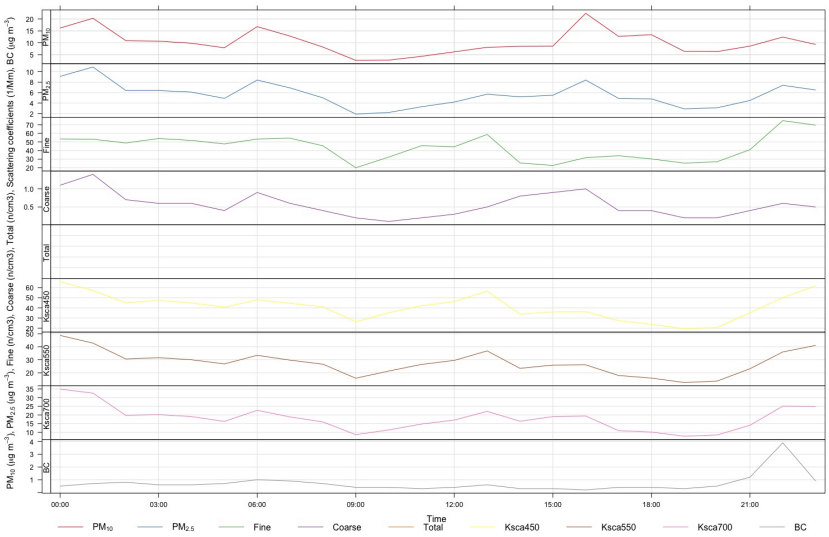

Event 13

(17 - 21 / 7 / 2015)

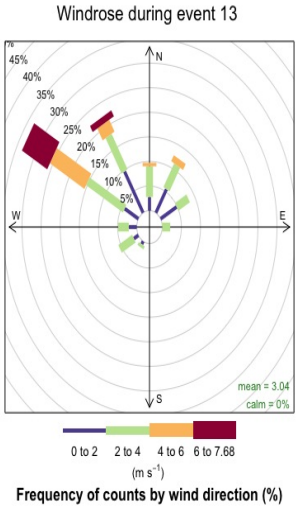

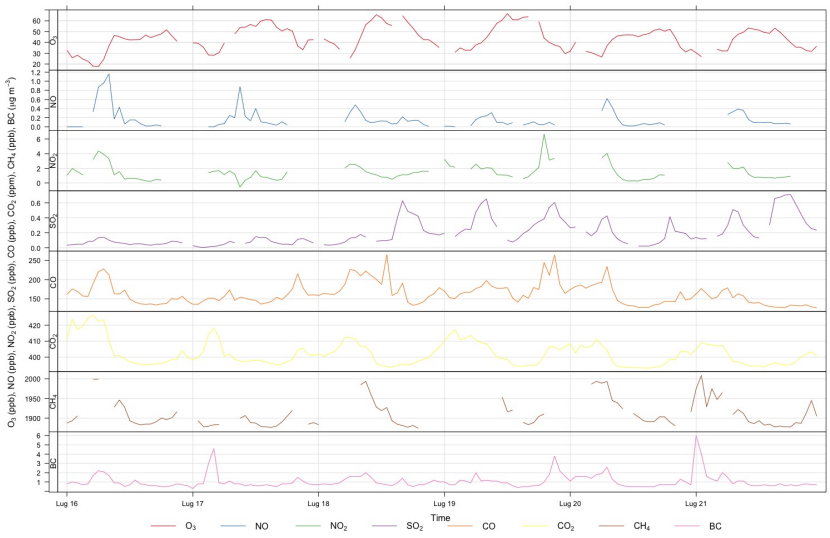

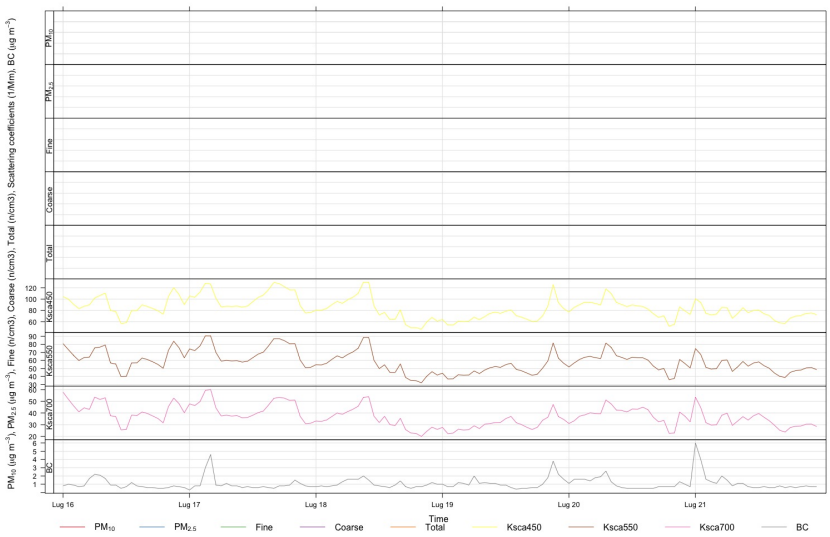

Event 14

(1 / 8 / 2015)

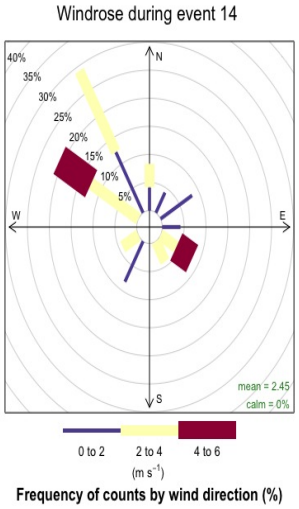

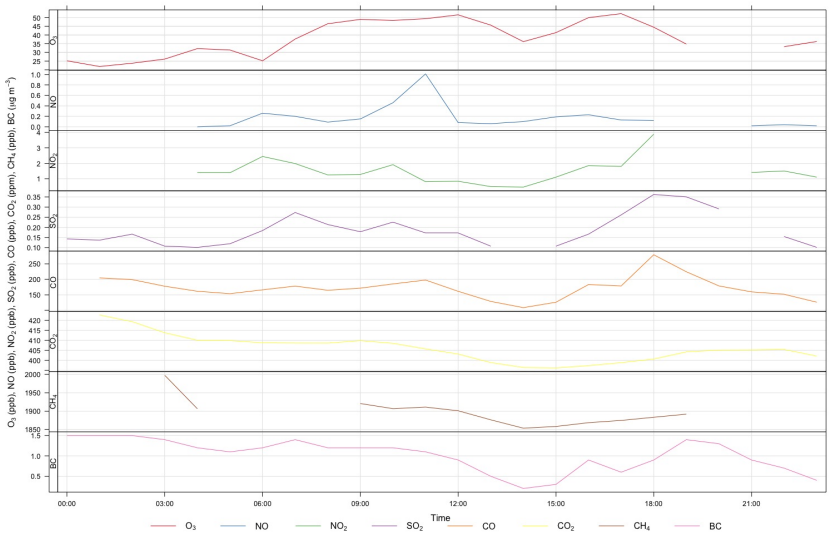

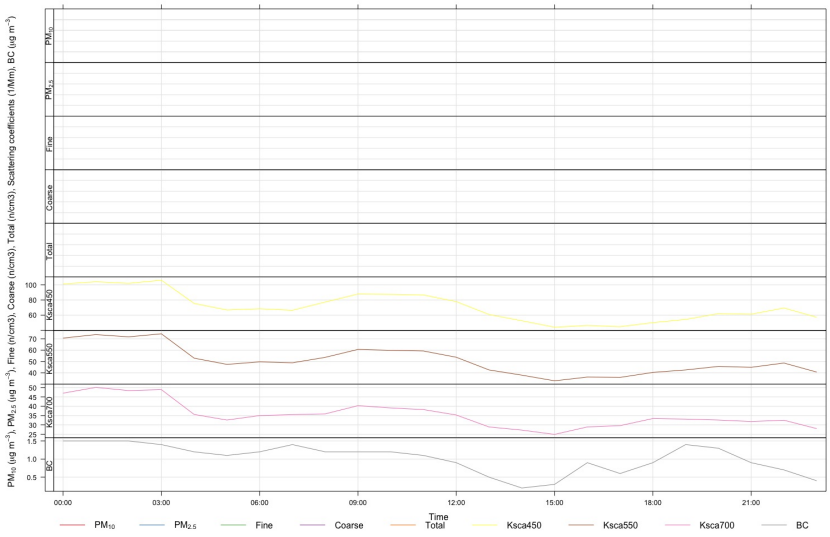

Event 15

(8 – 9 / 8 / 2015)

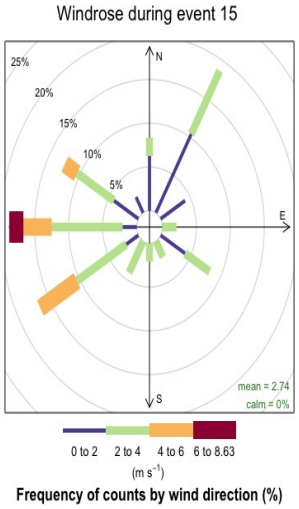

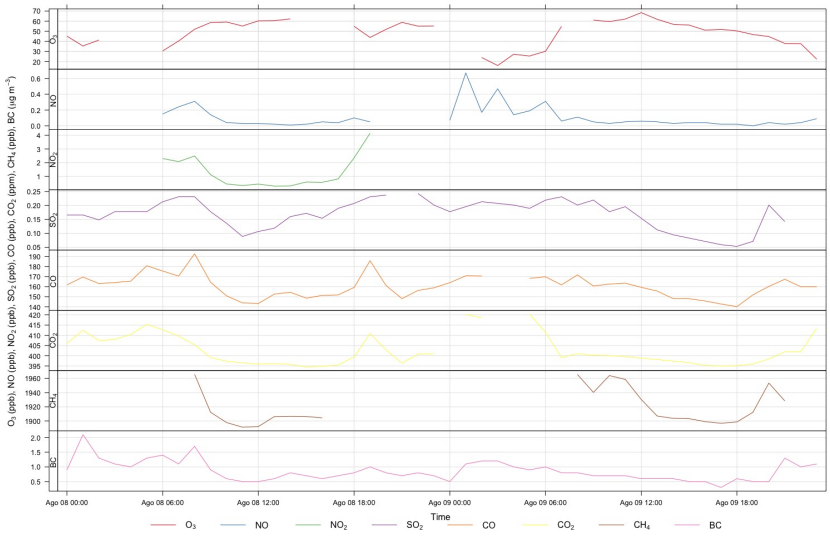

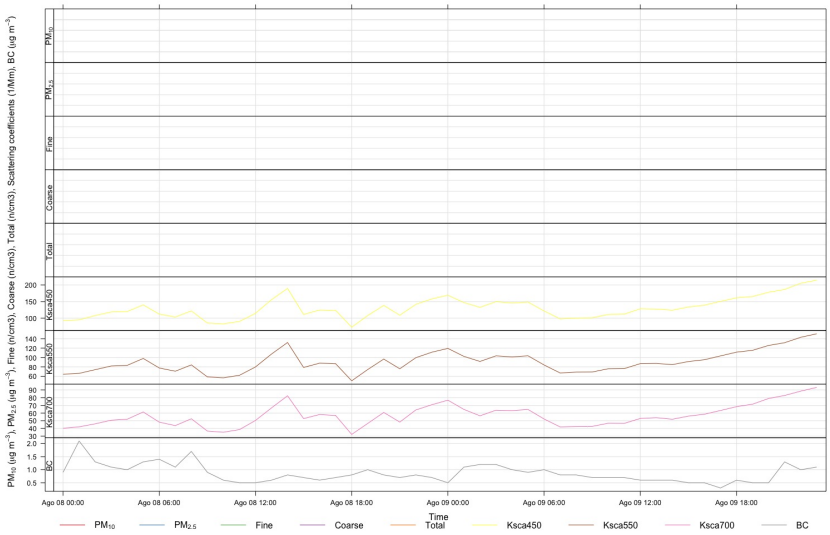

Event 16

(14 / 8 / 2015)

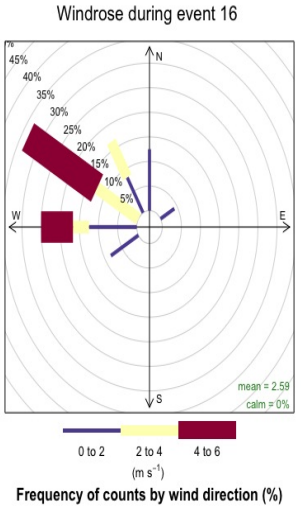

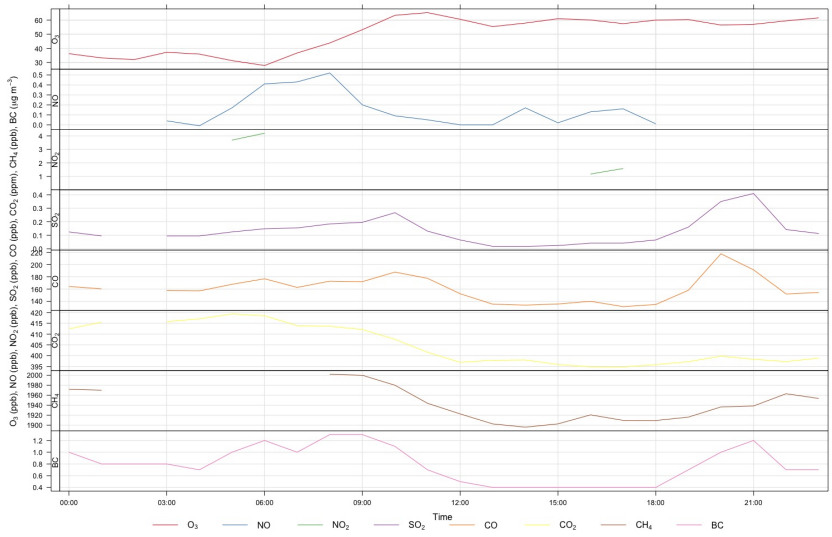

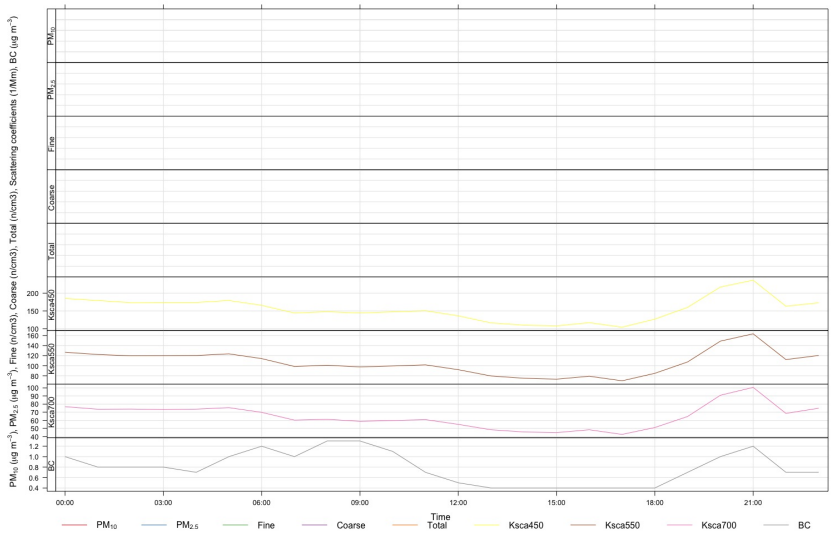

Event 17

(1 - 5 / 9 / 2015)

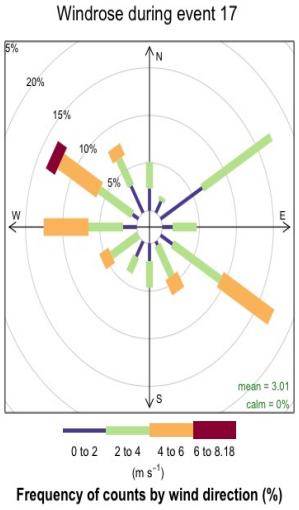

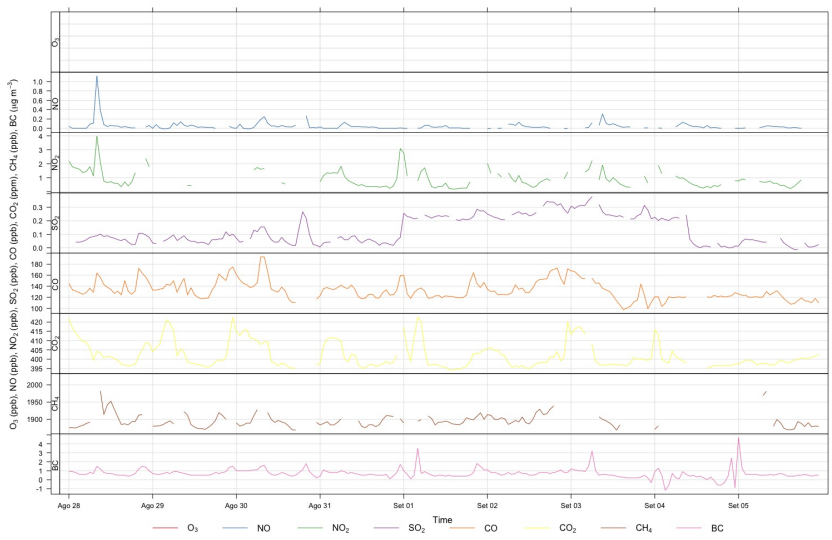

Event 18

(19 / 9 / 2015)

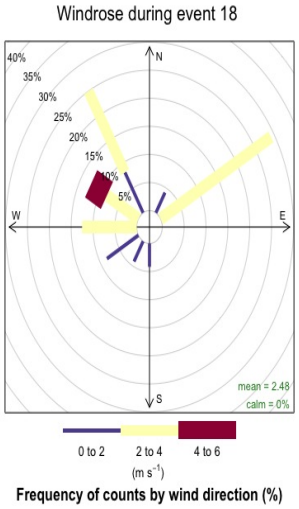

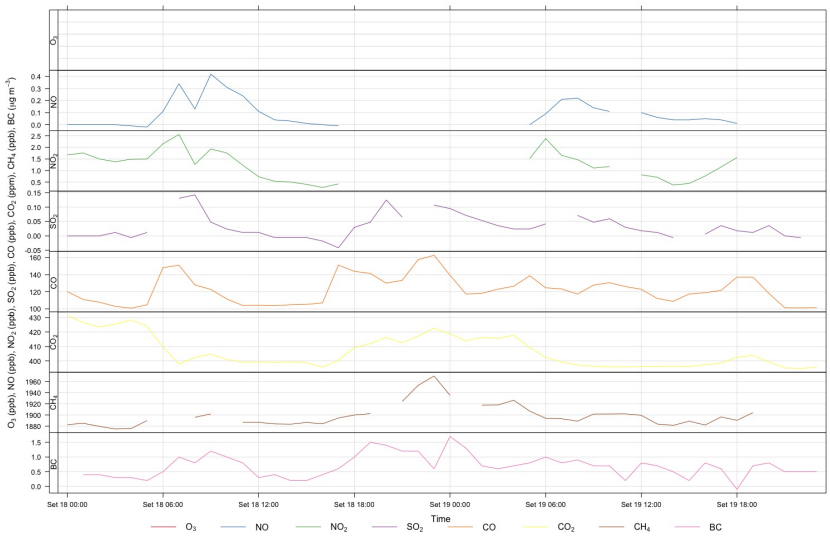

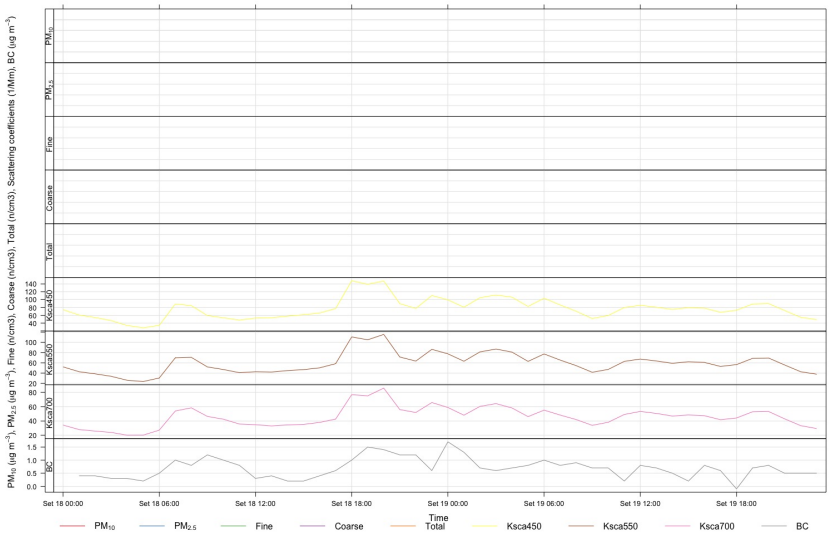

Event 19

(23 / 9 / 2015)

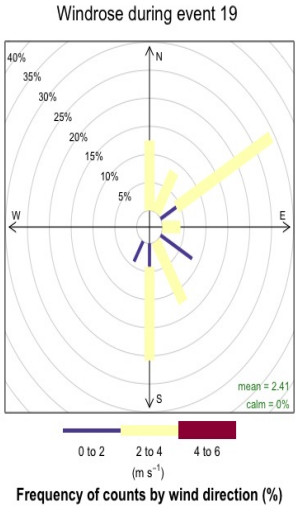

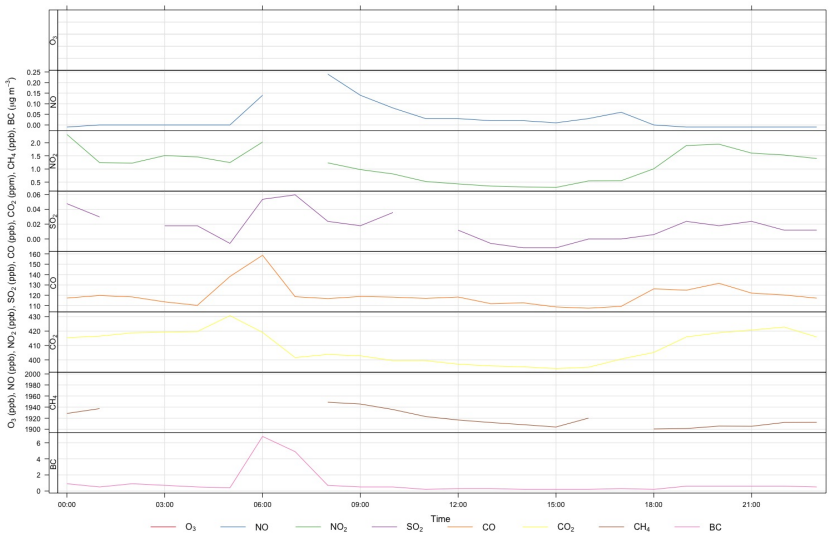

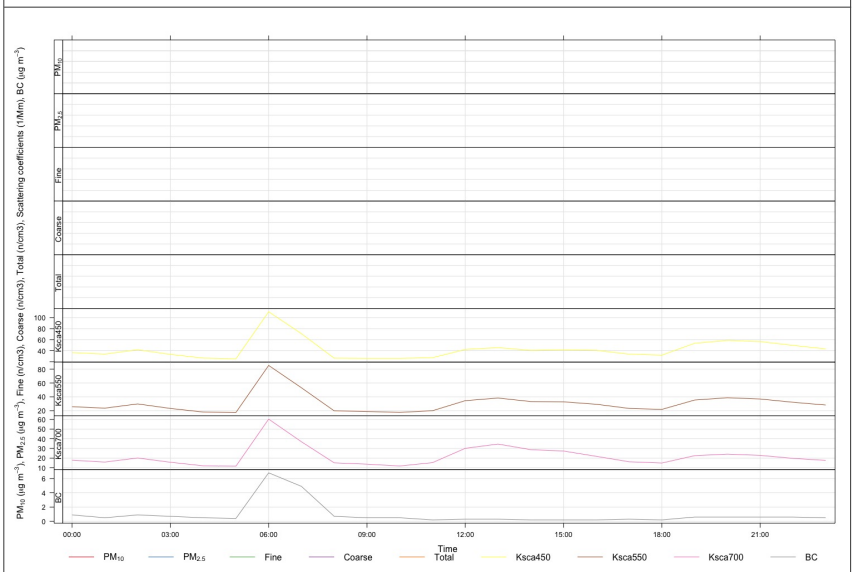

Event 20

(29 / 9 / 2015)

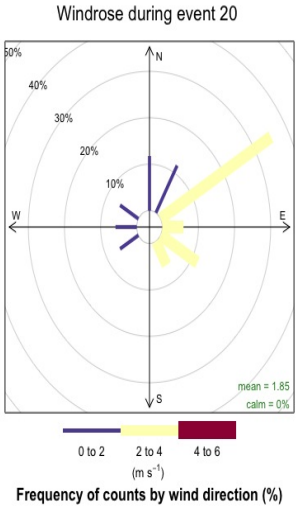

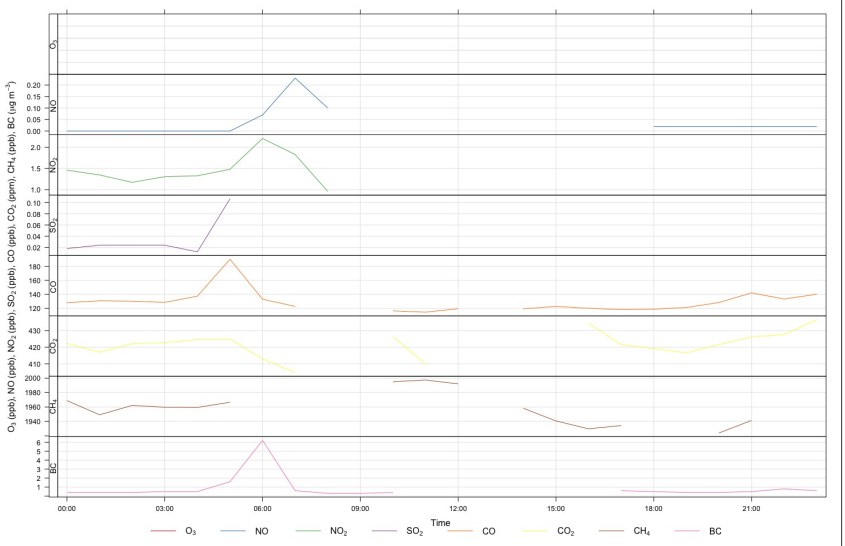

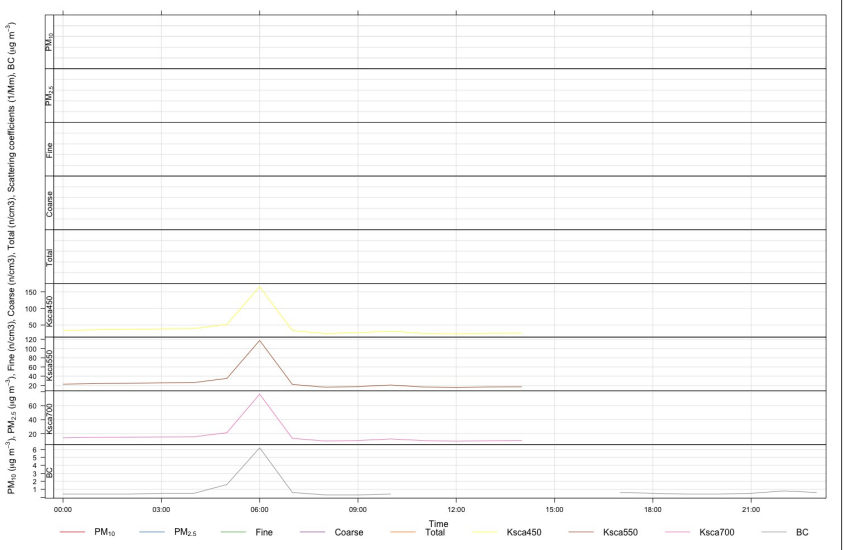

Event 21

(6 / 10 / 2015)

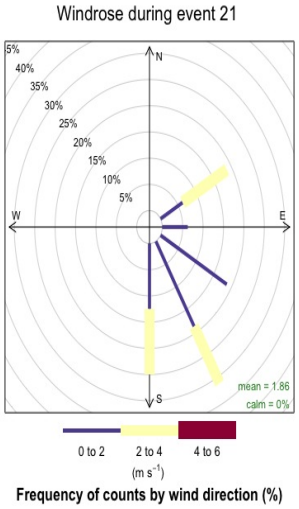

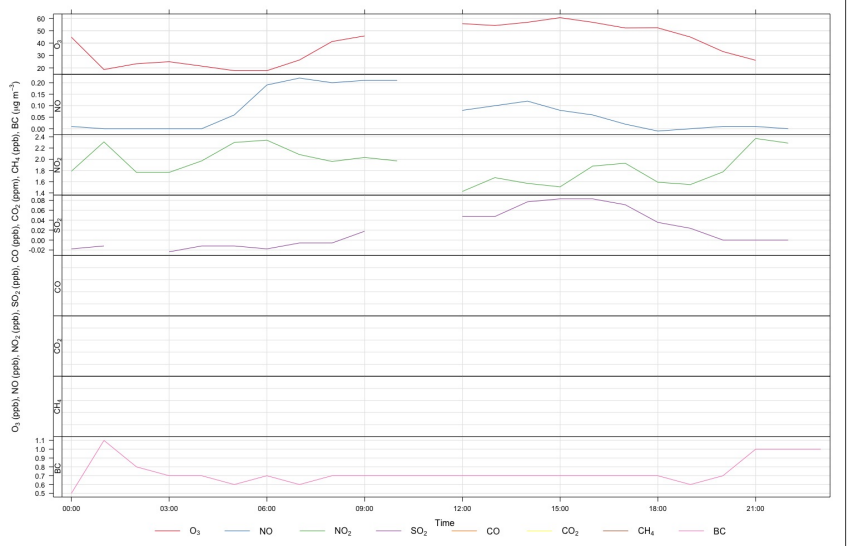

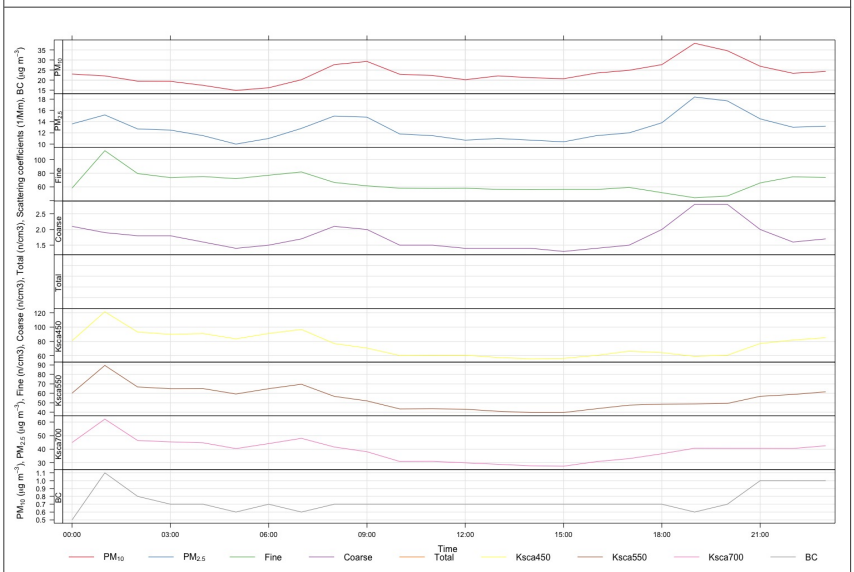

Event 22

(17 / 10 / 2015)

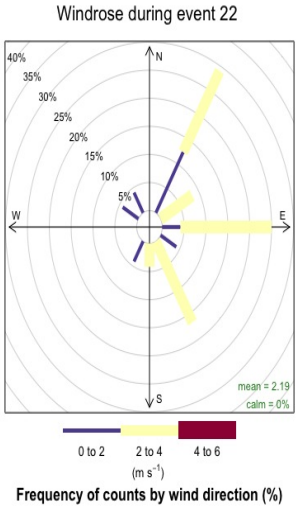

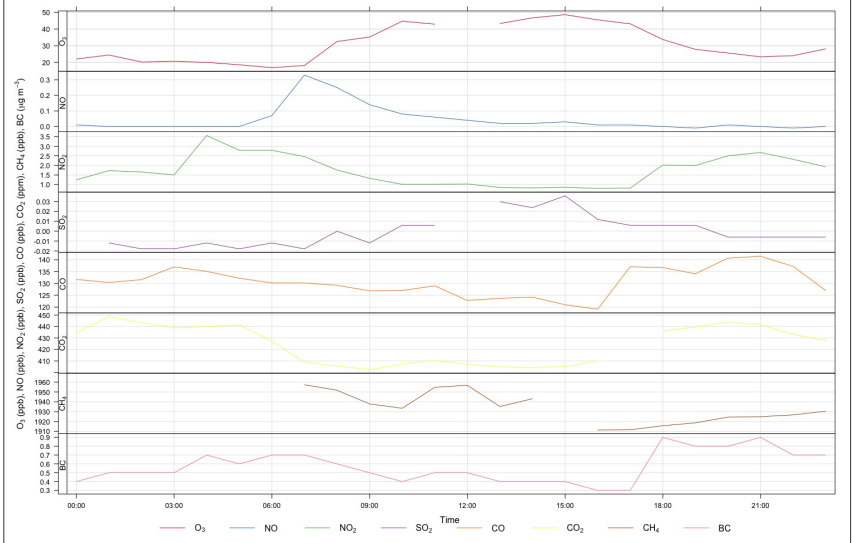

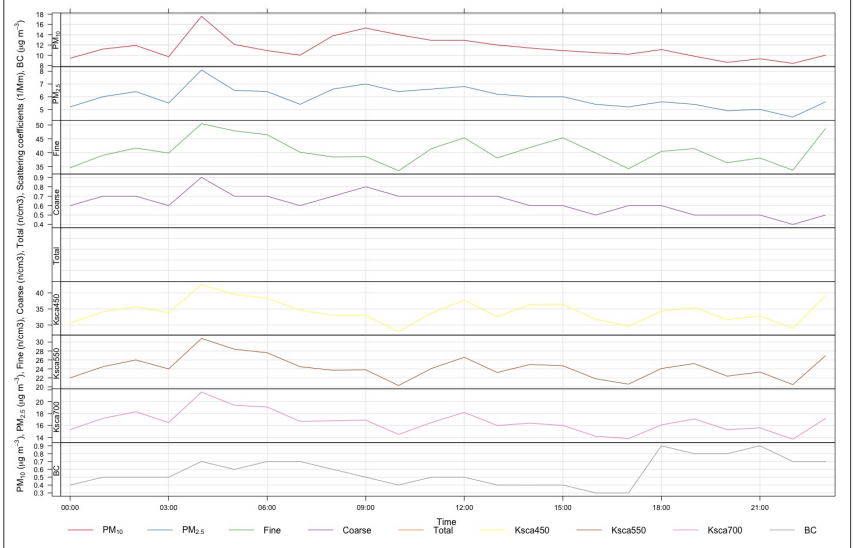

Event 23

(8 / 11 / 2015)

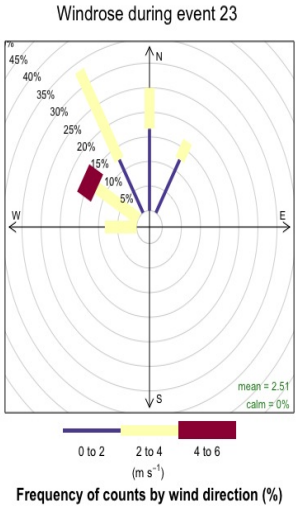

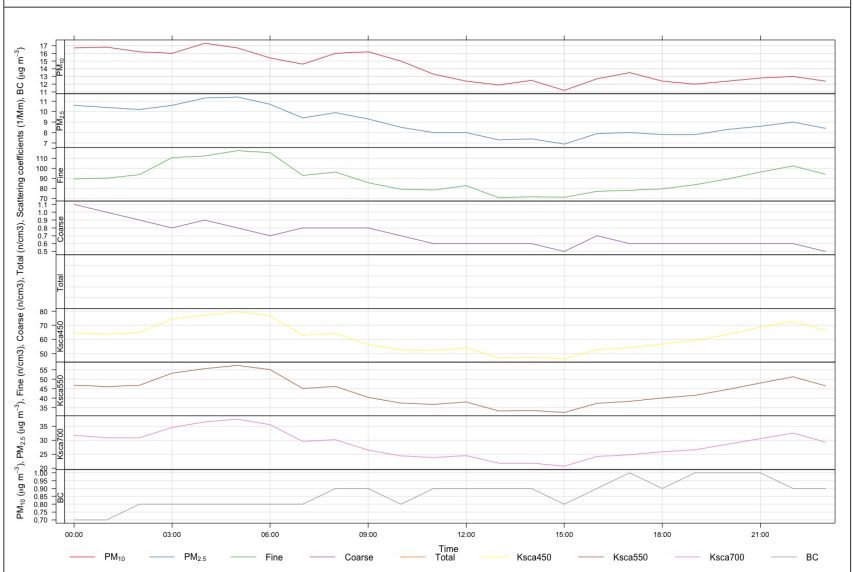

Event 24

(12 - 13 / 11 / 2015)

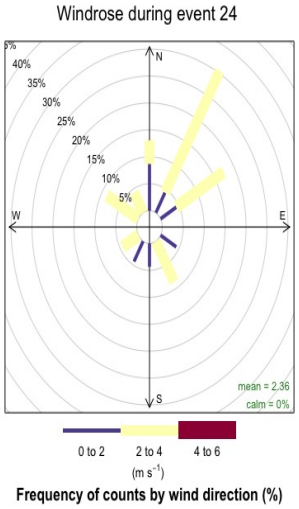

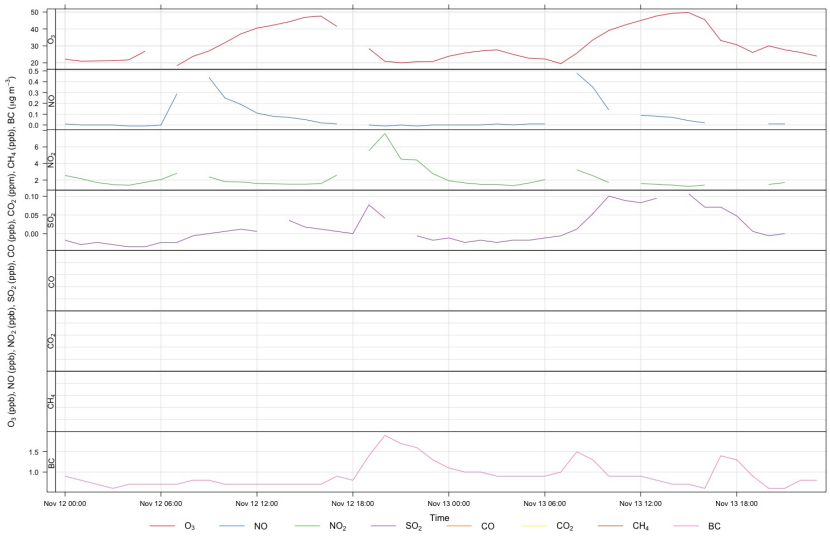

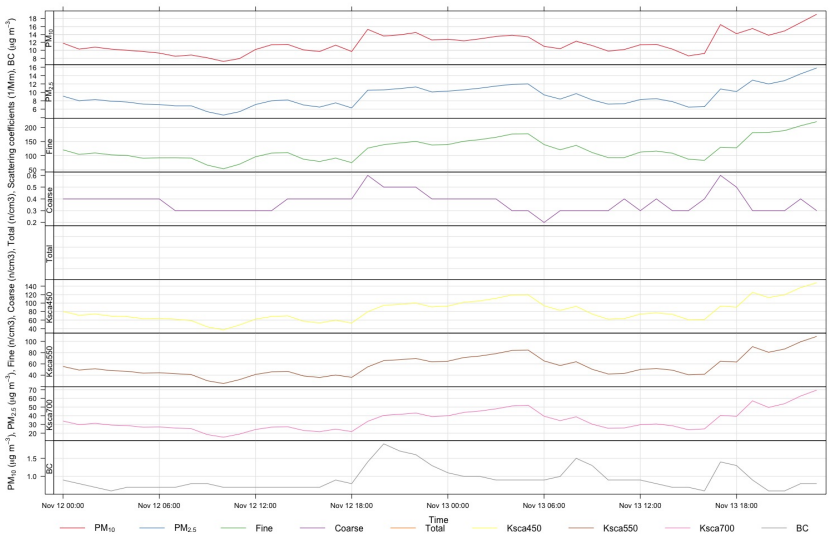

Event 25

(19 / 11 / 2015)

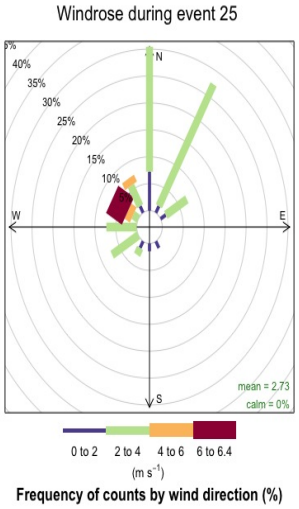

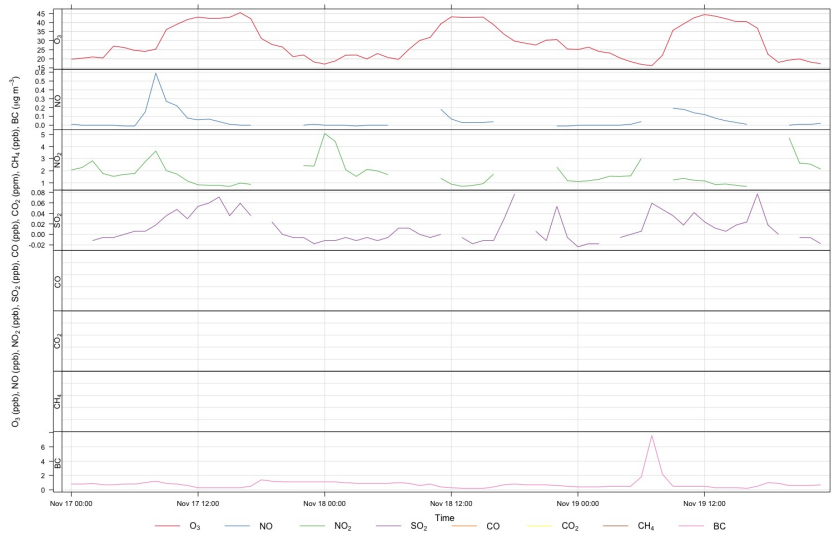

Event 26

(23 / 2 / 2016)

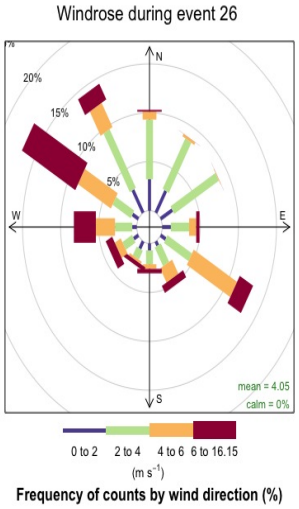

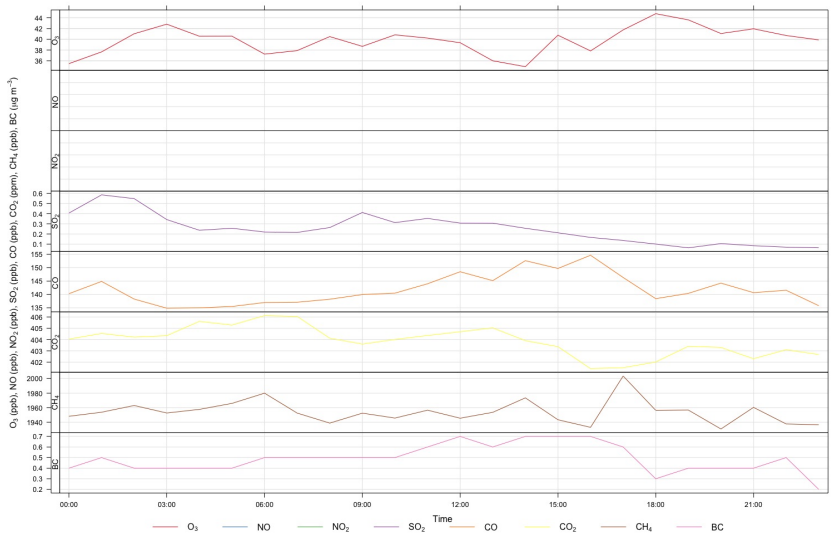

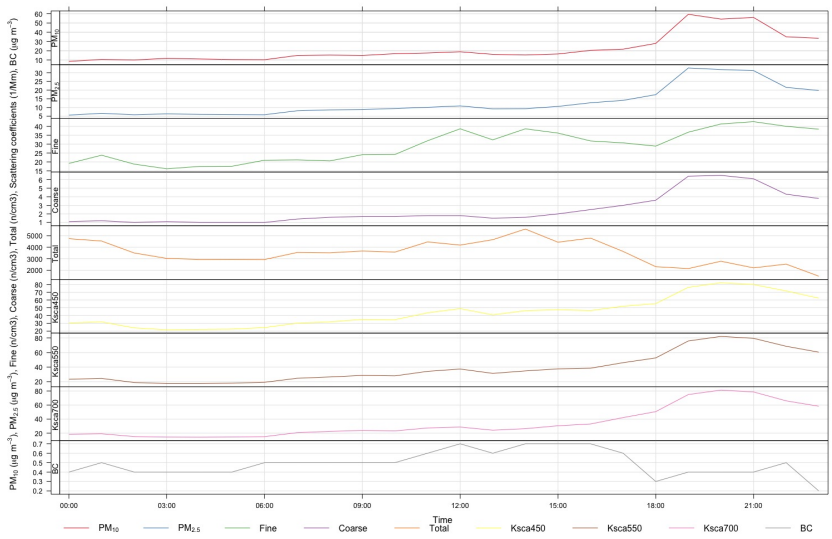

Event 27

(6 / 4 / 2016)

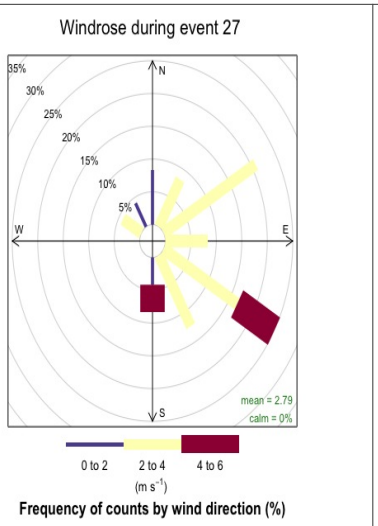

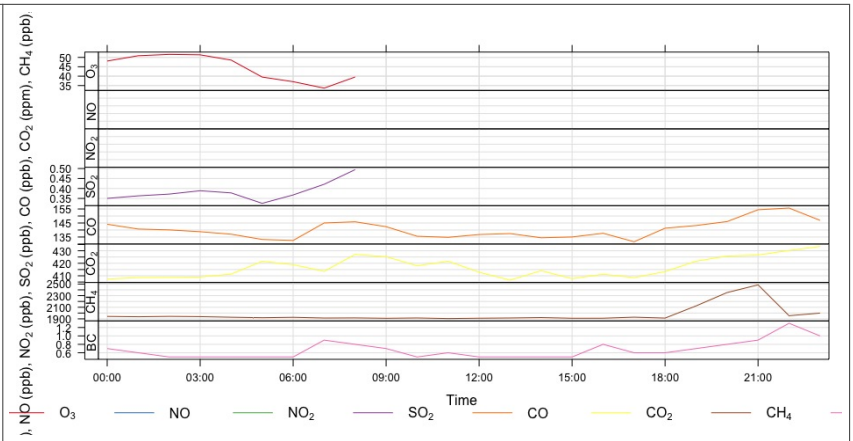

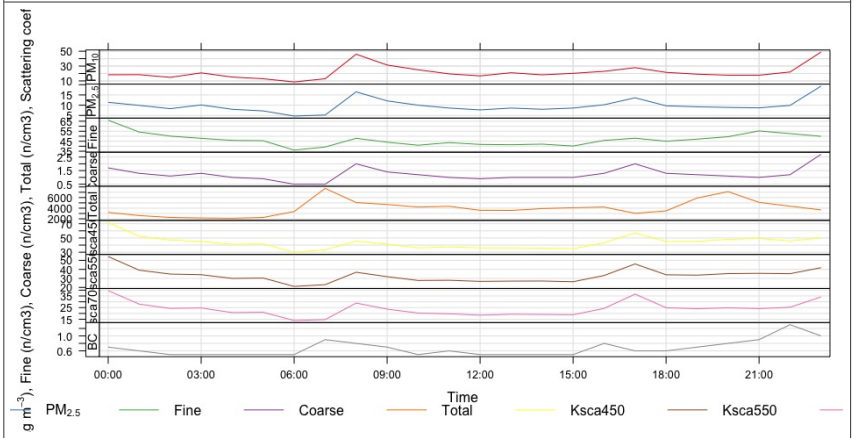

Event 28

(30 / 4 / 2016)

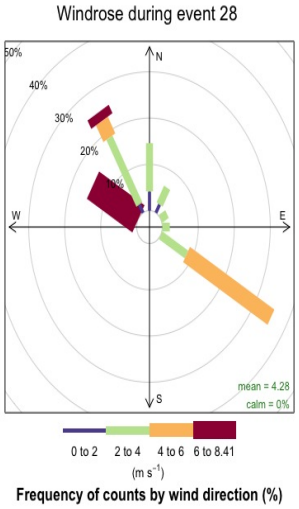

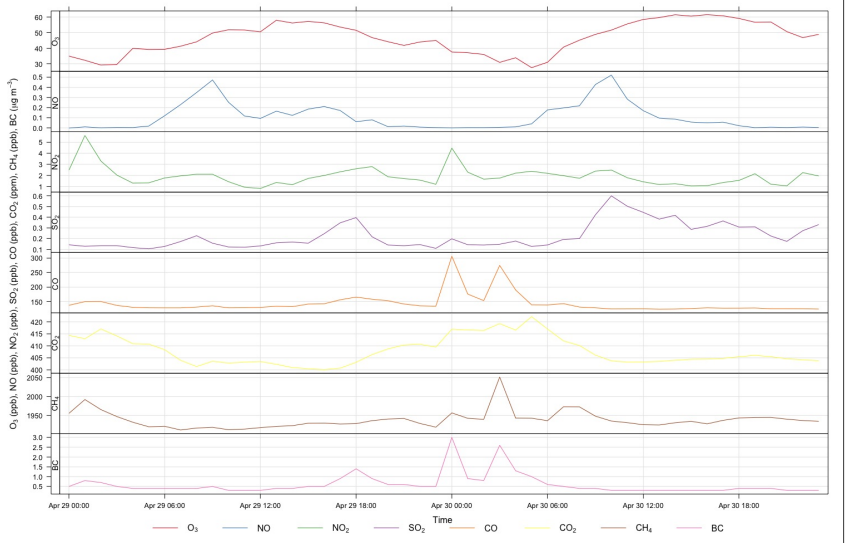

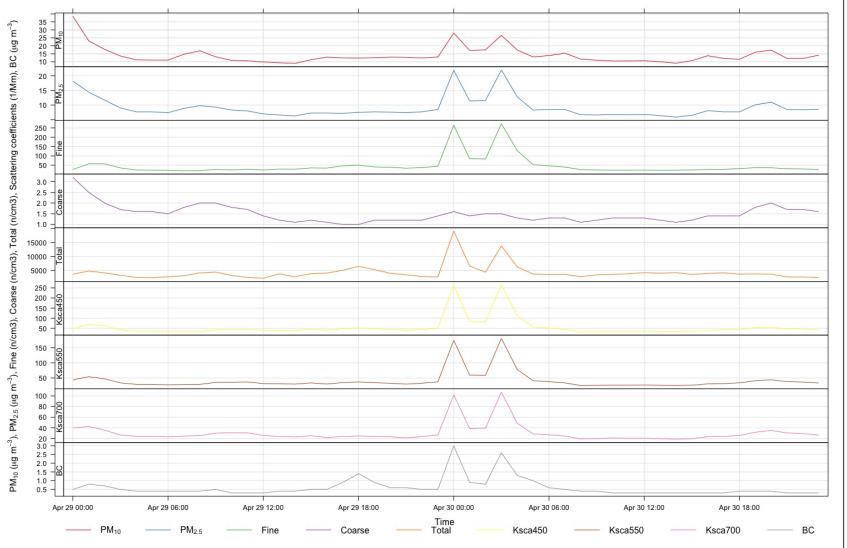

Event 29

(4 / 6 / 2016)

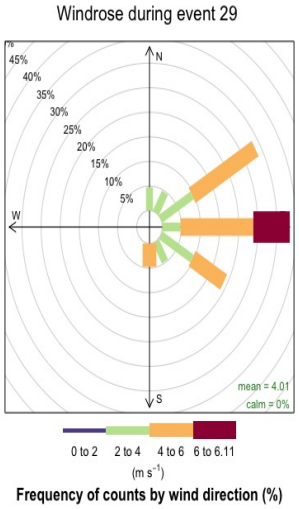

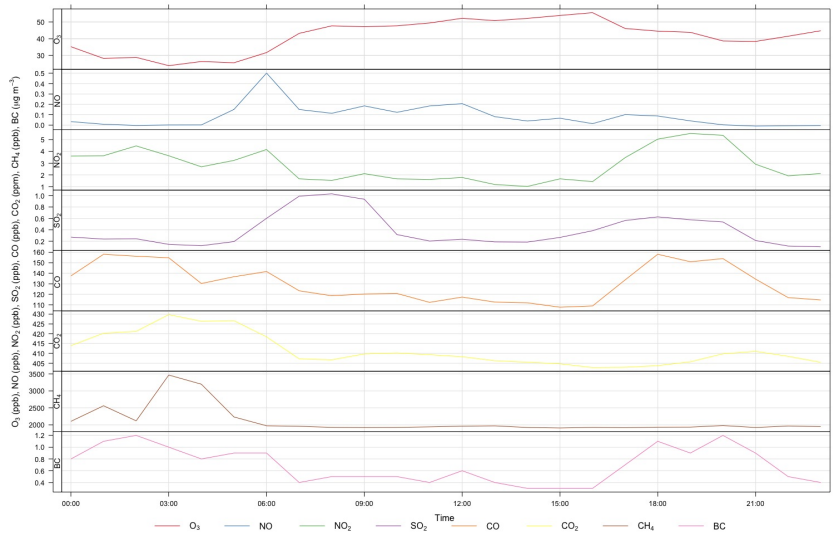

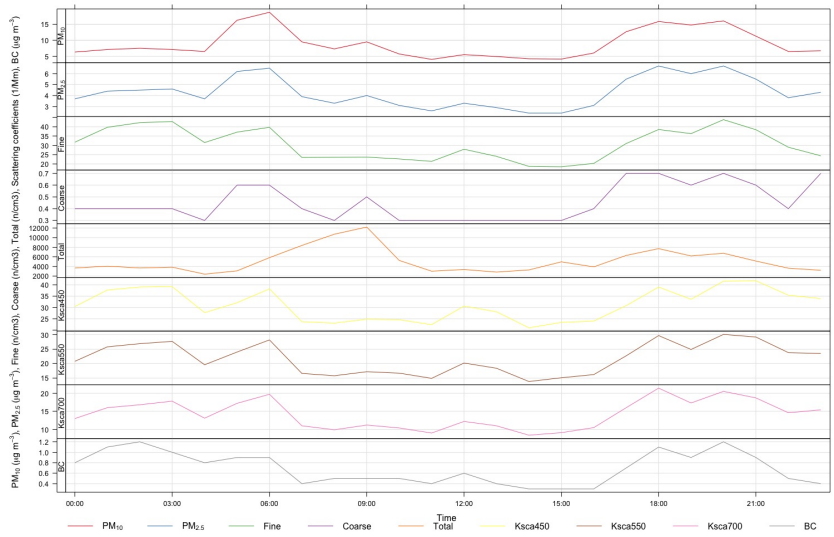

Event 30

(7 / 6 / 2016)

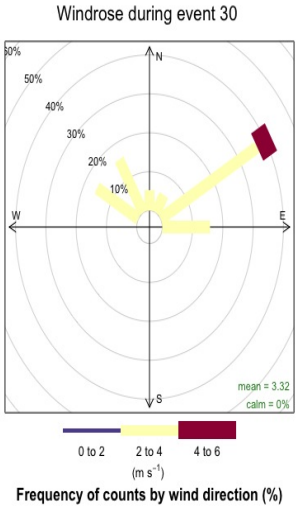

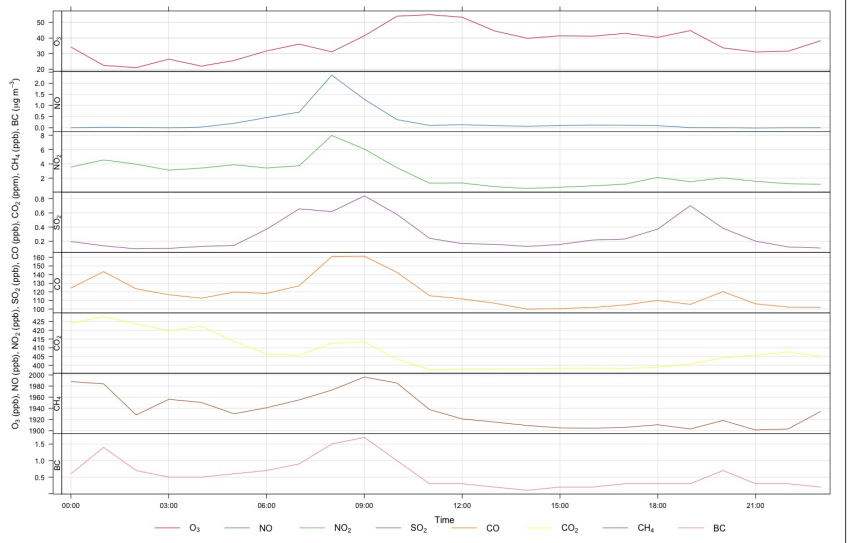

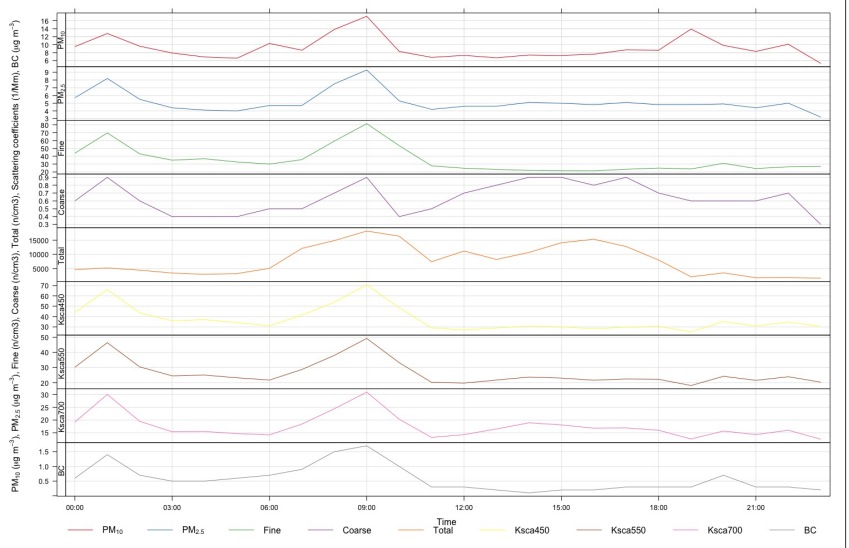

Event 31

(24- 26 / 6 / 2016)

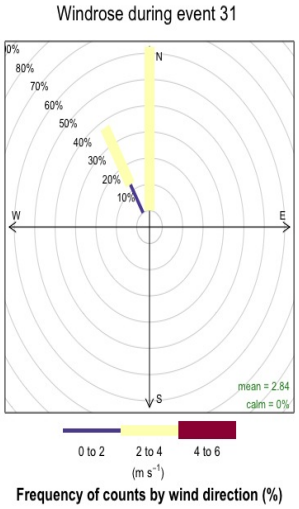

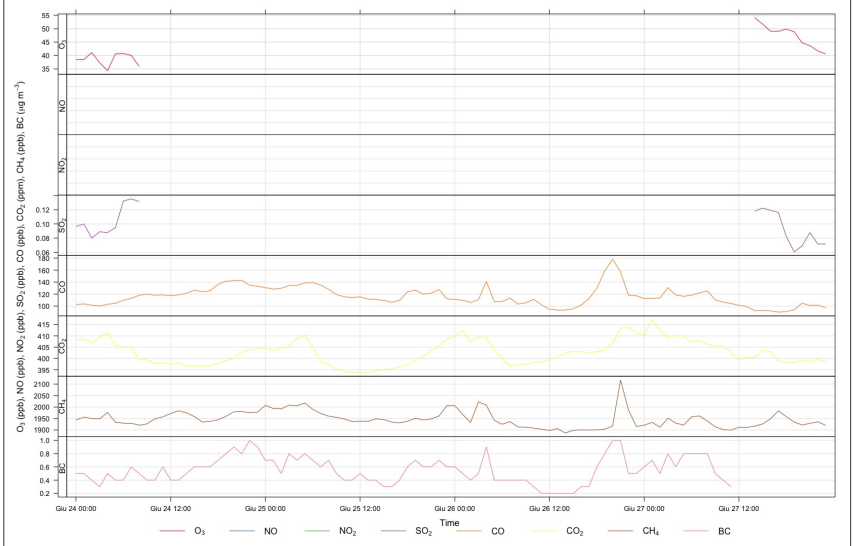

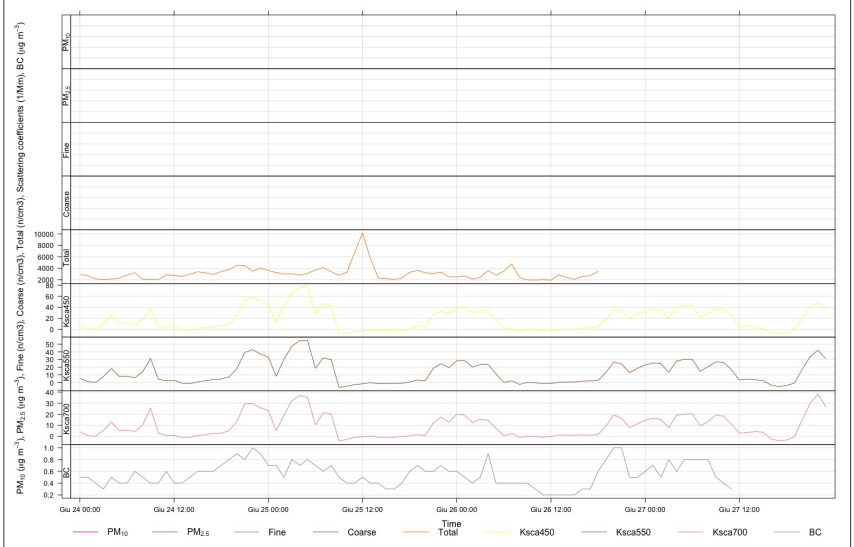

Event 32

(28 - 29 / 9 / 2016)

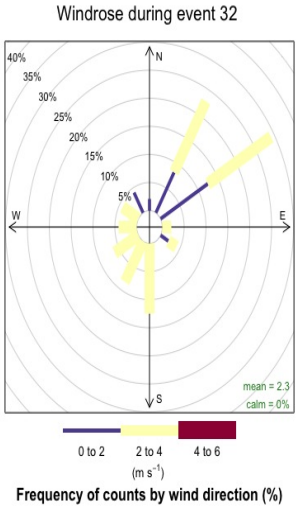

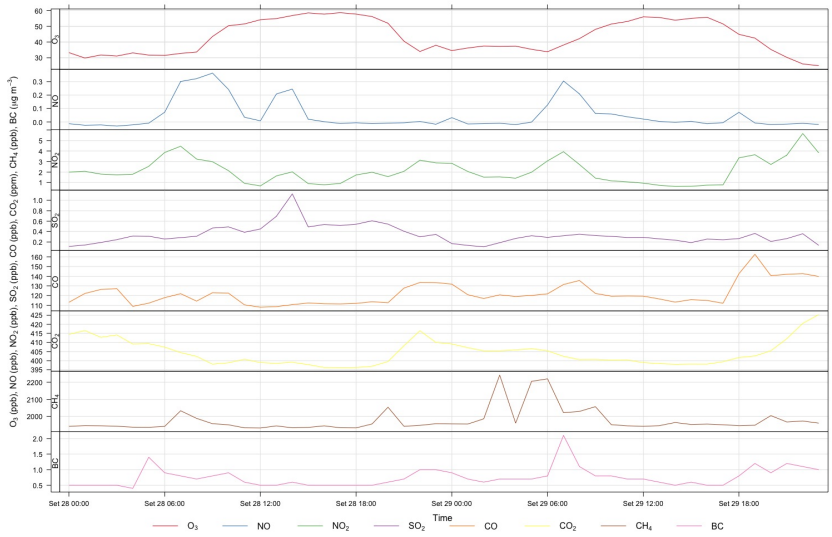

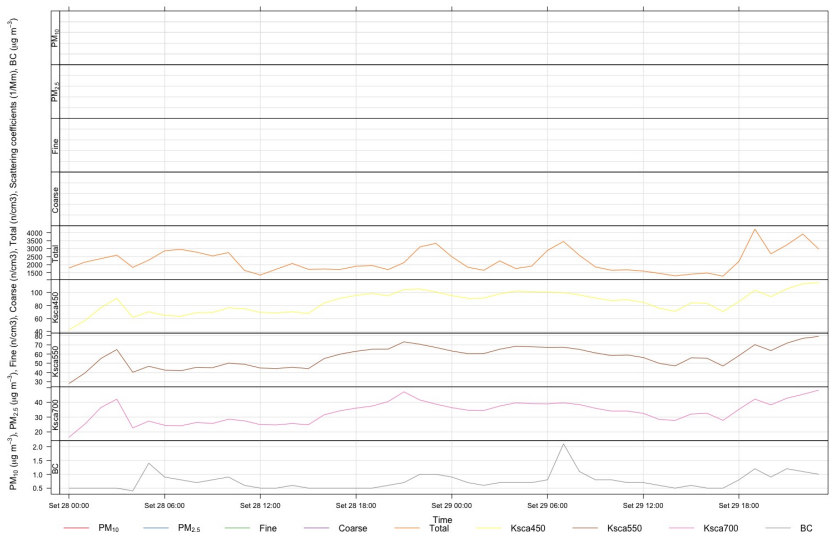

Event 33

(4 / 11 / 2016)

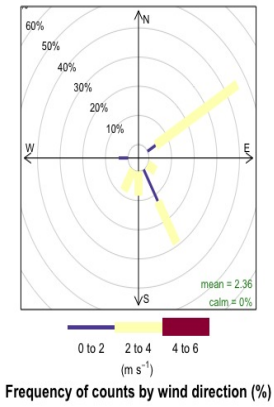

Frequency of counts by wind direction (%)

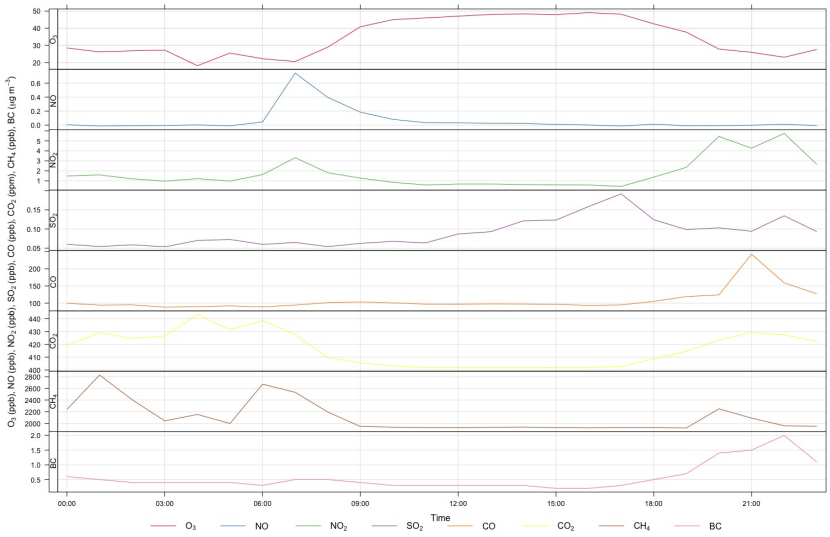

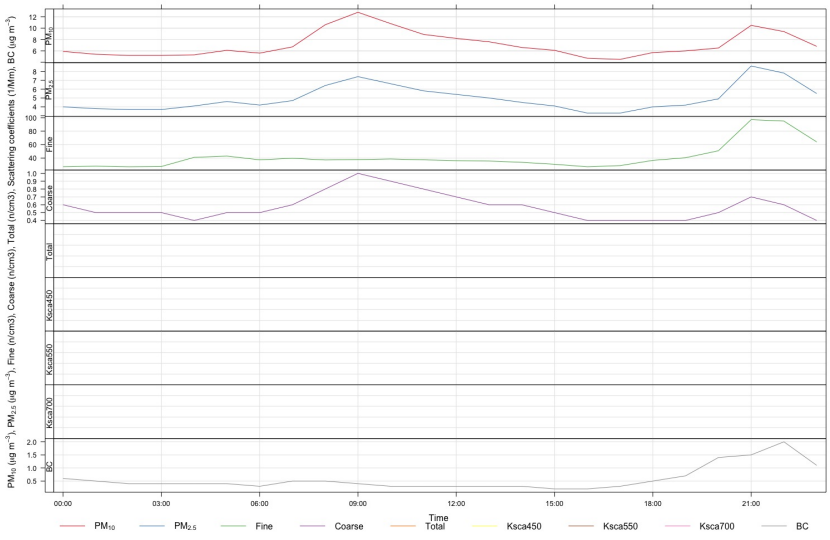

Event 34

(9 - 10 / 12 / 2016)

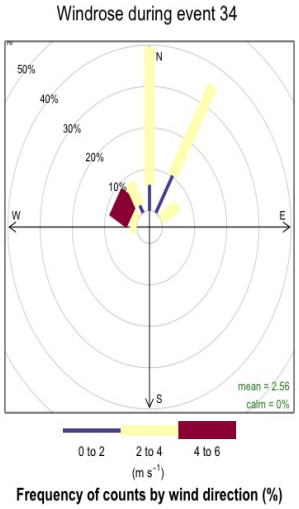

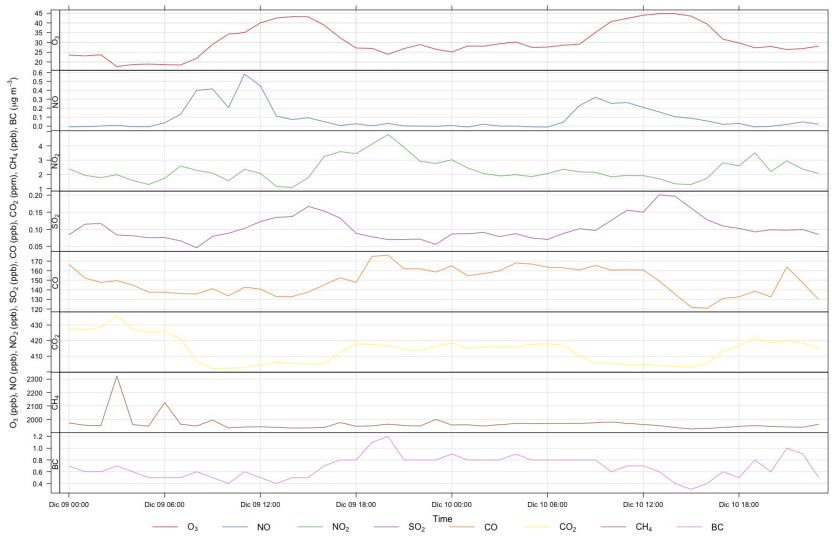

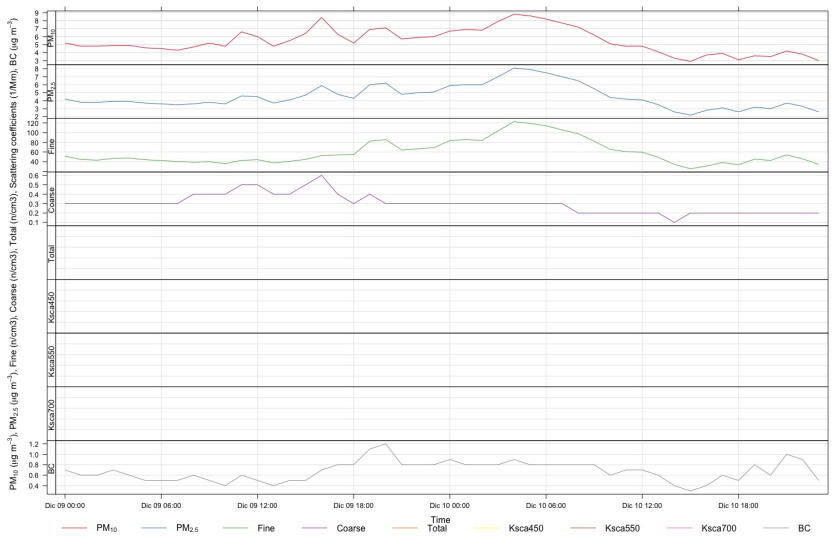

Event 35

(23 / 12 / 2016)

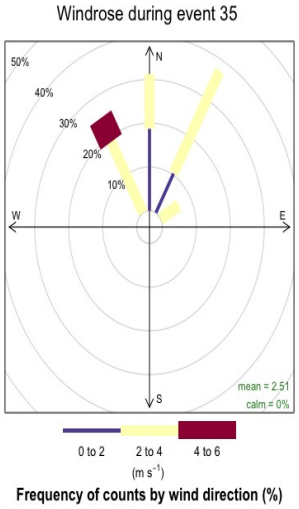

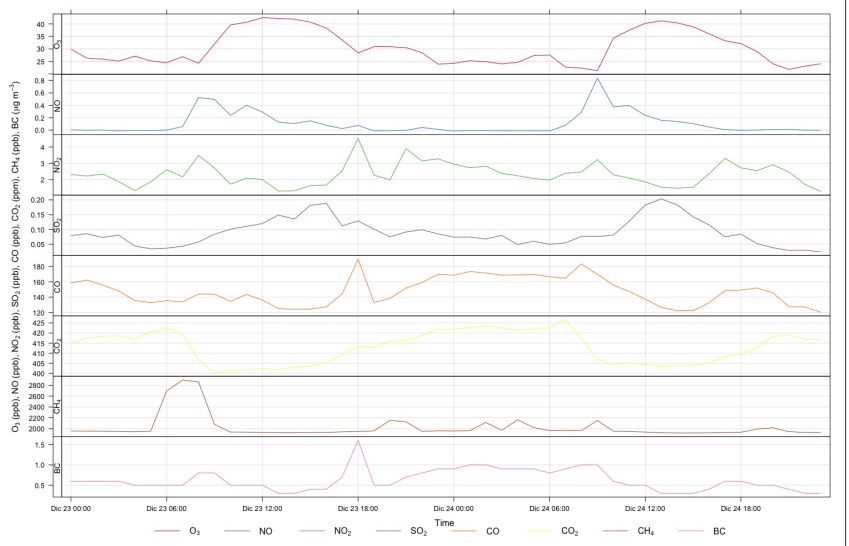

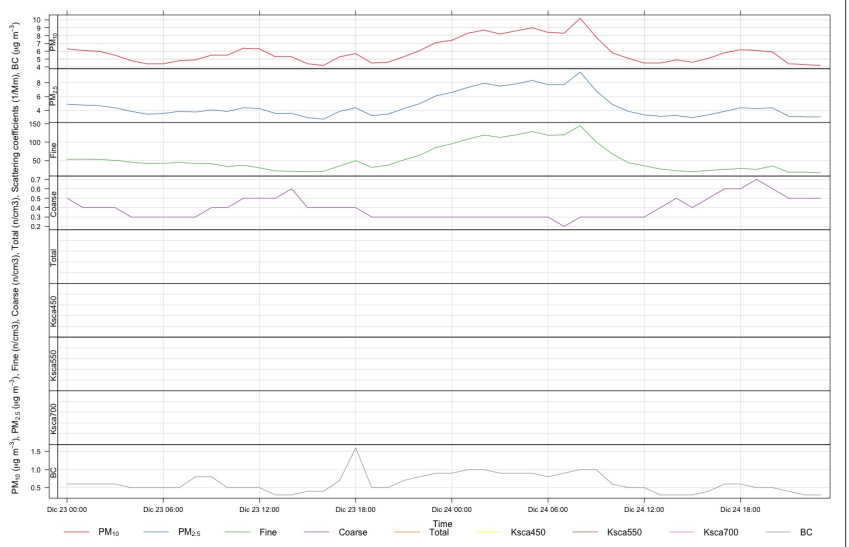

Wind rose in polluted days

During polluted days prevailing wind direction is WNW / ESE; as regards seasonal variation, this pattern is well respected in spring, as well as in autumn and winter, in some extent.

In summer, carrying - BC wind blows preferentially towards WNW.

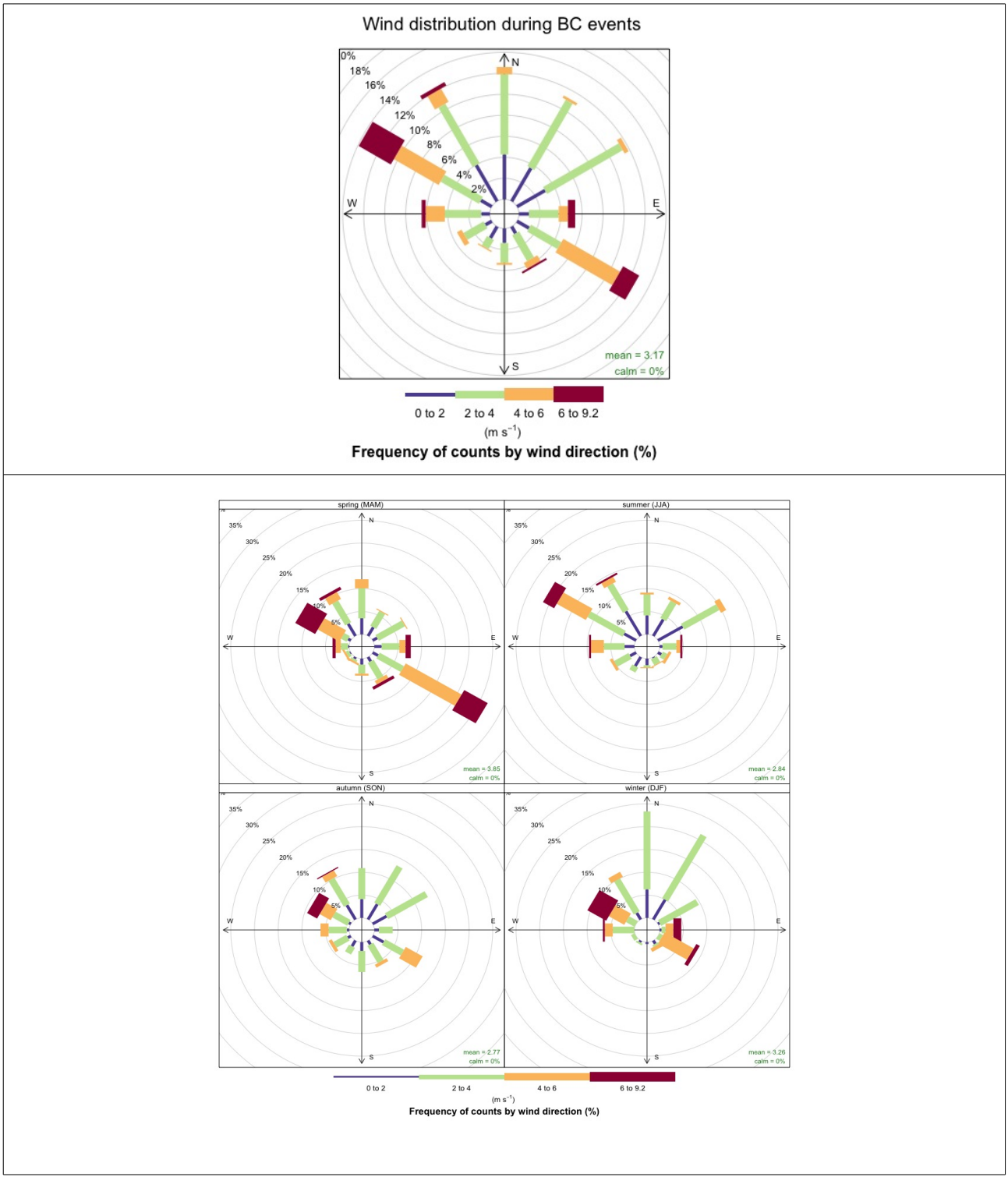

Scatter plot of BC and CO versus each monitored parameter (see Appendix 5) reported, together with the center detail (right column), clearly depict the absence of a clear correlation, except a somewhat link with CO concentration (p=0,4924), NO_2 concentration (p=0,4212), fine particles concentration (p=0,3828) and total particles concentration (p=0,3387).

Similarly, CO pattern resulted as more connectable to those ones of fine particles concentration (p=0,5740), total particles concentration (p=0,4981), scattering coefficients (p ranging from 0,3991 to 0,4578), NO_2 concentration (p=3861) and $PM_{2.5}$ mass concentration (p=0,3468).

4.2. Case studies

Afterwards, long – lasting events have been splitted because extending well beyond one - single - day time frame, for a sum of 52 elementary events, on overall.

Over this dataset, a threshold of 2,5 µg / m^3 was posed, as to select the most evident peak events in BC content, on hourly basis, and thus to facilitate the following case studies reasearch; the result was to isolate 18 elementary events from the initial 52 ones, on which a deeper analysis was conducted, to delucidate if air mass backtrajectory passed over the sea area of ship traffic dataset or land: in the first case a 6-h temporal horizon was considered, while in the last one 120-h backtrajectories were derived and contextual research for fires on satellite data was conducted.

17 selected events fall into 2015 year, just 1 into 2016 year.

EVENT	STARTING TIME (UTC)	BC PEAK VALUE (µg/m^3)
1	08/01/2015 20.00 UTC	14,7
02 a	14/01/2015 20.00 UTC	2,5
02 b	15/01/2015 20.00 UTC	3,4
04	03/03/2015 21.00 UTC	3,7
07 a	13/04/2015 2.00 UTC	2,7
07 b	21/04/2015 21.00 UTC	4,2
11b	06/06/2015 20.00 UTC	5,1
12	29/06/2015 21.00 UTC	3,9
13 a	17/07/2015 3.00 UTC	4,6
13 b	19/07/2015 20.00 UTC	3,8
13 c	20/07/2015 23.00 UTC	6
17 a	01/09/2015 3.00 UTC	3,5
17 b	03/09/2015 5.00 UTC	3,2
17 c	04/09/2015 23.00 UTC	4,7
19	23/09/2015 5.00 UTC	6,8
20	29/09/2015 5.00 UTC	6,2
25	19/11/2015 6.00 UTC	7,6
28	29/04/2016 23.00 UTC	3

Seasonal distribution of BC – pollution days in the most polluted subset resulted to be concentrated in summer, as represented in the following chart.

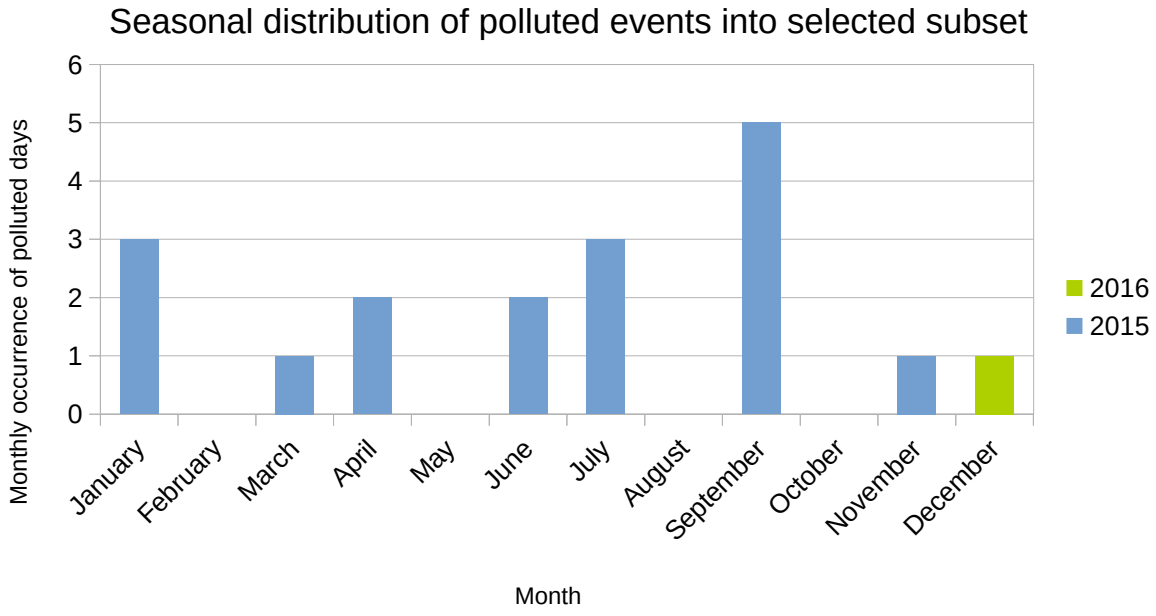

6 particularly considerable events were identified, during which backtrajectories had passed over meaningful ship traffic nuclei, according to ship traffic register, as well as 6 events in which backtrajectories crossed biomass burning locations, as reported by satellite data, 2 of which overlapping.

Of these ones, 7 cases remained unclassified because they have been ascertained as lacking of any meaningful ship traffic or biomass episode occurrence in the proximity of relative backtrajectories.

Selected subdataset of events and concerning data are following reported in chronological order.

Ship traffic case study 1 – Event 2b

(15/01/2015 - 20 UTC, BC = 3,4 µg / m^3)

BC event time span was about 4 hours, with a relative increment in BC mass concentration of about +600%.

Backtrajectory coming from SW overflied an intense ship traffic area, about 40 km off sicilian coast, crossing the route of a vehicle carrier travelling towards NW along sicilian coast 2 hours before the event, as well as the route of a fishing vessel just leaving the near harbour of Mazara del Vallo (TP) 3 hours before the event; going back in time (that means farther from the coast), 6 hours before the event backtrajectory had passed very close (lower than 5 km) to the route of a livestock carrier.

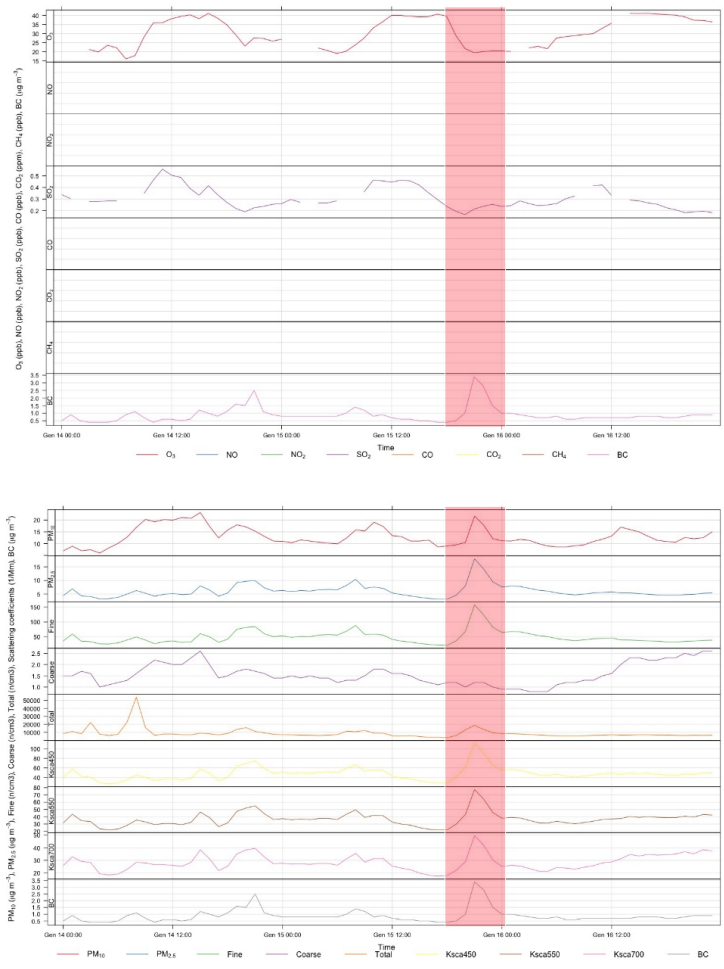

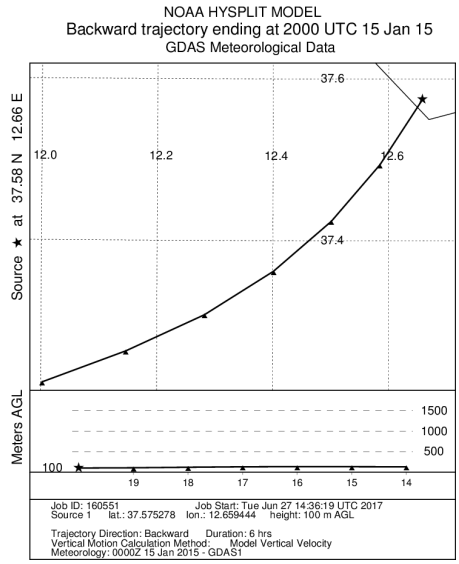

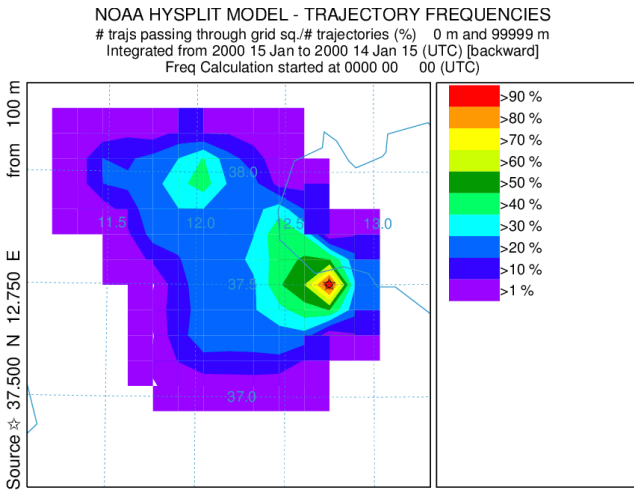

TIME DELAY (H)	DISTANCE (m)	SECTOR	LONG E	LAT N	YEAR BUILT	GROSS TONNAGE (t)
-2	28177,38	VEHICLES CARRIER	12,364437	37,474125	2012	60825
-3	28554,42	FISHING	12,613309	37,404302	NA	NA
-5	38522,49	LIVESTOCK CARRIER	11,726708	37,282270	1971	1879
-6	4590,98	LIVESTOCK CARRIER	11,979711	37,215922	1971	1879

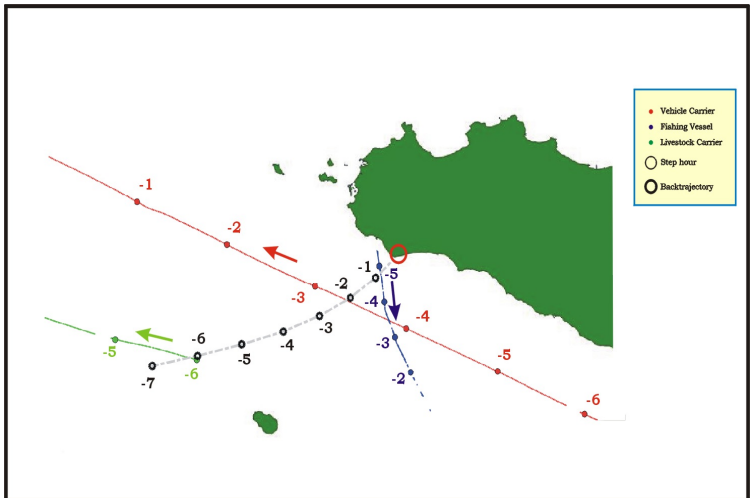

Ship traffic case study 2 – Event 4

(03/03/2015 - 21 UTC, BC = 3,7 µg / m^3)

BC event time span was about 5 hours, with a relative increment in BC mass concentration of about +270%.

Backtrajectory coming from NW was identified as crossing the route of a fishing vessel leaving the coast, as well as passing very close (lower than 6 km) the route of another fishing ship, 2 and 3 hours before the event, respectively.

In the same timeframe, during its travel, backtrajectory crossed the route of a passenger / ro-ro cargo ship, directed towards the near harbour of Trapani, where it arrived in about 1 hour.

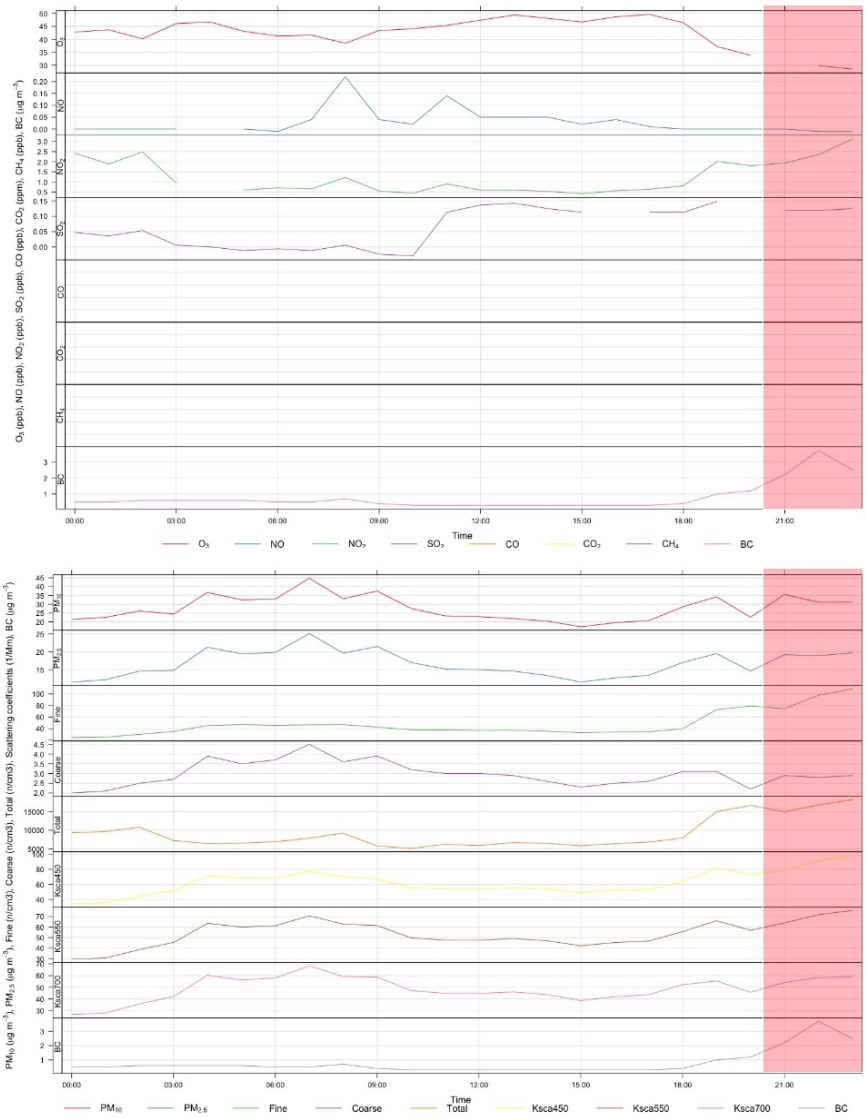

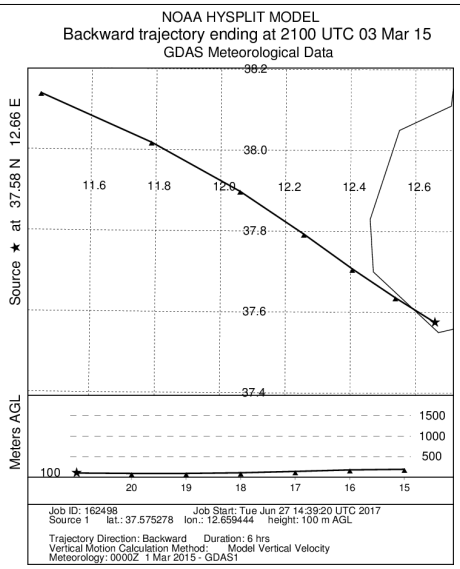

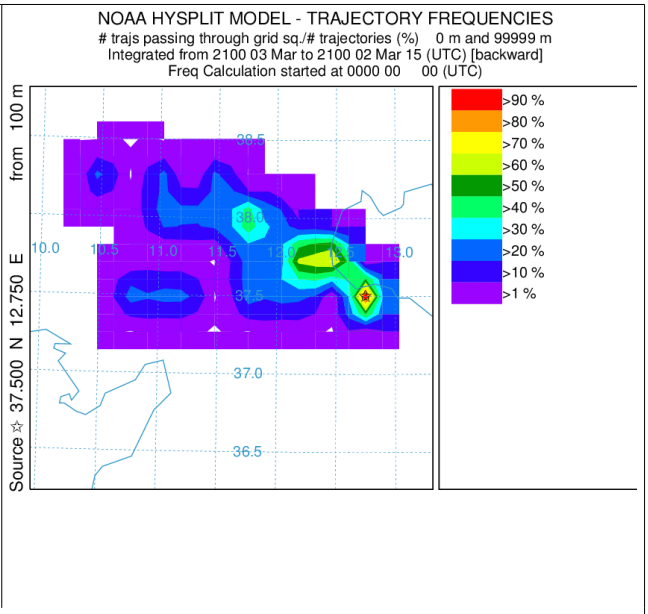

TIME DELAY (H)	DISTANCE (m)	SECTOR	LONG E	LAT N	YEAR BUILT	GROSS TONNAGE (t)
-2	17925,94	FISHING	12,206615	37,712876	NA	NA
-3	3379,68	PASSENGER / RO-RO CARGO	12,284779	37,797367	1979	4453
-3	5965,36	FISHING	12,209665	37,784478	NA	NA

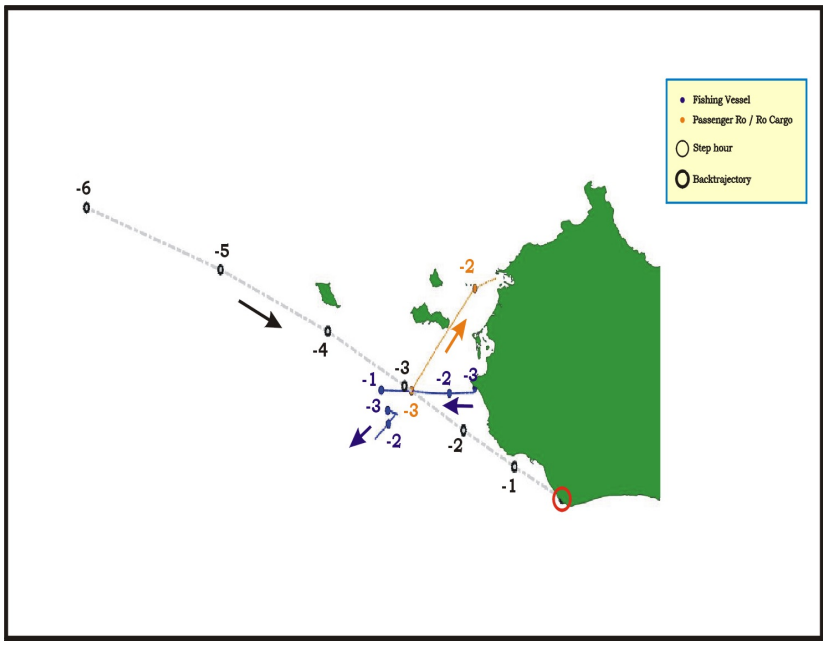

Ship traffic case study 3 – Event 7a

(13/04/2015 – 2 UTC, BC = 2,7 µg / m^3)

BC event time span was about 8 hours, with a relative increment in BC mass concentration of about +170%.

Backtrajectory coming from SE was identified as crossing the route of 5 fishing vessels directed towards NW, probably setting out from the near harbour of Sciacca (AG), in a timeframe between 3 and 2 hours before the event.

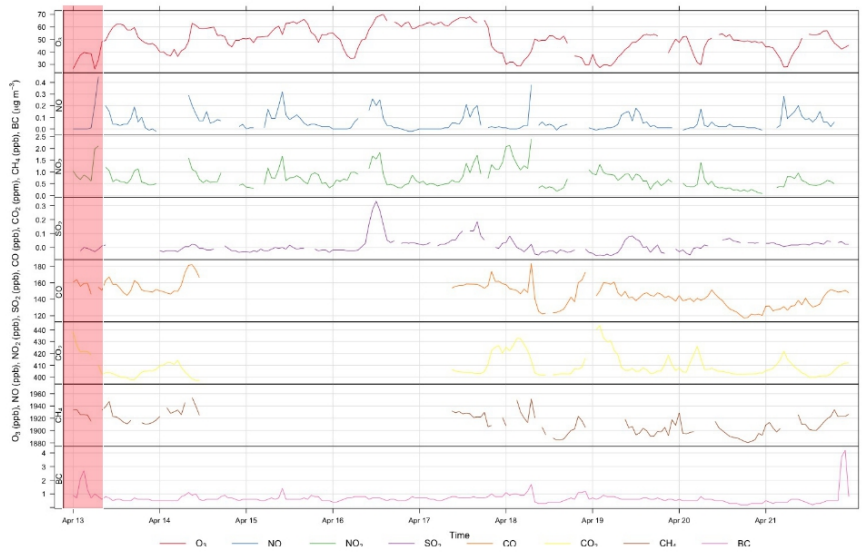

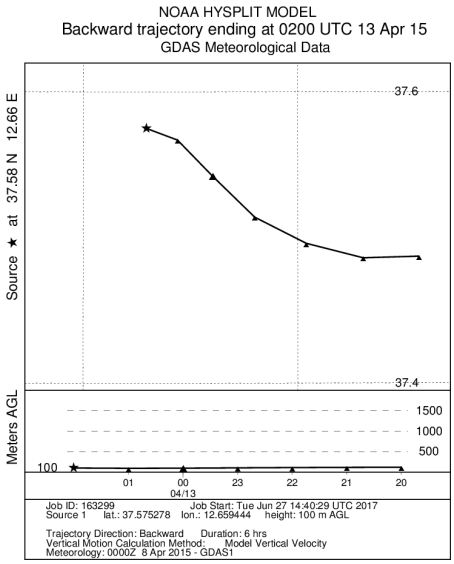

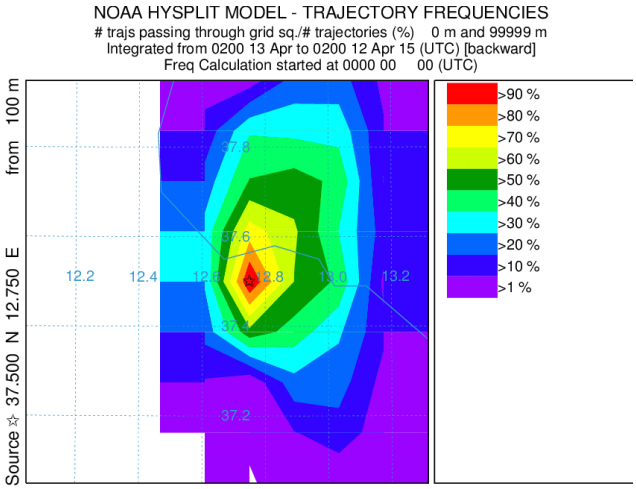

TIME DELAY (H)	DISTANCE (m)	SECTOR	LONG E	LAT N	YEAR BUILT	GROSS TONNAGE (t)
-1	9847,01	FISHING	12,602294	37,554661	NA	NA
-1	10237,62	FISHING	12,582292	37,558880	NA	NA
-1	10943,18	FISHING	12,596087	37,552610	NA	NA
-2	12041,43	FISHING	12,597372	37,551825	NA	NA
-2	12052,25	FISHING	12,601664	37,553374	NA	NA
-2	13321,55	FISHING	12,871084	37,540706	NA	NA
-2	13405,53	FISHING	12,587937	37,554545	NA	NA
-3	7639,49	FISHING	12,701661	37,525077	NA	NA
-3	9707,47	FISHING	12,692516	37,529060	NA	NA
-3	9793,00	FISHING	12,680467	37,527389	NA	NA
-3	11135,33	FISHING	12,851934	37,528947	NA	NA
-3	13214,97	FISHING	12,870991	37,531378	NA	NA
-4	16051,96	FISHING	12,858316	37,526377	NA	NA
-4	17406,88	FISHING	12,866282	37,528746	NA	NA
-4	20053,05	FISHING	12,691120	37,529822	NA	NA
-5	21429,82	FISHING	12,858518	37,528215	NA	NA
-5	23171,14	FISHING	12,850818	37,531613	NA	NA
-5	25919,51	FISHING	12,790955	37,535574	NA	NA
-6	20549,02	FISHING	13,055141	37,455023	NA	NA
-6	23130,41	FISHING	12,852069	37,531307	NA	NA
-6	23623,57	FISHING	12,846421	37,532062	NA	NA

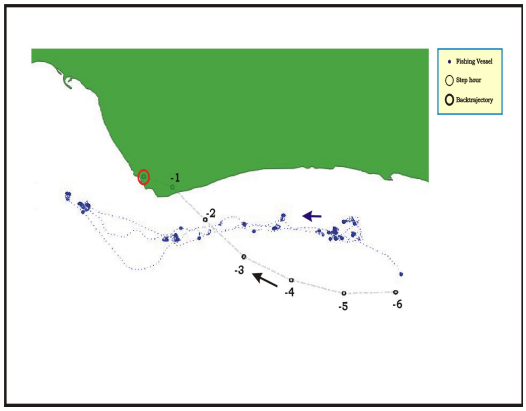

Ship traffic case study 4 – Event 13a

(17/07/2015 – 3 UTC, BC = 4,6 µg / m^3)

BC event time span was about 6 hours, with a relative increment in BC mass concentration of about +360%.

Backtrajectory coming from SE was identified as crossing the route of 9 fishing vessels directed towards SW, probably setting out from the near harbour of Sciacca (AG), in a timeframe between 4 and 5 hours before the event.

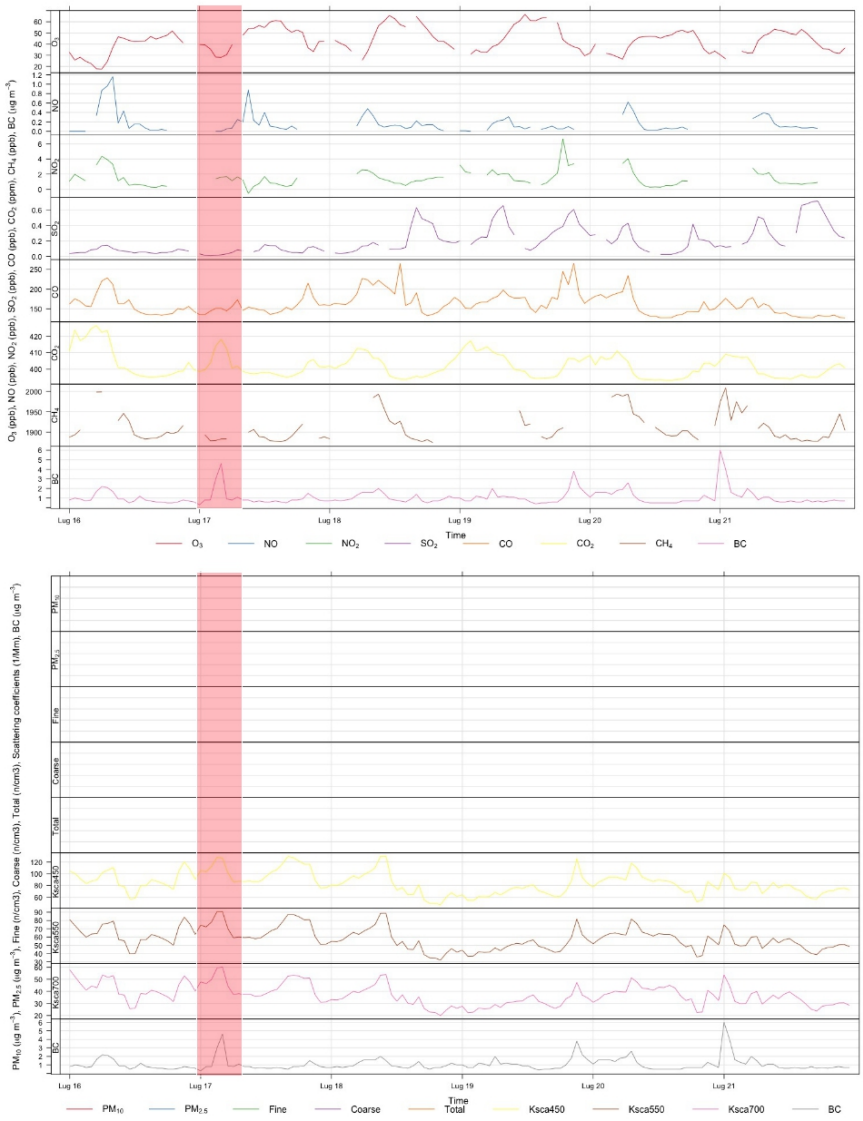

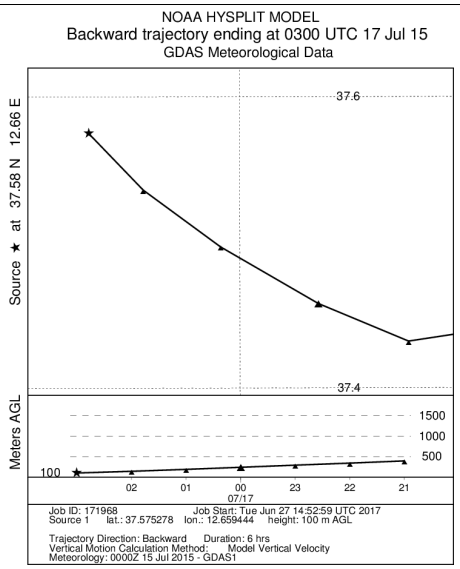

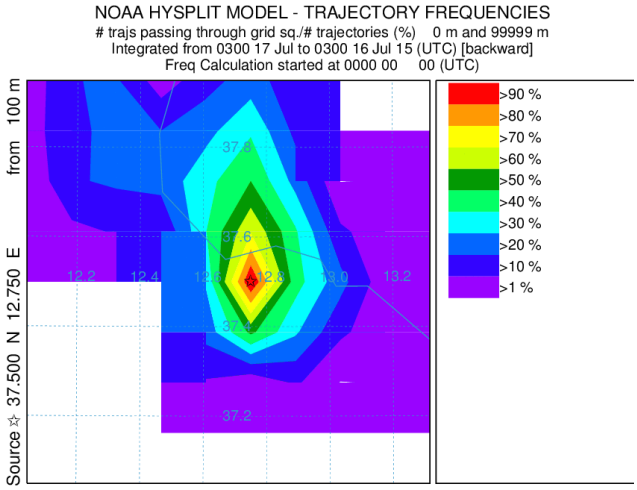

TIME DELAY (H)	DISTANCE (m)	SECTOR	LONG E	LAT N	YEAR BUILT	GROSS TONNAGE (t)
-2	7585,86	FISHING	12,712395	37,488308	NA	NA
-3	11100,09	FISHING	12,991646	37,451013	NA	NA
-3	11118,80	FISHING	12,995236	37,453096	NA	NA
-3	12609,39	FISHING	13,014379	37,455281	NA	NA
-3	12777,57	FISHING	13,016773	37,459774	NA	NA
-3	13788,22	FISHING	13,015046	37,469063	NA	NA
-3	14172,79	FISHING	12,911124	37,485115	NA	NA
-3	14263,69	FISHING	12,987663	37,438288	NA	NA
-3	17480,98	FISHING	13,021542	37,480648	NA	NA
-3	18951,61	FISHING	13,040802	37,481131	NA	NA

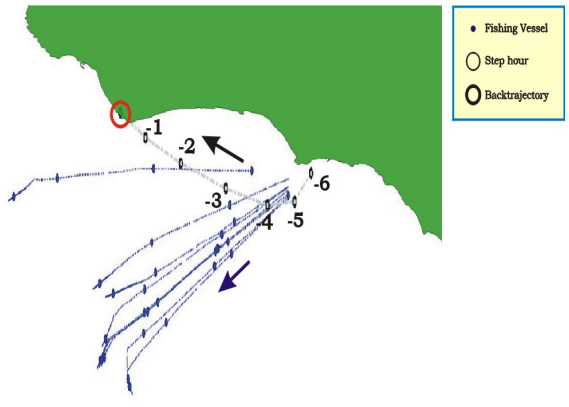

Ship traffic case study 5 – Event 17b

(03/09/2015 – 5 UTC, BC = 3,2 µg / m^3)

BC event time span was about 5 hours, with a relative increment in BC mass concentration of about +220%.

Backtrajectory coming from SW was identified as parallelling the route of 2 fishing vessels similarly directed towards the coast, in a long timeframe between 1 and 5 hours before the event.

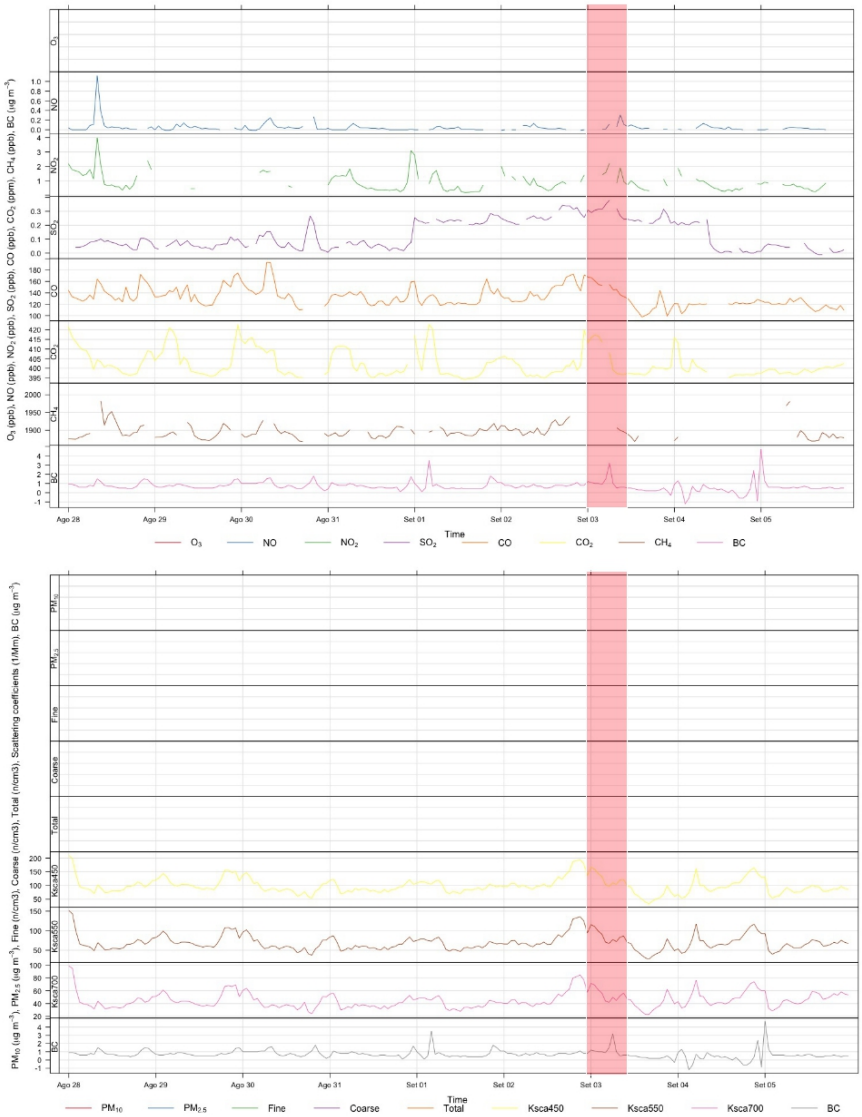

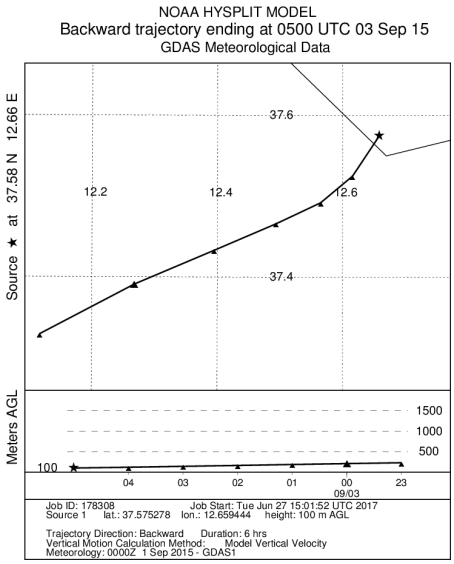

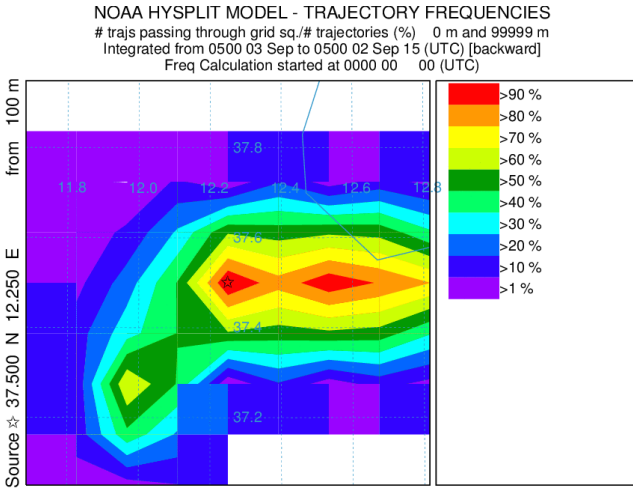

TIME DELAY (H)	DISTANCE (m)	SECTOR	LONG E	LAT N	YEAR BUILT	GROSS TONNAGE (t)
-1	22735,68	FISHING	12,367176	37,514153	NA	NA
-1	23468,98	FISHING	12,360252	37,513059	NA	NA
-2	21531,87	FISHING	12,322944	37,495490	NA	NA
-2	21782,43	FISHING	12,319603	37,494152	NA	NA
-3	24174,30	FISHING	12,246575	37,445981	NA	NA
-3	27989,55	FISHING	12,226099	37,436823	NA	NA
-4	17290,14	FISHING	12,209820	37,422311	NA	NA
-4	17574,22	FISHING	12,209044	37,421004	NA	NA
-5	13675,58	FISHING	12,155778	37,409485	NA	NA
-5	14505,83	FISHING	12,161148	37,412642	NA	NA

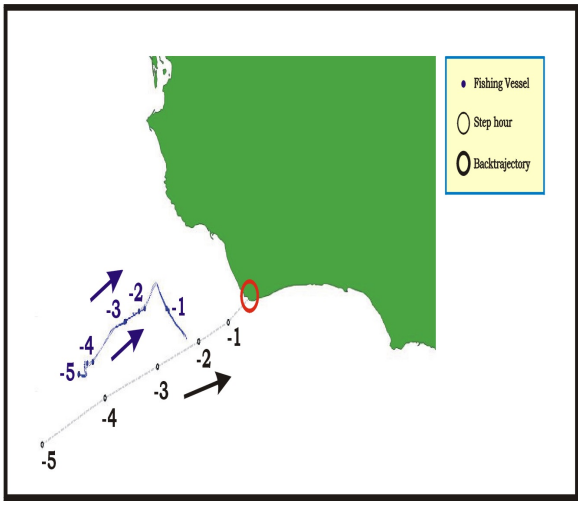

Ship traffic case study 6 – Event 19

(23/09/2015 – 5 UTC, BC = 6,8 µg / m^3)

BC event time span was about 3 hours, with a relative increment in BC mass concentration of about +1260%.

Backtrajectory coming from NW was identified as crossing the route of a fishing vessel leaving the coast in the immediate proximity of the event time; going back in time, backtrajectory crossed the oute of another fishing vessel directed towards W, 4 hours before the event, as well as that one of a passenger cruise ship going in SE direction (5 hours before the event) and that one of 2 chemical oil / products tankers similarly directed.

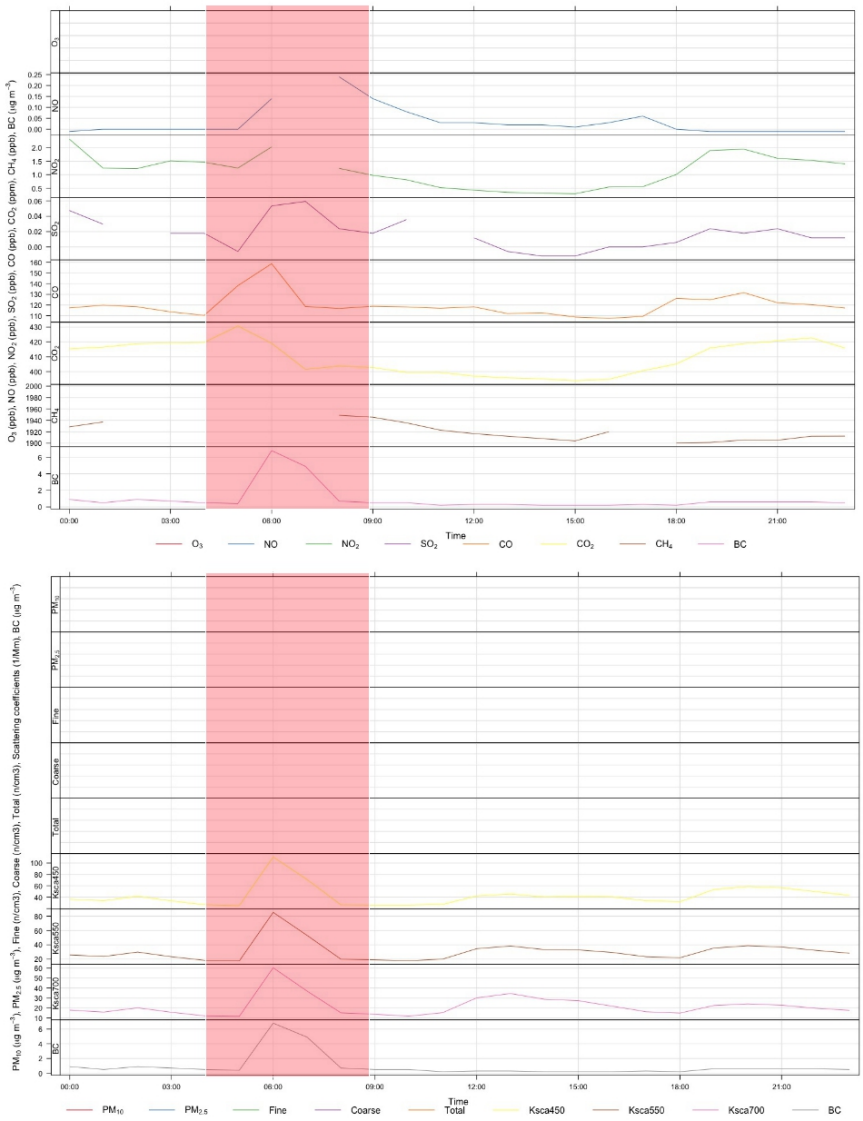

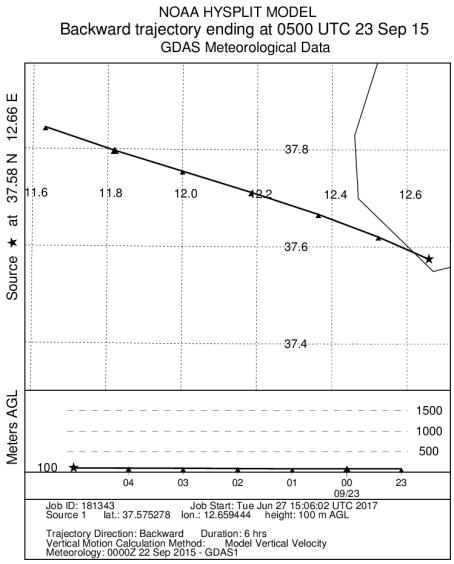

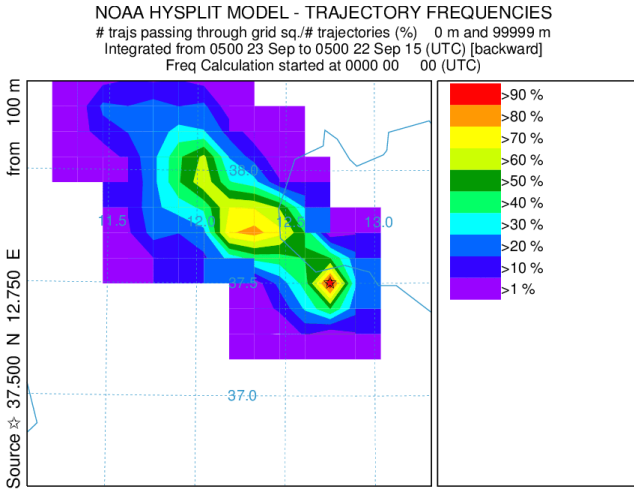

TIME DELAY (H)	DISTANCE (m)	SECTOR	LONG E	LAT N	YEAR BUILT	GROSS TONNAGE (t)
-1	5616,00	FISHING	12,586291	37,621471	NA	NA
-4	12079,83	FISHING	11,994622	37,731221	NA	NA
-5	2822,62	PASSENGER CRUISE SHIP	11,786643	37,796036	2012	113321
-5	6870,29	CHEMICAL / OIL PRODUCTS TANKER	11,816371	37,783469	2008	25467
-5	13747,81	CHEMICAL / OIL PRODUCTS TANKER	11,942119	37,813236	2011	7386
-6	15221,89	CHEMICAL / OIL PRODUCTS TANKER	11,576290	37,872304	NA	NA

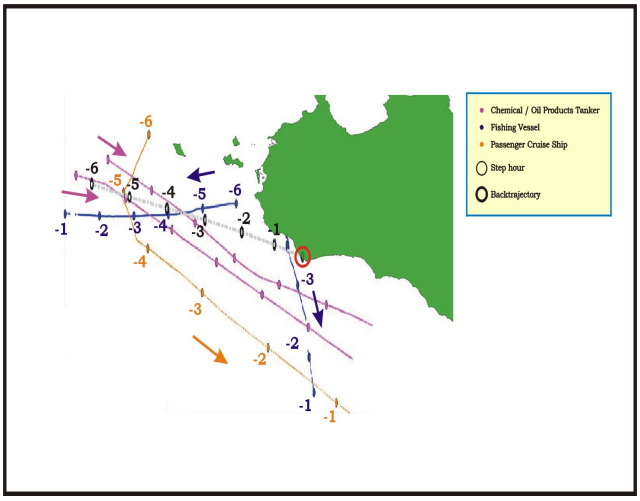

Wildfire case study 1 – Event 1

(08/01/2015 – 20 UTC, BC = 14,7 µg / m^3)

The event registered the January 8th 2015 was the main event registered during the two-year period, reaching the concentration of 14,7 µg / m^3 around 20.00 UTC. BC event time span was about 2 hours, with a relative increment in BC mass concentration of about +7300%.

Comparison between MODIS thermal fire / anomalies 8 days – dataset and HYSPLIT 120 – h backtrajectory coming from NW revealed the crossing of burning areas near the boundary between France and Spain, about 3 days before the event, whereas goig back in time backtrajectories meaningfully rises, quenching any possible fire – related contribution to sampled air mass composition.

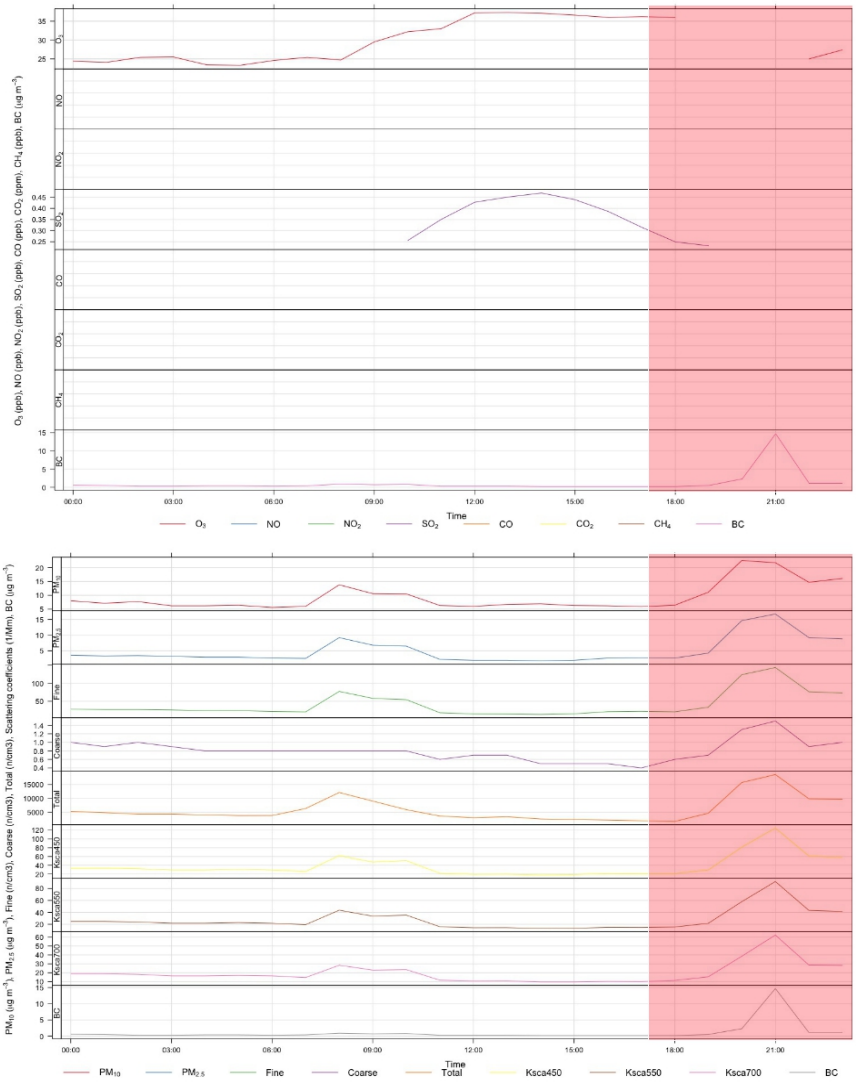

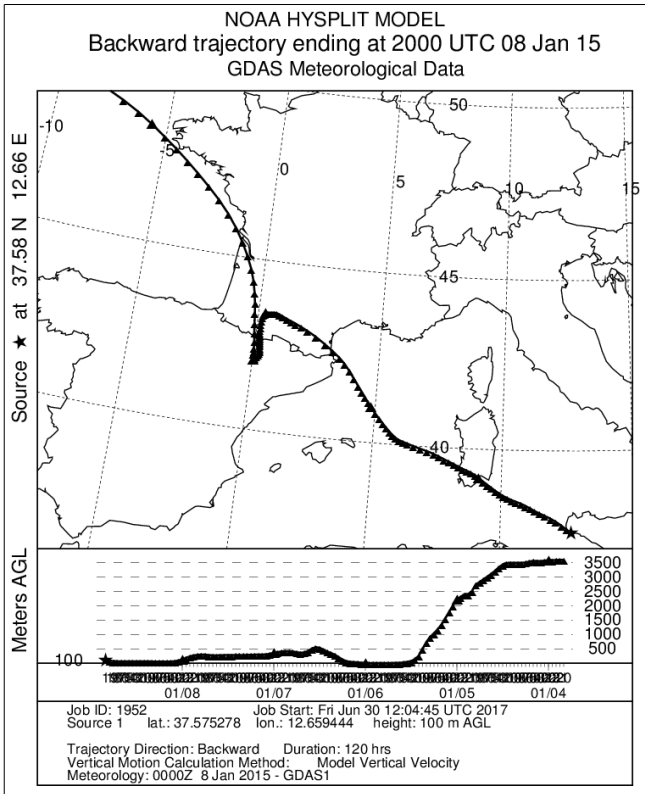

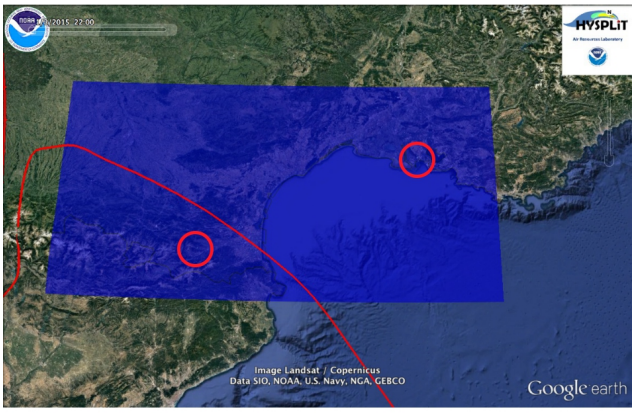

MODIS / Terra

MOD14A2.A2015001.h17v04.006.2015295052605.hdf
MOD14A2.A2015001.h18v04.006.2015295060428.hdf

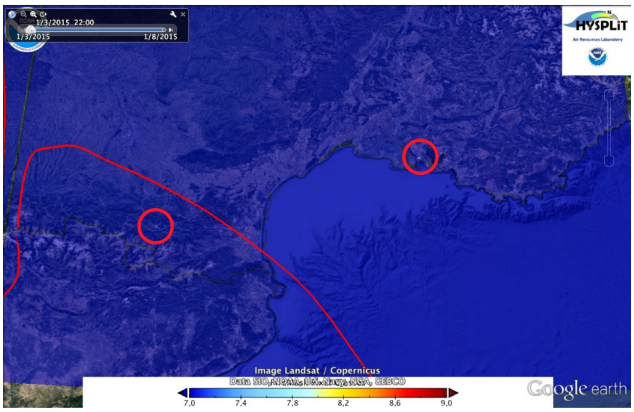

MODIS / Aqua

MYD14A2.A2015001.h17v04.006.2015295034935.hdf
MYD14A2.A2015001.h18v04.006.2015295041509.hdf

WILDFIRE COORDINATES

PROG.	LAT	LONG	COVER TYPE
01(1)	43°27'6.41"N	4°54'11.07"E	Urban area
01(2)	42°37'27.27"N	2°17'49.37"E	Mosaic HC / tree, shrub
01(3)	43°26'53.80"N	4°53'35.47"E	Shrub or herbaceous flooded
01(4)	42°29'59.08"N	2°18'57.14"E	Grassland

Wildfire case study 2 – Event 2(a/b)

(14-15/01/2015 – 20 / 20 UTC, BC = 2,5 – 3,4 µg / m^3)

BC event time span was about 5 (2a) + 5 (2b) hours, with relative increments in BC mass concentration of about +210% and +580%, respectively.

Comparison between MODIS dataset and HYSPLIT 120 – h backtrajectory coming from NW revealed the crossing of many burning areas near the boundary between Algeria and Tunisia, approximately 1 day before the event.

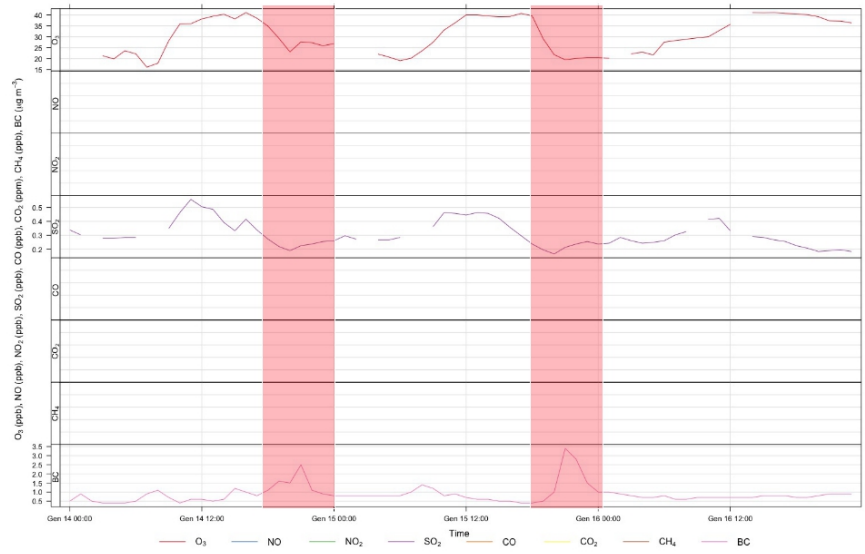

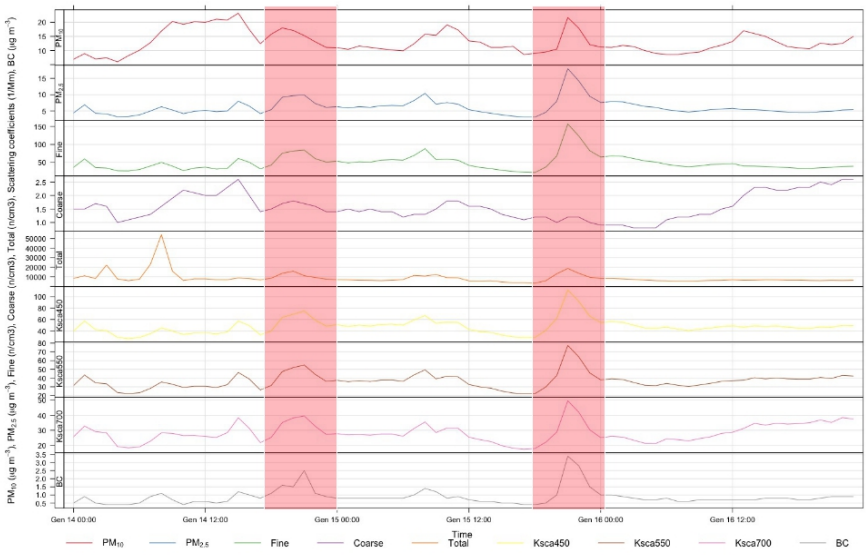

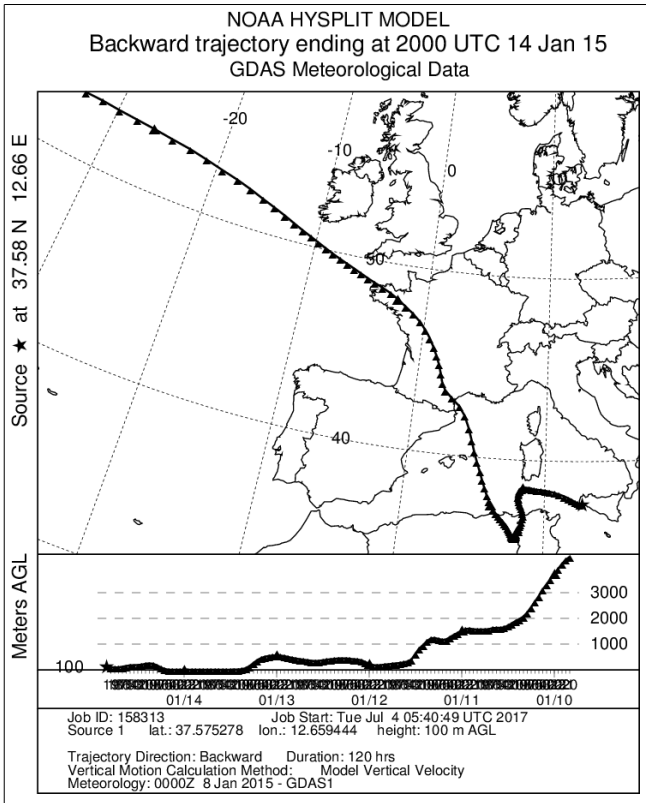

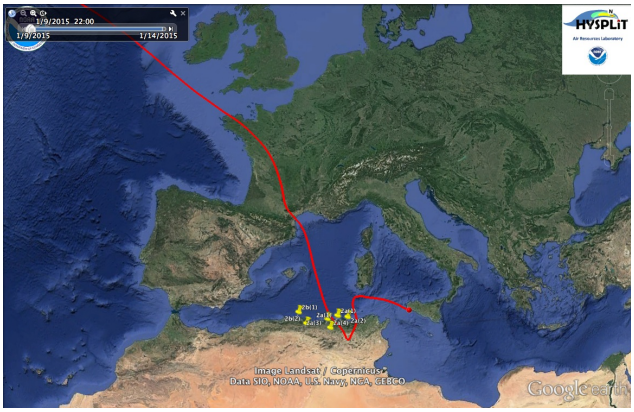

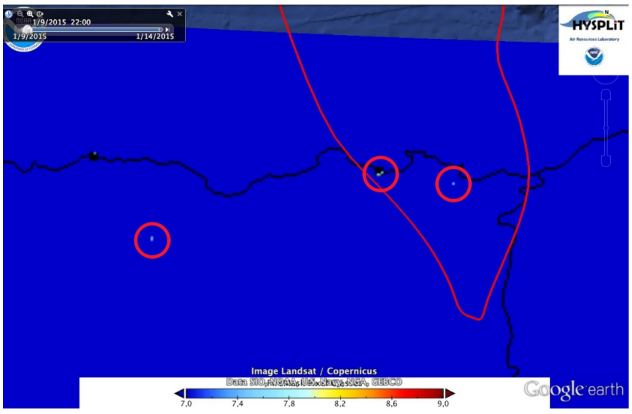

MODIS / Terra

MOD14A2.A2015313.h18v04.006.2015335131355.hdf
MOD14A2.A2015009.h19v05.006.2015295100919.hdf
MOD14A2.A2015009.h18v05.006.2015295101217.hdf

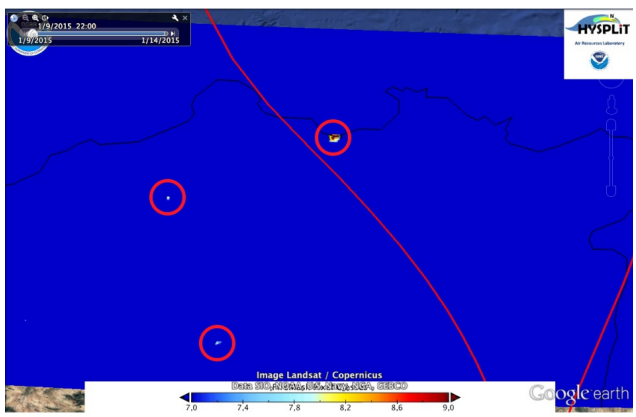

MODIS / Aqua

MYD14A2.A2015009.h18v06.006.2015295080644.hdf
MYD14A2.A2015009.h19v05.006.2015295081331.hdf
MYD14A2.A2015009.h18v05.006.2015295084913.hdf

WILDFIRE COORDINATES

PROG.	LAT	LONG	COVER TYPE
2 a(1)	36°52'6.39"N	6°55'49.45"E	Bare areas
2 a(2)	36°48'37.77"N	7°42'46.48"E	Tree broadleaved evergreen
2 a(3)	36°36'59.10"N	6° 9'37.82"E	Cropland, rainfed
2 a(4)	36° 4'4.39"N	6°25'42.81"E	Cropland, rainfed
2b(1)	36°54'45.50"N	3°54'10.63"E	Tree broadleaved deciduous
2b(2)	36°13'44.61"N	4°34'20.19"E	Shrubland

Wildfire case study 3 – Event 13a

(17/07/2015 – 3 UTC, BC = 4,6 µg / m^3)

BC event time span was about 5 hours, with a relative increment in BC mass concentration of about +475%.

Comparison between MODIS dataset and HYSPLIT 120 – h backtrajectory coming from N revealed the crossing of many large burning areas in central Sicily, no more than 1 day before the event, better highlighted by Terra sensor.

Particularly low - speed wind conditions over the investigated area, together with geographical proximity to the station, strengthen the correlation between fire occurrence and BC measurement.

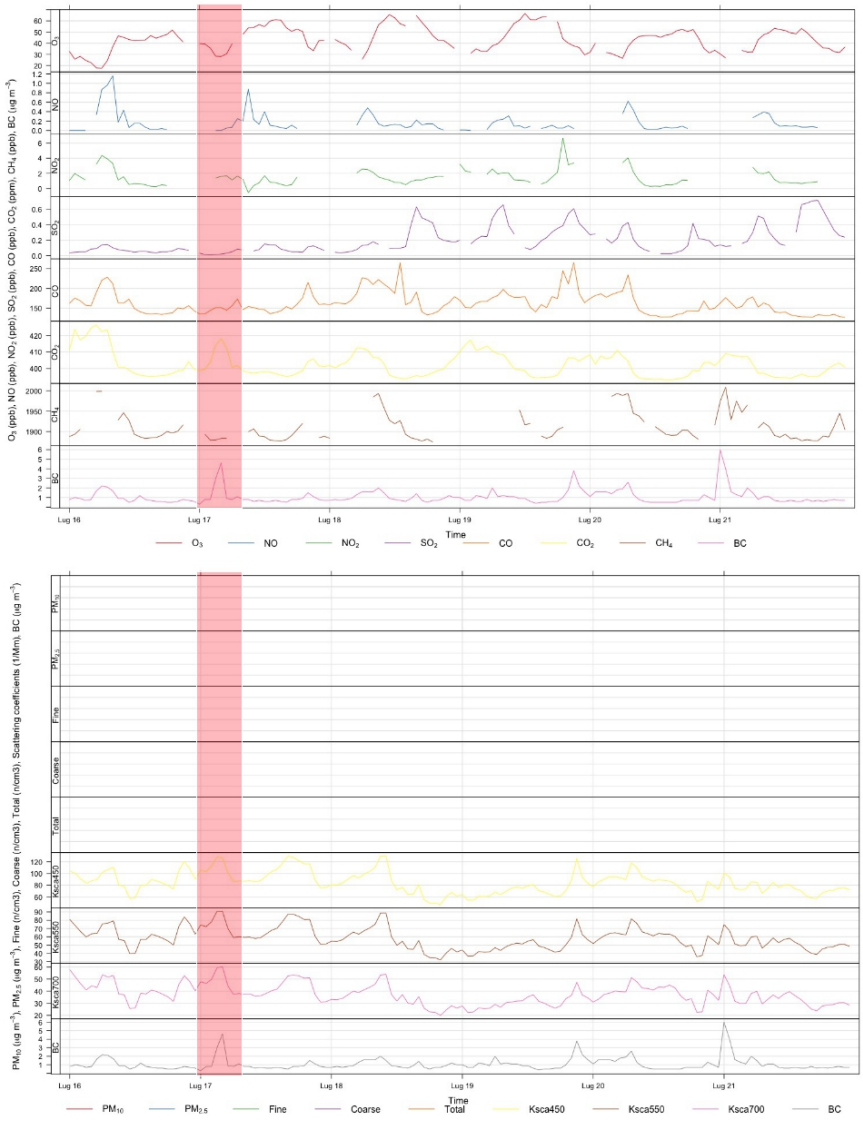

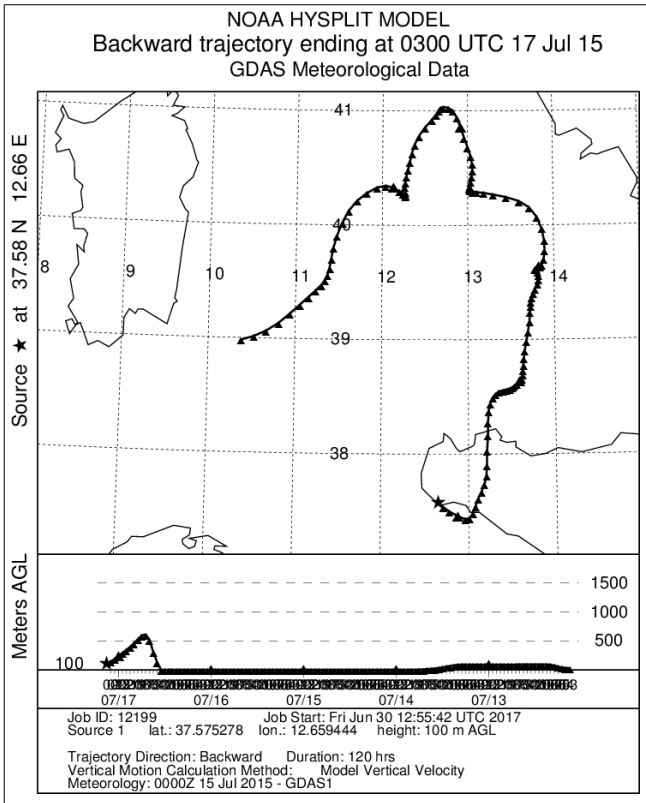

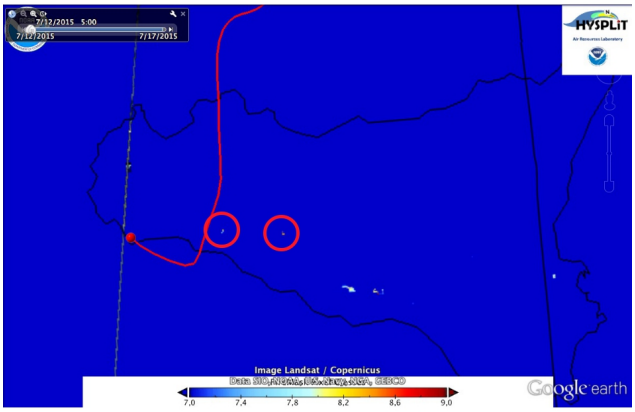

MODIS / Terra

MOD14A2.A2015193.h18v05.006.2015303024748.hdf
MOD14A2.A2015193.h19v05.006.2015303030037.hdf

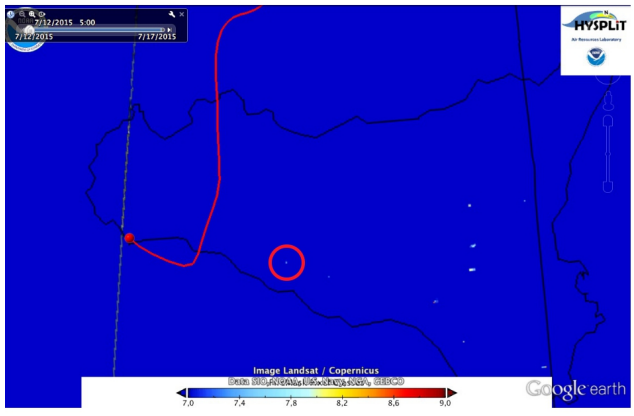

MODIS / Aqua

MYD14A2.A2015193.h18v05.006.2015303031329.hdf
MYD14A2.A2015193.h19v05.006.2015303031642.hdf

WILDFIRE COORDINATES

PROG.	LAT	LONG	COVER TYPE
13a(1)	37°24'40.25"N	13°32'44.64"E	Cropland, rainfed
13a(2)	37°34'1.90"N	13°11'17.97"E	Cropland, rainfed
13a(3)	37°32'22.43"N	13°32'6.50"E	Cropland, rainfed

Wildfire case study 4 – Event 13c

(20/07/2015 – 23 UTC, BC = 6,0 µg / m^3)

BC event time span was about 4 hours, with a relative increment in BC mass concentration of about +570%.

Comparison between MODIS dataset and HYSPLIT 120 – h backtrajectory coming from N revealed the crossing of many large burning areas in the western extremity of Sicily, no more than 1 day before the event.

Going back in time, backtrajectory height significantly raises, discouraging any further research of fire occurrence matching.

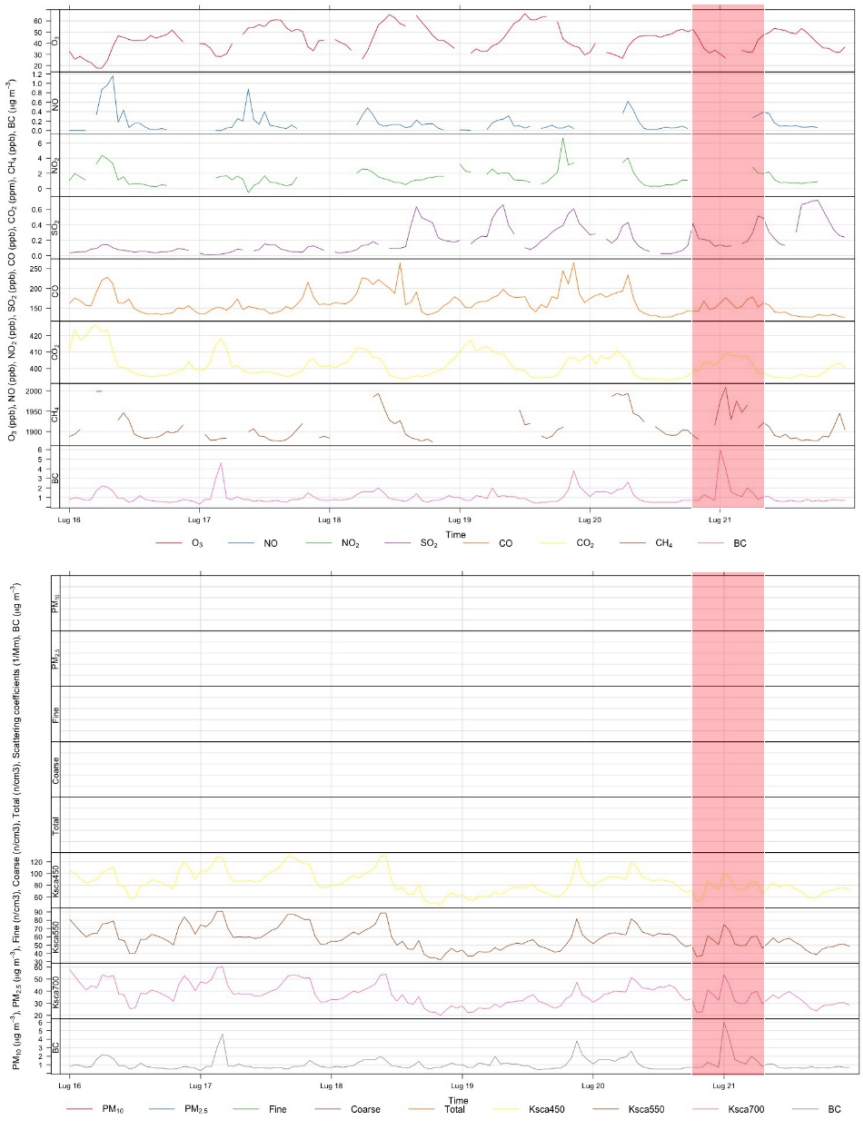

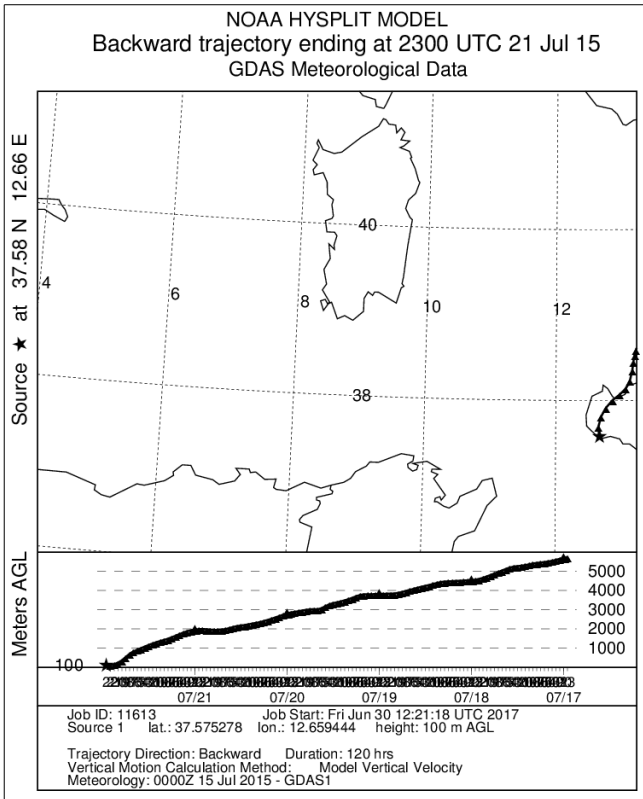

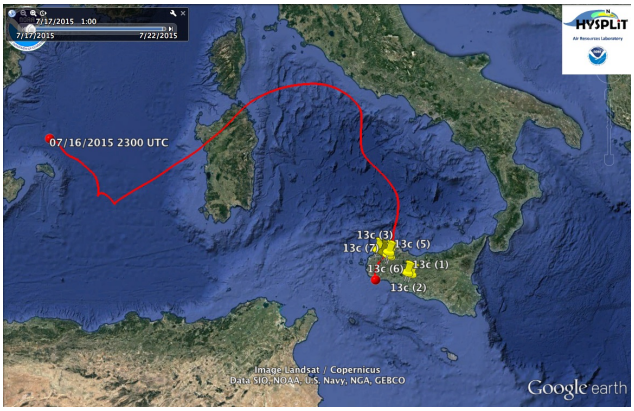

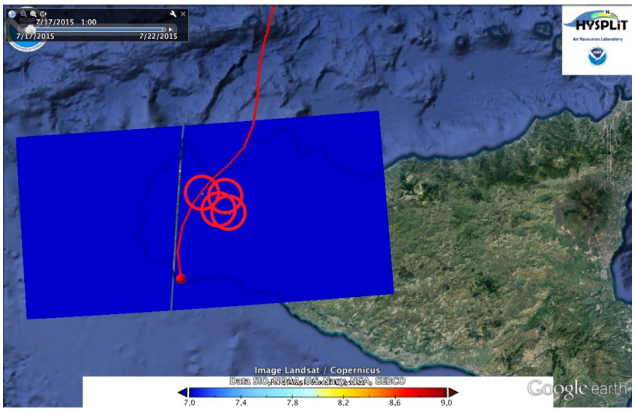

MODIS / Terra

MOD14A2.A2015201.h18v05.006.2015303232742.hdf
MOD14A2.A2015201.h19v05.006.2015303235202.hdf

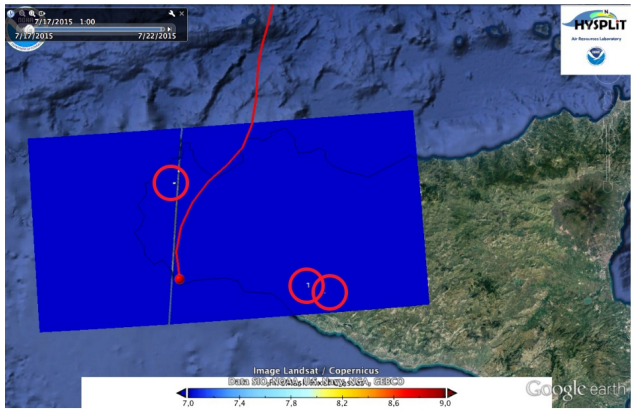

MODIS / Aqua

MYD14A2.A2015201.h19v05.006.2015303234030.hdf
MYD14A2.A2015201.h18v05.006.2015304000024.hdf

WILDFIRE COORDINATES

PROG.	LAT	LONG	COVER TYPE
13c (1)	37°29'58.89"N	13°22'40.94"E	Grassland
13c (2)	37°27'59.40"N	13°28'13.19"E	Grassland
13c (3)	38° 0'13.95"N	12°39'57.22"E	Cropland, rainfed
13c (4)	37°56'34.44"N	12°48'51.50"E	Cropland, rainfed
13c (5)	37°56'26.28"N	12°56'48.90"E	Cropland, rainfed
13c (6)	37°52'52.22"N	12°55'30.98"E	Cropland, rainfed
13c (7)	37°51'31.04"N	12°57'35.86"E	Cropland, rainfed

Wildfire case study 5 – Event 20

(29/09/2015 – 5 UTC, BC = 6,2 µg / m^3)

BC event time span was about 2 hours, with a relative increment in BC mass concentration of about +1900%.

Comparison between MODIS dataset and HYSPLIT 120 – h backtrajectory coming from N revealed the crossing of burning areas in Campania, about 3 days before the event.

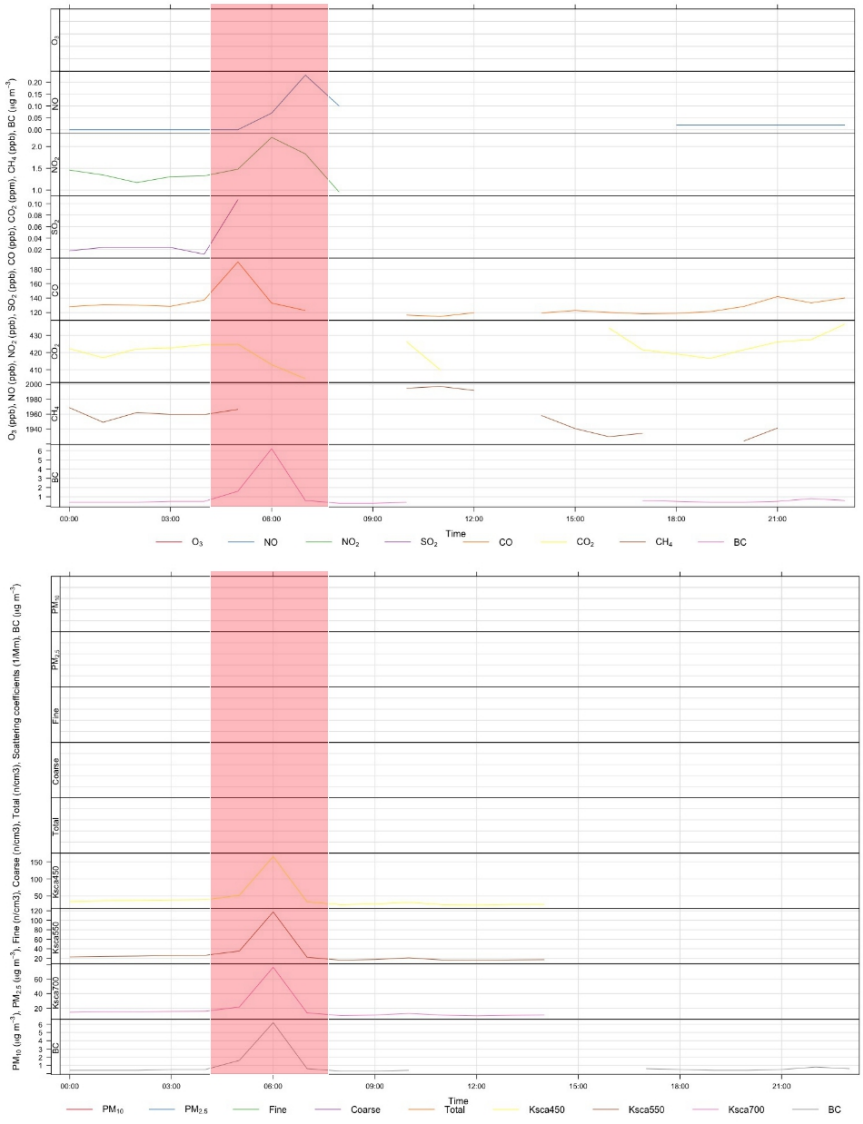

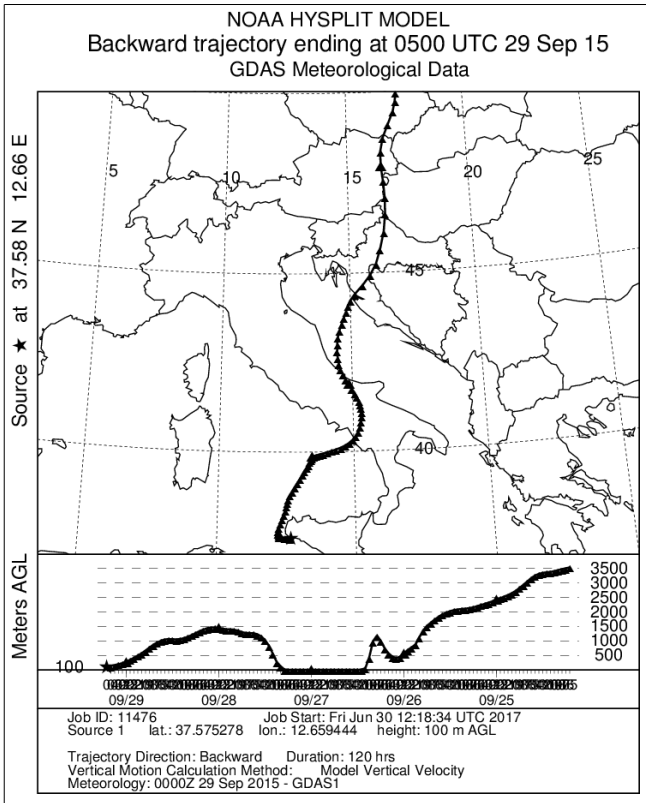

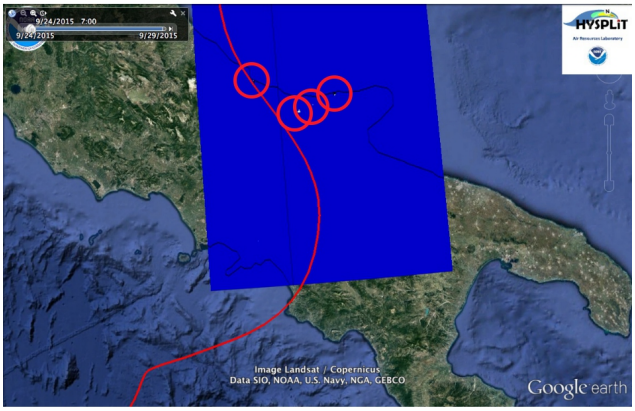

MODIS / Terra

MOD14A2.A2015265.h19v04.006.2015306145348.hdf

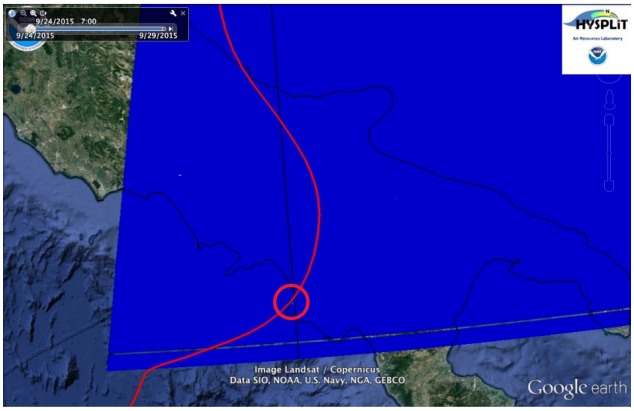

MODIS / Aqua

MYD14A2.A2015265.h19v04.006.2015307190916.hd

WILDFIRE COORDINATES

PROG.	LAT	LONG	COVER TYPE
20(1)	40°18'50.12"N	14°58'53.68"E	Cropland, rainfed
20(2)	41°47'48.36"N	15°12'12.33"E	Cropland, rainfed
20(3)	41°50'27.00"N	15°21'0.32"E	Mosaic cropland / vegetation
20(4)	41°54'8.71"N	15°35'34.19"E	Cropland, rainfed
20(5)	42° 3'45.72"N	14°45'15.78"E	Urban areas

Wildfire case study 6 – Event 25

(19/11/2015 – 6 UTC, BC = 7,6 µg / m^3)

BC event time span was about 5 hours, with a relative increment in BC mass concentration of about +1800%.

Comparison between MODIS dataset and HYSPLIT 120 – h backtrajectory coming from N revealed the approach to burning areas in Corsica island about 5 days before the event; going even back in time, it is possible to speculate on probable crossing of burning areas in northern Italy.

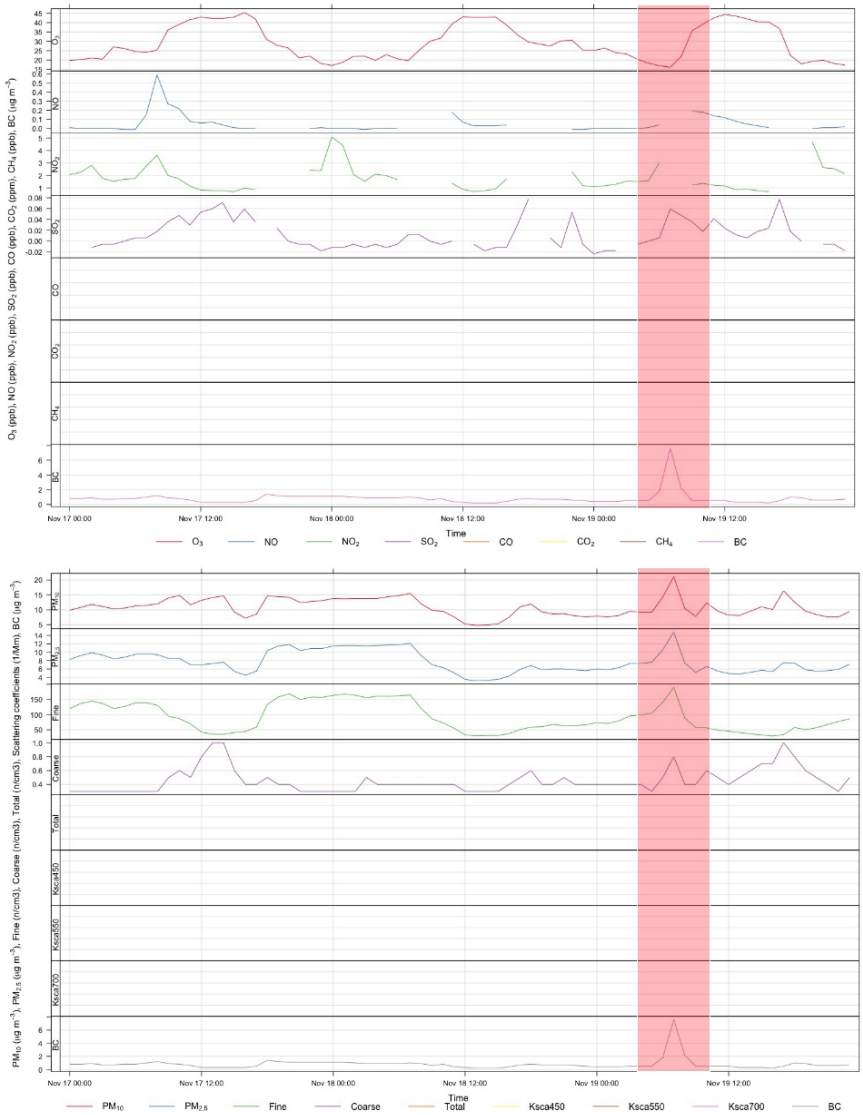

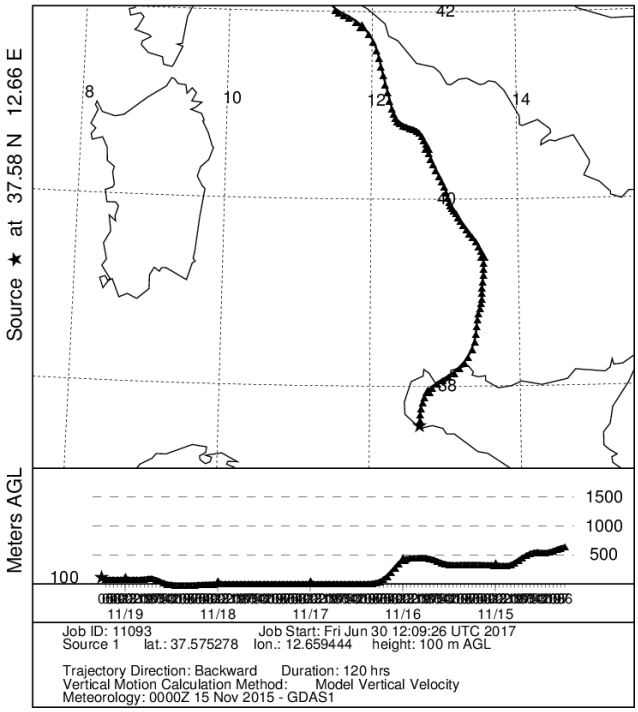

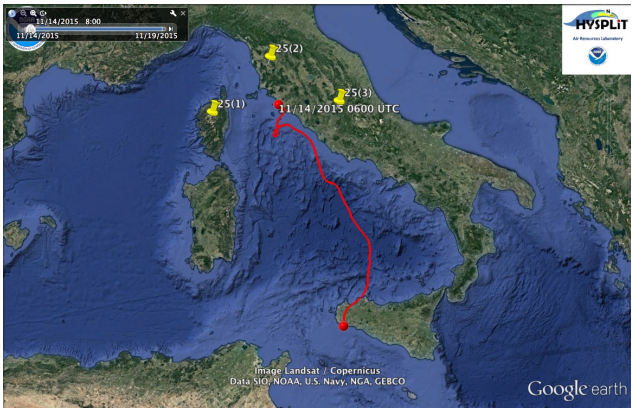

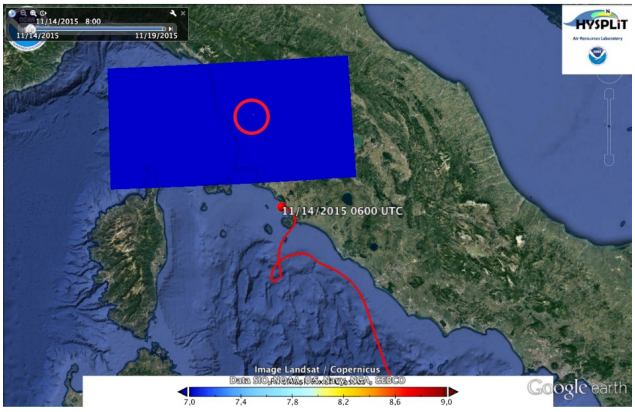

MODIS / Terra

MOD14A2.A2015313.h18v04.006.2015335131355.hdf

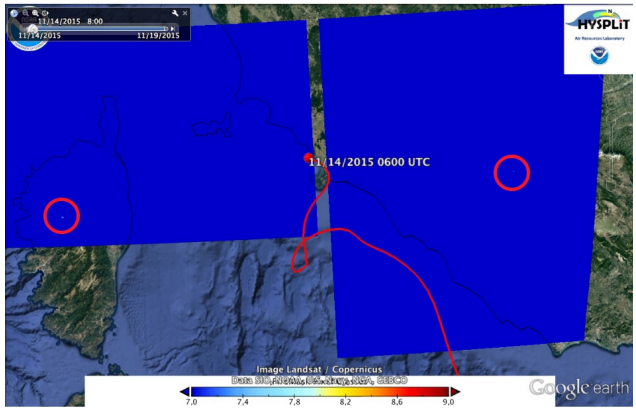

MODIS / Aqua

MYD14A2.A2015313.h18v04.006.2015334234230.hdf

WILDFIRE COORDINATES

PROG.	LAT	LONG	COVER TYPE
25(1)	42°14'51.02"N	8°58'42.94"E	Grassland
25(2)	43°27'5.59"N	10°46'51.86"E	Cropland, rainfed
25(3)	42°22'55.92"N	12°48'19.00"E	Tree broadleaved deciduous

5. CONCLUSIONS

The present project has substantially centered attention on the characterization of ship and wildfire emission transport events identified at the GAW Regional Station of Capo Granitola, in the southern of Sicily, thanks to black carbon observation analysis during 2015-2016.
Identification and analysis of 64 BC – pollution days during biennium 2015 – 2016, as detected by instrumental set, has been followed by the identification of 35 most salient events, during which the entire 22 – parameter dataset has been explored.

Among polluted days, 35 BC pollution events have been identified on the biennium basis, 1 to 9 days long, whose occurrence resulted to be concentrated on 2015 (25 out of 35 events).
Interestingly, scatter plots restricted to 35 polluted events confirmed the starting assumption of BC and CO as combustion tracers, expressing a somewhat link between BC and CO concentration (p=0,4924); BC peaks closer analysis of parameters variations during BC pollution events revealed that the prevailing wind direction in conjunction with BC peaks is north – westernly, with a secondary south – easternly occurrence peak on winter and spring; moreover, a well pronounced increment in scattering coefficients, CO, NO_2, fine particles and $PM_{2,5}$ parallel BC peaks.

Afterwards, a subset of 18 elementary events overcoming the threshold of 2,5 $\mu g/m^3$ in BC concentration has been furtherly investigated to elucidate the possible contribution of ship traffic and wildfire / biomass burning occurence in determining the value peak, as well as to try to localize their potential sources, in consideration of small and medium – scale circulation conditions in the hours before the event.

For each event, backtrajectories (BT) have been elaborated in a gathered way in order to help to discriminate if atmospheric circulation locally occurred upon ground or sea; afterwards, the most polluted events in which BT arrived by sea and by ground were chosen, respectively, and separately treated.
In consideration of limited spatial extension of ship traffic register available, BT were calculated in the timespan of previous 6 hours, with respect to the event BC peak time, when passing over sea, while were calculated in the timespan of previous 120 hours when passing over sea, because of the absenceof such a restriction whn dealing with satellite data.
Additionally, trajectory frequencies maps were produced, as to visualize the dynamic air mass transfer situation in the investigated area.

Data mining procedures have been applied on raw data from instrumental atmospheric monitoring and subsequently intersected with data from Automatic Information System (AIS) ship position tracking register and Moderate Resolution Imaging Spectroradiometer (MODIS) satellite remote sensing observation systems, in order to trace back and investigate the most remarkable case studies. The model' s computational approach HYSPLIT, which is extensively used in the atmospheric sciences community, has been extensively adopted for HYSPLIT backtrajectory (BT) analysis to determine the origin of air masses responsible for measures during event, taking into consideration travel times, in the intent to track air mass history and behavior and establish source-receptor relationships, on the basis of comparison with meteorological data.

Average BT were chosen as to ease spatial recognition of their eventual matching with ships and / or burning biomass points, and their contemporary travel altitude consideration allowed to exclude some BT sector in which air stream became excessively high.

The intersection between BT, satellite data and ship traffic register proved a powerful and promising instrument to take into account complexity of the instanteous BC pollution source configuration, which is dually in evolution, in space and time.
Such an integrated approach was adopted during the preliminary spatial analysis of BT for all 18 high - BC pollution events, to distinguish potentially ship – produced BC pollution events (BT passing over sea) from potentially fire – produced ones (BT passing over land); by this way, 12 case studies have been identified, 6 linked to ship traffic and 6 to wildfire occurrence.

Case studies analysis allowed to provide an outlook of richness and complexity of real – world situations falling into the investigated categories.
Case studies seasonal distribution is well balanced, with ship traffic – related BC – pollution events slightly prevailing on spring and autumn, while accountable wildfire centers detection prevailed on Sicily and Italy on summer and autumn, during wildfire – related BC – pollution events.

Among the investigated case studies, in 2 cases both types of occurrence resulted overlapped (ship case study 1 and wildfrire case study 2, during event 2b, and ship case study 4 and wildfrire case study 3, during event 13a) as a result of the particular backtrajectory direction, seeming to suggest a shared accountability between ship and wildfire contribution: this aspect provides a further confirmation of the extreme vulnerability of the Mediterranean basin as a climatic hotspot, for which new development paradigms will need to be elaborated.

In particular, the extremely intense and diversified ship traffic, even if prevalently devoted to fishing activities, can account for BC pollution signalled in the observational site, notwithstanding the spatial exiguity of dataset analyzed, because of spatial proximity to impact receptor and temporal coincidence of emission.

On the other hand, when dealing with wildfires, in some case studies the distance between potential source and receptor appears excessive to support an unequivocal identification of real pollution core.
Geographical and temporal identification of fires was provided by the MODIS fire product MOD14A2 and MYD14A2, summing up 8 days of satellite observations, thus it has not been always useful in estimating if a fire occurred in the proximity of backtrajectory, thus requiring the consideration of 2 temporally contiguous images to appreciate the presence of fires in the far past with respect to the event time.
Land cover data analysis for reported burning areas, even if categorical, provided an indirect confirmation of the exact identification o fires, since all fires resulted to happen on potentially fire – prone vegetation patterns.
Fire data analysis confirmed the potential responsibility of fire episodes on western Sicily and north Africa for determining BC peaks at the observational site, with the intriguing possibility that even more distant sources could be identified; despite this, it must be clarified that no confirmation is provided in this work. On the whole, the seasonal trend of biomass burning contribution was found to prevail during the hotter and drier spring / summer period, even if more relevant episodes can account for BC peaks in autumn / winter semester.

Because of the lack of chemical data for the BC – polluted days, together with the unavailability of quantitative data as regards ship engines and emission rate on one side and fire conditions on the other side, this investigation should be considered as an exploratory study needing for further improvement, but sheding light on the innovative valence of such a multidisciplinary approach for the development of reliable environmental monitoring observation networks for characterization of atmospheric pollution phenomena at mediterranean scale, particularly in the sicilian context.
On the whole, case studies analyses allowed to confirm the environmental burden of marine transport and wildfire occurrence on mediterranean coastal atmosphere composition.

In conclusion, the precious role of the coastal area investigated, placed far away from industrial plants, relies in its position in a remote coastal rather unpolluted mediterranean area: this feature has

the double benefit to ensure scientific atmospheric assessment in a background (pristine) area, as well as to provide data for modelization of forecasting tools for evaluation of impacts coming from sea – derived and ground – based events.

At the same time, the observational data acquired at the Capo Granitola Observatory, the only GAW-WMO station present on the island of Sicily, will help to better characterize the climate aspects of the Mediterranean Basin and, together with what is shown in this thesis, will facilitate the promotion of mitigation policies, paying particular attention to SLCF.

6. BIBLIOGRAPHY

Andreae M. O., 1995. *Climate effects of changing atmospheric aerosol levels*. In: World Survey of Climatology, Future Climate of the World, Vol. 16, Henderson-Sellers, A. (Ed.), 341–392, Elsevier, Amsterdam, 1995.Andreae M. O., 1991. Biomass burning: its history, use, and distribution and its impact on environmental quality and global climate, in Global Biomass Burning, edited by J. S. Levine, pp. 3–21, MIT Press, Cambridge, Mass.

Becagli S., Sferlazzo D. M., Pace G., Di Sarra A., Bommarito C., Calzolai G., Ghedini C., Lucarelli F., Meloni D., Monteleone F., Severi M., Traversi R., Udisti R., 2012. *Evidence for heavy fuel oil combustion aerosols from chemical analyses at the island of Lampedusa: a possible large role of ships emissions in the Mediterranean*. Atmos. Chem. Phys. 12: 3479 - 3492.

Becagli S., Sferlazzo D. M., Pace G., Di Sarra A., Bommarito C., Calzolai G., Ghedini C., Lucarelli F., Meloni D., Monteleone F., Severi M., Traversi R., Udisti R., 2011. *Evidence for ships emissions in the central Mediterranean Sea from aerosol chemical analyses at the island of Lampedusa* . Atmos. Chem. Phys. Discuss., 11, 29915–29947, 2011.

Bonasoni P., Cristofanelli P., Calzolari F., Bonafè U., Evangelisti F., Stohl A., Zauli Sajani S., van Dingenen R., Colombo T., Balkanski Y., 2004. *Aerosol-ozone correlations during dust transport episodes*. Atmos. Chem. Phys., 4, 1201–1215, 2004.

Bond T. C., Doherty S. J., Fahey D. W., Forster P. M., Berntsen T., De Angelo B. J., Flanner M. G., Ghan S., Kärcher B., Koch D., Kinne S., Kondo Y., Quinn P. K., Sarofim M. C., Schultz M. G., Schulz M., Venkataraman C., Zhang H., Zhang S., Bellouin N., Guttikunda S. K., Hopke P. K., Jacobson M. Z., Kaiser J. W., Klimont Z., Lohmann U., Schwarz J. P., Shindell D., Storelvmo T., Warren S. G., Zender C. S., 2013. *Bounding the role of black carbon in the climate system: A scientific assessment*. Journal of Geophysical Research: Atmospheres, Vol. 118, 5380 – 5552, 2013.

Bond T. C., Streets D. G., Yarber K. F., Nelson S. M., Woo J. H., Klimont Z., 2004. *A technology-based global inventory of black carbon and organic carbon emissions from combustion*. J. Geophys. Res., 109, D14203, 2004.

Cesari D., Donateo A., Conte M., Merico E., Giangreco A., Giangreco F., Contini D., 2016. *An inter-comparison of PM2.5 at urban and urban background sites: Chemical characterization and source apportionment*. Atmosperic Research 174 - 175 (2016) 106 - 119.

Chen Y., Paytan A., Chase Z., Measures C., Beck A. J., San˜udo-Wilhelmy S. A., Post A. F., 2008. *Sources and fluxes of atmospheric trace elements to the Gulf of Aqaba, Red Sea*. Journal of Geophysical Research, vol. 113, 2008.

CIMAC. 2012. *Background information on black carbon emissions form large marine and stationary diesel engines – definition, measurement methods, emission factors and abatement technologies*. CIMAC Working Group 5 "Exhaust Emissions Control", January 2012.

CNR, 2014. *Progetto PONa3_00363 - INFRASTRUTTURA AMICA, Infrastruttura di Alta tecnologia per il Monitoraggio Integrato Climatico-Ambientale*. Gennaio 2012 – Dicembre 2014. Dati salienti del Progetto.

Corbett J. J., Winebrake J. J., Green E. H., Kasibhatla P., Eyring V., Lauer A., 2007. *Mortality from ship emissions: a global assessment*. Environ. Sci. Technol., 41(24), 8512–8518, 2007.

Cristofanelli P., Fierli F., Marinoni A., Calzolari ., Duchi R., Burkhart J., Stohl A., Maione M., Arduini J., Bonasoni P., 2013. *Influence of biomass burning and anthropogenic emissions on ozone, carbon monoxide and black carbon at the Mt. Cimone GAW-WMO global station (Italy, 2165 m a.s.l.)*. Atmos. Chem. Phys., 13, 15–30, 2013.

Crutzen P. J., Andreae M. O., 1990. *Biomass burning in the tropics: impact on atmospheric chemistry and biogeochemical cycles*. Science, 250, 1669–1678.

Derwent R., Stevenson D. S., Doherty R. M, Collins W. J., Sanderson M. G., Amann M., Dentener F., 2005. *The contribution from ship emissions to air quality and acid deposition in Europe*. Ambio, 34, 54–59, 2005.

Devasthale A., Kruger O., Graßl H., 2006. *Impact of ship emissions on cloud properties over coastal areas*. Geophys. Res. Lett., 33, L02811, 2006.

Di Natale F., Carotenuto C., 2015. *Particulate matter in marine diesel engines exhausts: Emissions and control strategies*. Transportation Research Part D 40 (2015) 166–191.

Dickerson R. R., Kondragunta S., Stenchikov G., Civerolo K. L., Doddrige B. G., Holben B. N., 1997. *The impact of aerosols on solar ultraviolet radiation and photochemical smog*. Science, 278, 827–830, 1997.

Draxler R. R., Hess G. D., 1998. *An overview of the HYSPLIT 4 modeling system of trajectories, di-*

spersion and deposition. Austral. Met. Mag. 47, 295 – 308.

Draxler R. R., Taylor A. D., 1982. *Horizontal dispersion parameters for long - range transport modeling*. J. Appl. Meteor., 21, 367–372.

EEA, 2015. *State of the Environment 2015 — The European environment — State and outlook 2015*. EEA, Copenhagen, 2015.

EEA, 2013. *The impact of international shipping on European air quality and climate forcing*. Tech report No 4/2013. EEA, Copenhagen, 2013.

EEA, 2012a. *The contribution of transport to air quality. TERM 2012: transport indicators tracking progress towards environmental targets in Europe*. EEA Technical Report 10 / 2012.

EEA, 2012b. *Particulate matter from natural sources and related reporting under the EU Air Quality Directive in 2008 and 2009*. EEA Technical report No 10/2012, 43 pp.

EPA, 2012. *Report to Congress on Black Carbon*. Department of the Interior, Environment, and Related Agencies Appropriations Act, 2010.

Forster P., Ramaswamy V., Artaxo P., Berntsen T., Betts R., Fahey D.W., Haywood J., Lean J., Lowe D.C., Myhre G., Nganga J., Prinn R., Raga G., Schulz M., Van Dorland R., 2007. *Changes in Atmospheric Constituents and in Radiative Forcing*. In: Climate Change 2007: The Physical Science Basis. Contribution of Working Group I to the Fourth Assessment Report of the Intergovernmental Panel on Climate Change [Solomon S., Qin D., Manning M., Chen Z., Marquis M., Averyt K.B., TignorM. Miller H.L. (eds.)]. Cambridge University Press, Cambridge, United Kingdom and New York, NY, USA.

Gauss M., Myhre G., Pitari G., et al., 2003. *Radiative forcing in the 21st century due to ozone changes in the troposphere and the lower stratosphere*. J. Geophys. Res., 108, 4292, 2003.

Giglio L., Csiszar I., Justice C. O., 2006. *Global distribution and seasonality of active fires as observed with the Terra and Aqua Moderate Resolution Imaging Spectroradiometer (MODIS) sensors*. Journal of Geophysical Research, vol. 111, G02016, 2006.

Hansen J., Nazarenko L., 2003. *Soot climate forcing via snow and ice albedos*. PNAS January 13, 2004, Vol. 101, No. 2, pagg. 423 – 428.

Hill J., Stellmes M., Udelhoven T., Roder A., Sommer S., 2008. *Mediterranean desertification and land degradation: Mapping related land use change syndromes based on satellite observations*. Global Planetary Change, Vol. 64, Issues 3-4, December 2008, Pages 146–157.

Ichoku C., Kaufman Y. J., 2005. *A Method to derive Smoke Emission Rates From MODIS Fire Radiative Energy Measurements*. IEEE Transactions on Geoscience and Remote Sensing, Vol. 43, No. 11, November 2005.

IPCC, 2014. *Climate Change 2014: Synthesis Report. Contribution of Working Groups I, II and III to the Fifth Assessment Report of the Intergovernmental Panel on Climate Change* [Core Writing Team, R.K. Pachauri and L.A. Meyer (eds.)]. IPCC, Geneva, Switzerland, 151 pp.

ISAC - CNR, 2016. *Report 2015 of the Capo Granitola Climate Environmental Observatory, GAW - WMO Regional Station.*

Janssen, N. A., 2011. *Black carbon as an additional indicator of the adverse health effects of airborne particles compared with PM_{10} and $PM_{2.5}$*. Environ. Health Perspect., 119, 1691–1699.

Johnson K., Miller W., Durbin T., Jiang Y., Yang J., Karavalakis G., Cocker D., 2016. *Black carbon measurement methods and emission factors from ships*. Prepared for: International Council on Clean Transportation.

JRC, 2007. *Contribution of natural sources to air pollution levels in the EU - a technical basis for the development of guidance for the Member States*. European Commission, Joint Research Centre Institute for Environment and Sustainability, Report EUR 22779 EN.

Justice C. O., Giglio L., Korontzi S., Owens J., Morisette J., Roy D., Descloitres J., Alleaume S., Petitcolin ., Kaufman Y., 2002. *The MODIS fire products*. Remote Sens. Environ., 83, 244–262.

Kaiser, J., 2005. *Mounting evidence indicts fine-particle pollution*. Science, 307, 1858–1861.

Kanakidou M., Mihalopoulos N., Kindap T., Im U., Vrekoussis M., Gerasopoulos E., Dermitzaki E., Unal A., Koçak M., Markakis K., Melas D., Kouvarakis G., Youssef A. F., Richter A., Hatzianastassiou N., Hilboll A., Ebojie F., Wittrock F., von Savigny C, Burrows J. P., Ladstaetter-Weissenmayer A., Moubasher H., 2011. *Megacities as hot spots of air pollution in the East Mediterranean.* Atmospheric Environment 45 (2011) 1223 – 1235.

Kaufman Y. J., Ichoku C., Gigio L., Korontzi S., Chu D.A., Hao W. M., Li R. R., Justice C. O.,

2003. *Fire and smoke observed from the Earth Observing System MODIS instrument - products, validation, and operational use*. Int. J. Remote Sensing, 2003, vol. 24, no. 8, 1765 – 1781.

Kaufman Y. J., Justice C. O., Flynn L. P., Kendall J. D., Prins E. M., Giglio L., Ward D. E., Menzel W. P., Setzer A. W., 1998. *Potential global fire monitoring from EOS-MODIS*. J. Geophys. Res., 103(D24), 32,315 – 32,338.

Lack D., Corbett J. J., Onasch T., Lerner B., Massoli P., Quinn P. K., Bates T. S., Covert D. S., Coffman D., Sierau B., Herndon S., Allan J., Baynard T., Lovejoy E., Ravishankara A. R., Williams E., 2009. *Particulate emissions from commercial shipping: chemical, physical, and optical properties*. Geophys. Res. Lett., 114, D00F04, 2009.

Marenco F., Bonasoni P., Calzolari F., Ceriani M., Chiari M., Cristofanelli P., D'Alessandro A., Fermo P., Lucarelli F., Mazzei F., Nava S., Piazzalunga A., Prati P., Valli G, Vecchi R., 2006. *Characterization of atmospheric aerosols at Monte Cimone, Italy, during summer 2004: source apportionment and transport mechanisms*. Jounal of Geophysical Research, Vol. 111, D24202, 2006.

Marinoni A., Bonasoni P., Cristofanelli P., Calidonna C., Ammoscato I., Gulli D., Dinoi A., Contini D., Cesari D., Sprovieri F., Andreoli V., Naccarato A., Tirimberio G., Chianese E., Riccio A., 2016. *Caratterizzazione chimica invernale di $PM_{2.5}$ e PM_{10} presso cinque siti di misura nell'Italia meridionale*. Poster submitted at PM 2016 - VII National Conference on Atmospheric Particulate Matter, Rome 17 - 20 may 2016.

Marinoni A., Cristofanelli P., Laj P., Duchi R., Putero D., Calzolari F., Landi T. C., Vuillermoz E., Maione M., Bonasoni P., 2013. *High black carbon and ozone concentration during pollution transport in the Himalayas: five years of continuous observations at NCO-P global GAW station*. Journal of Environmental Sciences 2013, 25(8) 1618 – 1625.

Merico E., Donateo A., Gambaro A., Cesari D., Gregoris E., Barbaro E., Dinoi A., Giovanelli G., Masieri S., Contini D., 2016. *Influence of in - port ships emissions to gaseous atmospheric pollutants and to particulate matter of different sizes in a Mediterranean harbour in Italy*. Atmospheric Environment 139 (2016) 1 – 10.

Naeher L. P., Brauer M., Lipsett M., Zelikoff J. T., Simpson C. D., Koenig J. Q., Smith K. R, 2007. *Woodsmoke health effects: a review*. Inhal. Toxicol., 19(1), 67–106.

Novelli P. C., Masarie K. A., Lang P. M., Hall B. D., Myers R. C., Elkins J. W., 2003. *Reanalysis of*

tropospheric CO trends: effects of the 1997–1998 wildfires J. Geophys. Res., 108(D15), 4464, 2003.

Penner, J. E., Andreae, M., Annegarn, H., Barrie, L., Feichter, J., Hegg, D., Jayaraman, A., Leaitch, R., Murphy, D., Nganga, J., and Pitari, G., 2001. *Aerosols, their direct and indirect Effects*. In: Climate Change 2001: the Scientific basis, Contribution of Working Group 1 to the Third Assessment Report of Intergovernmental Panel on Climate Change, edited by Houghton J. T., Ding Y., Griggs D. J., Noguer M., van der Linden P. J., Dai X., Maskell K., Johnson C. A. Cambridge Univ. press, Cambridge, UK and New York, NY USA, 881, 2001.

Putero D., Landi T. C., Cristofanelli P., Marinoni A., Laj P., Duchi R., Calzolari F., Verza G. P., Bonasoni P., 2014. *Influence of open vegetation fires on black carbon and ozone variability in the southern Himalayas (NCO-P, 5079 m a.s.l.)*. Environmental Pollution 184 (2014) 597 - 604.

Pyne, S., 2002: *Small particles add up to big disease risk*. Science, 295, 1994.

San-Miguel-Ayanz J., Schulte E., Schmuck G., Camia A., Strobl P., Liberta G., Giovando C., Boca R., Sedano F., Kempeneers P., McInerney D., Withmore C., Santos de Oliveira S., Rodrigues M., Durrant T., Corti P., Oehler F., Vilar L., Amatulli G., 2012. *Comprehensive monitoring of wildfires in Europe: The European Forest Fire Information System (EFFIS)*. In: Approaches to Managing Disaster - Assessing Hazards, Emergencies and Disaster Impacts, Tiefenbacher J. (Ed), 87 – 108.

Simmonds P., Manning A., Derwent R., Ciais P., Ramonet M., Kazan V., Ryall D., 2005. *A burning question: can recent growth rate anomalies in the greenhouse gases be attributed to large - scale biomass burning events ?* Atmos. Environ., 39, 2513–2517, 2005.

Stein A. F., Draxler R. R., Rolph G. D., Stunder B. J. B., Cohn M. D., Ngan F., 2015. *NOAA'S HYSPLIT Atmospheric transport and dispersion modeling system*. American Meteorological Society, December 2015, 2059 - 2077.

UNCTAD, 2015. *Review of Marine Transport 2015*. UNCTAD/RMT/2015 United Nations Publication Sales no. E. 15.II.D.6

UNEP / MAP, 2009. *UNEP / MAP-Plan Bleu: State of the Environment and Development in the Mediterranean*. Athens, 2009.

Urbanski S., Hao W., Baker S., 2009. *Chemical composition of wildland fire emissions*. In: Bytnerowicz A., Arbaugh M., Riebau A., Andersen C. (eds), Developments in Environmental Science, Volu-

me 8, 79.

Whelan R. J., 2006. *The ecology of fire – Developments since 1995 and outstanding questions.* Proceeding of Bushfire 2006 - Life In A Fire-Prone Environment: Translating Science into practice conference, Griffith University, Brisbane, 6–9 June 2006.

WMO / GAW, 2016. *Aerosol Measurement Procedures, Guidelines and Recommendations, 2nd Edition*. GAW Report No. 227 – 2016

Wooster M. J., Zhukov B., Oertel D., 2003. *Fire radiative energy for quantitative study of biomass burning: derivation from the BIRD experimental satellite and comparison to MODIS fire products*. Remote Sens. Environ., 86, 83–107.

APPENDIX 1: Basic regulatory and legislative framework

To pursue its goal, the Project has unavoidably taken as a basis the international and community regulation framework.

Accordingly to **Intergovernmental Panel on Climate Change (IPCC)** "warming of the climate system is unequivocal, and since the 1950s, many of the observed changes are unprecedented over decades to millennia"; recent climate changes "have had widespread impacts on human and natural systems […] on all continents and across the oceans" and expose "people, societies, economic sectors and ecosystems to risk" (IPCC, 2014).

IPCC is the leading international body for the assessment of climate change, established by the **United Nations Environment Programme (UNEP)** and the **World Meteorological Organization (WMO)** in 1988, with the endorsement to review and assess the most recent climate - change concerning scientific, technical and socio - economic information produced worldwide, with impartial and rigorous evaluation criteria, in the aim to support appropriate regulations and technical upgrading in mitigation techniques by member countries.

Evidences for climate change are indisputable, concordant and compelling: focusing on, regulatory conventions, international treaties and technical reports recognized an important role in climate - change triggering to **forcing external agents**, both natural and linked to human activities; their influence can be described exhaustively by introducing the **concept of radiative forcing (RF)** of different human and natural agents, describing their strength in causing changes in the radiative balance of the Earth, due to an increase in absorption of sunlight within the atmosphere.

RF is expressed in terms of energy contribution, in Wm^{-2}, to global atmosphere, and allows mutual comparations among forcing agents (EEA, 2013; Andreae, 1995): while a positive forcing agent tends to increase the surface temperature, a negative one pushes toward a temperature cooling.

Since 1750, combined anthropogenic RF is estimated to be +1.6 W m^{-2}, indicating substantial human warming influence on climate (Forster et al., 2007).

In the light of IPCC projections of what the future increase in global mean temperature might mean, the international treaty known as **Kyoto Protocol** was conceived and ratified in 1997 with the purpose of a legally binding agreement, under which industrialized countries formally commit to reduce their collective emissions of 6 greenhouse gases (CO_2, CH_4, NO_2, HFC_s, PFC_s and SF_6) by 5.2% compared to the year 1990, in such a way to invert their accumulation trend into the atmosphere, reported in the industrial era (Forster et al., 2007).

Instituted in 1948 and entered into force 10 years later, the **International Maritime Organization (IMO)** is the United Nations specialized agency with responsibility for the safety and security of shipping and the prevention of marine pollution by ships, particularly oil - carrying tankers, through actions coordinated at the international level.

IMO addressed air pollution issue, too, through the drawing up of the **International Convention for the Prevention of Pollution from Ships (MARPOL)**, ratified in 1973 and entered into force in 1983, embodying the effort to minimize pollution of the marine environment by ships from operational or accidental causes: all ships flagged under countries that are signatories of the Convention are subject to its requirements. In particular, Annex VI, come into force in 2005, introduces requirements to regulate the air pollution being emitted by ships, including the emission of Ozone-Depleting Substances (ODS), Nitrogen Oxides (NO_x), Sulphur Oxides (SO_x) and Volatile Organic Compounds (VOCs), as well as to encourage the reduction of fuel consumption and consequent air pollutants release, by instituting **Sulphur Emission Control Areas** (**SECAs**) in sea areas where controls were introduced to minimize airborne emissions from ships (EEA, 2013).

In 2012 Annex VI was revised to introduce a reduction of the global sulphur limit of marine fuels from 4.5 % to 3.5 % and stepwise to 0.5 % afterwards; reductions of NO_x emissions from marine diesel engines were in parallel regulated in the new ships built from 2000 as a function of speed and engine installation year, in the so - called **NO_x Emission Control Areas (NECAs)**.

Mediterranean basin does not fall in any Emission Control Areas, yet.

United Nations Framework Convention on Climate Change (UNFCCC) was adopted in the "Rio Earth Summit" of 1992 and entered into force on 1994 with the specific aim to involve all countries to share the mission to stabilize atmospheric composition of greenhouse gases concentrations to prevent irreversible human interference with the climate system and related threats to ecosystem resilience, food production and sustainable economic development and progress: the threshold level of human pressure on climate system has been set by the need to preserve global coastlines, in consideration of their particular vulnerability to sea level rise.

Collecting scientific evidence on the current state in climate change is required to figure out the most likely environmental and socio - economic impacts in industrialized and developing countries, according to the well established precautionary principle.

European Union has developed an extensive body of legislation to establish health - based standards

and objectives for a number of pollutants in air: as concerns fine particles ($PM_{2.5}$) the limit has been introduced by the **Directive 2008 / 50 / EC on Ambient Air Quality and Cleaner Air for Europe** and is 25 $\mu g/m^3$, on a year averaging period.

This document entered into force on 2015 to monitor long - term air quality tendencies drawn from data through shared methods and criteria, in an effort to estimate the appropriateness of national mitigation measures.

As regards coarse particles (PM_{10}), since 2005 the limit has been set to 40 $\mu g/m^3$ on a year averaging period and 50 $\mu g/m^3$ on a 24 hours averaging period, in the latter case with the possibility to exceed the threshold for a maximum of 35 times per year, as stated by the **Directive 1999 / 30 / EC** relating to limit values for sulphur dioxide, nitrogen dioxide and oxides of nitrogen, particulate matter and lead in ambient air.

European Environment Agency (EEA) is the agency of the European Union aiming to preserve people from environment - related health risks, support sustainable development and to asses and help to achieve significant improvement in Europe's environment and quality of life through sustaining European environmental knowledge - based policy implementation; to pursue this goal it publishes a **State of the Environment Report (SOER)** every five years, based on reliable current information on the environment trends and prospects, considered as a basis for building actions which support sustainable development and help achieve significant and measurable environmental improvement; the last one is SOER 2015 (EEA, 2015).

In this document EEA, moved by the underlying awareness is that environmental drivers, trends and impacts are becoming increasingly globalized, clarifies that climate change is estimated to have direct impacts on many features of the Earth System, like nature and biodiversity, natural resources exploitation and waste disposal, and that, to protect the "natural capital" which economic prosperity and human well-being are founded on, it is necessary to recalibrate existing economic and social development in the direction of conjugating mitigation, adaptation, reduction and restoration.

Previously, EEA published the **technical report "The contribution of transport to air quality - TERM 2012: transport indicators tracking progress towards environmental targets in Europe"** (EEA, 2012a), in which European regulation to make tentative progress in reducing the impacts from transport comes out clearly in terms of reinforcement of quantitative - targets policy and support to technical improvements of transport efficiency.

In the **technical report "Particulate matter from natural sources and related reporting under the EU Air Quality Directive in 2008 and 2009"** (EEA, 2012b), EEA recognize the role played by natural particulate matter sources, included wild - land fire particulate matter, and provides instrument to help member countries to take this aspect into consideration before to compare ambient air pollutant concentrations in the framework of legally binding limit values introduced by **Air Quality Directive 2008 / 50 / EC** of the European Parliament and of the Council on ambient air quality and cleaner air for Europe, issued on 21 May 2008 and entered into force on 11 June 2008.

In its **technical report "The impact of international shipping on European air quality and climate forcing"** (EEA, 2013) EEA provides a comprehensive review of state - of - the - art literature on the impact on air quality and climate forcing from activities linked to the maritime transport sector, on a european scale, as well as on monitoring of maritime fuel consumption and resulting emissions.

EU Thematic Strategy on Air Pollution, signed in 2005 in order to attain air - quality levels that do not give rise to significant negative impacts on human health and environment, intervenes on the current european legislation introducing objectives to be achieved by 2020; for the purposes of this Project, the strategy provides concrete measures to reduce SO_x, NO_x and PM emission from ships (EEA, 2013).

International strategies for mitigation of emissions in harbor areas and well specific zones was introduced with the **Directive 2005 / 33 / CE on the sulphur content of marine fuels**, designating the Baltic Sea, the English Channel and the North Sea as SECAs.

In 1975, the Mediterranean States and UNEP for European Community approved the **Mediterranean Action Plan (MAP)** to encourage regional cooperative effort involving 21 countries bordering the Mediterranean Sea in concretely addressing marine environmental degradation; this initiative was promoted by **United Nations Environment Programme (UNEP)** to assist the Mediterranean Governments meet the challenges of assessing and controlling pollution of marine and coastal environment, while boosting regional and national plans by formulating effective national marine protection policies to achieve a coherent and sustainable development. In 1995, MAP was revised, moving the focus from marine pollution control to pollution prevention, socio-economic sustainable development and integrated coastal zone management / planning, in the belief that environmental protection is effective and lasting just if it is integrated in social and economic development and support national efforts towards achieving Good Environmental Status

(GES) in the Mediterranean basin in synergy with European Union **Marine Strategy Framework Directive 2008 / 56 / EC**, the environmental pillar of the EU Integrated Maritime Policy.

In 1995 the **UNEP / MAP Convention for the Protection of the Marine Environment and the Coastal Region of the Mediterranean**, commonly known as **Barcelona Convention**, was adopted, providing a critical framework for setting standards and targets to trigger lasting improvements of the environment in the Mediterranean Sea area. To assess whether progress is being made and to identify where better performance is needed, the Contracting Parties established to periodically report on the state of the environment, measures undertaken to implement the Barcelona Protocols and their effectiveness, as well as to provide public access to information on the State of the Environment in fields where the Barcelona Convention and its Protocols apply.

The italian threshold air particulate matter concentration is established by **Legislative Decree no. 155 / 2010** together with data quality objectives, and calculated on an annual time basis, whose Annex XI substantially confirming european legislation as regards concentration thresholds.

In the U.S.A. framework, the **Clean Air Act** was a federal law ratified in 1963 and many times amended under the thrust of U. S. Environmental Protection Agency (US EPA); its primary intent is controlling air pollution by regulating total particles and air pollutants concentration levels by chemistry, requiring EPA to set **National Ambient Air Quality Standards (NAAQS)** for six principal pollutants ("criteria air pollutants"), i.e. carbon monoxide, lead, nitrogen dioxide, ozone, particle pollution and sulphur dioxide, considered harmful to public health and the environment, included fuel pollutants.

In particular, EPA showed to have incorporated today widespread scientific awareness that rules based on the numeric concentration of particles with a diameter of 10 micron or less (PM_{10}) aren't adequate to preserve public health, because of the epidemiological evidence against fine particles (Corbett et al., 2007; Kaiser, 2005).

NAAQS are periodically revised and updated to ensure an updated and effective protection of human health and the environment; EPA regulates air concentration of particles which are narrower than 10 micrometers and current values regarding particle pollution in outdoor air, differentiated on size basis, are listed in the following page.

Size fraction	Standard	Averaging time	Level	Form
$PM_{2.5}$	primary (public health protection)	1 year	12 μg/m^3	annual mean, averaged over 3 years
	secondary (public welfare protection)	1 year	15 μg/m^3	annual mean, averaged over 3 years
	primary and secondary	24 hours	35 μg/m^3	98th percentile, averaged over 3 years
PM_{10}	primary and secondary	24 hours	150 μg/m^3	Not to be exceeded more than once per year on average over 3 years

APPENDIX 2: I-AMICA Project: a network for the reinforcement of observative structures in southern Italy

The Air Quality Directive 2008 / 50 / EC requires the Member States to divide their territory into a number of zones in which to undertake separate assessments of air pollution levels and to adopt timely countermeasures every time compliance with the limit value has to be restored, prior the limit value formally enters into force: this requirement gives further strength to the demand for a spatially representative observatory network setup. Widening the view, an integrated observational network for weather and climate monitoring is greatly required to qualify and quantify the state of health of the Mediterranean basin (CNR - ISAC / IAMC, 2016; CNR, 2014); currently it hosts very few atmospheric research observatories in its central portion, hence quantity and quality of scientific reliable environmental data are unsatisfactory.

The Italian peninsula, with its about 8300 Km - long coastline, is among the regions most likely exposed to possible serious repercussions related to climate change in the Mediterranean basin scale: it occupies a crucial position within its western part, in which it intrudes for over 1200 km and 12° latitude (CNR, 2014): as a consequence of this, Italy can be considered as an elective observation platform for monitoring Mediterranean and south - Europe climate and environment. Additionally, as a matter of fact the understanding of coastal processes dynamics is of paramount importance as it strongly influences italian populations' health and quality of life and environmental resources economy; such a purpose requires the availability of continuous and high-quality information about atmospheric composition (ISAC / IAMC, 2016).

Financed by Italian Government and European Union through the tool PON "Ricerca e Competitività" 2007-2013, the **I-AMICA Project "Infrastructure of High Technology for Integrated Climate and Environmental Monitoring"** (PONa3_00363, www.i-amica.it) falls within EU cohesion policy strategy introduced with **Regulation (CE) n.1083 / 2006 of the Council**, specifically aimed to encourage social and economic relaunch of italian most disadvantaged geographical areas ("Convergence Regions"), being Puglia, Calabria, Sicilia and Campania, by promoting technology transfer and industrial development, with the final result of maximizing synergies among italian regions and increasing their own competitiveness, at the same time.

Officially closed at the end of July 2015, the project globally turned its attention to the Mediterranean Basin by realizing or strengthening / upgrading a set of integrated infrastructures for

the execution of continuous monitoring actions of atmosphere, climate, agriculture, forestry and coastal systems, through Observing Systems based on innovative sensor systems, parallel computing infrastructures for an adequate data acquisition, management and storage of information on air quality, as well as on air - quality services for forecasting and advanced analyses.

In an effort to offer a deeper insight of environmental keystone issues (air quality, forest fires, transformation of coastal ecosystem, intrusion of salt wedge, energy production from wind, etc) to the management authorities, the observational network I-AMICA was created by CNR - Dipartimento Scienze del Sistema Terra e Tecnologie per l'Ambiente, with the support of seven CNR Institutes: IAMC, IBAF, ICAR, IIA, IREA, ISAC and ISAFOM, with the purpose to create a system able to collect up - to - date and reliable information on the environmental status and to strategically increase knowledge about climate and atmosphere, considering the complex relationship between air pollution and climate change and the Mediterranean hotspot vulnerability to climate change.

By this way a technological gap has been bridged towards atmospheric data collection and management; this initiative has provided improved and deeper scientific knowledge and offered appropriate support to stakeholders engaged in integrated environmental policies development and management, consistently with the European Environment Agency's mission (EEA, 2015).

The I-AMICA Observing Systems are integrated to international programs, with the result to foster technology transfer and to encourage a strong integration between public and private activities for the development of innovative environmental instrumentations and regional promotion and development.

The I-AMICA network constitutes an opportunity for italian and european climate and environmental monitoring, as well as early warning activities following to monitoring and detection of episodes of pollutant transport in the atmosphere, towards which EU shows great interest, and is in activity since the end of 2014 (CNR, 2014).

Station of I-AMICA network	Region	Tipology
Capo Granitola	Sicilia	Climatic - environmental observatory
Lamezia Terme	Calabria	Climatic - environmental observatory Atmospheric profiling
Monte Curcio	Calabria	Climatic - environmental observatory
Bacino del Bonis - Monti della Sila	Calabria	Agro - forestry ecosystems
Lecce	Apulia	Climatic - environmental observatory Atmospheric profiling
Parco della Murgia	Apulia	Agro - forestry ecosystems
Eboli - Borgo Cioffi	Apulia	Agro - forestry ecosystems
Napoli - Capodimonte	Campania	Atmospheric profiling Agro - forestry ecosystems
Napoli - Castel Volturno	Campania	Coastal marine ecosytems

APPENDIX 3: Plots of main parameters observed at Capo Granitola during the years 2015-2016

1 January 2015 / 31 December 2015 (hourly frequency, 8760 records)

Parameter	NAs	Data coverage (%)	Minimum	25th percentile	50th percentile	Mean	75th percentile	Maximum
Temperature (°C)	452	94.84	0.4	13.7	17.4	18.0	22.7	37.4
Relative humidity (%)	437	95.01	10.6	69.4	77.6	75.4	83.3	94.9
Atmospheric pressure (hPa)	446	94.91	985.8	1011.5	1014.7	1015.5	1019.0	1035.8
Wind speed ($m\ s^{-1}$)	438	95.00	0.4	2.3	3.3	4.1	5.4	16.1
Rain ($mm\ h^{-1}$)	435	95.03	0.0	0.0	0.0	0.1	0.0	25.76
O_3 (ppb)	1949	77.75	11.5	33.6	42.2	41.6	49.5	74.2
NO (ppb)	2560	70.78	0.00	0.00	0.02	0.05	0.07	3.29
NO_2 (ppb)	2863	67.32	0.00	0.46	0.76	1.02	1.32	16.57
SO_2 (ppb)	1784	79.63	0.00	0.00	0.03	0.06	0.08	1.44
CO (ppb)	3463	60.47	84.3	116.2	126.8	131.1	142.2	308.1
CO_2 (ppm)	3514	59.89	388.8	398.3	402.8	405.1	409.2	450.8
CH_4 (ppb)	4465	49.03	1850	1901	1918	1924	1941	2124
PM_{10} (ug/m^3)	2324	73.47	0.0	1.4	2.4	4.2	5.0	126.5
$PM_{2.5}$ (ug/m^3)	2324	73.47	0.2	5.1	7.5	9.0	11.4	85.7

Parameter	NAs	Data coverage (%)	Minimum	25th percentile	50th percentile	Mean	75th percentile	Maximum
Fine particles (n/cm^3)	2324	73.47	1.1	22.9	38.0	50.5	66.2	403.0
Coarse particles (n/cm^3)	2324	73.47	0.0	0.6	1.0	1.4	1.9	17.3
Total particles (n/cm^3)	5460	37.67	705.8	3648.6	5085.7	6133.4	7394.8	63669.2
BC (ug/m^3)	909	89.62	0.0	0.2	0.4	0.4	0.6	14.7
$Ksca_{450}$ (Mm^{-1})	654	92.53	1.3	28.6	44.3	53.2	68.8	299.8
$Ksca_{550}$ (Mm^{-1})	654	92.53	1.0	21.6	33.8	40.5	51.9	290.0
$Ksca_{700}$ (Mm^{-1})	654	92.53	0.5	16.0	25.5	30.7	39.1	289.7

1 January 2016 / 31 December 2016 (hourly frequency, 8784 records)

Parameter	NAs	Data coverage (%)	Minimum	25th percentile	50th percentile	Mean	75th percentile	Maximum
Temperature (°C)	2939	66.54	4.7	13.9	16.1	16.3	19.0	33.7
Relative humidity (%)	2936	66.58	25.9	66.4	74.7	72.7	80.9	91.4
Atmospheric pressure (hPa)	2941	66.52	985.4	1011.5	1015.0	1015.5	1019.3	1033.8
Wind speed ($m\ s^{-1}$)	2980	66.07	0.5	2.6	3.8	4.5	6.0	15.5
Rain ($mm\ h^{-1}$)	2936	66.58	0.0	0.0	0.0	0.0	0.0	16.6
O_3 (ppb)	581	93.39	12.2	33.5	41.4	40.9	48.4	70.4

Parameter	NAs	Data coverage (%)	Minimum	25th percentile	50th percentile	Mean	75th percentile	Maximum
NO (ppb)	2157	75.44	0.00	0.00	0.02	0.06	0.08	2.37
NO_2 (ppb)	2158	75.43	0.00	0.90	1.36	1.67	2.08	14.12
SO_2 (ppb)	1515	82.75	0.00	0.07	0.12	0.17	0.19	4.58
CO (ppb)	1293	85.28	65.4	106.8	122.8	127.0	138.2	1337.3
CO_2 (ppm)	1305	85.14	353.9	401.5	404.3	406.6	409.7	511.3
CH_4 (ppb)	1308	85.11	1859	1919	1936	1961	1957	4610
PM_{10} (ug/m^3)	3394	61.36	1.7	6.9	11.2	15.1	17.6	663.3
$PM_{2.5}$ (ug/m^3)	3394	61.36	1.1	4.5	6.9	9.0	10.8	276.5
Fine particles (n/cm^3)	3394	61.36	2.2	15.9	26.1	33.4	41.1	387.8
Coarse particles (n/cm^3)	3394	61.36	0.1	0.6	1.2	1.5	1.9	46.4
Total particles (n/cm^3)	4995	43.14	230.4	1825.2	2571.8	2960.0	3603.8	20164.6
BC (ug/m^3)	2740	68.81	0.0	0.2	0.3	0.3	0.4	3.6
$Ksca_{450}$ (Mm^{-1})	2844	67.62	-16.2	17.9	33.1	37.1	49.0	488.0
$Ksca_{550}$ (Mm^{-1})	2844	67.62	-12.5	14.4	26.2	30.0	39.7	504.6
$Ksca_{700}$ (Mm^{-1})	2844	67.62	-8.3	11.1	20.0	24.6	32.3	504.6

Summary plot of weather-related sub-dataset on 2015 and 2016

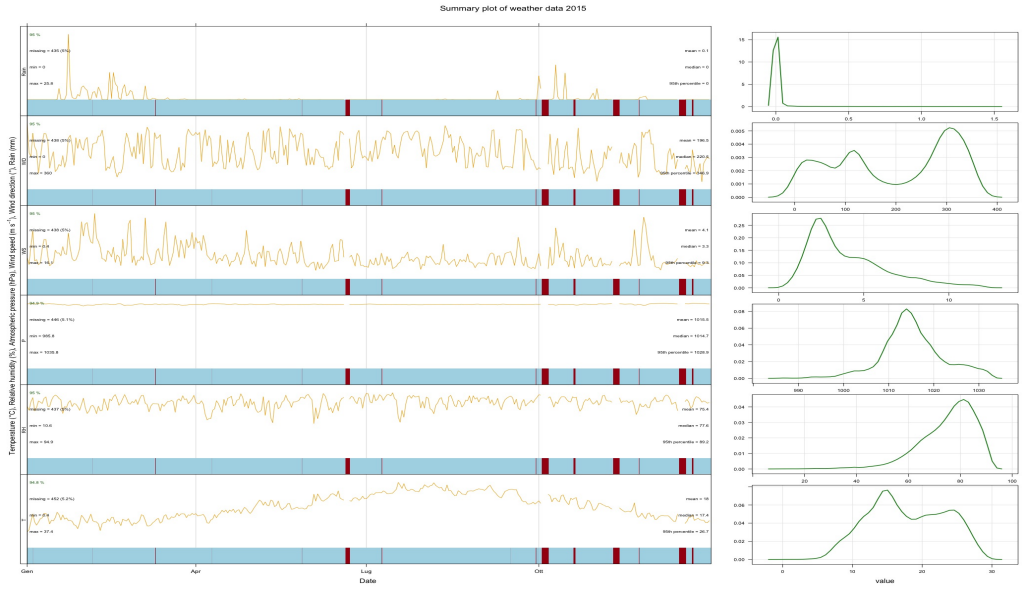

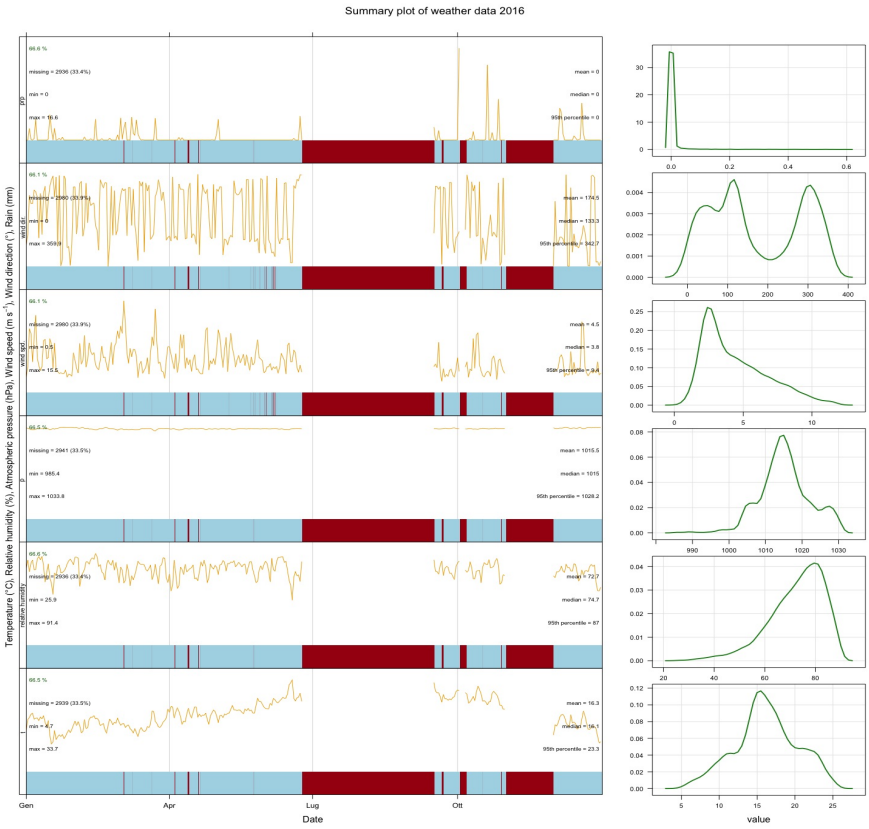

Summary plot of gas-related subdataset on 2015 and 2016

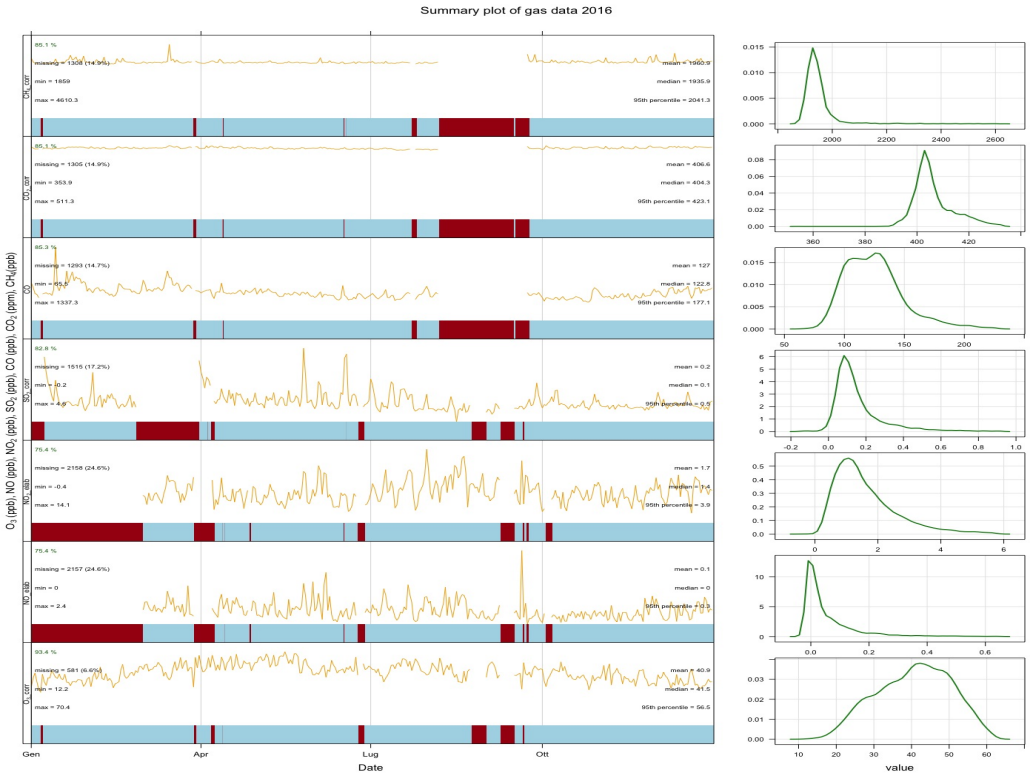

Summary plot of aerosol-related subdataset on 2015 and 2016

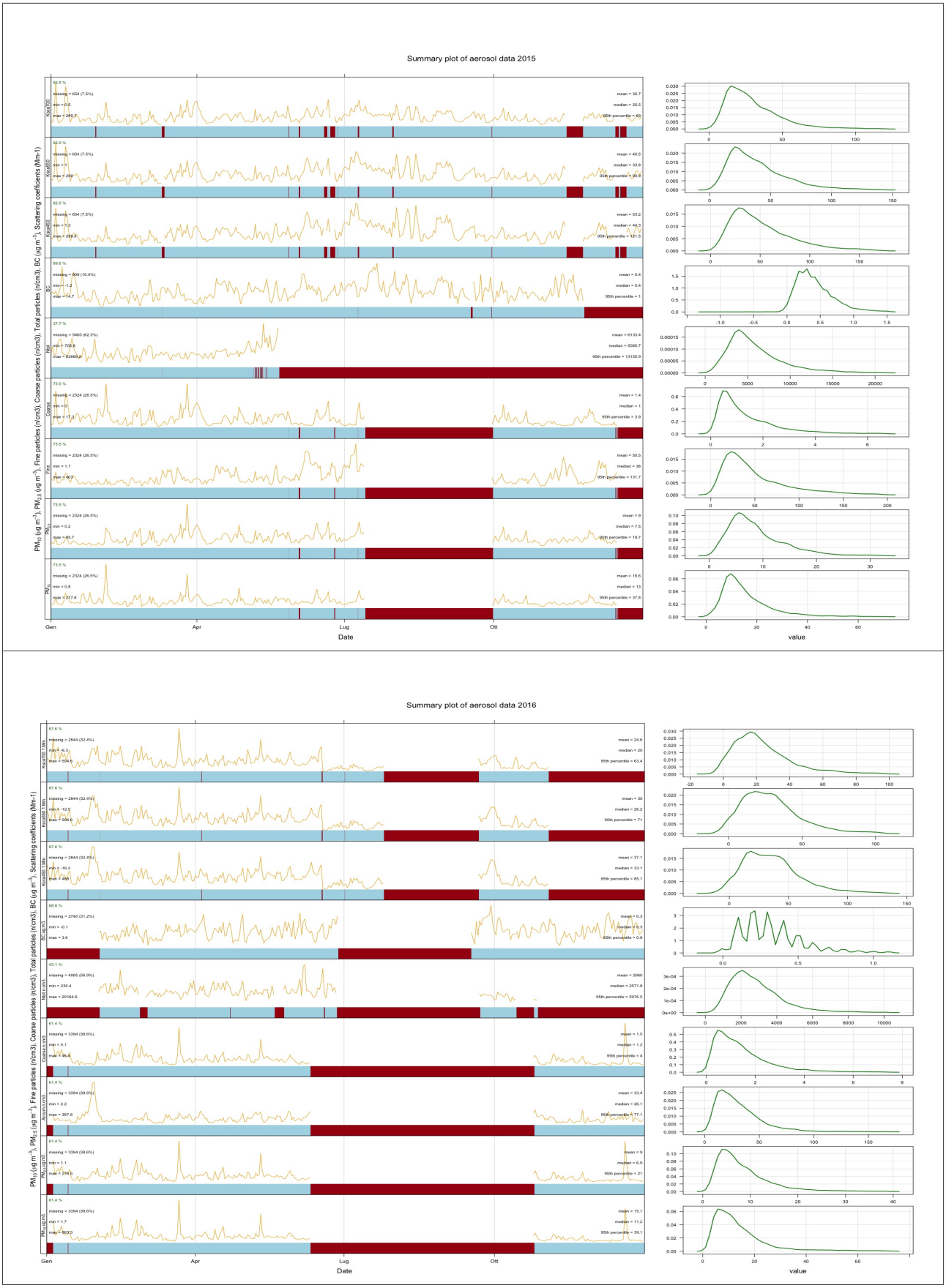

Time series of daily averaged temperature and relative humidity – biennium 2015 / 2016 (thick line: average / shaded area: 95 % confidence level)

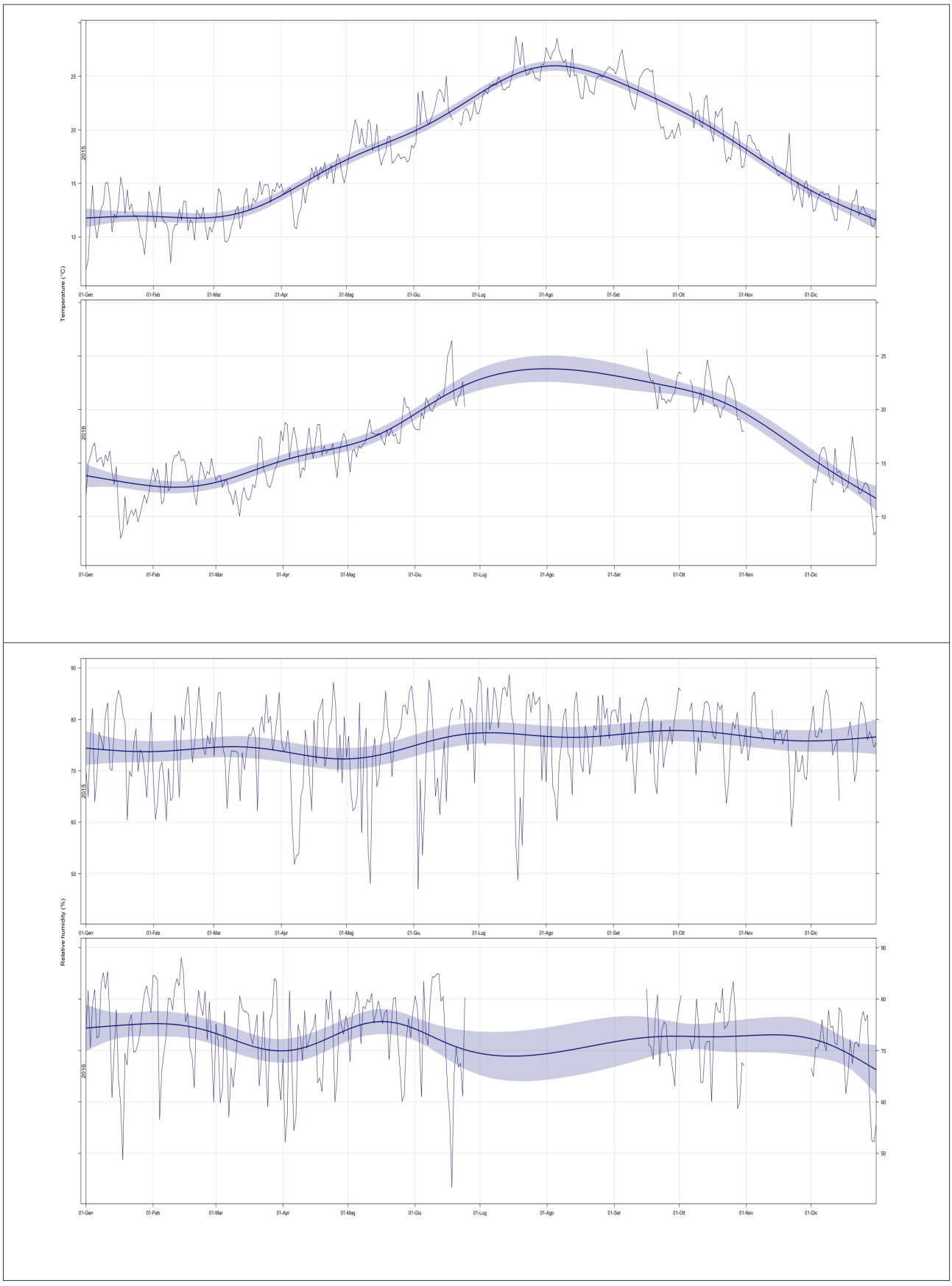

Time series of daily averaged atmospheric pressure and rain – biennium 2015 / 2016
(thick line: average / shaded area: 95 % confidence level)

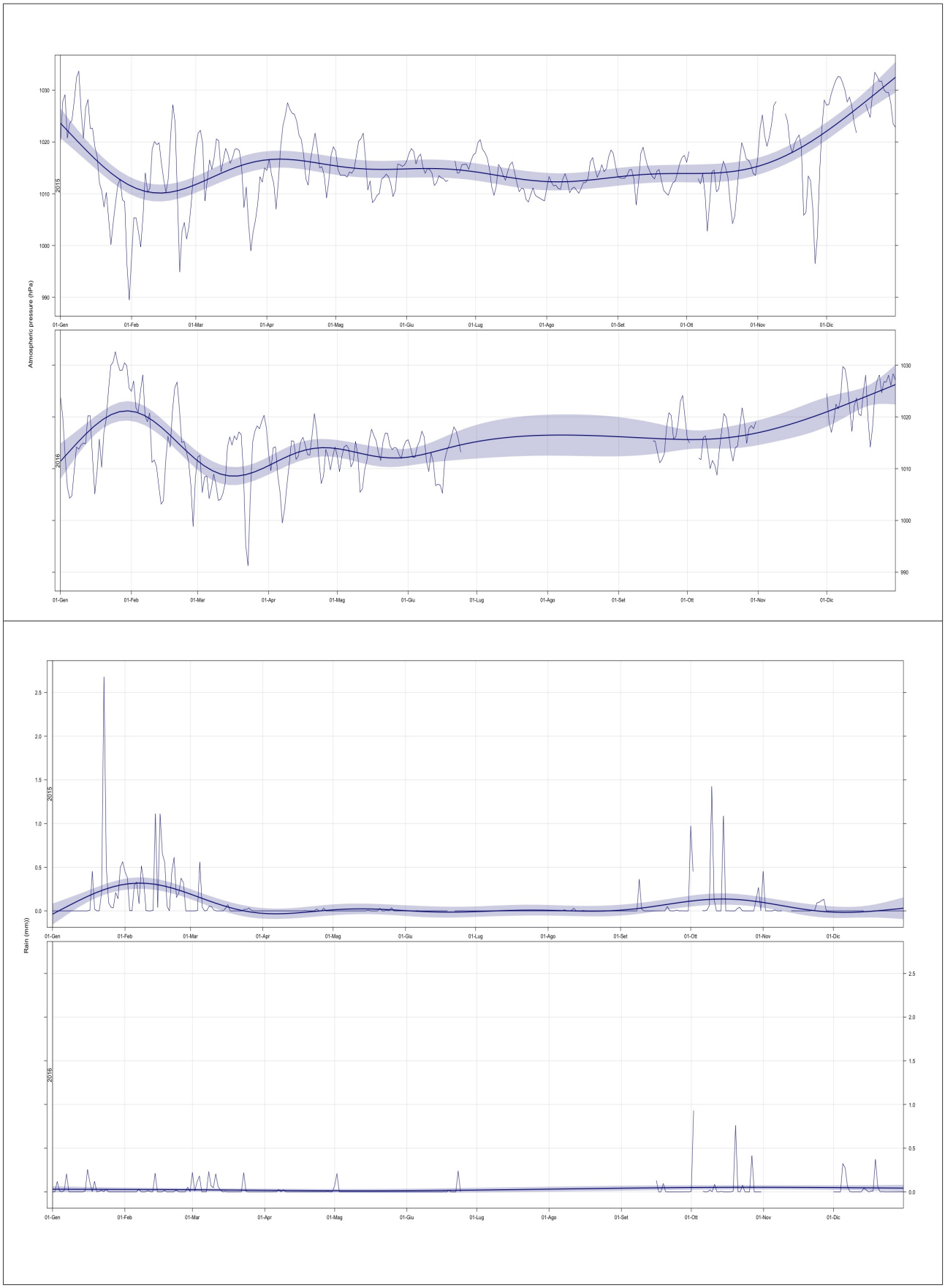

Time series of daily averaged wind speed and wind direction– biennium 2015 / 2016 (thick line: average / shaded area: 95 % confidence level)

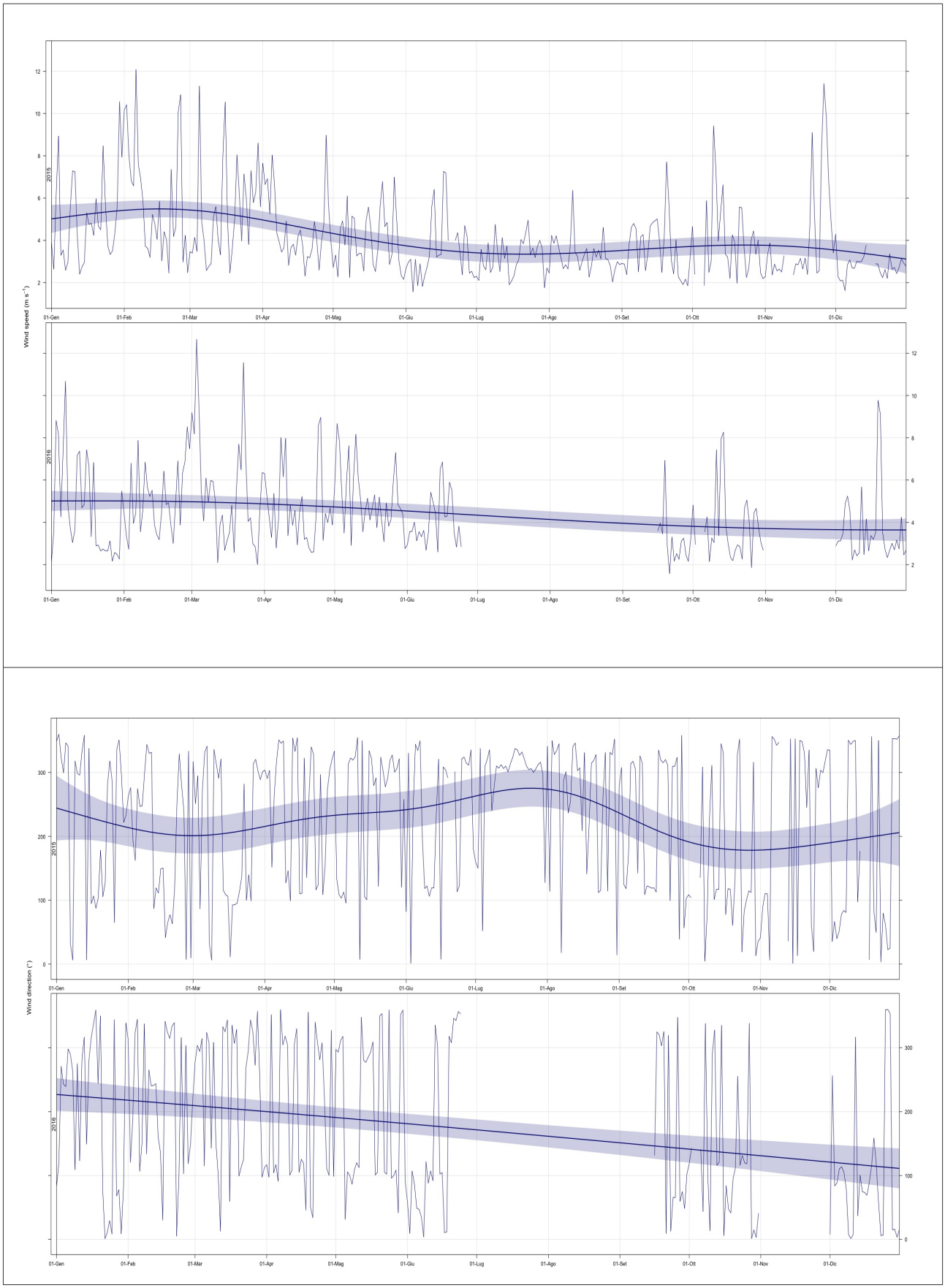

Time series of daily averaged O_3 and SO_2 concentration (ppb) – biennium 2015 / 2016 (thick line: average / shaded area: 95 % confidence level)

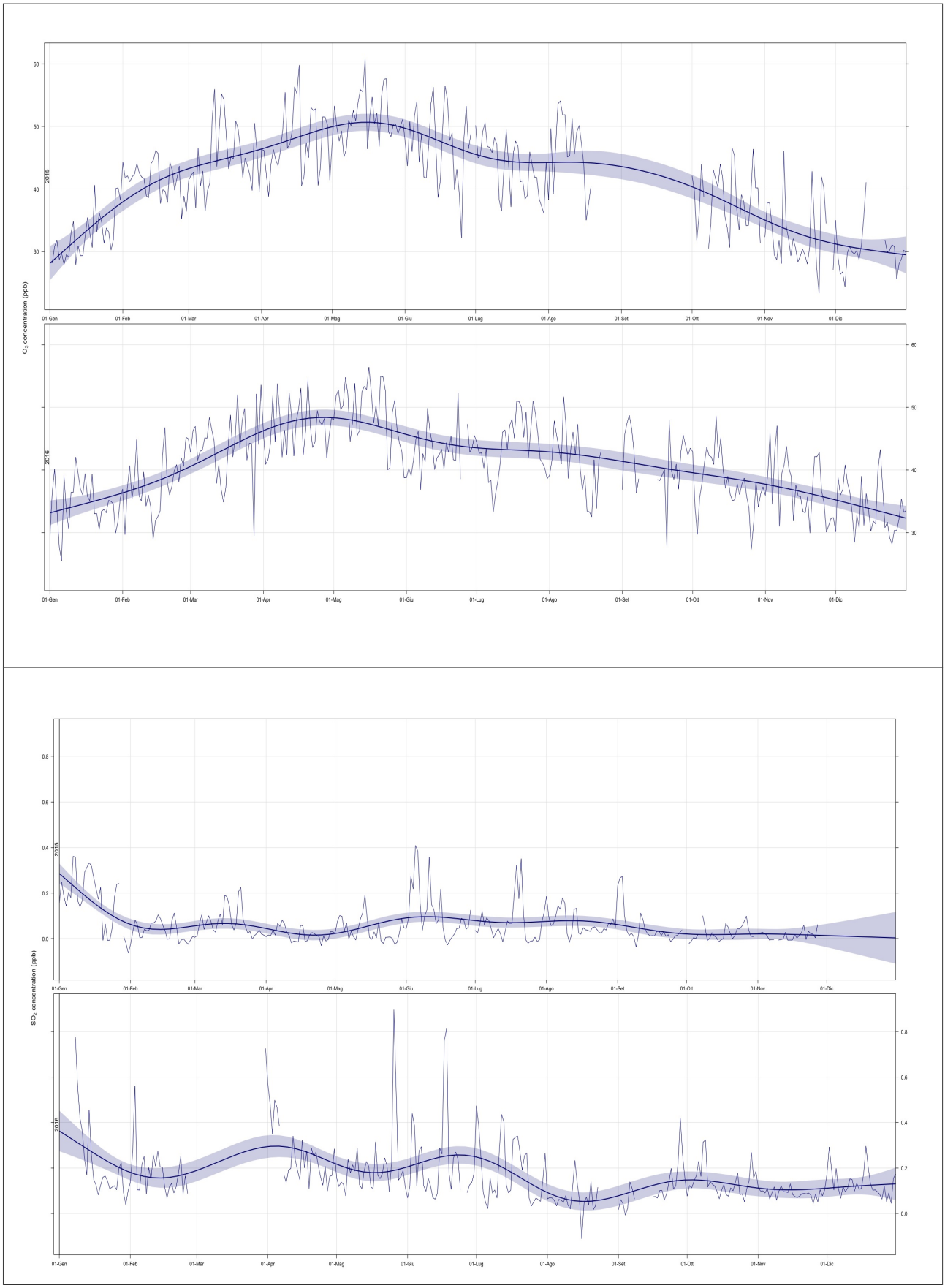

Time series of daily averaged NO and NO_2 concentration (ppb) – biennium 2015 / 2016 (thick line: average / shaded area: 95 % confidence level)

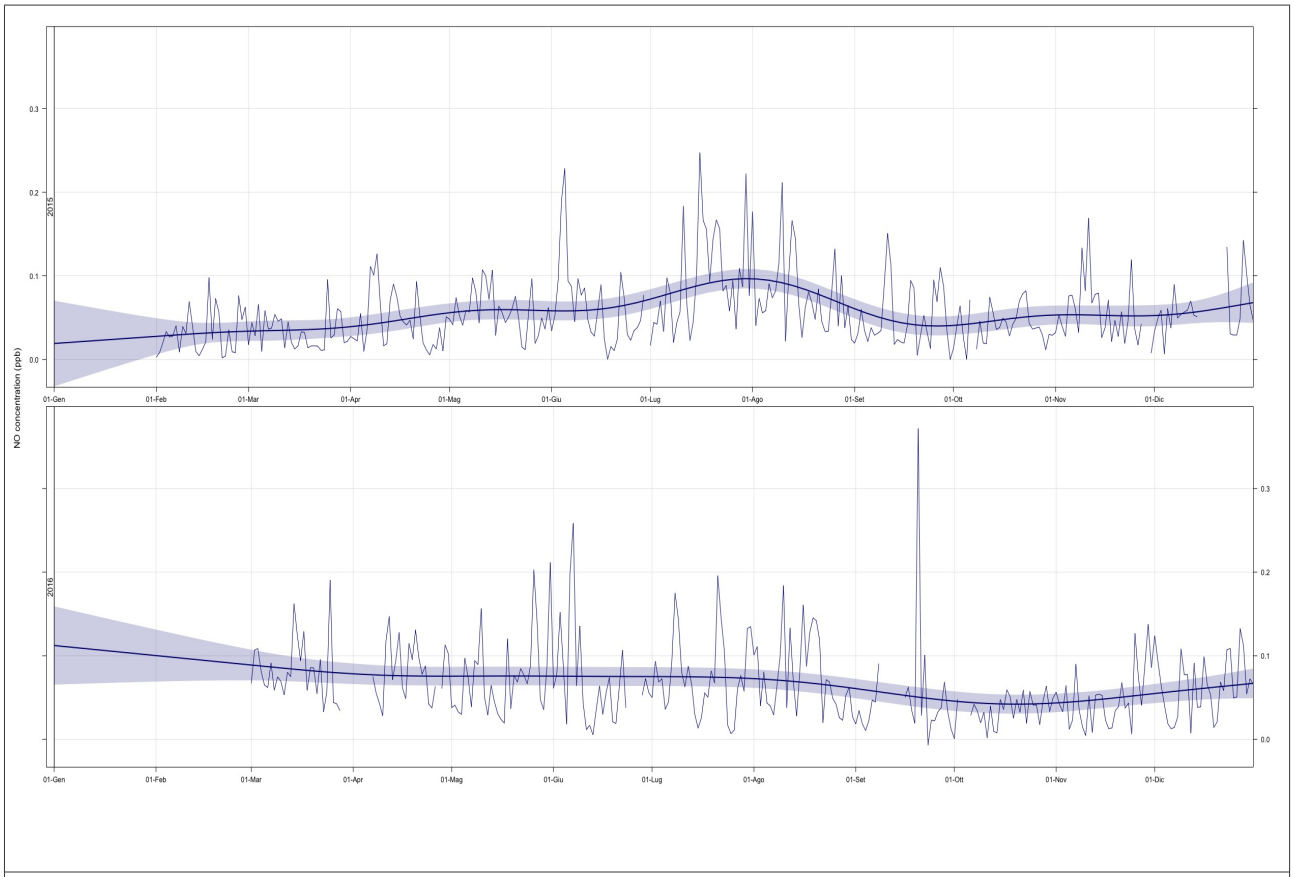

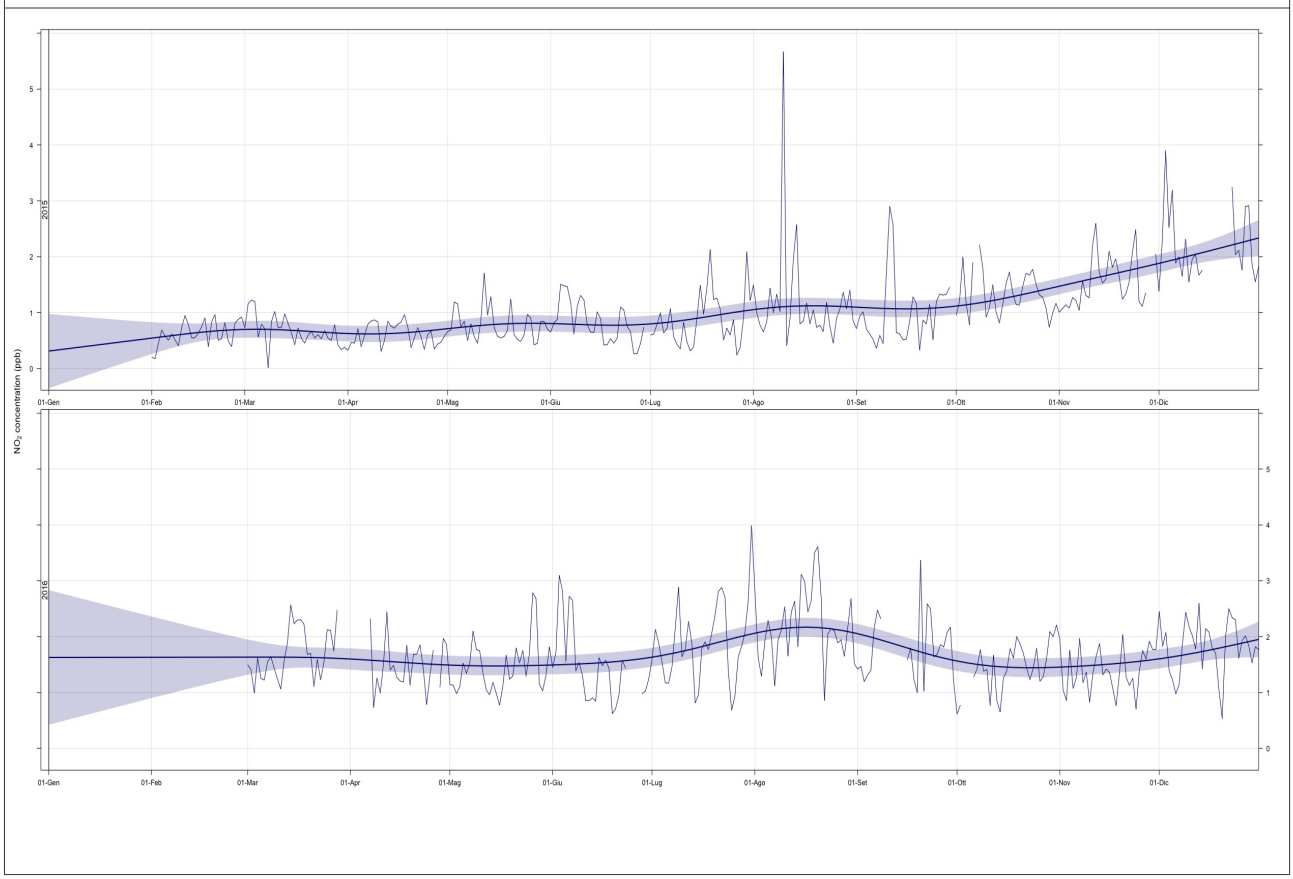

Time series of daily averaged CO and CO_2 concentration (ppb / ppm) – biennium 2015 / 2016 (thick line: average / shaded area: 95 % confidence level)

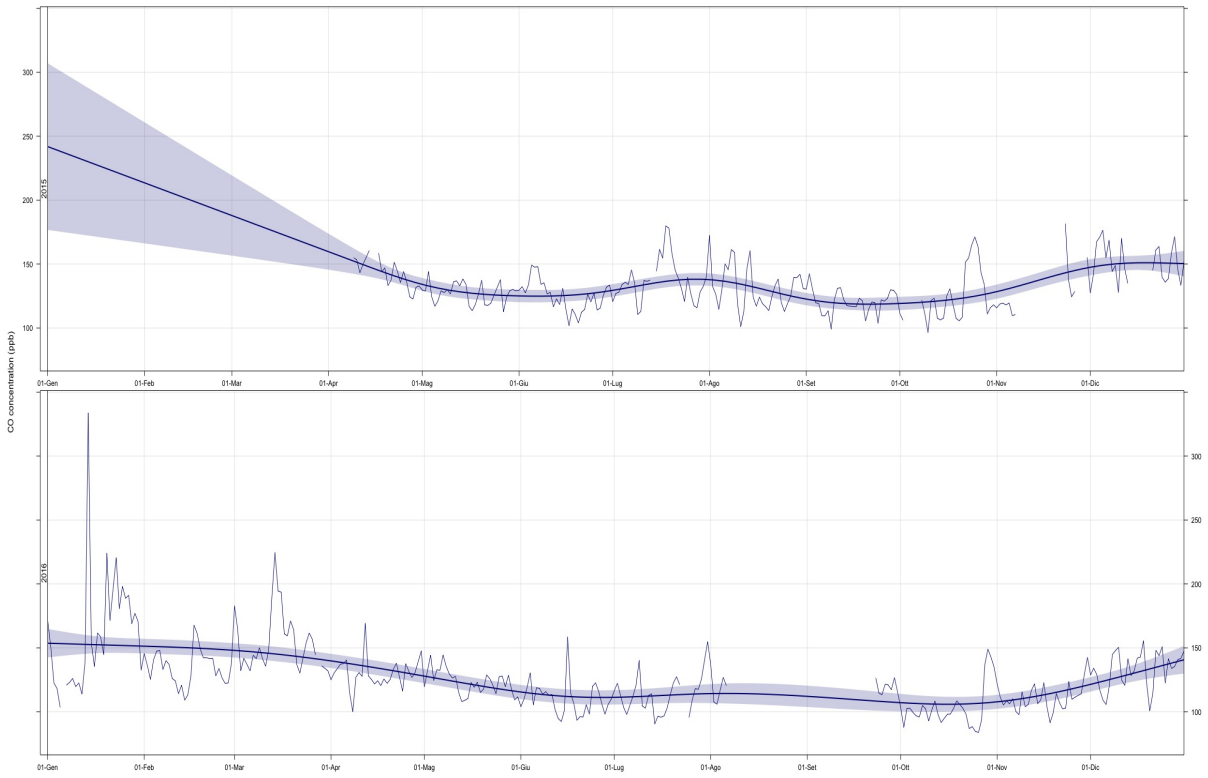

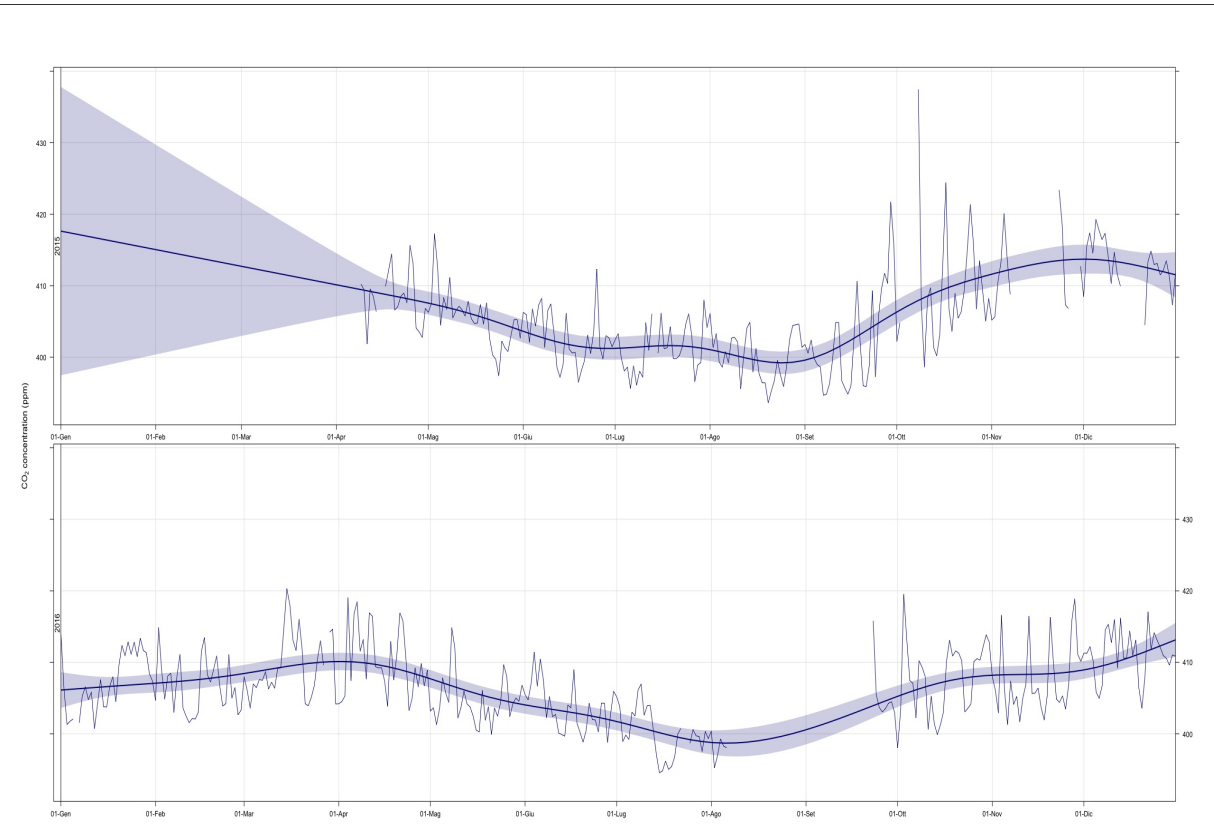

Time series of daily averaged CH_4 concentration (ppb) and PM_{10} ($\mu g/m^3$)
biennium 2015 / 2016
(thick line: average / shaded area: 95 % confidence level)

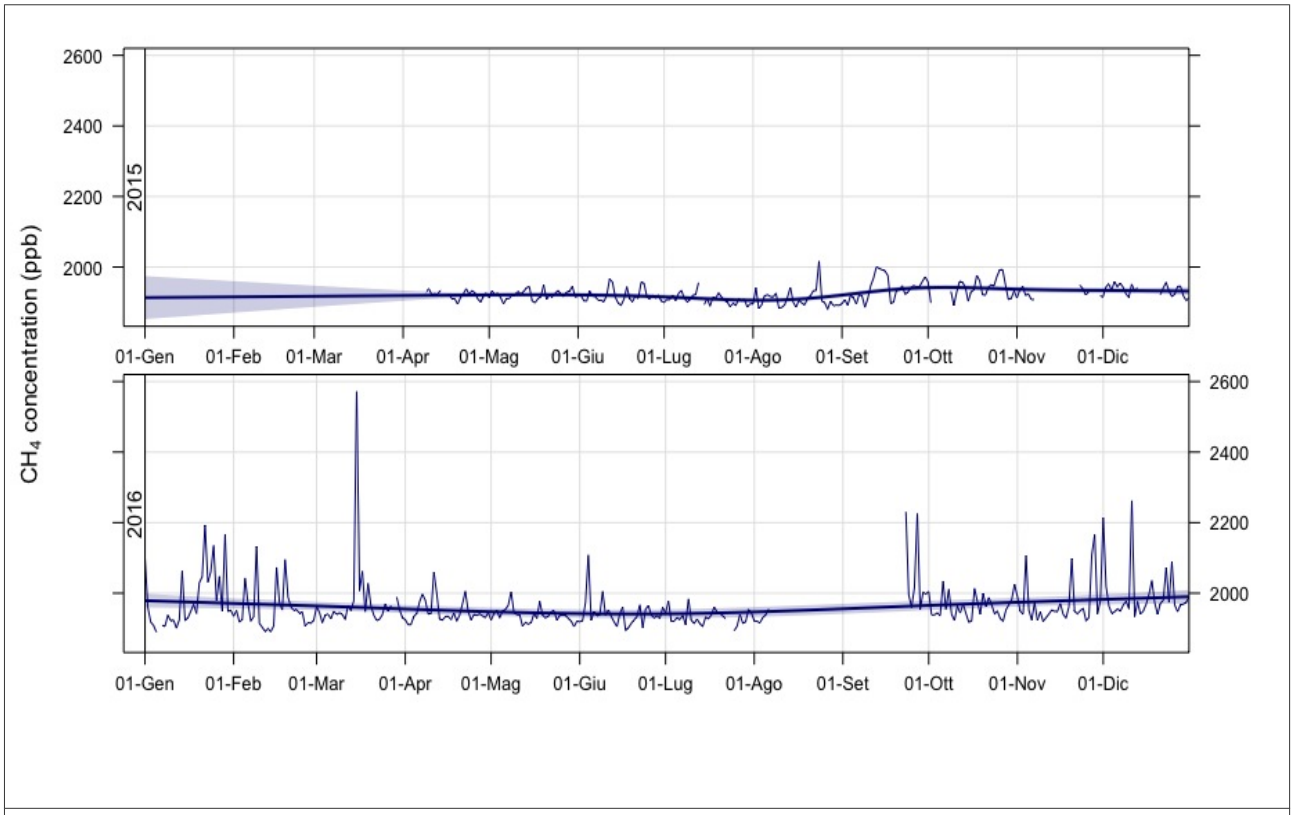

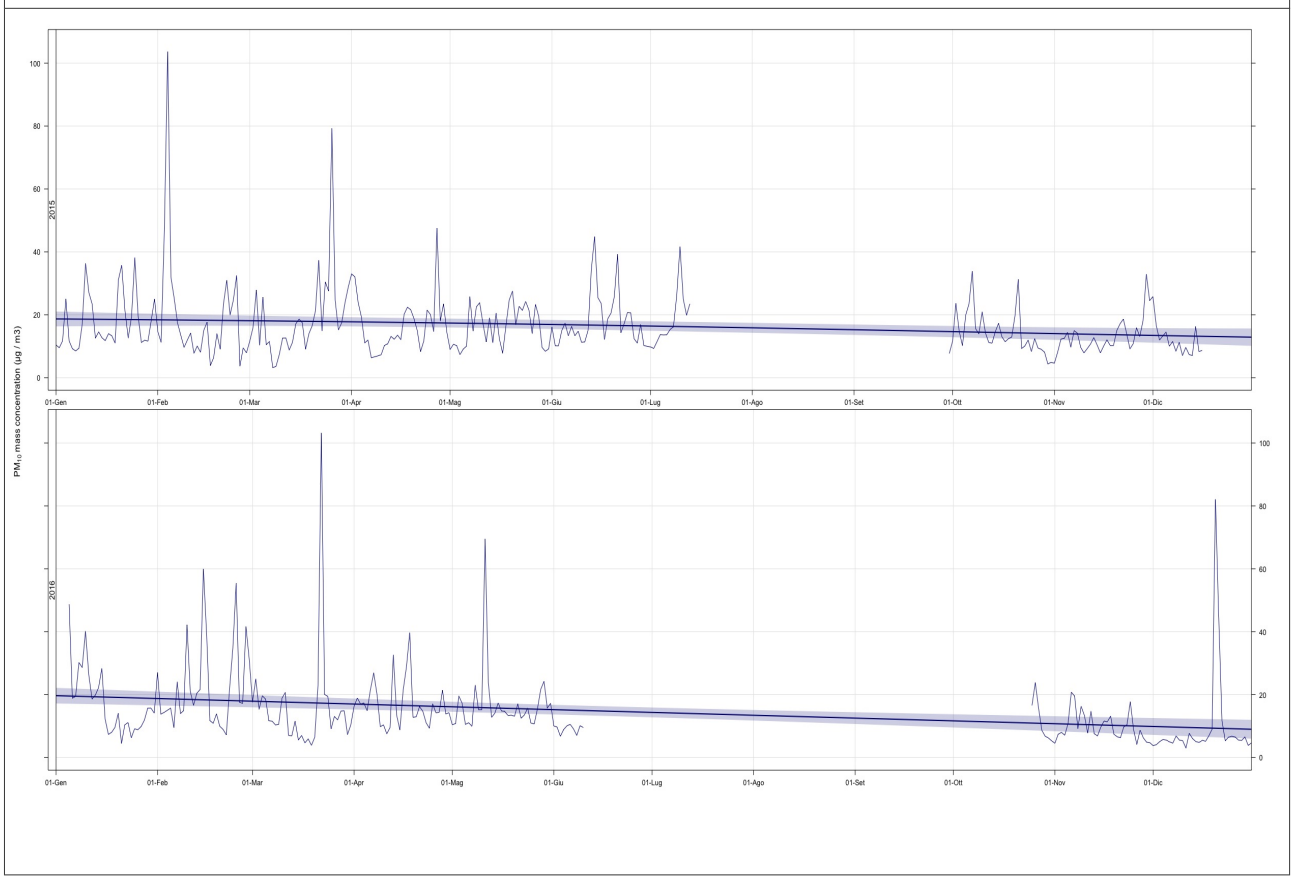

Time series of daily averaged $PM_{2.5}$ (µg/m^3) and total particles concentration (n cm^{-3}) biennium 2015 / 2016
(thick line: average / shaded area: 95 % confidence level)

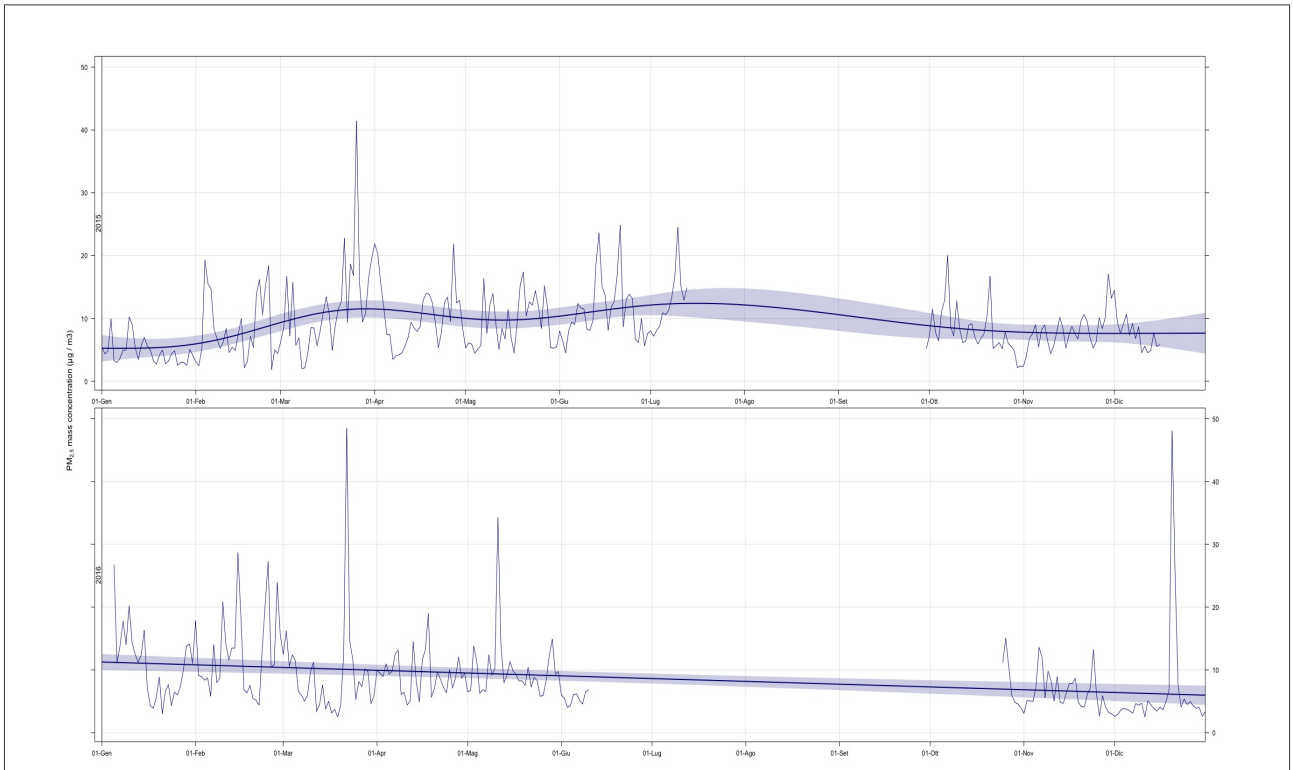

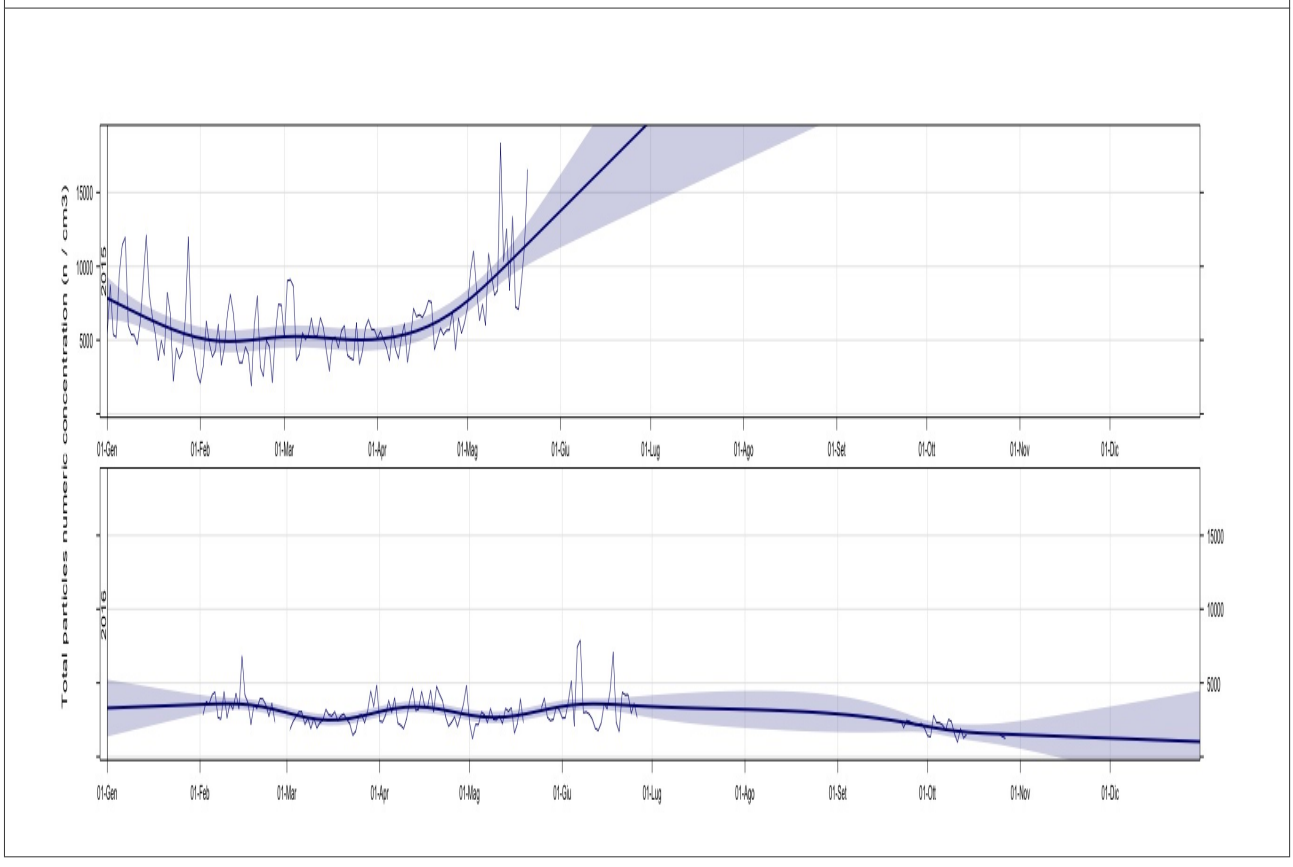

Time series of daily averaged fine and coarse particles concentration (n/cm^3)
biennium 2015 / 2016
(thick line: average / shaded area: 95 % confidence level)

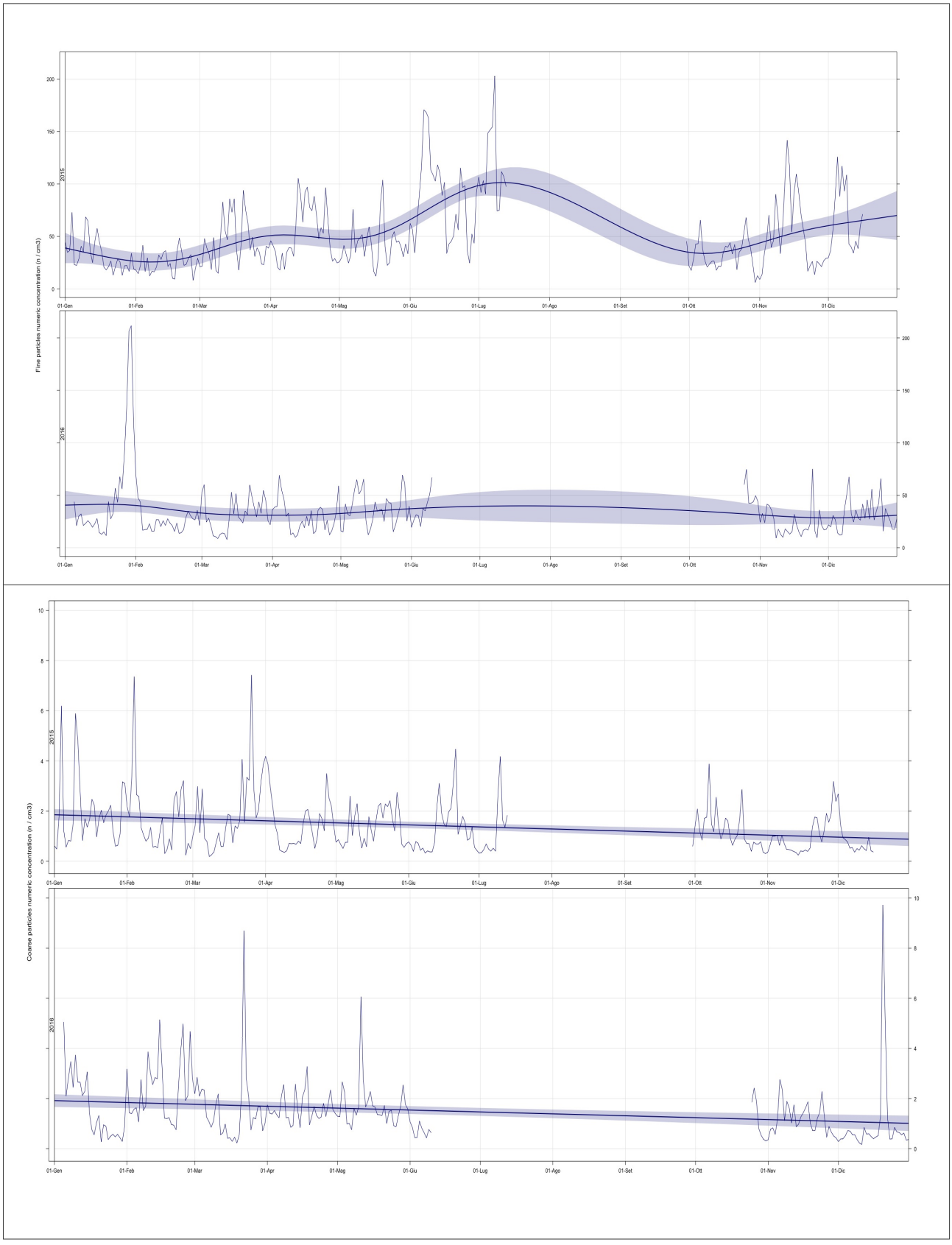

Time series of hourly and daily averaged black carbon concentration (µg/m^3)
(thick line: average / shaded area: 95 % confidence level)

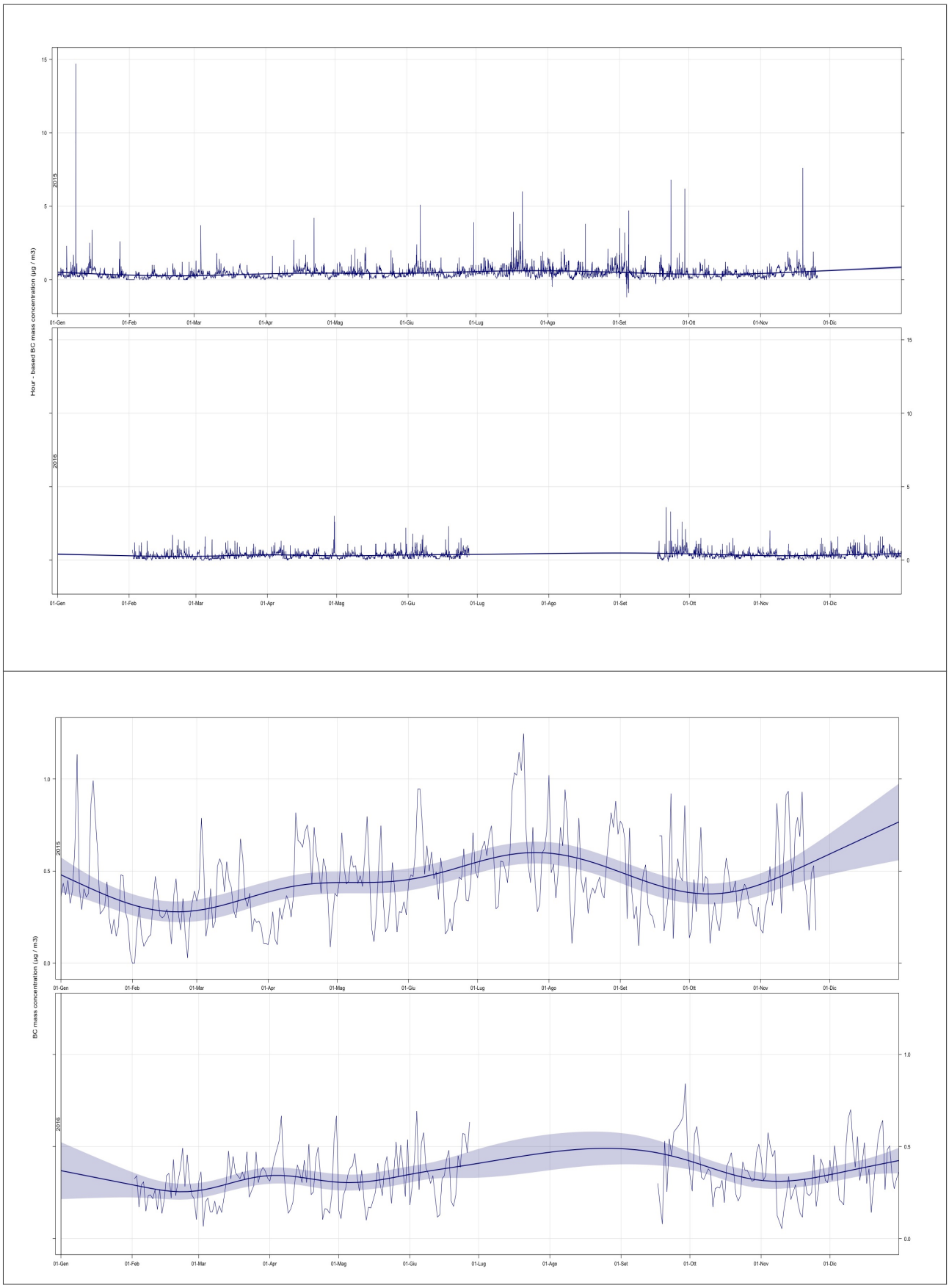

Time series of daily averaged scattering coefficients at 450, 550 and 700 nm biennium 2015 / 2016

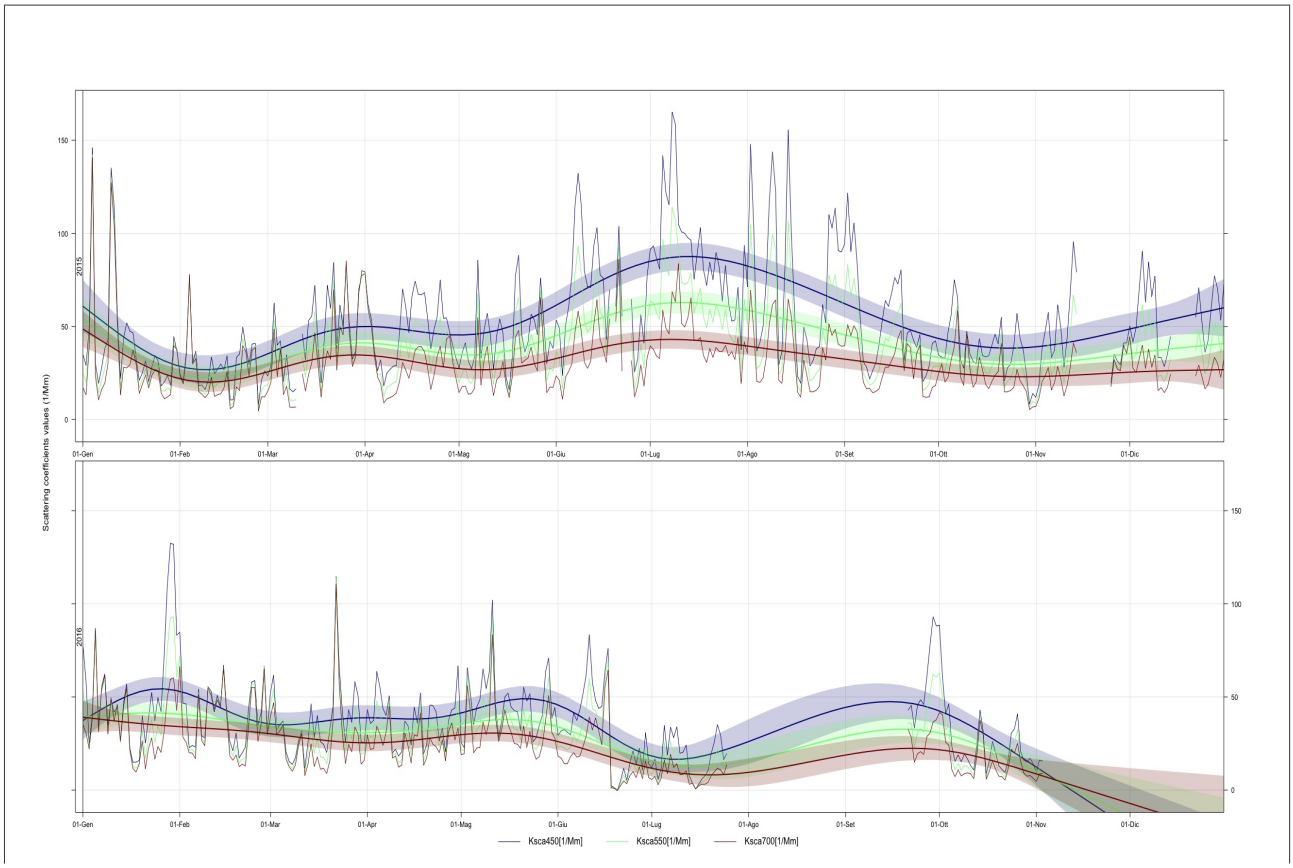


Daily average of weather parameters
Temperature (°C), Relative humidity (%), Atmospheric pressure (hPa), Rain (mm), Wind speed (m s-1), Wind direction (°)
T
RH
P
Rain
WS
WD
Gen
Apr
Lug
Ott
Gen
Apr
Lug
Ott
Time
T
RH
P
Rain
WS
WD

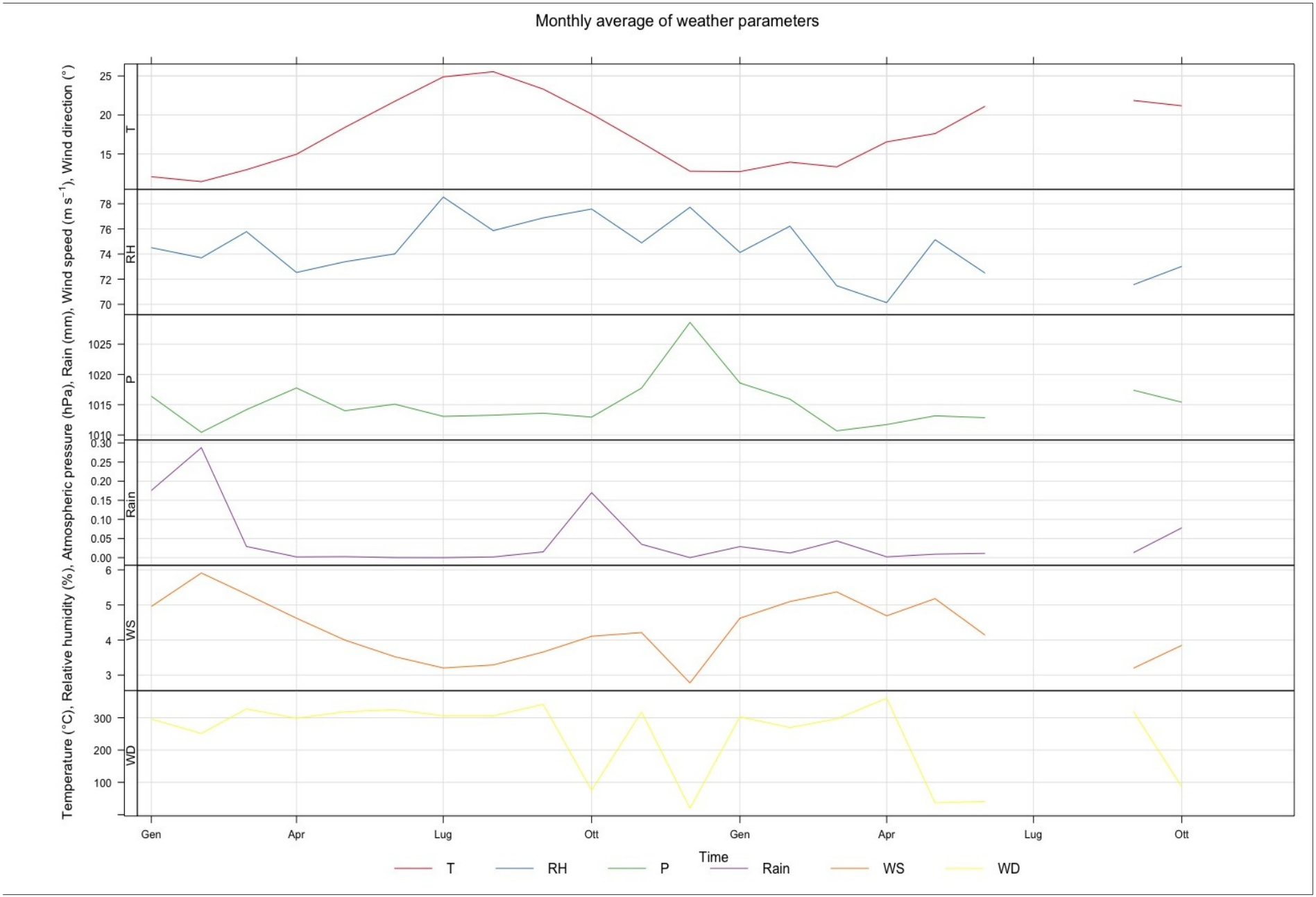
Monthly average of weather parameters
Temperature (°C), Relative humidity (%), Atmospheric pressure (hPa), Rain (mm), Wind speed (m s-1), Wind direction (°)
T
RH
P
Rain
WS
WD
Gen
Apr
Lug
Ott
Gen
Apr
Lug
Ott
Time
T
RH
P
Rain
WS
WD

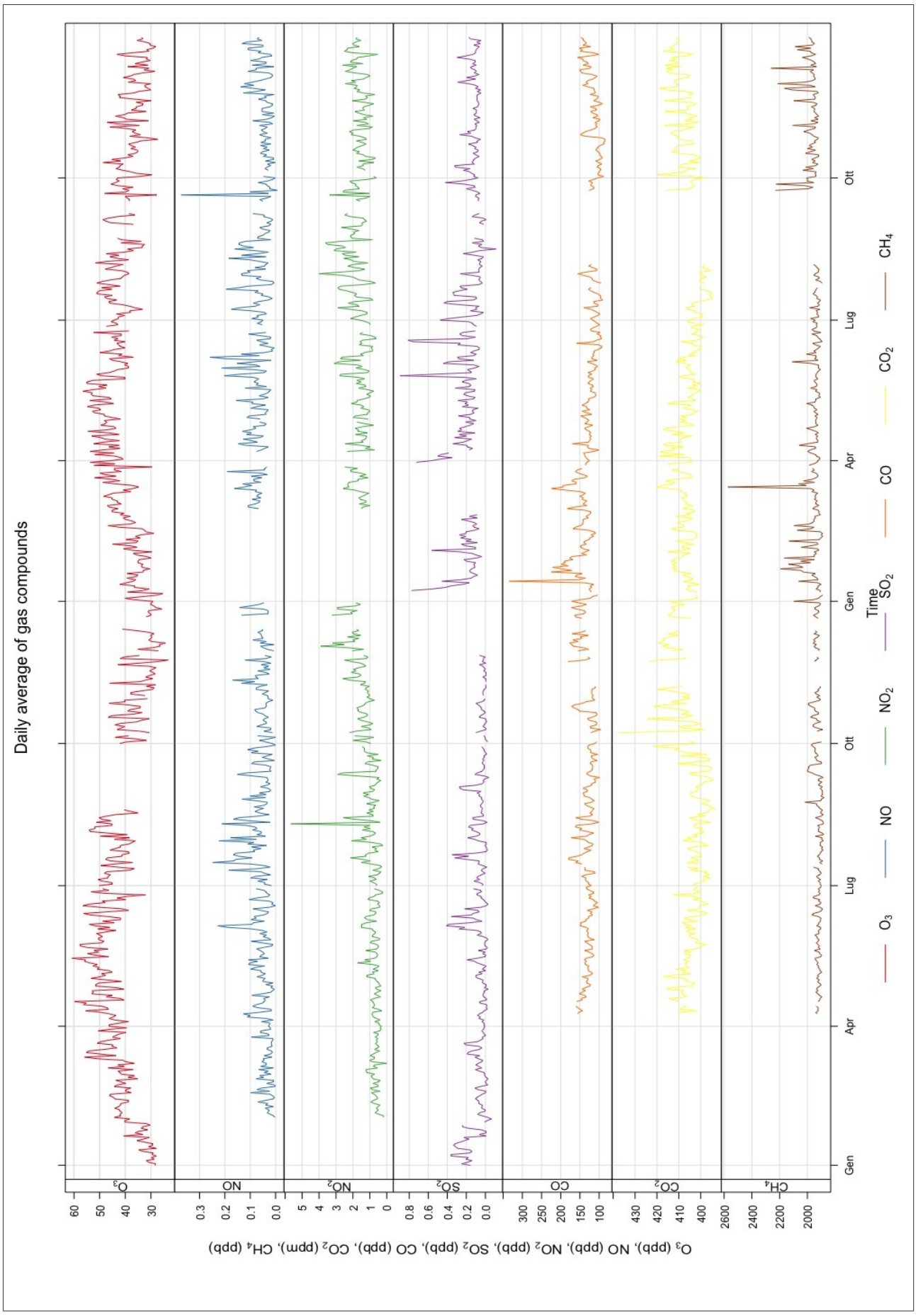
Daily average of gas compounds
O3 (ppb), NO (ppb), NO2 (ppb), SO2 (ppb), CO (ppb), CO2 (ppm), CH4 (ppb)
O3
NO
NO2
SO2
CO
CO2
CH4
Gen
Apr
Lug
Ott
Gen
Apr
Lug
Ott
Time
O3
NO
NO2
SO2
CO
CO2
CH4

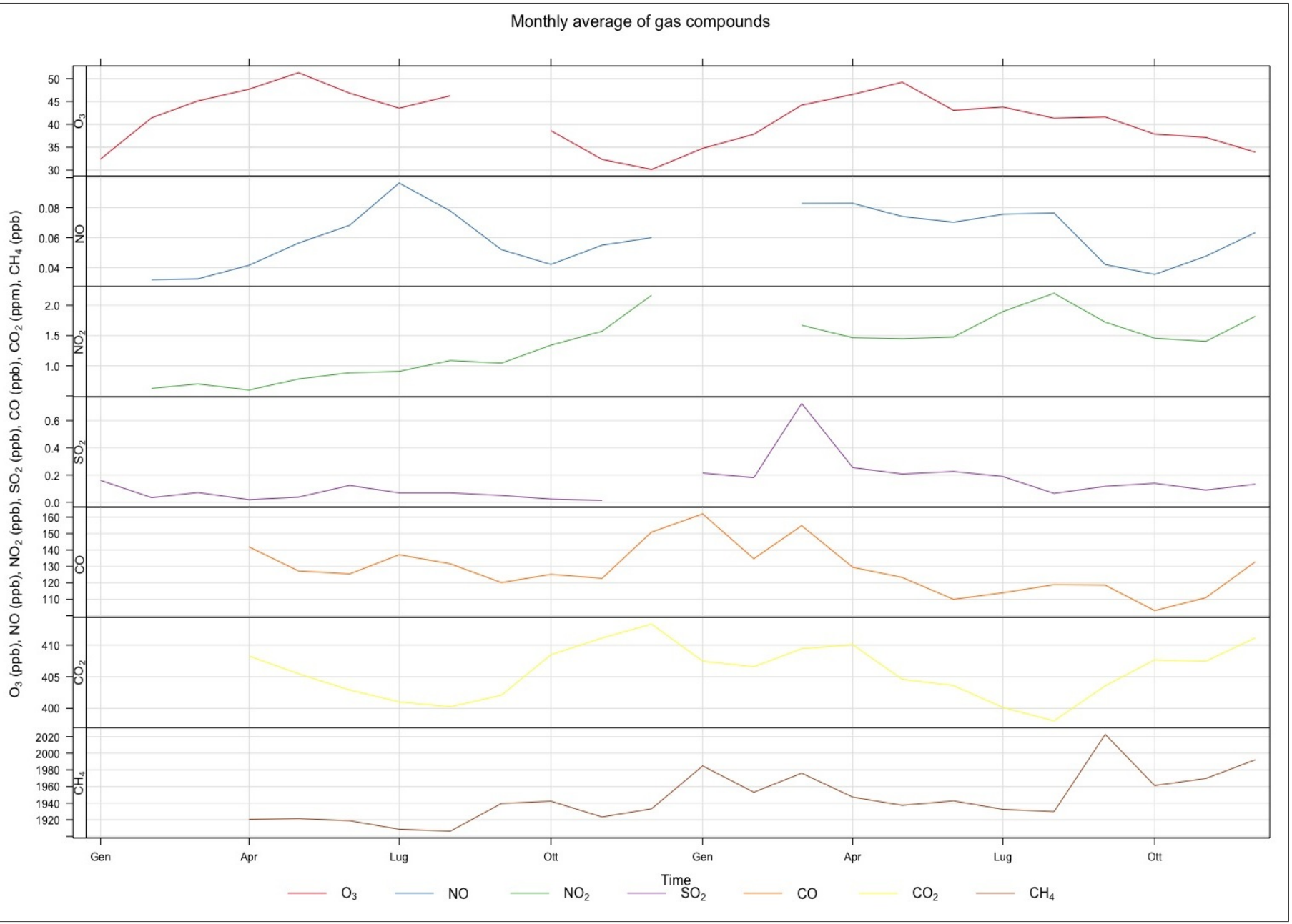
Monthly average of gas compounds
O3 (ppb), NO (ppb), NO2 (ppb), SO2 (ppb), CO (ppb), CO2 (ppm), CH4 (ppb)
O3
NO
NO2
SO2
CO
CO2
CH4
Gen
Apr
Lug
Ott
Time
O3
NO
NO2
SO2
CO
CO2
CH4

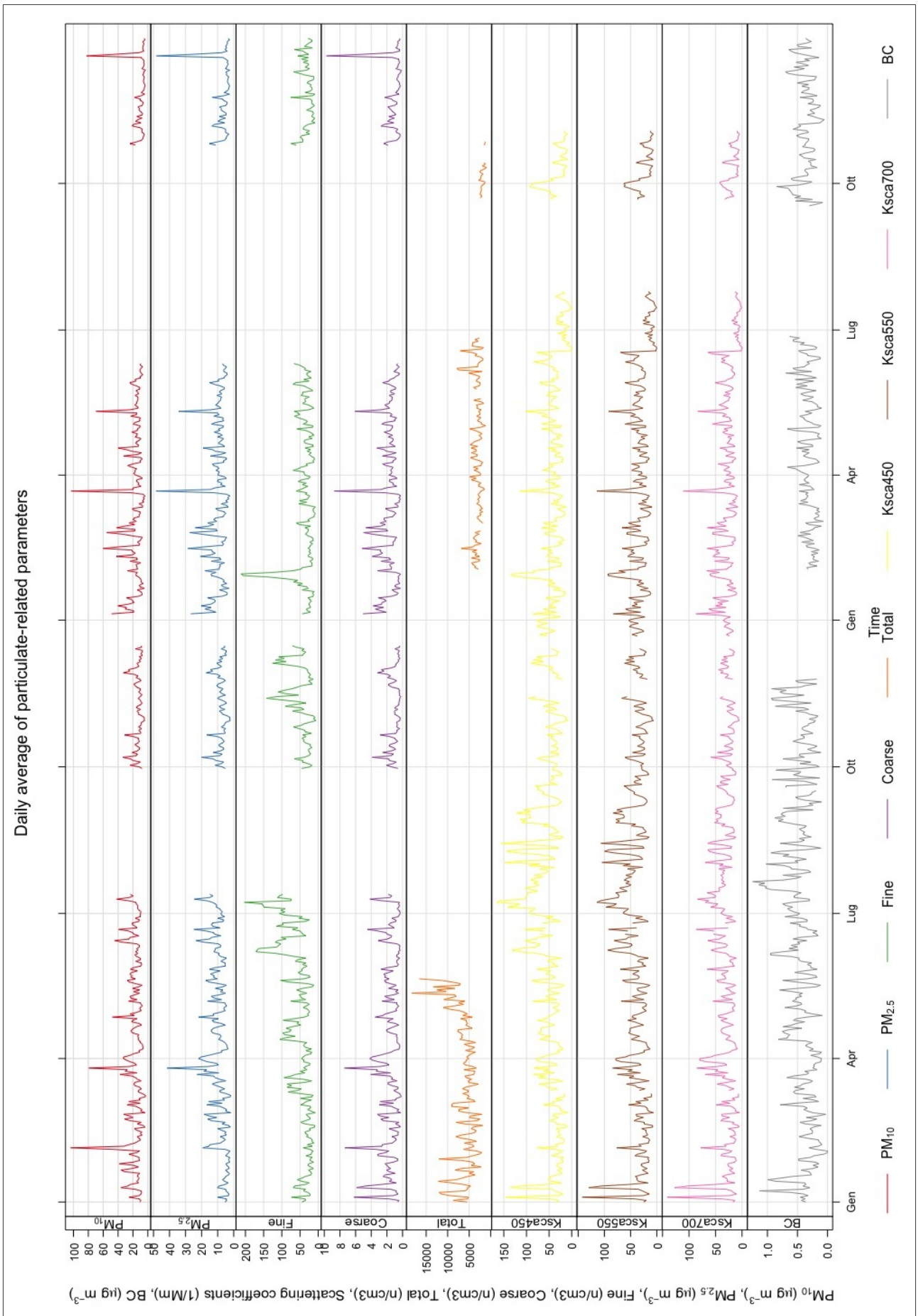
Daily average of particulate-related parameters
PM10 (µg m-3), PM2.5 (µg m-3), Fine (n/cm3), Coarse (n/cm3), Total (n/cm3), Scattering coefficients (1/Mm), BC (µg m-3)
PM10
PM2.5
Fine
Coarse
Total
Ksca450
Ksca550
Ksca700
BC
Gen
Apr
Lug
Ott
Gen
Apr
Lug
Ott
Time
PM10
PM2.5
Fine
Coarse
Total
Ksca450
Ksca550
Ksca700
BC

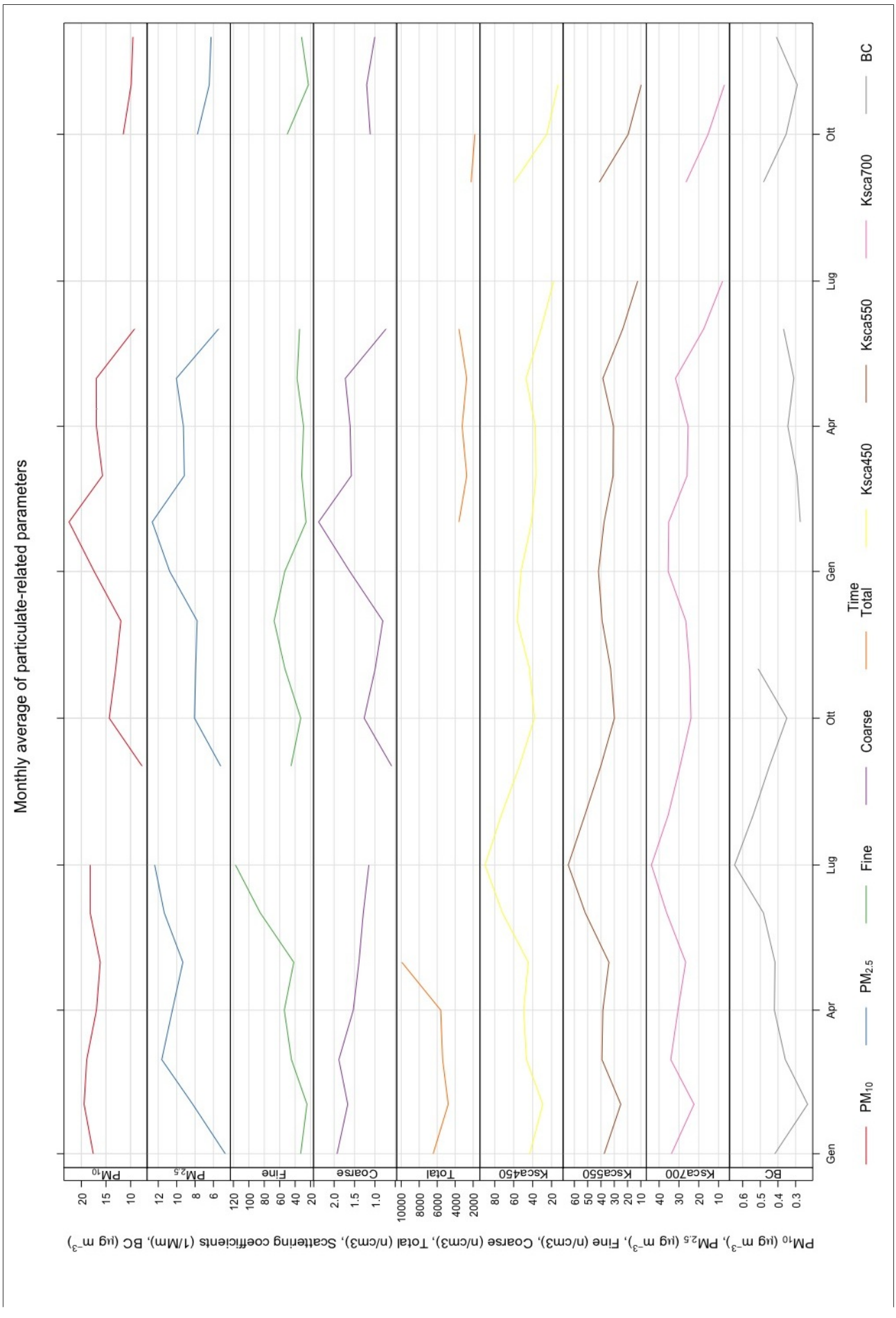
Monthly average of particulate-related parameters
PM10 (µg m-3), PM2.5 (µg m-3), Fine (n/cm3), Coarse (n/cm3), Total (n/cm3), Scattering coefficients (1/Mm), BC (µg m-3)
PM10
PM2.5
Fine
Coarse
Total
Ksca450
Ksca550
Ksca700
BC
Gen
Apr
Lug
Ott
Gen
Apr
Lug
Ott
Time
PM10
PM2.5
Fine
Coarse
Total
Ksca450
Ksca550
Ksca700
BC

Windrose - 2015

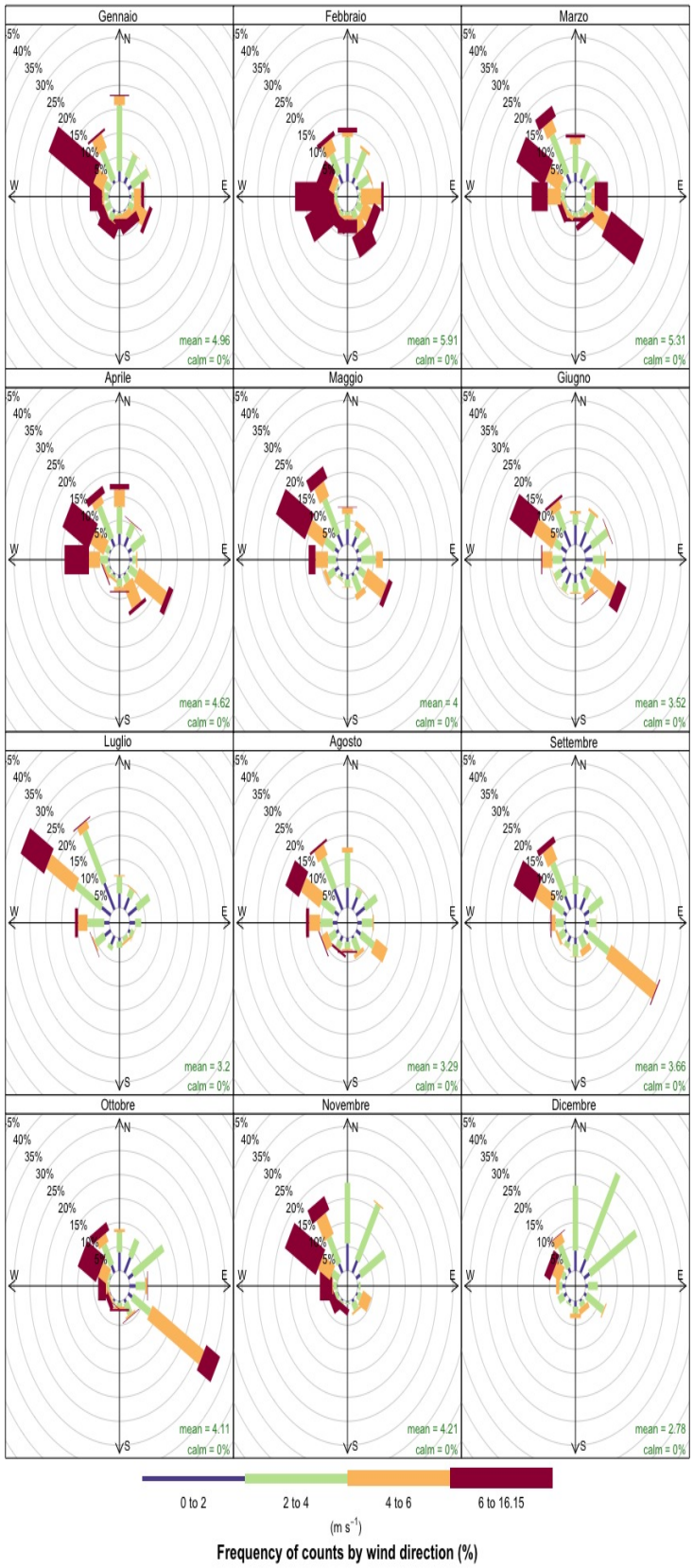

Windrose - 2016

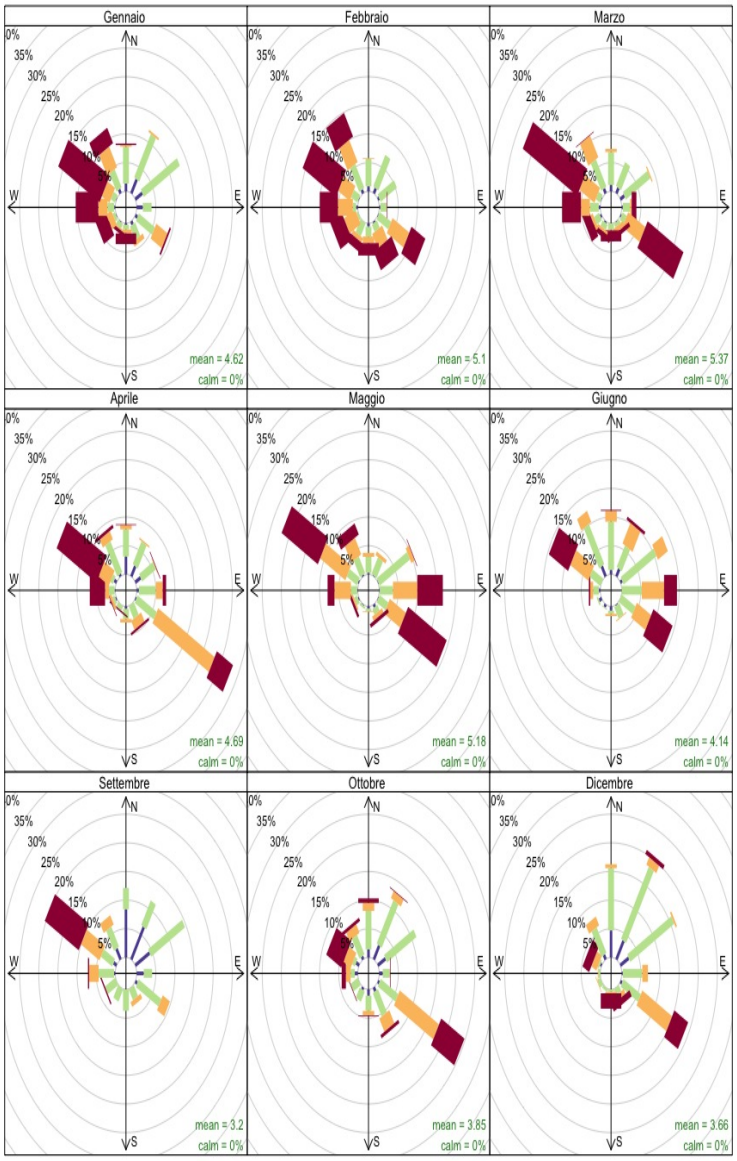

Inter – year wind rose comparison

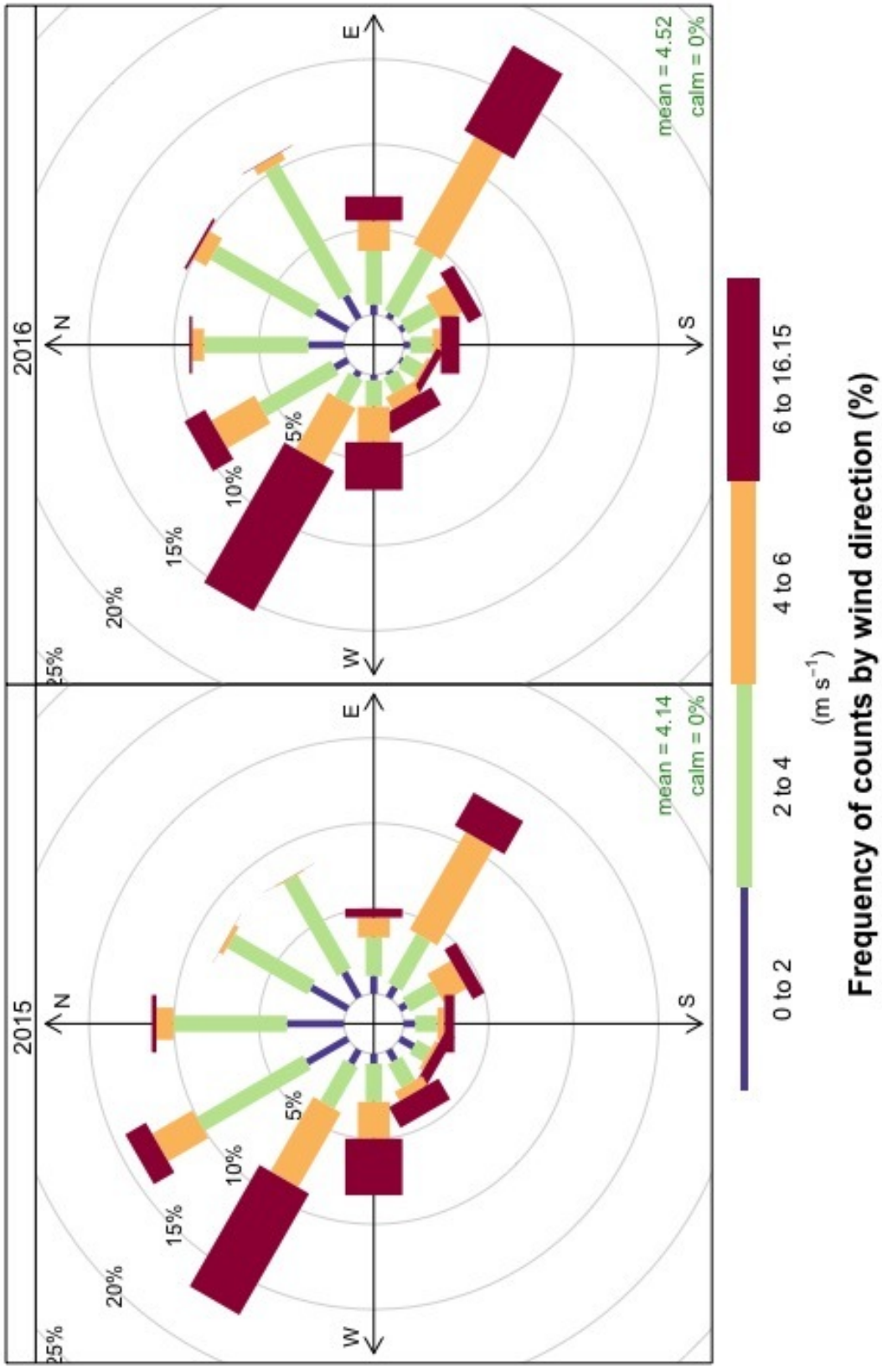

Seasonal wind direction in 2015

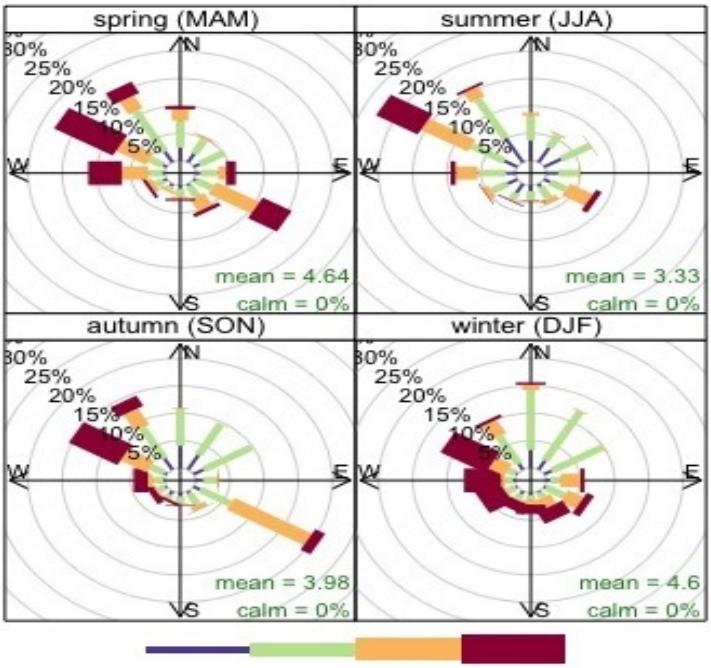

Frequency of counts by wind direction (%)

Seasonal wind direction in 2016

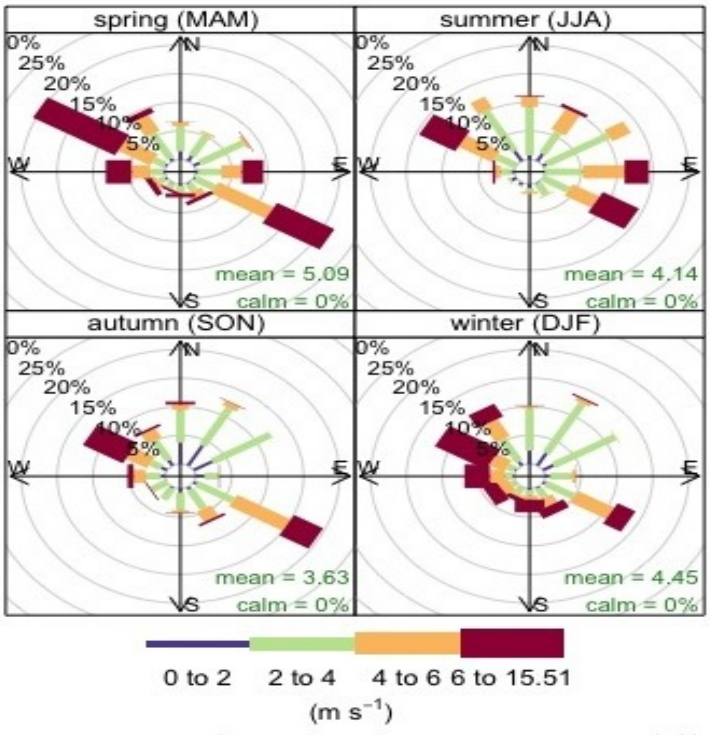

Frequency of counts by wind direction (%)

Seasonal variation of parameters v/s wind direction

O_3 seasonal variations in 2015

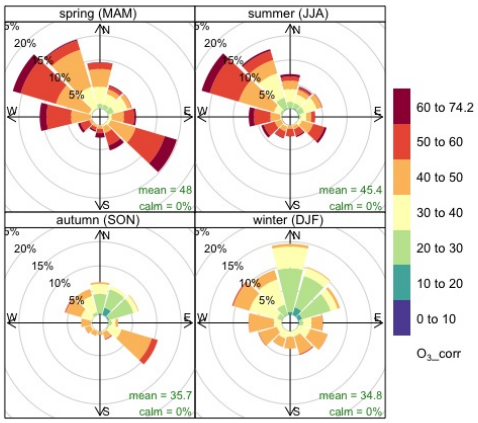

Frequency of counts by wind direction (%)

O_3 seasonal variations in 2016

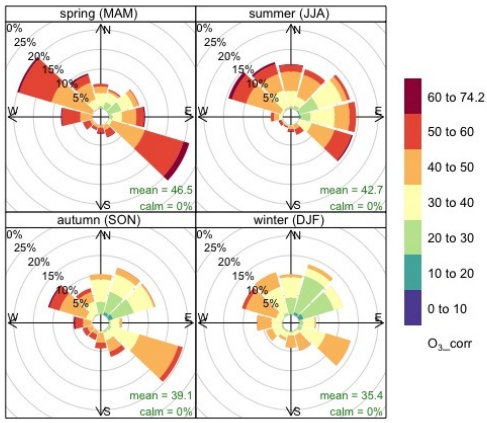

Frequency of counts by wind direction (%)

SO_2 seasonal variations in 2015

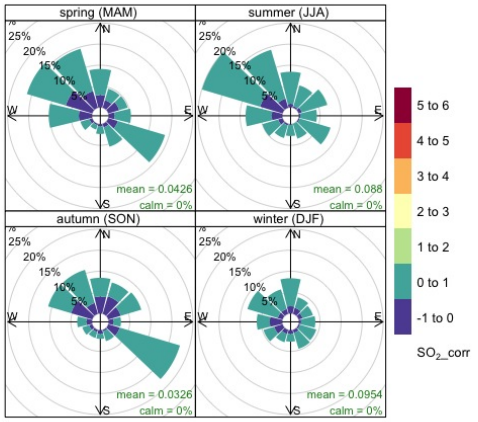

Frequency of counts by wind direction (%)

SO_2 seasonal variations in 2016

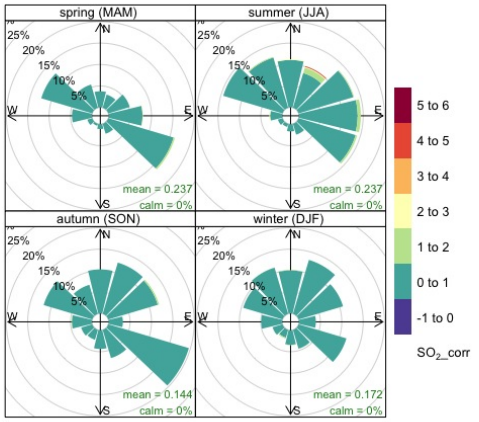

Frequency of counts by wind direction (%)

NO seasonal variations in 2015

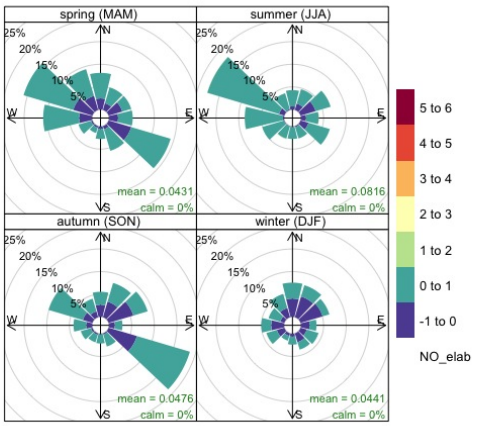

Frequency of counts by wind direction (%)

NO seasonal variations in 2016

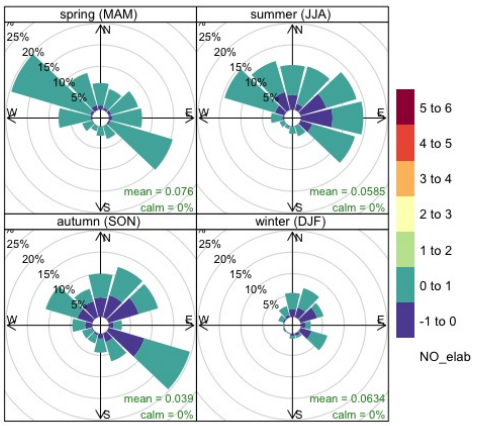

Frequency of counts by wind direction (%)

NO_2 seasonal variations in 2015

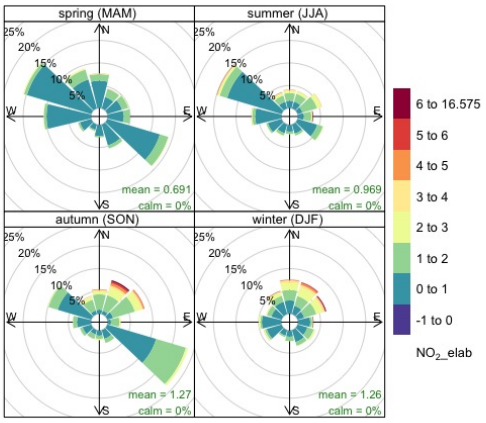

Frequency of counts by wind direction (%)

NO_2 seasonal variations in 2016

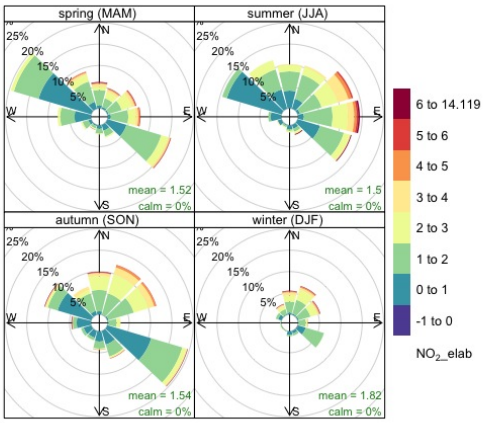

Frequency of counts by wind direction (%)

CO seasonal variations in 2015

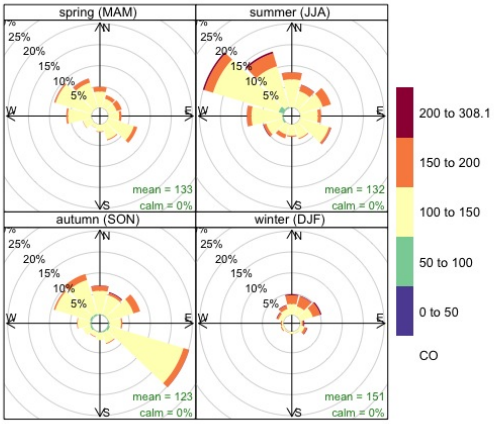

Frequency of counts by wind direction (%)

CO seasonal variations in 2016

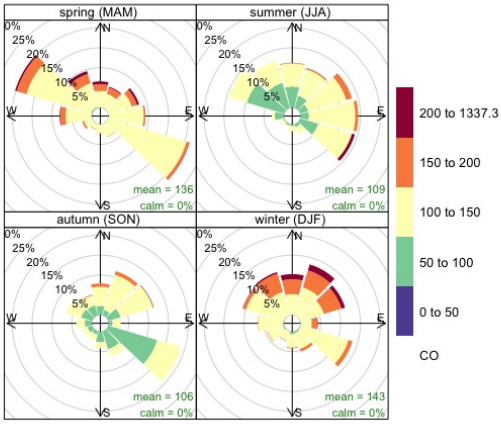

Frequency of counts by wind direction (%)

CO_2 seasonal variations in 2015

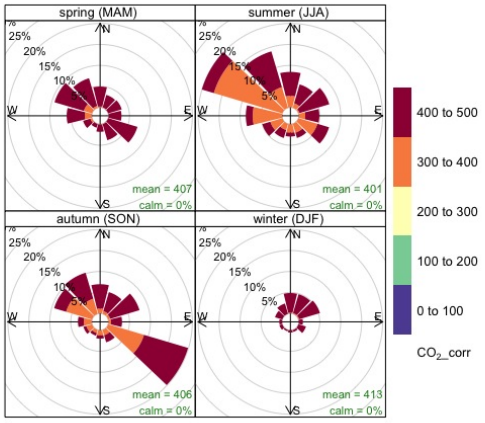

Frequency of counts by wind direction (%)

CO_2 seasonal variations in 2016

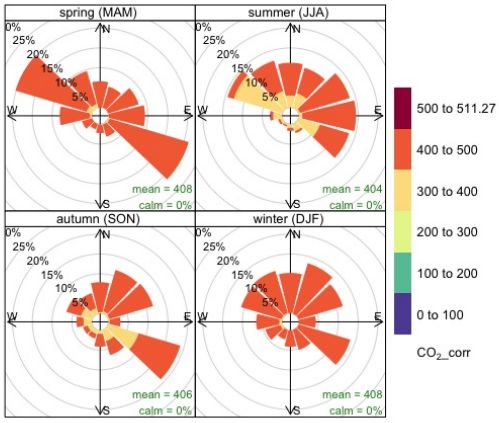

Frequency of counts by wind direction (%)

CH_4 seasonal variations in 2015

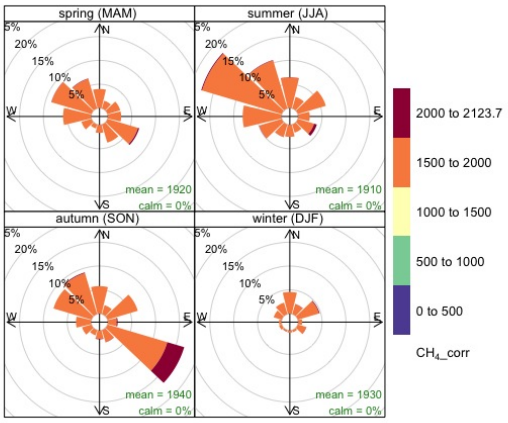

Frequency of counts by wind direction (%)

CH_4 seasonal variations in 2016

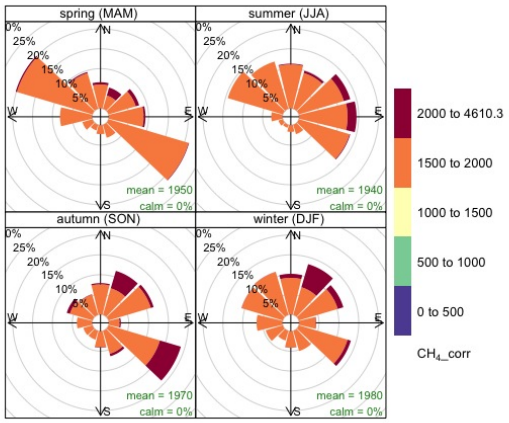

Frequency of counts by wind direction (%)

PM_{10} seasonal variations in 2015

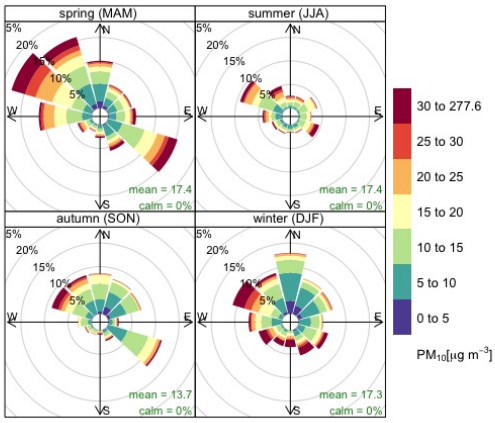

Frequency of counts by wind direction (%)

PM_{10} seasonal variations in 2016

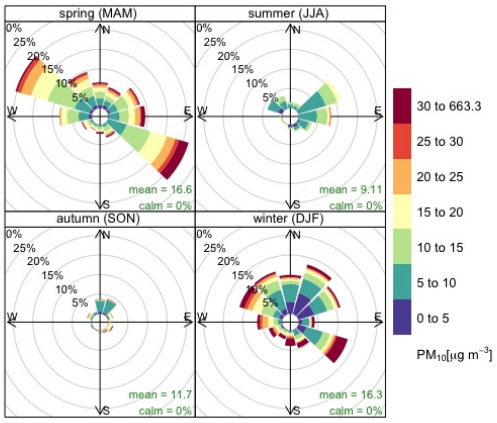

Frequency of counts by wind direction (%)

$PM_{2.5}$ seasonal variations in 2015

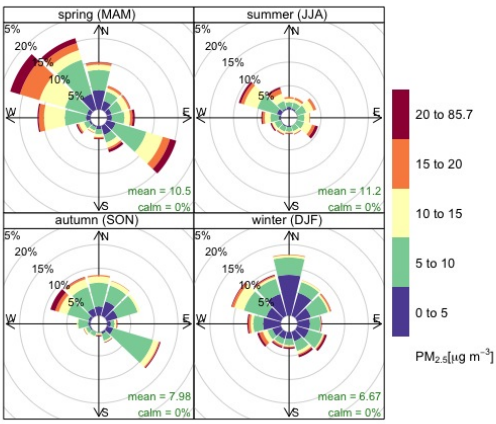

Frequency of counts by wind direction (%)

$PM_{2.5}$ seasonal variations in 2016

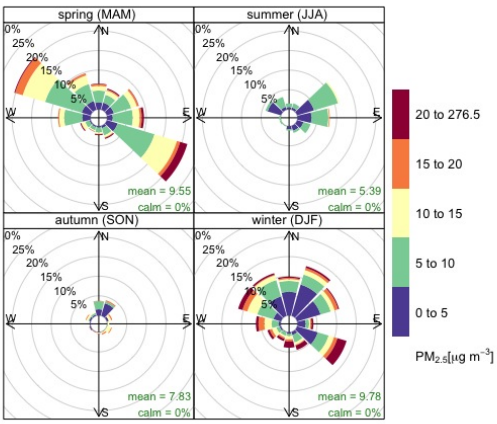

Frequency of counts by wind direction (%)

Fine particles (n/cm3) variations in 2015

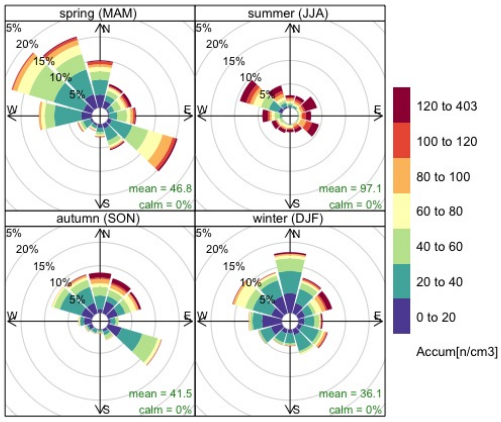

Frequency of counts by wind direction (%)

Fine particles (n/cm3) variations in 2016

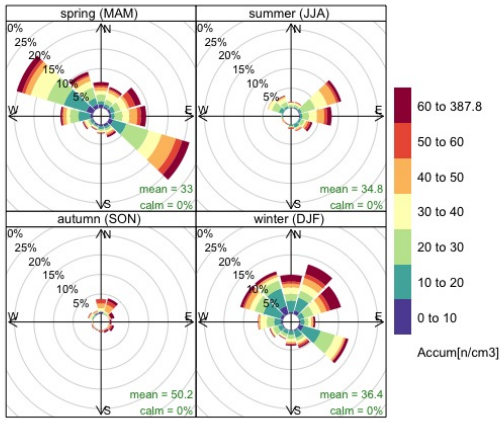

Frequency of counts by wind direction (%)

Coarse particles (n/cm3) variations in 2015

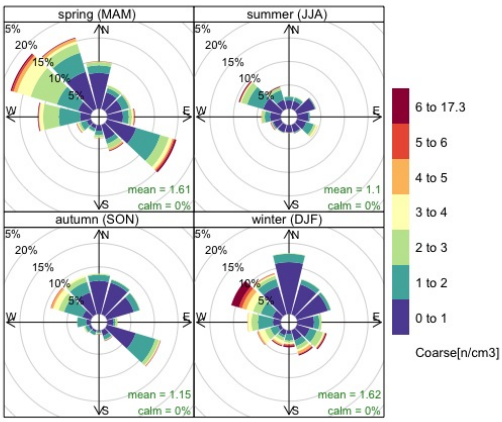

Frequency of counts by wind direction (%)

Coarse particles (n/cm3) variations in 2016

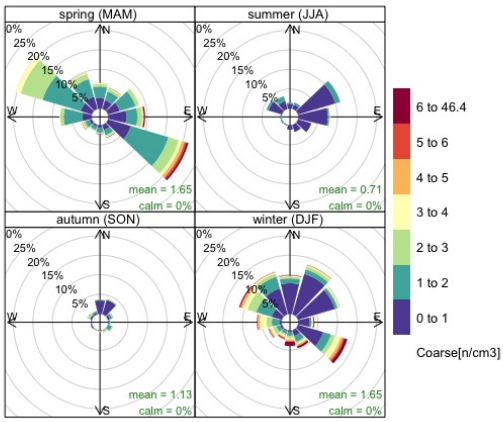

Frequency of counts by wind direction (%)

PM numeric concentration variations in 2015

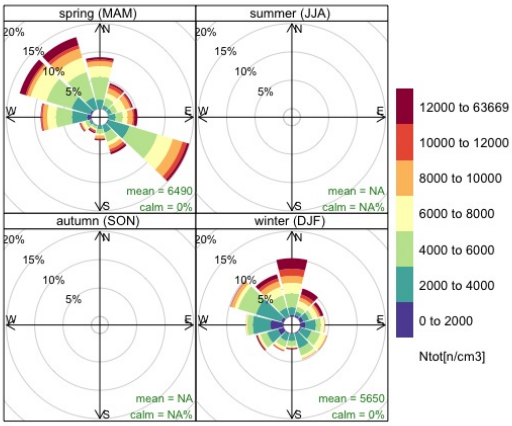

Frequency of counts by wind direction (%)

PM numeric concentration variations in 2016

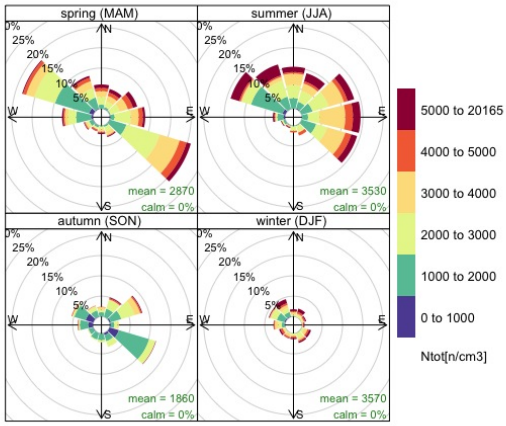

Frequency of counts by wind direction (%)

BC seasonal variations in 2015

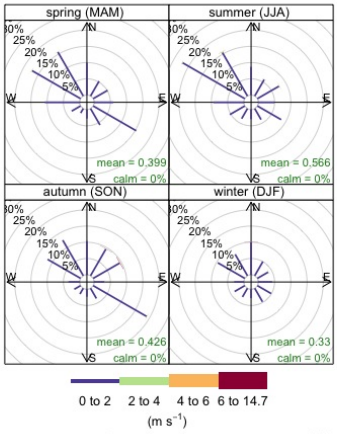

Frequency of counts by wind direction (%)

BC seasonal variations in 2016

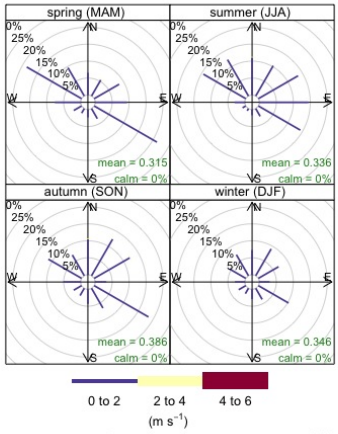

Frequency of counts by wind direction (%)

Calendar plots

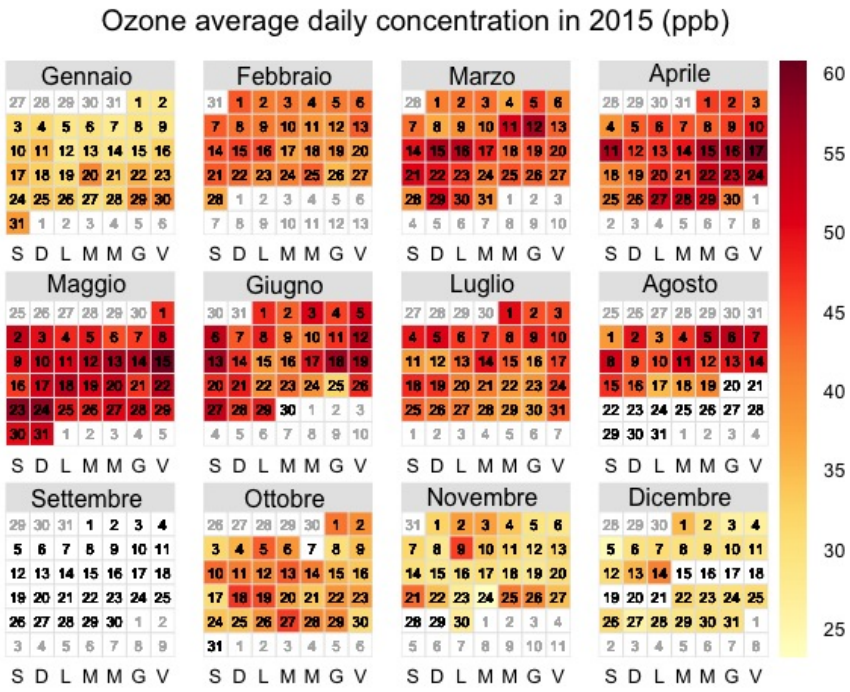

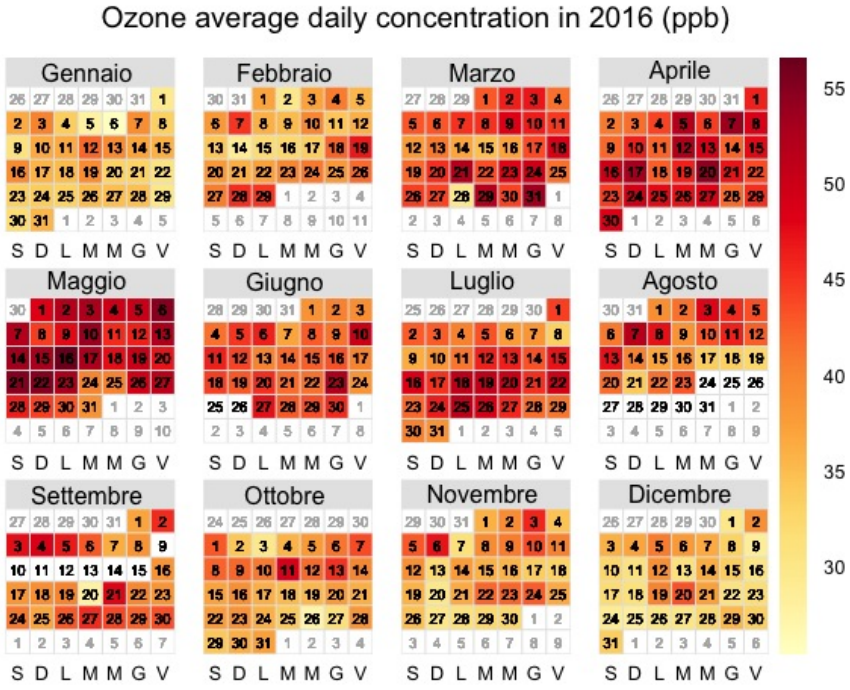

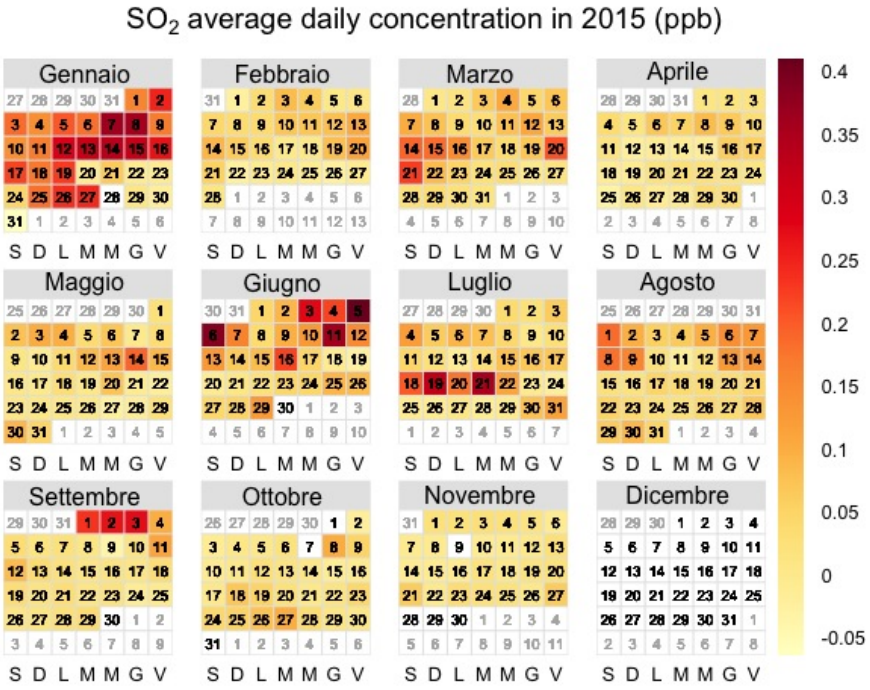
SO2 average daily concentration in 2015 (ppb)
Gennaio
Febbraio
Marzo
Aprile
Maggio
Giugno
Luglio
Agosto
Settembre
Ottobre
Novembre
Dicembre
S D L M M G V
0.4
0.35
0.3
0.25
0.2
0.15
0.1
0.05
0
-0.05

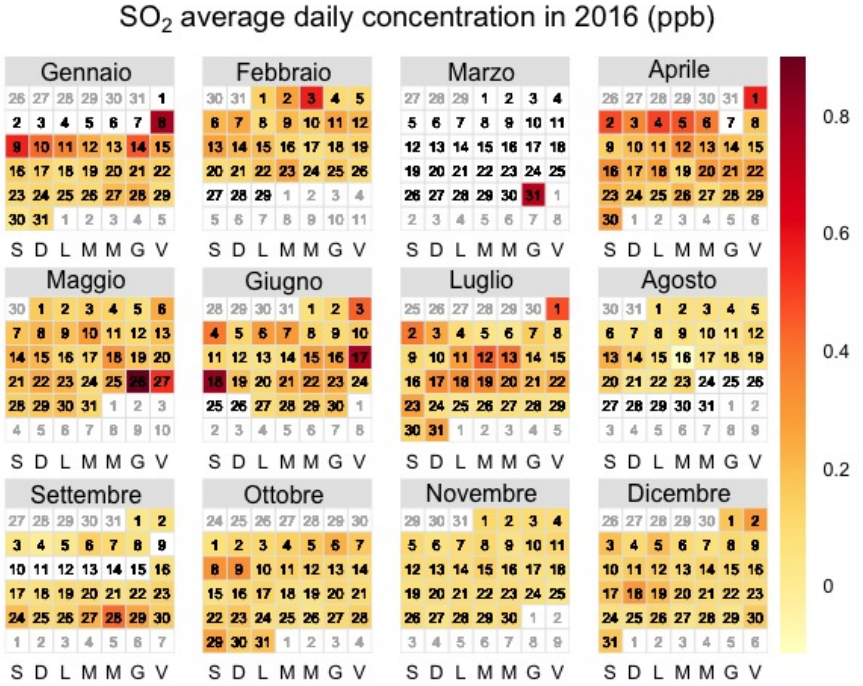
SO2 average daily concentration in 2016 (ppb)
Gennaio
Febbraio
Marzo
Aprile
Maggio
Giugno
Luglio
Agosto
Settembre
Ottobre
Novembre
Dicembre
S D L M M G V
0.8
0.6
0.4
0.2
0

NO average daily concentration in 2015 (ppb)

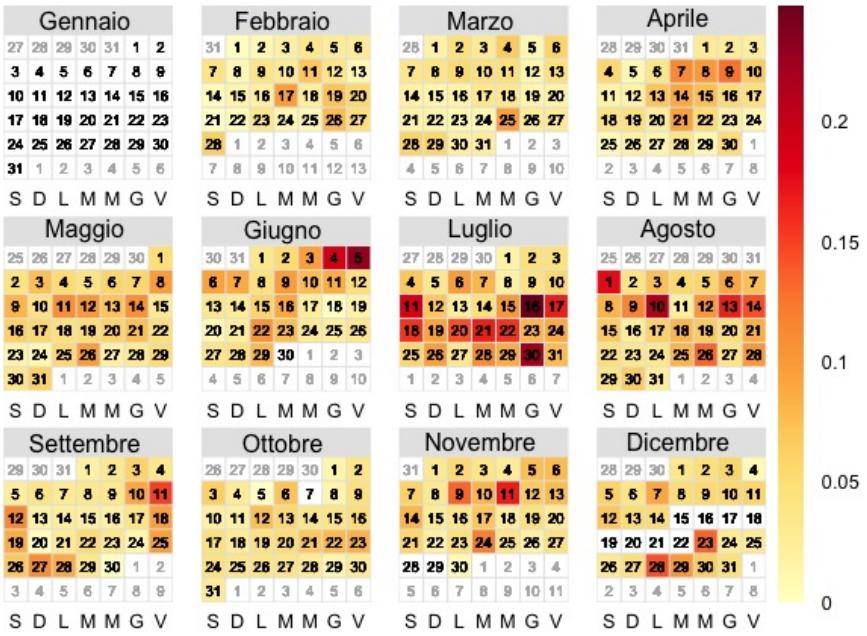

NO average daily concentration in 2016

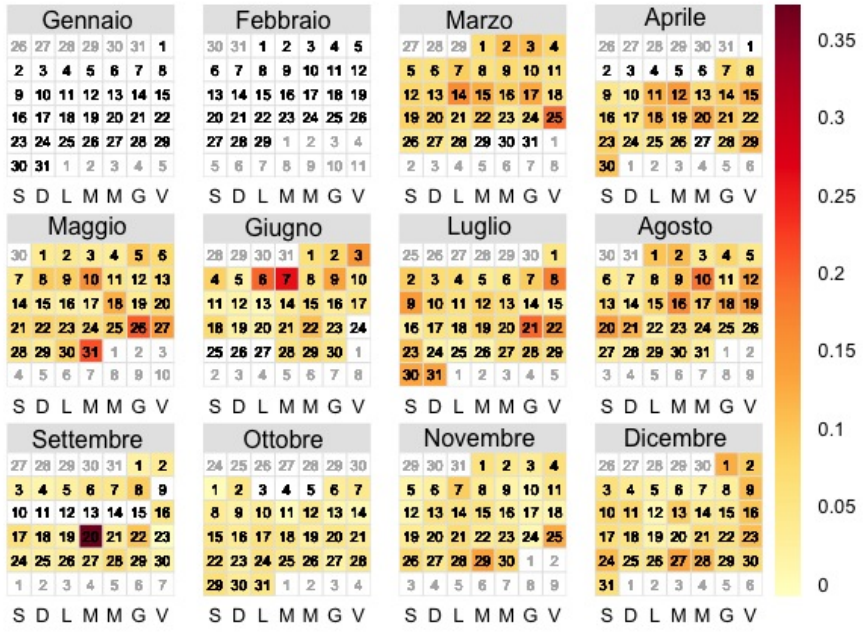

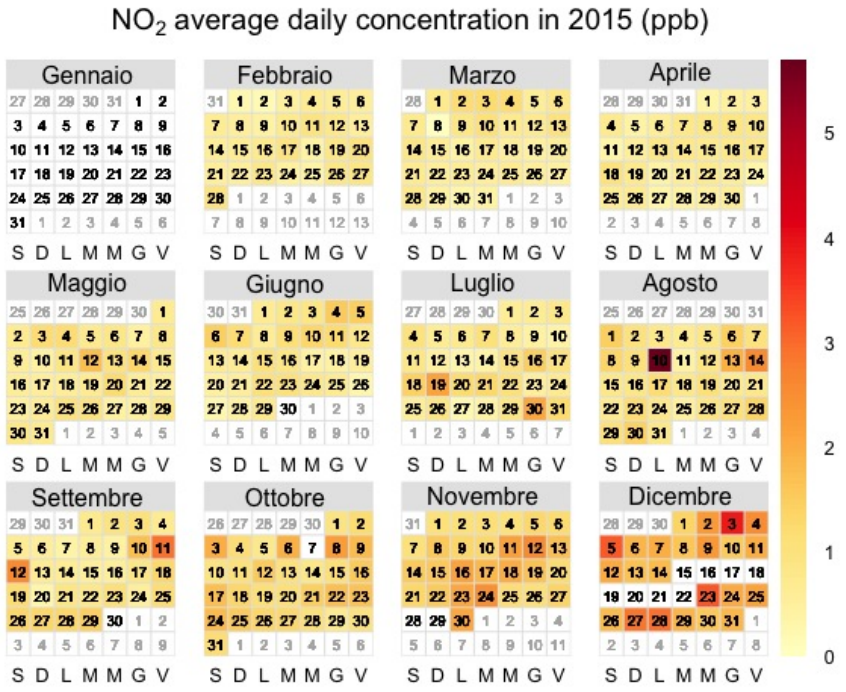
NO2 average daily concentration in 2015 (ppb)
Gennaio
Febbraio
Marzo
Aprile
Maggio
Giugno
Luglio
Agosto
Settembre
Ottobre
Novembre
Dicembre
S D L M M G V
5
4
3
2
1
0

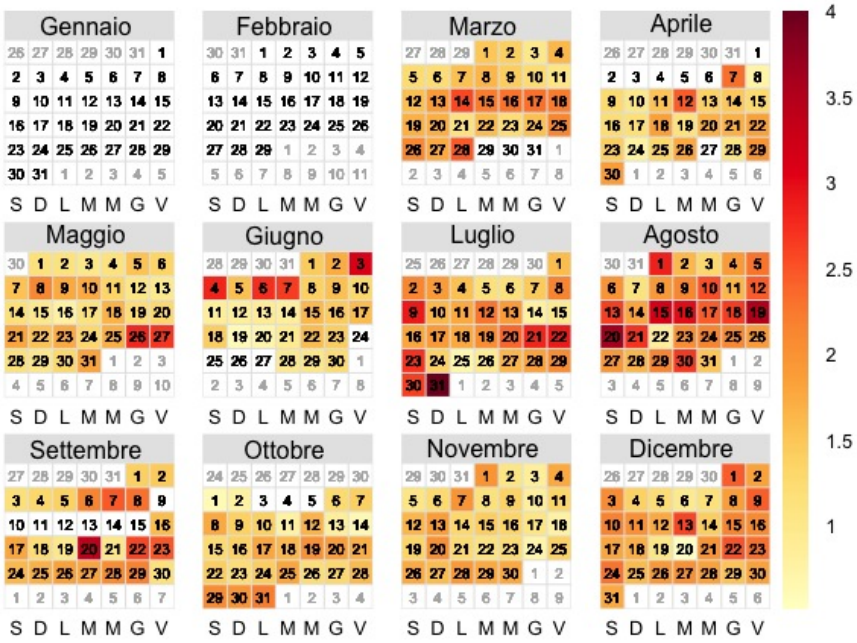
NO2 average daily concentration in 2016 (ppb)
Gennaio
Febbraio
Marzo
Aprile
Maggio
Giugno
Luglio
Agosto
Settembre
Ottobre
Novembre
Dicembre
S D L M M G V
4
3.5
3
2.5
2
1.5
1

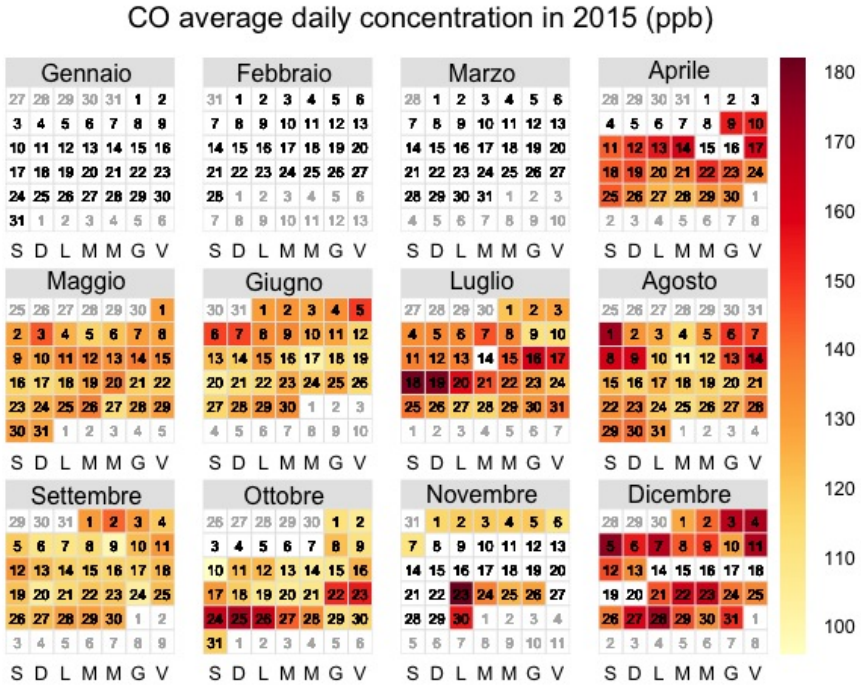
CO average daily concentration in 2015 (ppb)
Gennaio
Febbraio
Marzo
Aprile
Maggio
Giugno
Luglio
Agosto
Settembre
Ottobre
Novembre
Dicembre
S D L M M G V
180
170
160
150
140
130
120
110
100

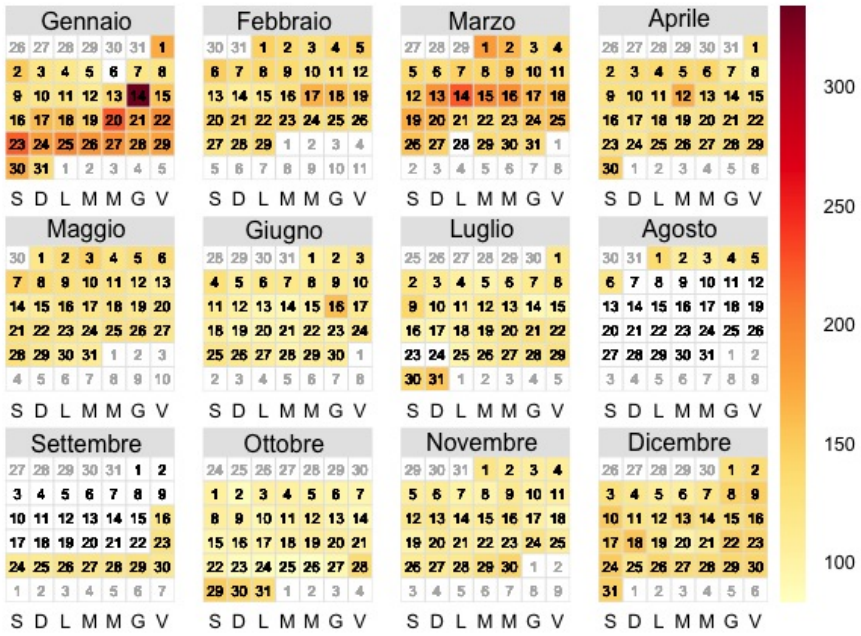
CO average daily concentration in 2016 (ppb)
Gennaio
Febbraio
Marzo
Aprile
Maggio
Giugno
Luglio
Agosto
Settembre
Ottobre
Novembre
Dicembre
S D L M M G V
300
250
200
150
100

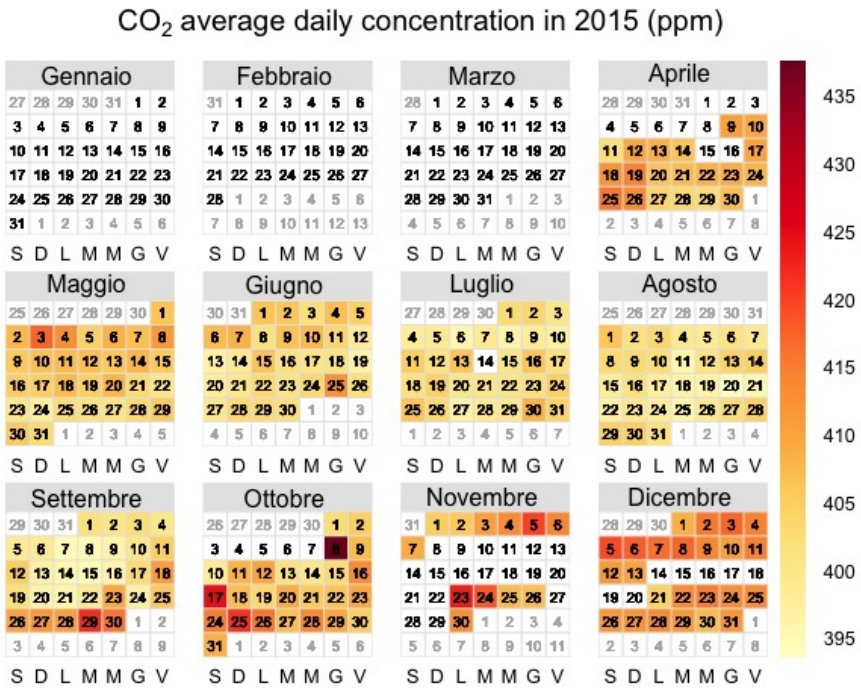
CO_2 average daily concentration in 2015 (ppm)
Gennaio
Febbraio
Marzo
Aprile
Maggio
Giugno
Luglio
Agosto
Settembre
Ottobre
Novembre
Dicembre
S D L M M G V
435
430
425
420
415
410
405
400
395

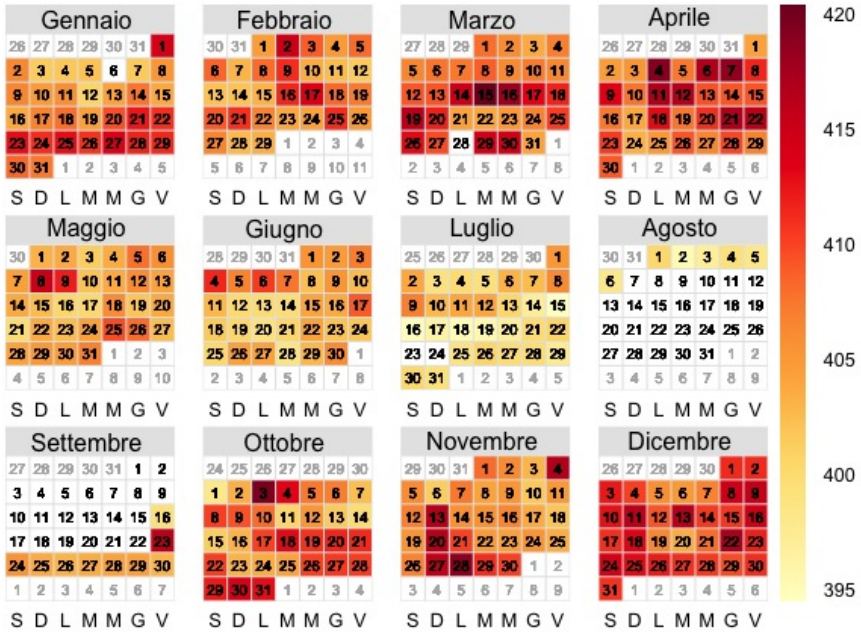
CO_2 average daily concentration in 2016 (ppm)
Gennaio
Febbraio
Marzo
Aprile
Maggio
Giugno
Luglio
Agosto
Settembre
Ottobre
Novembre
Dicembre
S D L M M G V
420
415
410
405
400
395

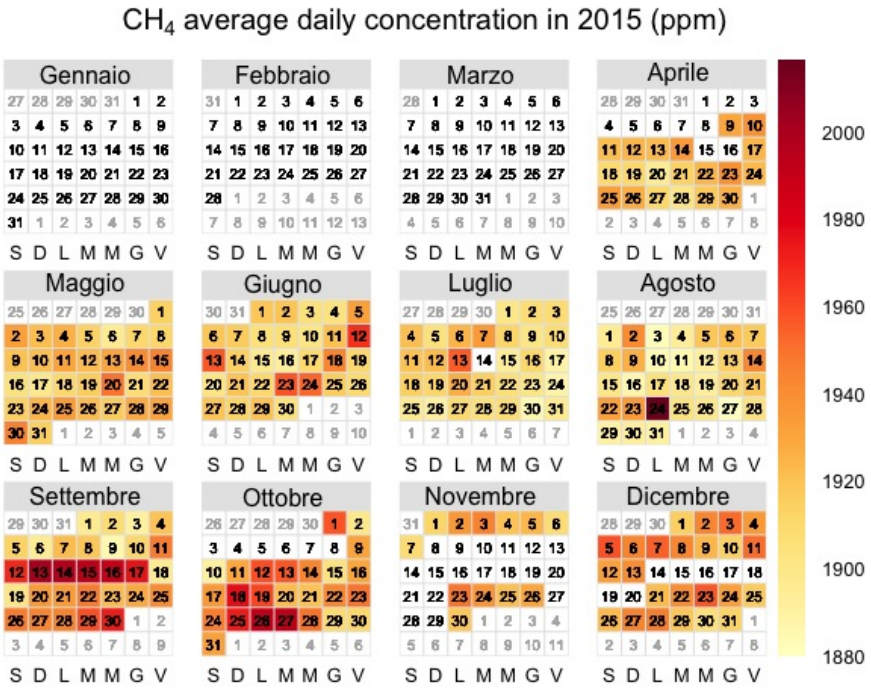
CH4 average daily concentration in 2015 (ppm)
Gennaio
Febbraio
Marzo
Aprile
Maggio
Giugno
Luglio
Agosto
Settembre
Ottobre
Novembre
Dicembre
S D L M M G V
2000
1980
1960
1940
1920
1900
1880

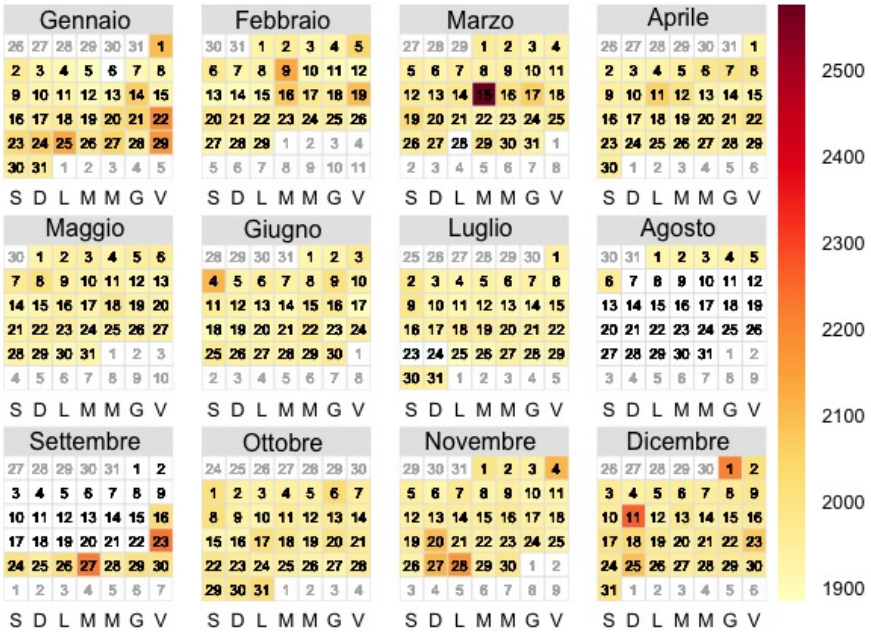
CH4 average daily concentration in 2016 (ppm)
Gennaio
Febbraio
Marzo
Aprile
Maggio
Giugno
Luglio
Agosto
Settembre
Ottobre
Novembre
Dicembre
S D L M M G V
2500
2400
2300
2200
2100
2000
1900

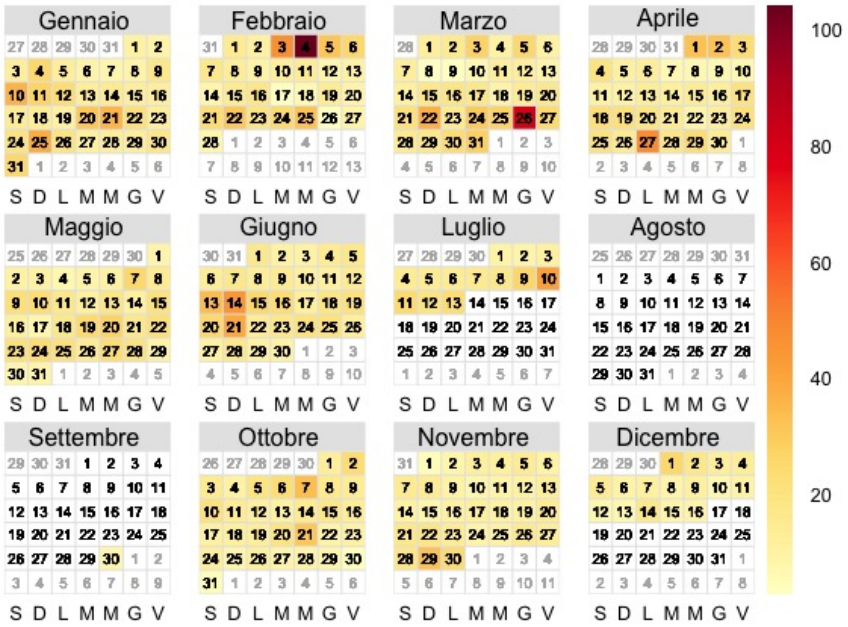
PM10[µg m−3] in 2015
Gennaio
Febbraio
Marzo
Aprile
Maggio
Giugno
Luglio
Agosto
Settembre
Ottobre
Novembre
Dicembre
S D L M M G V
100
80
60
40
20

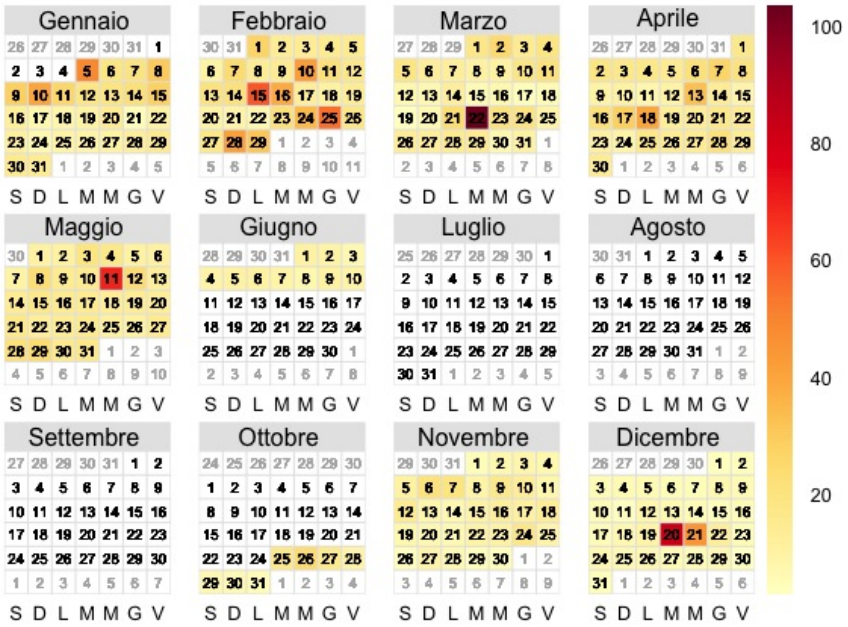
PM10[µg m−3] in 2016
Gennaio
Febbraio
Marzo
Aprile
Maggio
Giugno
Luglio
Agosto
Settembre
Ottobre
Novembre
Dicembre
S D L M M G V
100
80
60
40
20

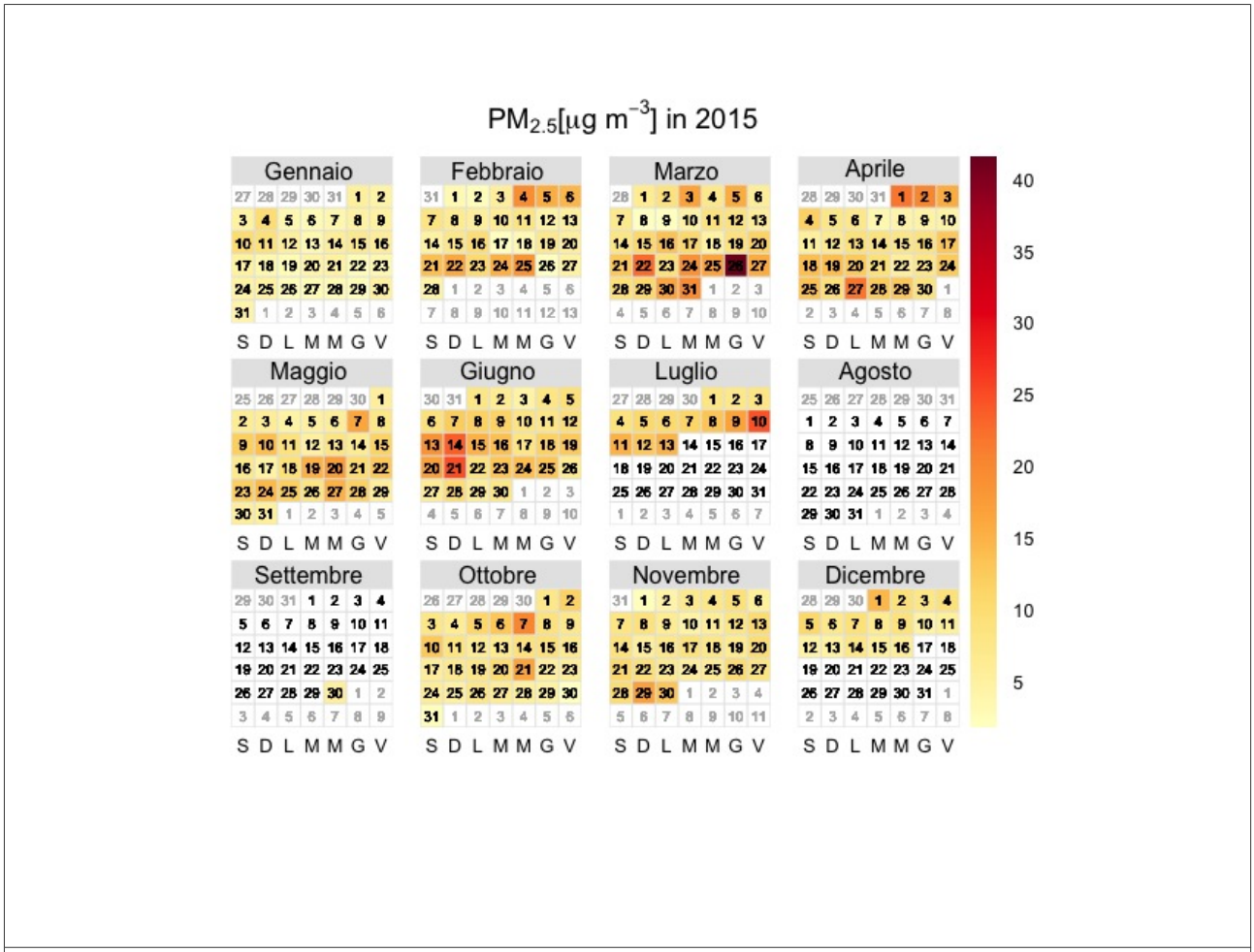
PM2.5[µg m−3] in 2015
Gennaio
Febbraio
Marzo
Aprile
Maggio
Giugno
Luglio
Agosto
Settembre
Ottobre
Novembre
Dicembre
S D L M M G V
40
35
30
25
20
15
10
5

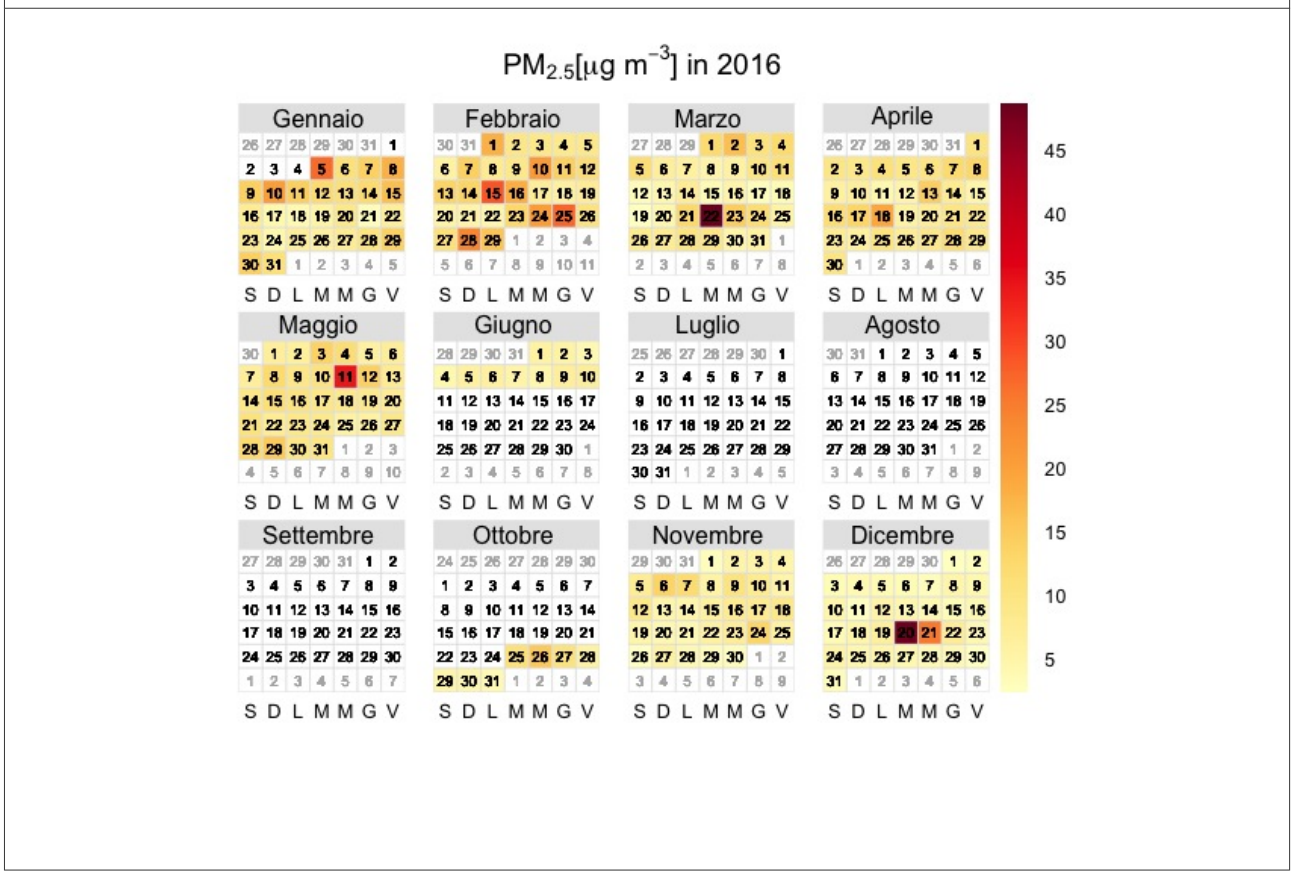
PM2.5[µg m−3] in 2016
Gennaio
Febbraio
Marzo
Aprile
Maggio
Giugno
Luglio
Agosto
Settembre
Ottobre
Novembre
Dicembre
S D L M M G V
45
40
35
30
25
20
15
10
5

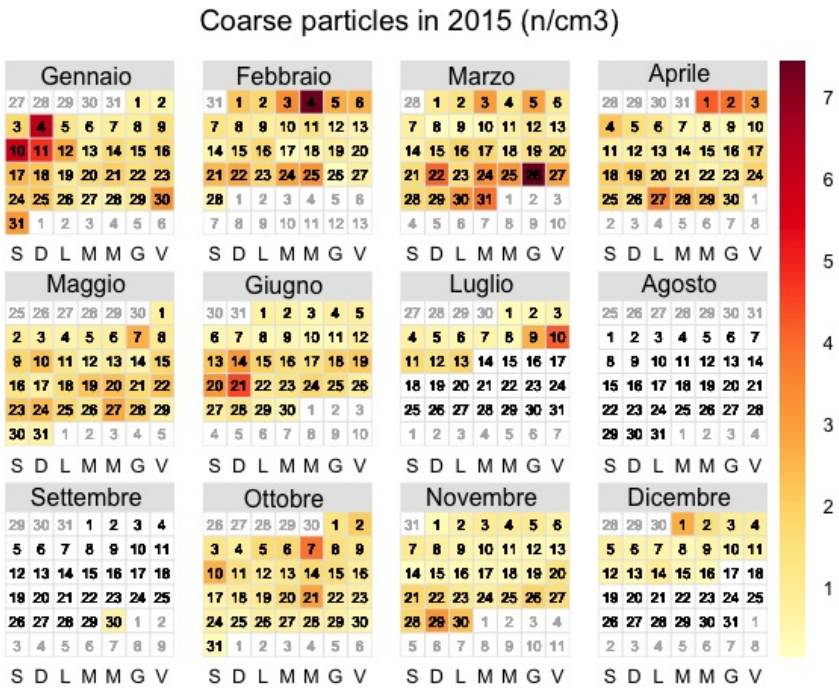
Coarse particles in 2015 (n/cm3)
Gennaio
Febbraio
Marzo
Aprile
Maggio
Giugno
Luglio
Agosto
Settembre
Ottobre
Novembre
Dicembre
S D L M M G V
7
6
5
4
3
2
1

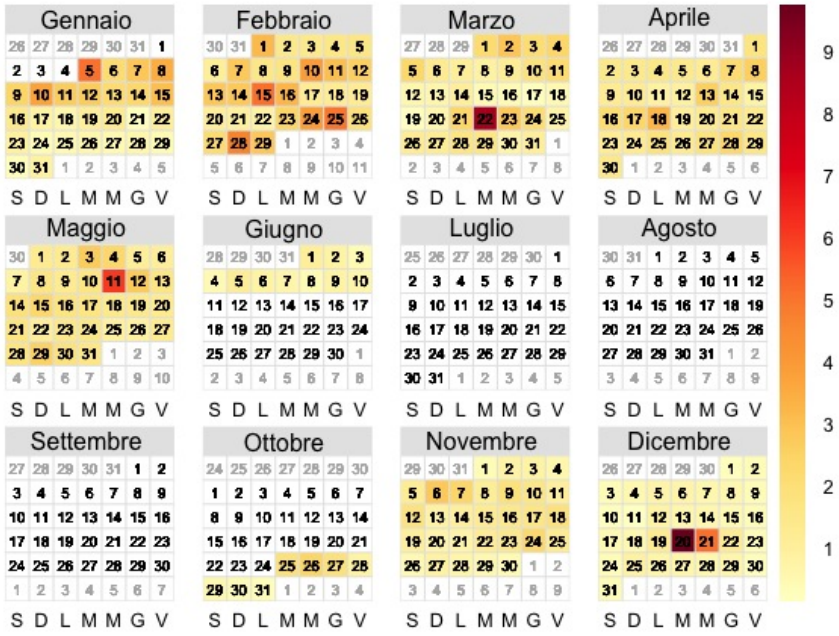
Coarse particles in 2016 (n/cm3)
Gennaio
Febbraio
Marzo
Aprile
Maggio
Giugno
Luglio
Agosto
Settembre
Ottobre
Novembre
Dicembre
S D L M M G V
9
8
7
6
5
4
3
2
1

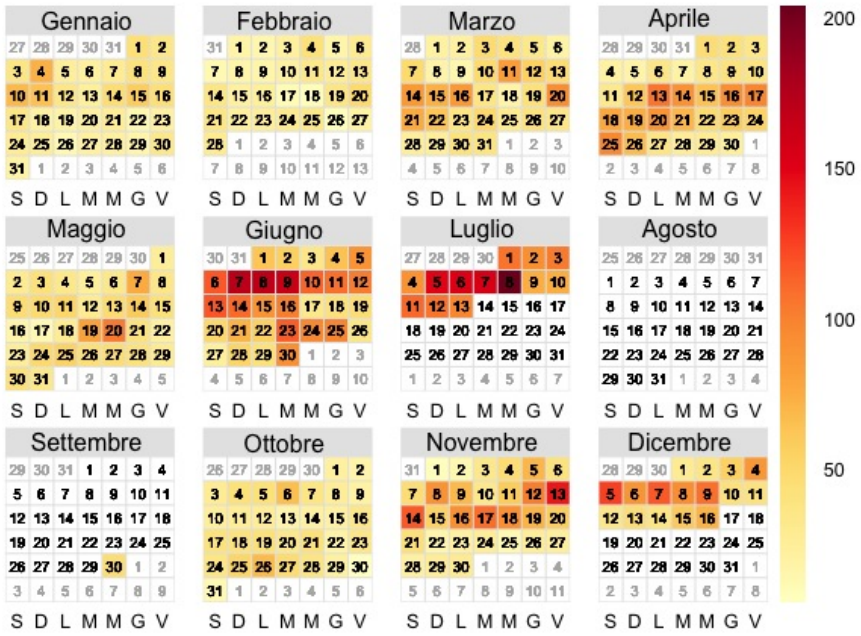
Fine particles in 2015 (n/cm3)
Gennaio
Febbraio
Marzo
Aprile
Maggio
Giugno
Luglio
Agosto
Settembre
Ottobre
Novembre
Dicembre
S D L M M G V
200
150
100
50

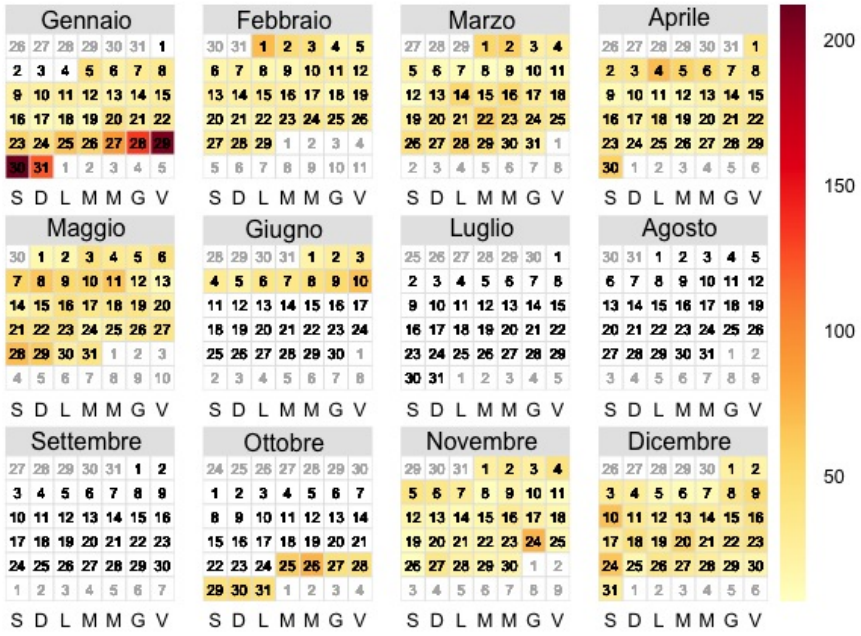
Fine particles in 2016 (n/cm3)
Gennaio
Febbraio
Marzo
Aprile
Maggio
Giugno
Luglio
Agosto
Settembre
Ottobre
Novembre
Dicembre
S D L M M G V
200
150
100
50

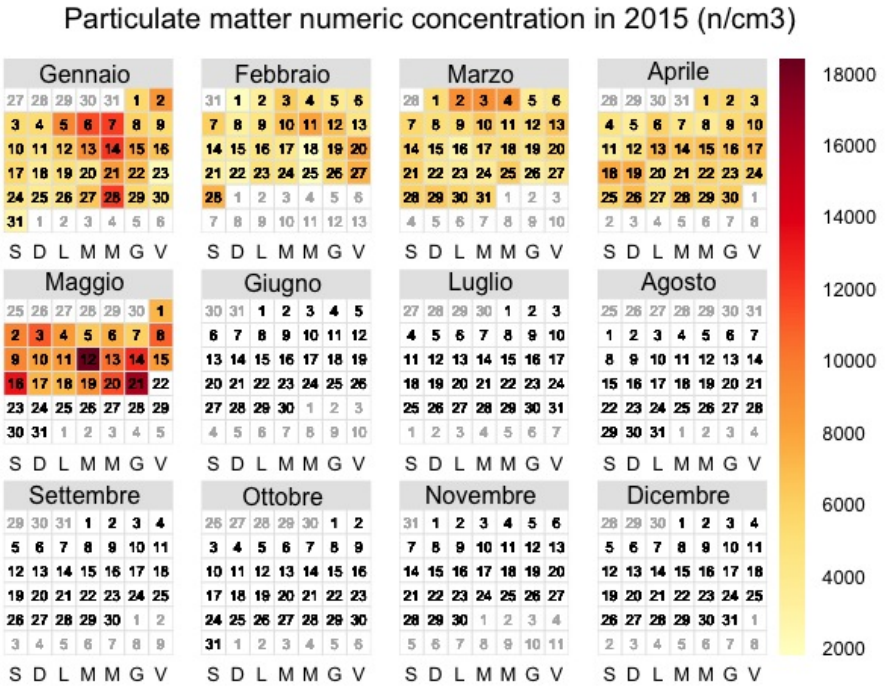
Particulate matter numeric concentration in 2015 (n/cm3)
Gennaio
Febbraio
Marzo
Aprile
Maggio
Giugno
Luglio
Agosto
Settembre
Ottobre
Novembre
Dicembre
S D L M M G V
18000
16000
14000
12000
10000
8000
6000
4000
2000

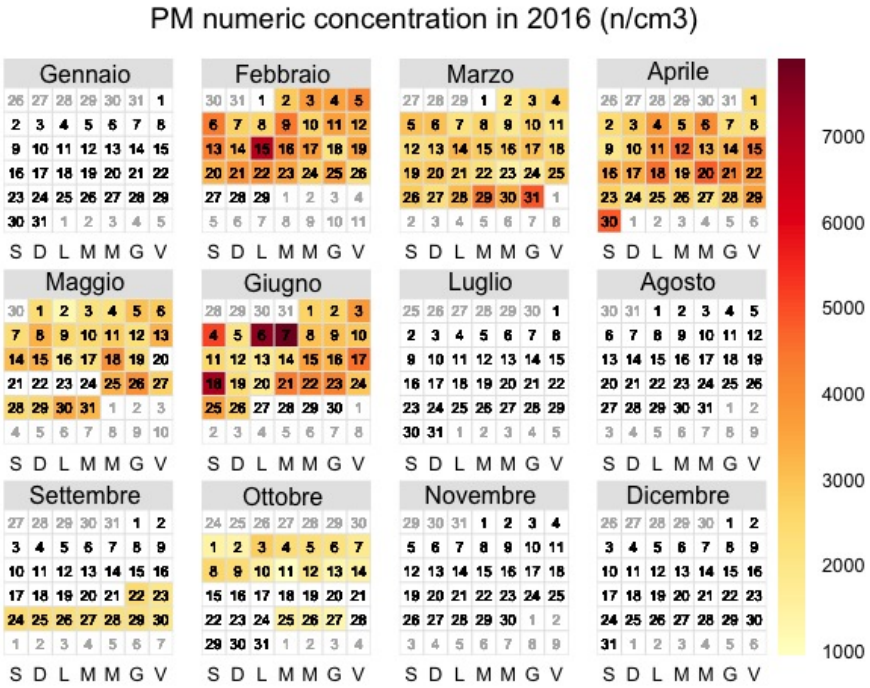
PM numeric concentration in 2016 (n/cm3)
Gennaio
Febbraio
Marzo
Aprile
Maggio
Giugno
Luglio
Agosto
Settembre
Ottobre
Novembre
Dicembre
S D L M M G V
7000
6000
5000
4000
3000
2000
1000

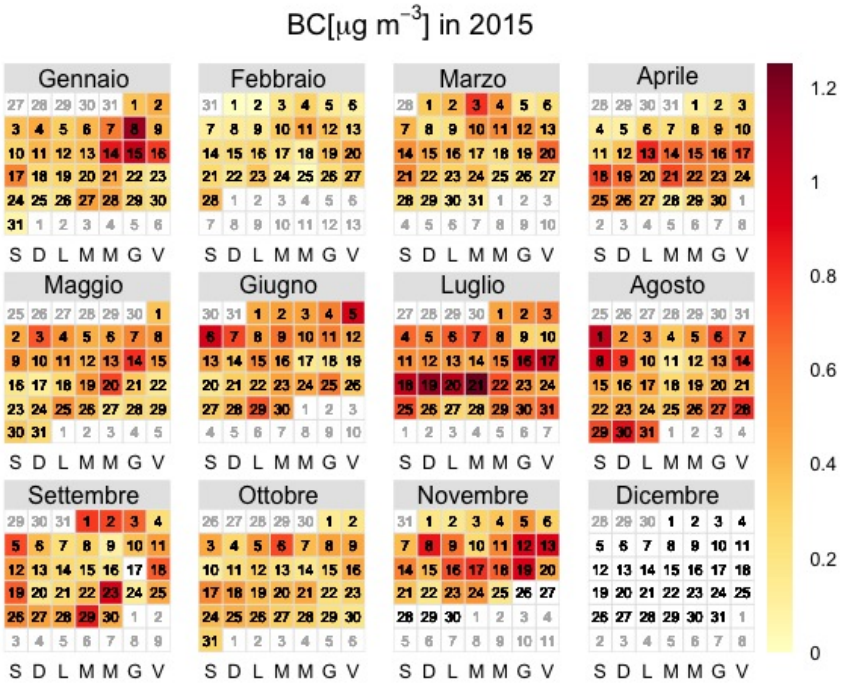
BC[μg m^{-3}] in 2015
Gennaio
Febbraio
Marzo
Aprile
Maggio
Giugno
Luglio
Agosto
Settembre
Ottobre
Novembre
Dicembre
S D L M M G V
1.2
1
0.8
0.6
0.4
0.2
0

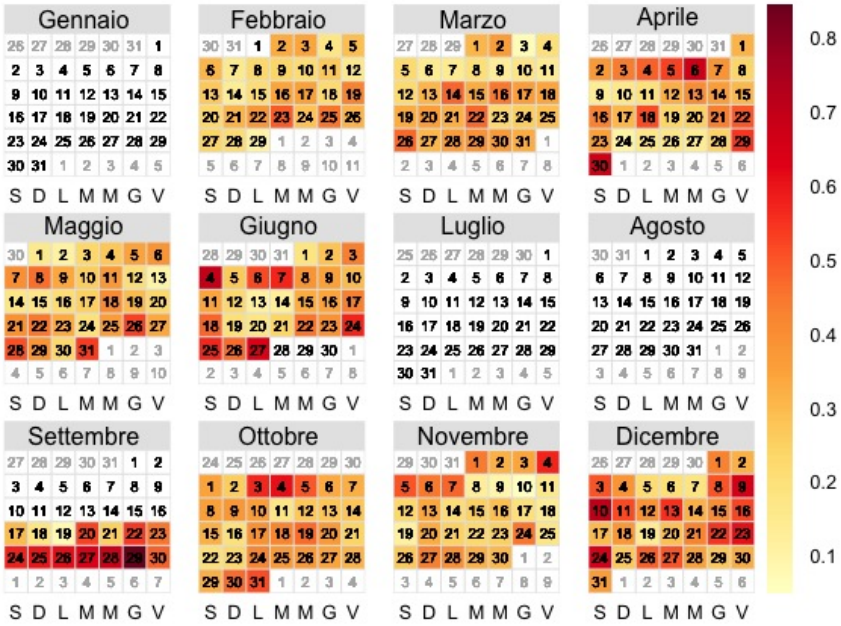
BC[μg m^{-3}] in 2016
Gennaio
Febbraio
Marzo
Aprile
Maggio
Giugno
Luglio
Agosto
Settembre
Ottobre
Novembre
Dicembre
S D L M M G V
0.8
0.7
0.6
0.5
0.4
0.3
0.2
0.1

Weekday trends on 2015

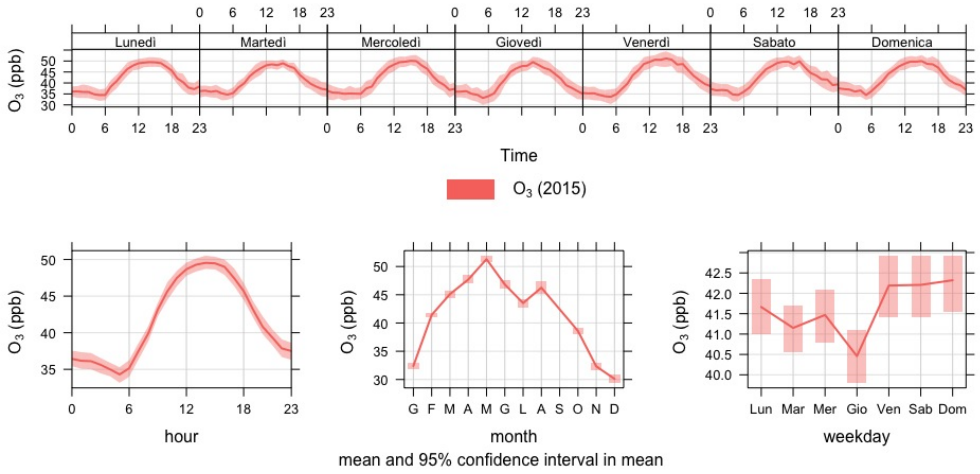

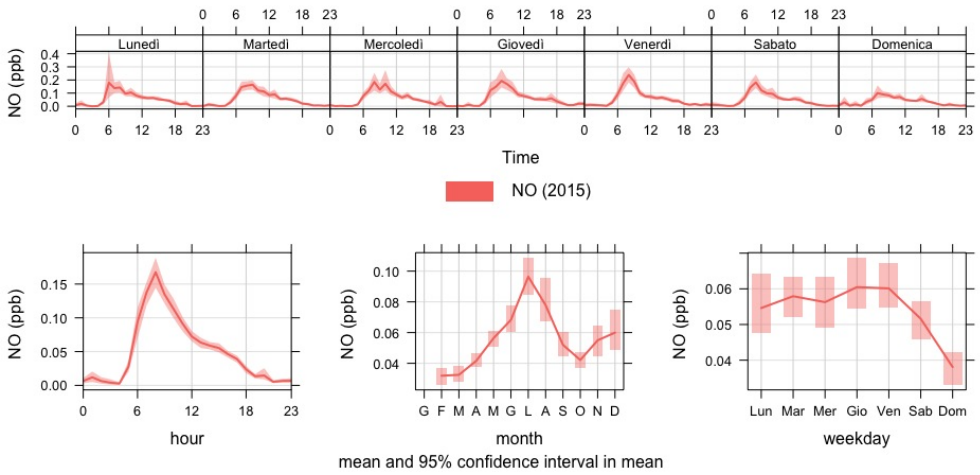

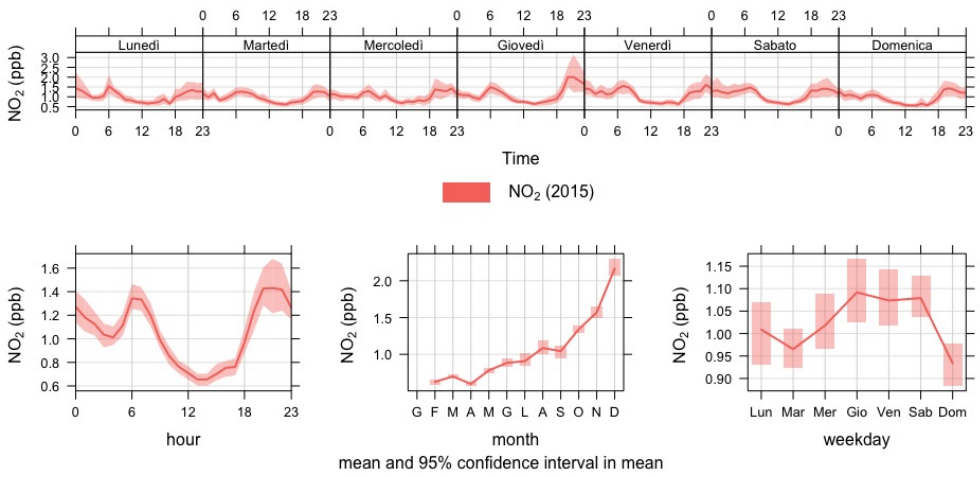
Lunedì
Martedì
Mercoledì
Giovedì
Venerdì
Sabato
Domenica
NO2 (ppb)
Time
NO2 (2015)
hour
month
weekday
mean and 95% confidence interval in mean

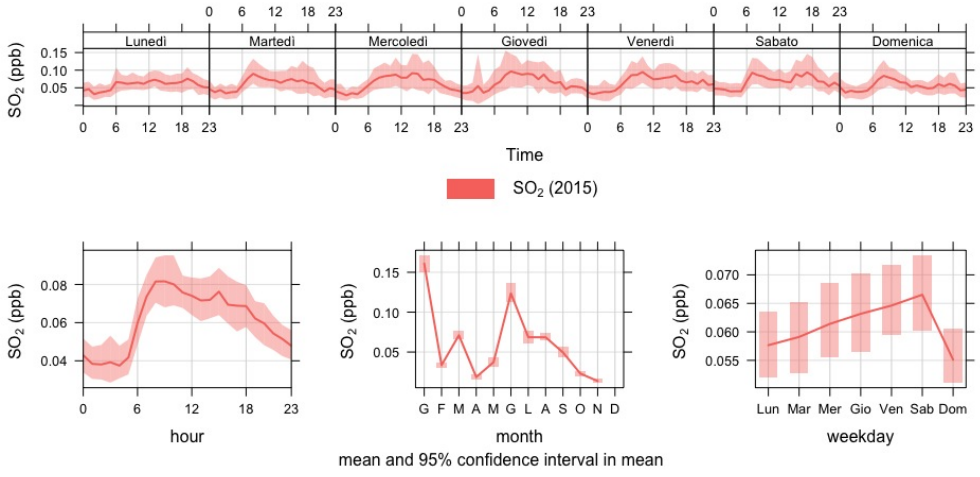
Lunedì
Martedì
Mercoledì
Giovedì
Venerdì
Sabato
Domenica
SO2 (ppb)
Time
SO2 (2015)
hour
month
weekday
mean and 95% confidence interval in mean

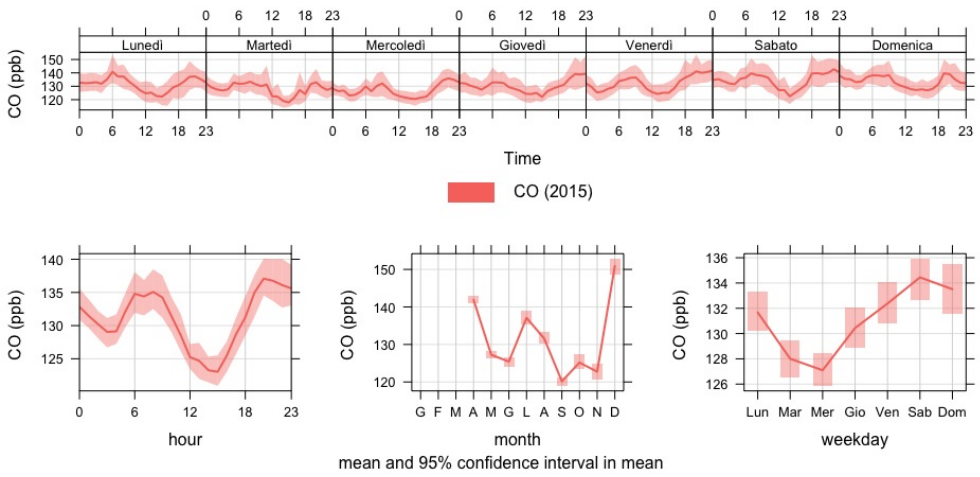
Lunedì
Martedì
Mercoledì
Giovedì
Venerdì
Sabato
Domenica
CO (ppb)
Time
CO (2015)
hour
month
weekday
mean and 95% confidence interval in mean

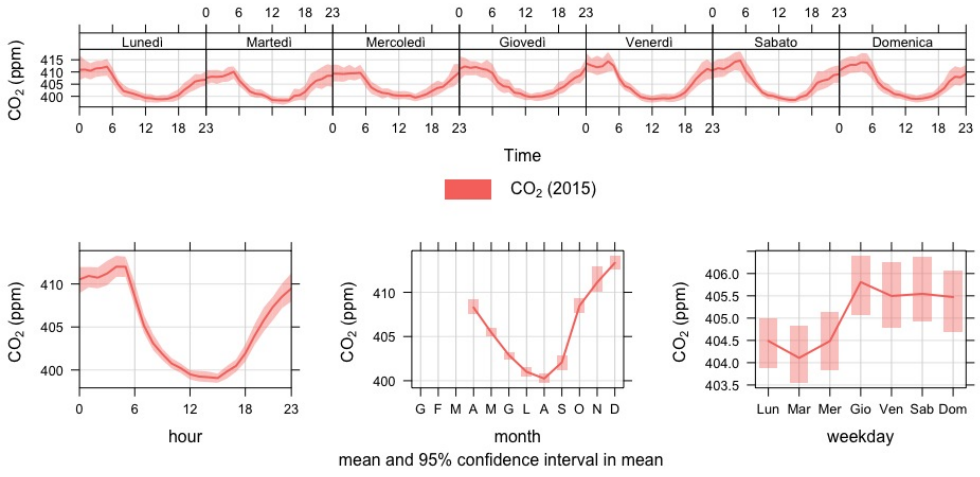
Lunedì
Martedì
Mercoledì
Giovedì
Venerdì
Sabato
Domenica
CO2 (ppm)
Time
CO2 (2015)
hour
month
weekday
mean and 95% confidence interval in mean

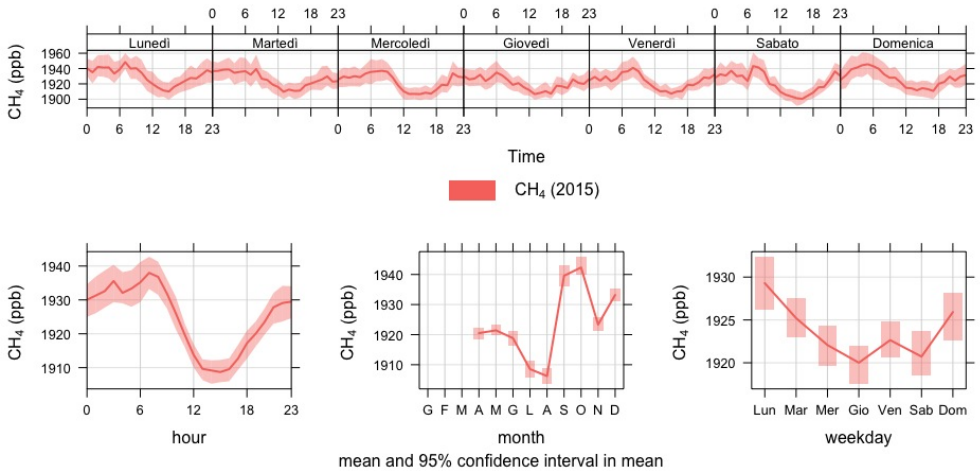
Lunedì
Martedì
Mercoledì
Giovedì
Venerdì
Sabato
Domenica
CH4 (ppb)
Time
CH4 (2015)
hour
month
weekday
mean and 95% confidence interval in mean

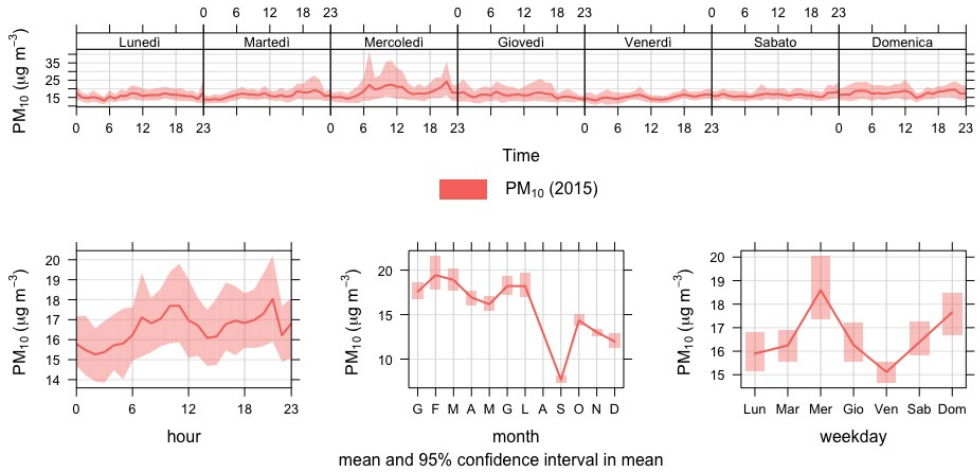
Lunedì
Martedì
Mercoledì
Giovedì
Venerdì
Sabato
Domenica
PM10 (µg m−3)
Time
PM10 (2015)
hour
month
weekday
mean and 95% confidence interval in mean

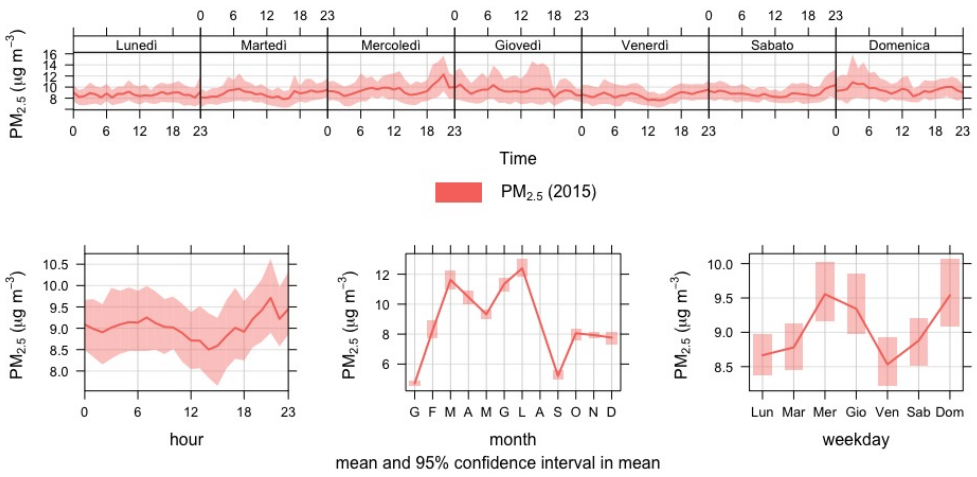
Lunedì
Martedì
Mercoledì
Giovedì
Venerdì
Sabato
Domenica
PM2.5 (µg m-3)
Time
PM2.5 (2015)
hour
month
weekday
mean and 95% confidence interval in mean

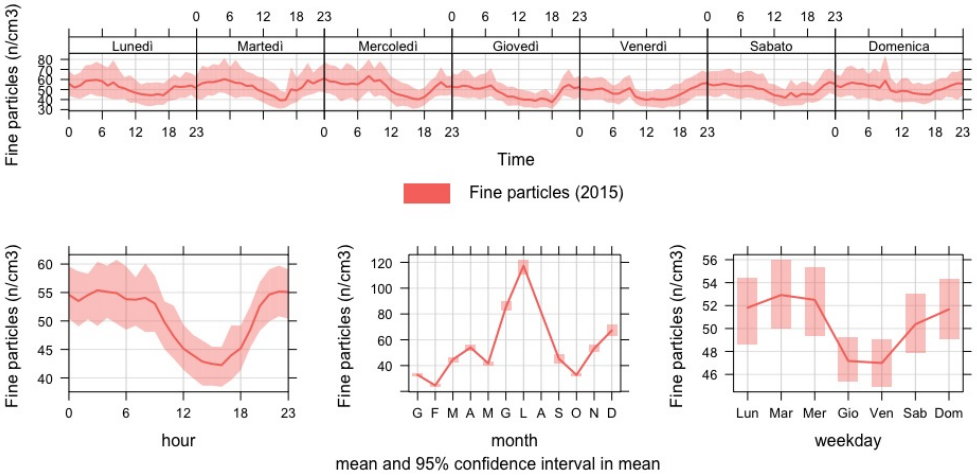
Lunedì
Martedì
Mercoledì
Giovedì
Venerdì
Sabato
Domenica
Fine particles (n/cm3)
Time
Fine particles (2015)
hour
month
weekday
mean and 95% confidence interval in mean

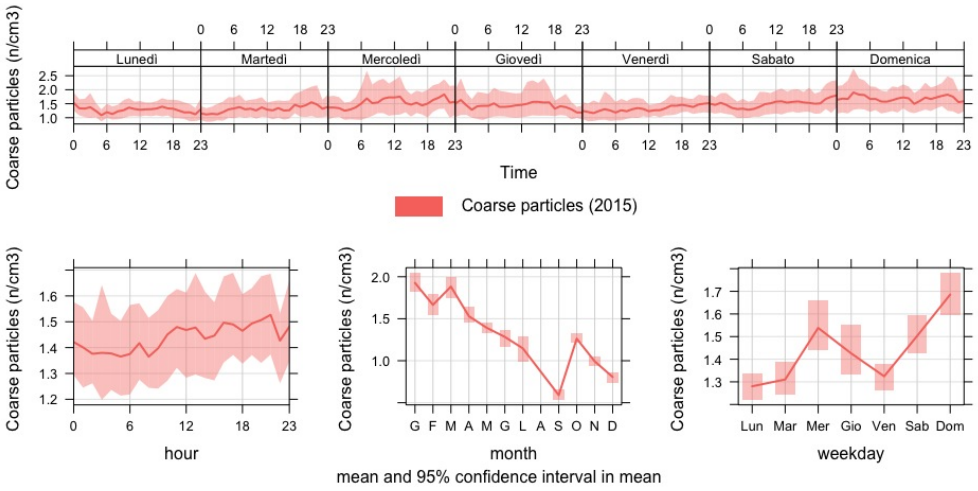
Coarse particles (n/cm3)
Lunedì
Martedì
Mercoledì
Giovedì
Venerdì
Sabato
Domenica
Time
Coarse particles (2015)
hour
month
weekday
mean and 95% confidence interval in mean

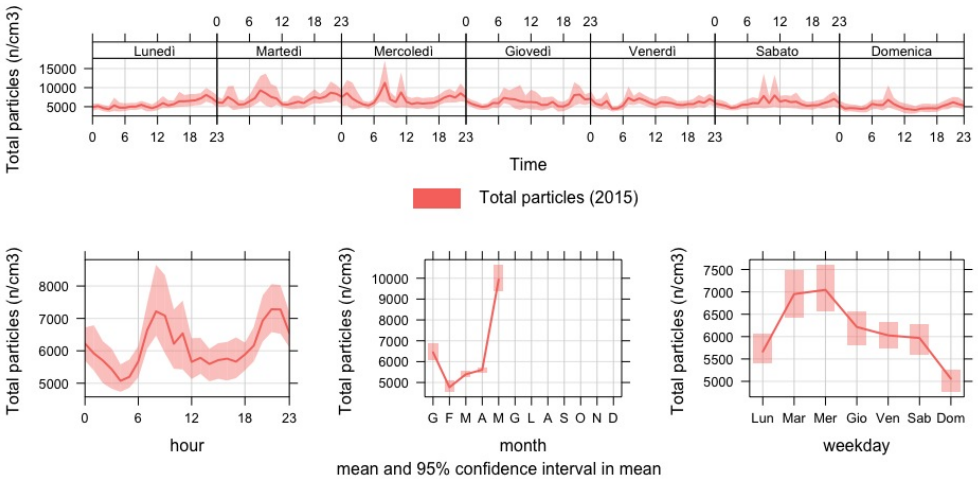
Total particles (n/cm3)
Lunedì
Martedì
Mercoledì
Giovedì
Venerdì
Sabato
Domenica
Time
Total particles (2015)
hour
month
weekday
mean and 95% confidence interval in mean

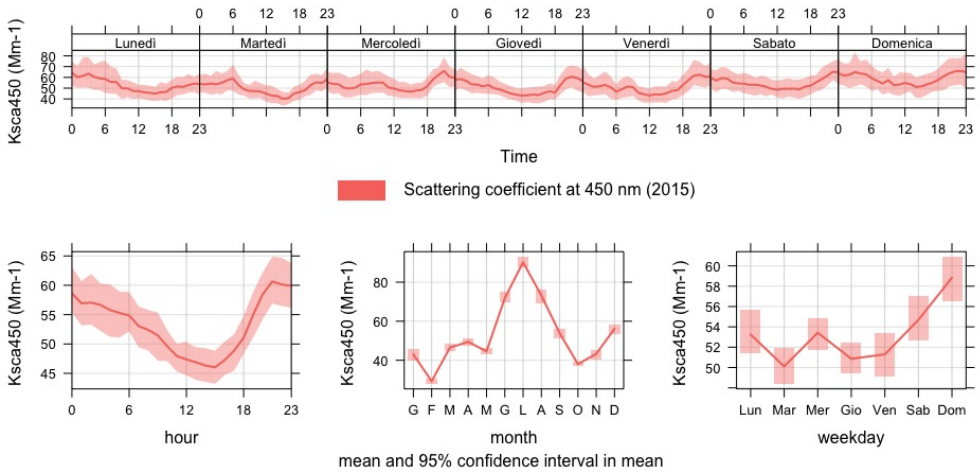
Ksca450 (Mm-1)
Lunedì
Martedì
Mercoledì
Giovedì
Venerdì
Sabato
Domenica
Time
Scattering coefficient at 450 nm (2015)
hour
month
weekday
mean and 95% confidence interval in mean

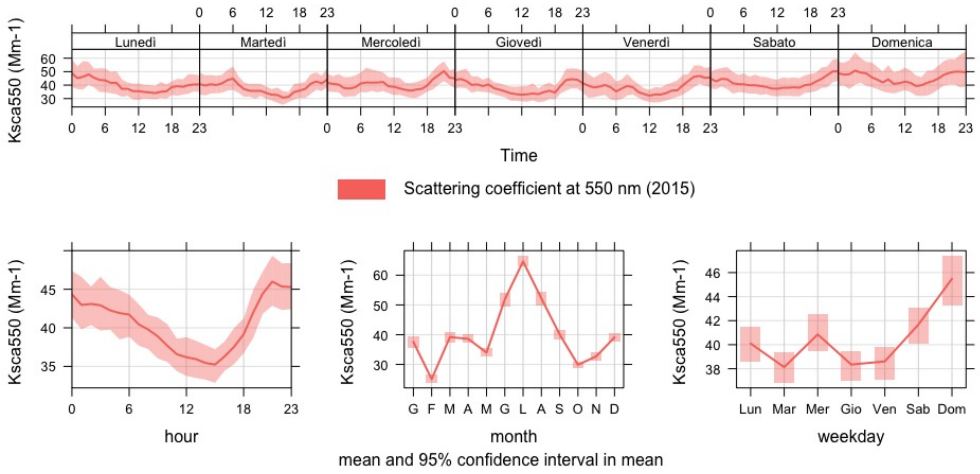
Ksca550 (Mm-1)
Lunedì
Martedì
Mercoledì
Giovedì
Venerdì
Sabato
Domenica
Time
Scattering coefficient at 550 nm (2015)
hour
month
weekday
mean and 95% confidence interval in mean

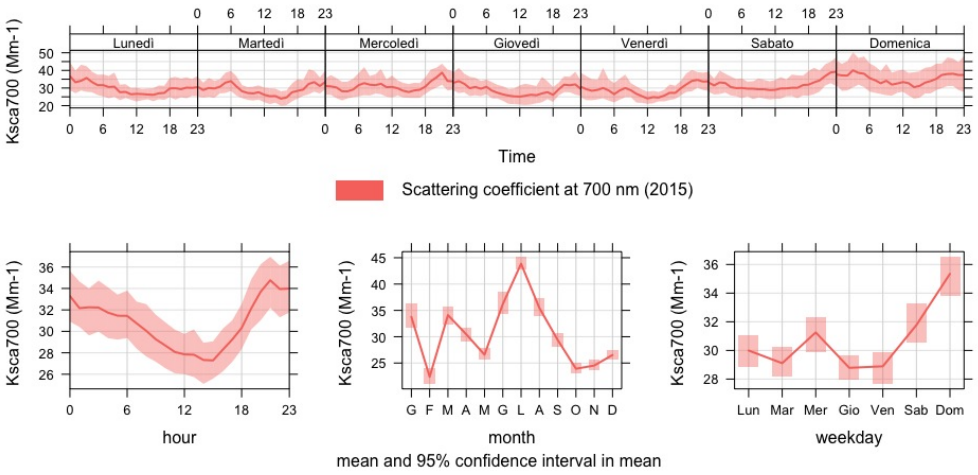
Ksca700 (Mm-1)
Lunedì
Martedì
Mercoledì
Giovedì
Venerdì
Sabato
Domenica
Time
Scattering coefficient at 700 nm (2015)
hour
month
weekday
mean and 95% confidence interval in mean

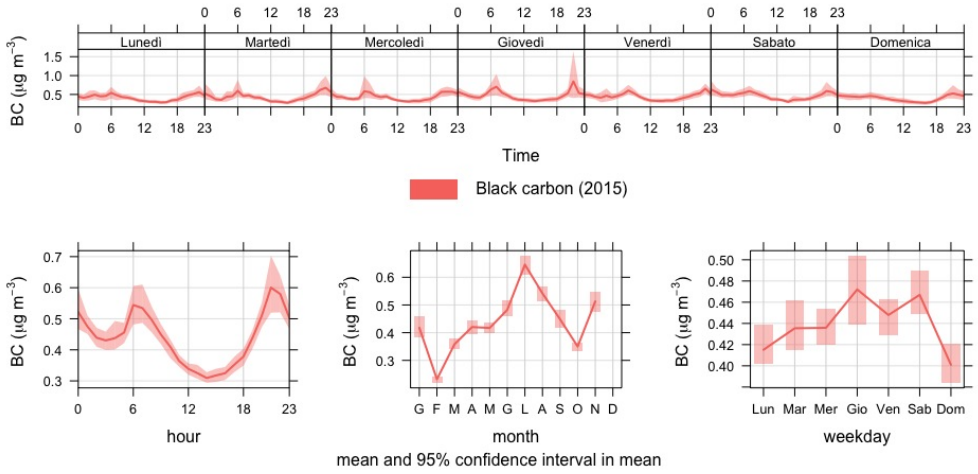
BC (µg m-3)
Lunedì
Martedì
Mercoledì
Giovedì
Venerdì
Sabato
Domenica
Time
Black carbon (2015)
hour
month
weekday
mean and 95% confidence interval in mean

Weekday trends on 2016

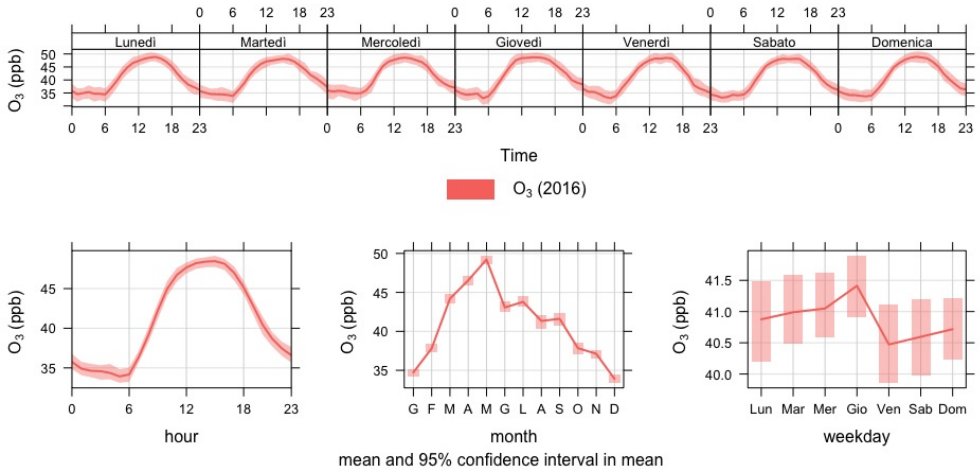

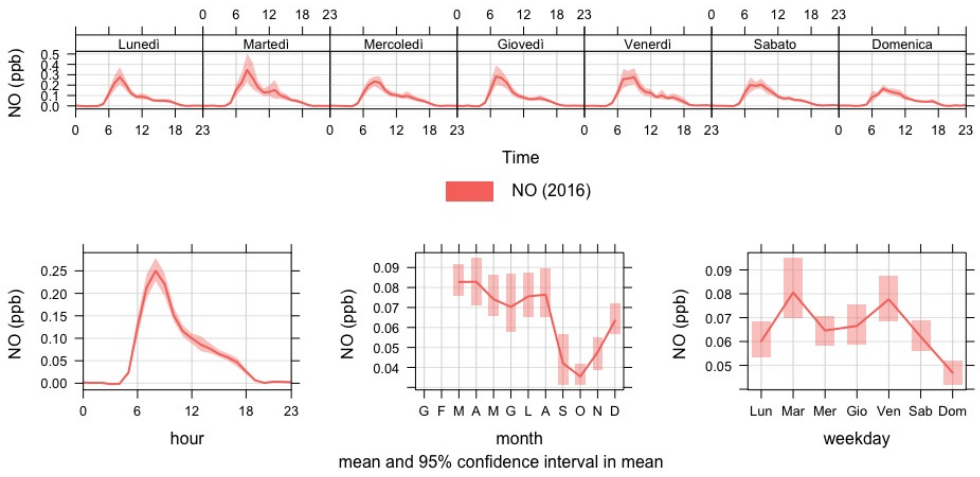

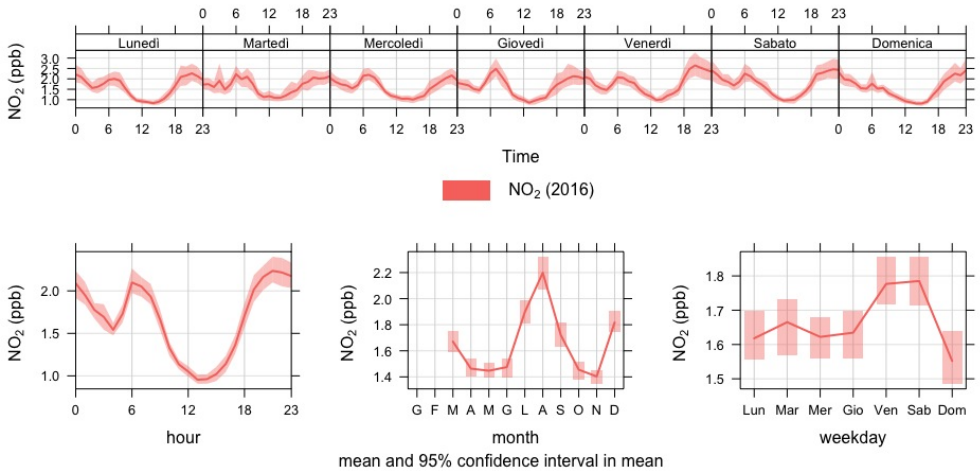
Lunedì
Martedì
Mercoledì
Giovedì
Venerdì
Sabato
Domenica
NO2 (ppb)
Time
NO2 (2016)
hour
month
weekday
mean and 95% confidence interval in mean

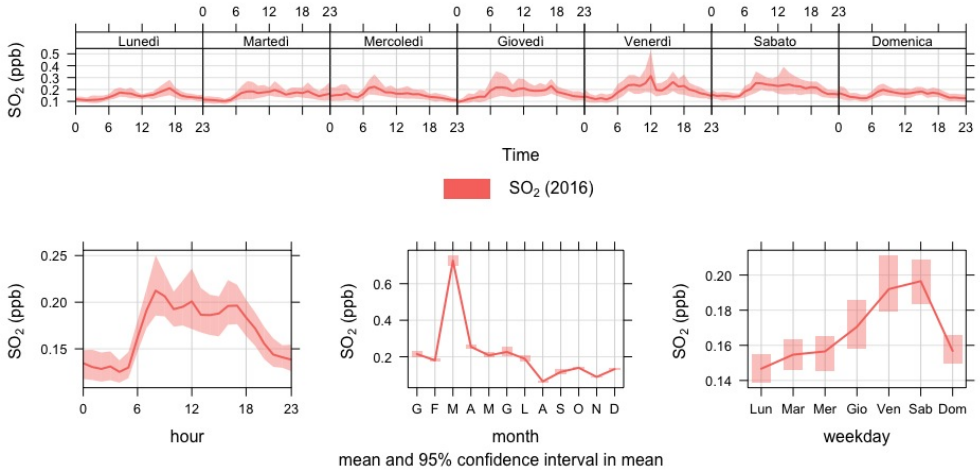
Lunedì
Martedì
Mercoledì
Giovedì
Venerdì
Sabato
Domenica
SO2 (ppb)
Time
SO2 (2016)
hour
month
weekday
mean and 95% confidence interval in mean

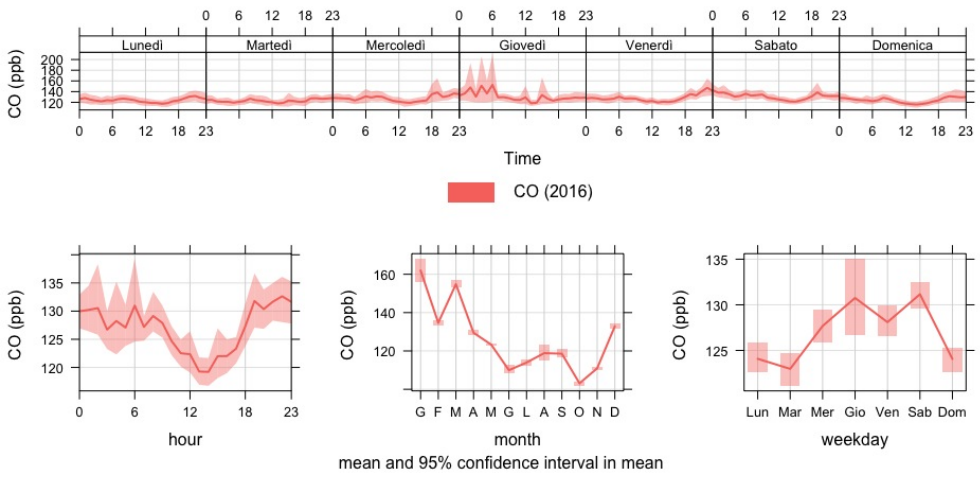
Lunedì
Martedì
Mercoledì
Giovedì
Venerdì
Sabato
Domenica
CO (ppb)
Time
CO (2016)
hour
month
weekday
mean and 95% confidence interval in mean

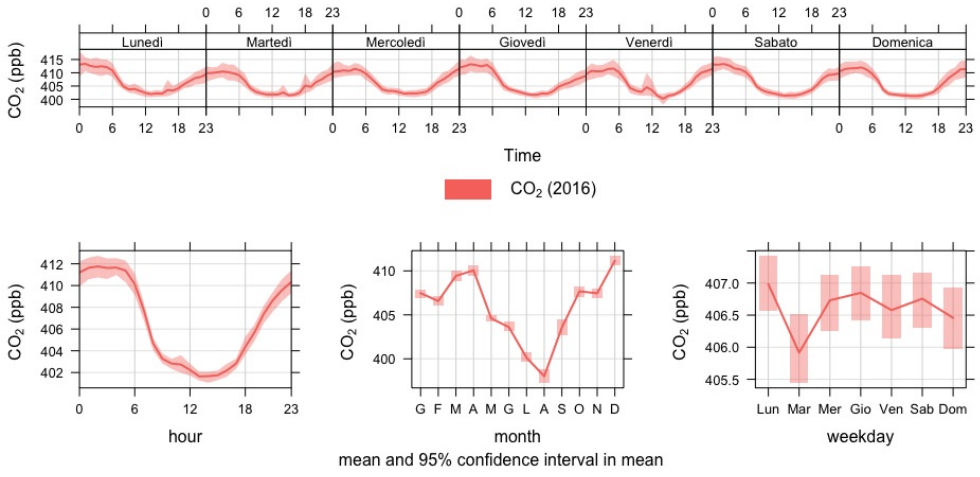
Lunedì
Martedì
Mercoledì
Giovedì
Venerdì
Sabato
Domenica
CO2 (ppb)
Time
CO2 (2016)
hour
month
weekday
mean and 95% confidence interval in mean

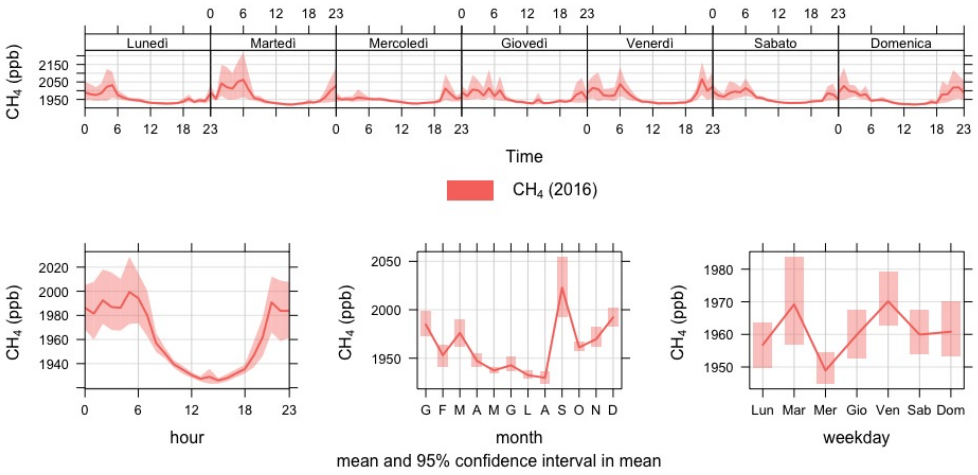
Lunedì
Martedì
Mercoledì
Giovedì
Venerdì
Sabato
Domenica
CH4 (ppb)
Time
CH4 (2016)
hour
month
weekday
mean and 95% confidence interval in mean

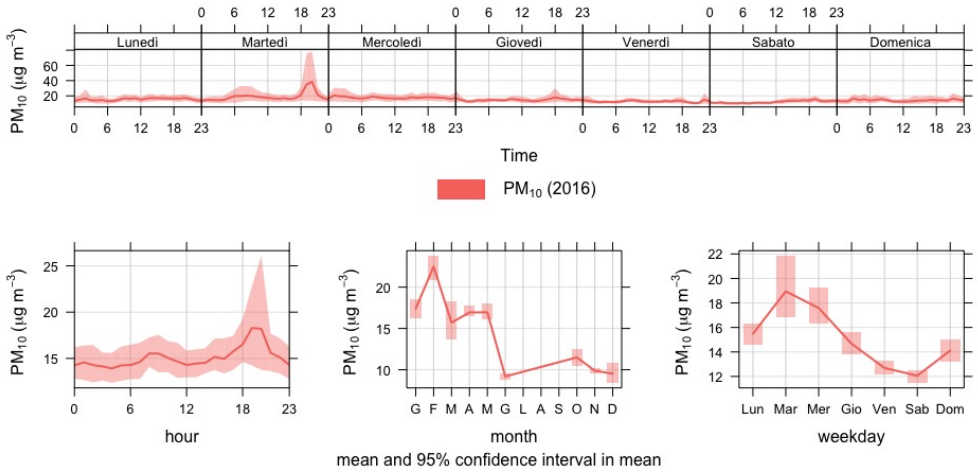
Lunedì
Martedì
Mercoledì
Giovedì
Venerdì
Sabato
Domenica
PM10 (µg m−3)
Time
PM10 (2016)
hour
month
weekday
mean and 95% confidence interval in mean

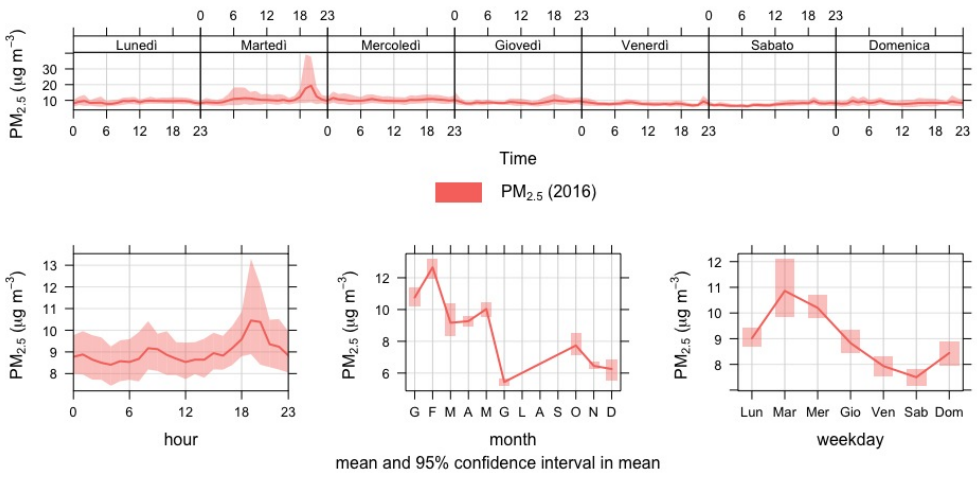
Lunedì
Martedì
Mercoledì
Giovedì
Venerdì
Sabato
Domenica
PM2.5 (µg m-3)
Time
PM2.5 (2016)
hour
month
weekday
mean and 95% confidence interval in mean

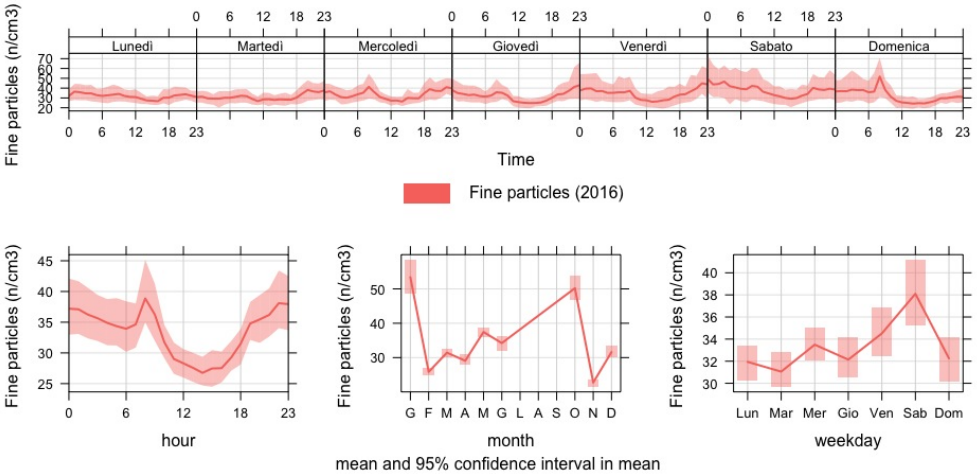
Lunedì
Martedì
Mercoledì
Giovedì
Venerdì
Sabato
Domenica
Fine particles (n/cm3)
Time
Fine particles (2016)
hour
month
weekday
mean and 95% confidence interval in mean

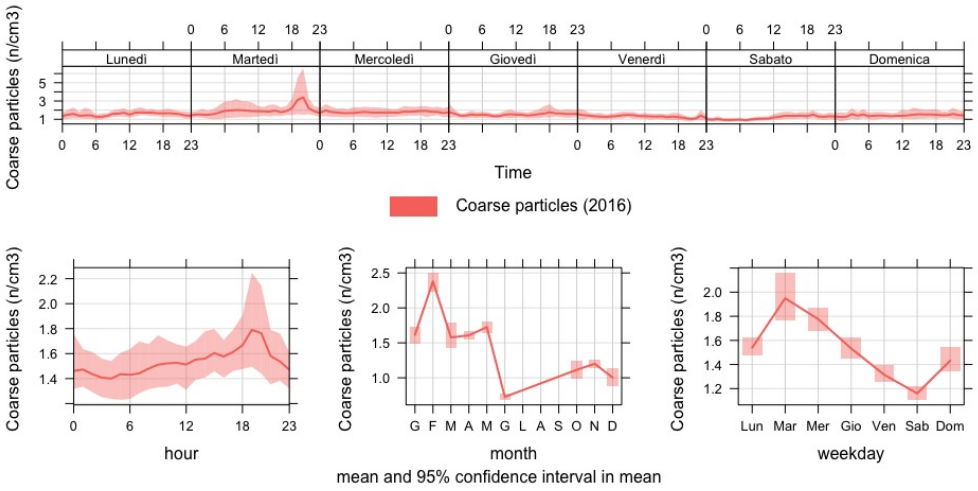
Coarse particles (n/cm3)
Lunedì
Martedì
Mercoledì
Giovedì
Venerdì
Sabato
Domenica
Time
Coarse particles (2016)
hour
month
weekday
mean and 95% confidence interval in mean

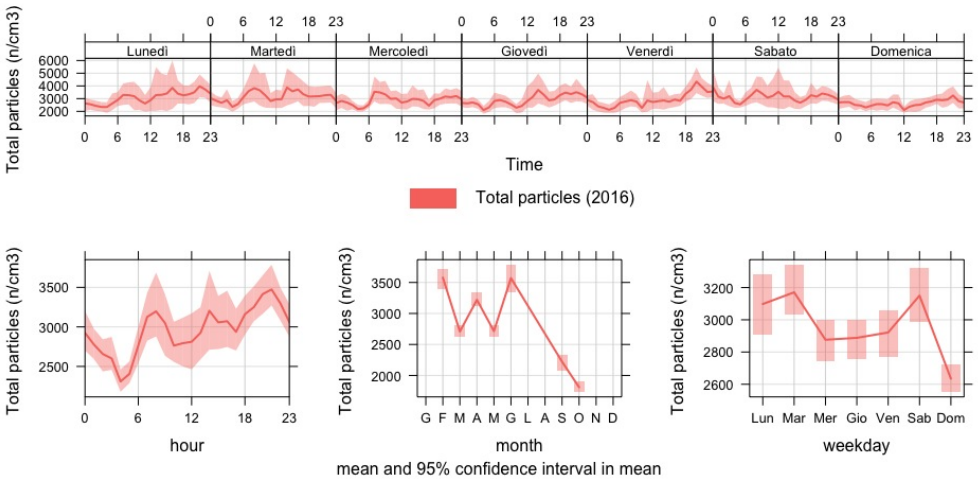
Total particles (n/cm3)
Lunedì
Martedì
Mercoledì
Giovedì
Venerdì
Sabato
Domenica
Time
Total particles (2016)
hour
month
weekday
mean and 95% confidence interval in mean

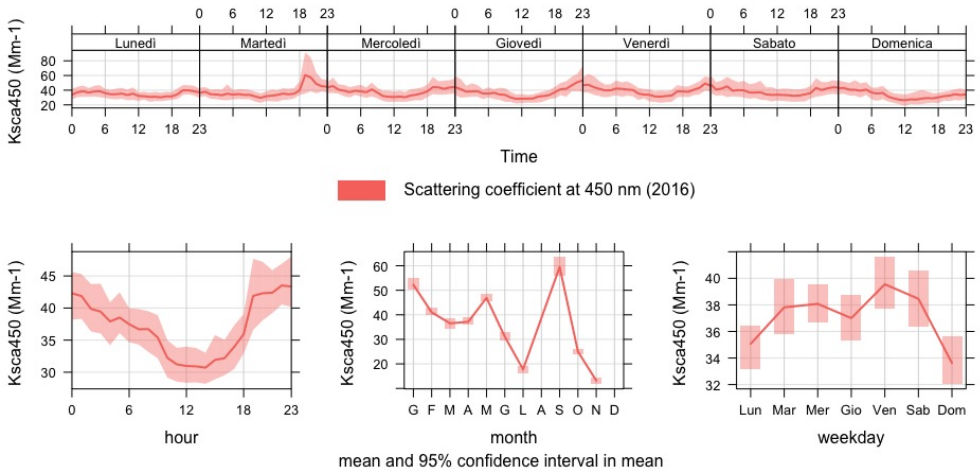
Ksca450 (Mm-1)
Lunedì
Martedì
Mercoledì
Giovedì
Venerdì
Sabato
Domenica
Time
Scattering coefficient at 450 nm (2016)
hour
month
weekday
mean and 95% confidence interval in mean

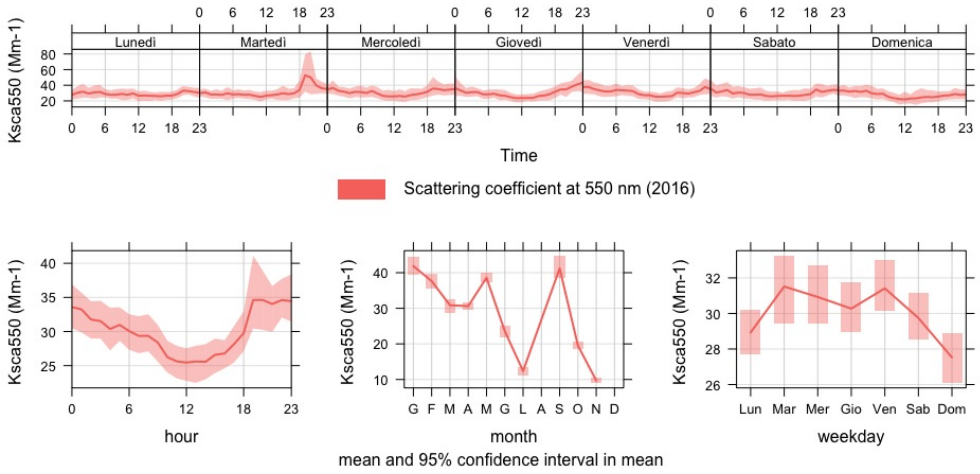
Ksca550 (Mm-1)
Lunedì
Martedì
Mercoledì
Giovedì
Venerdì
Sabato
Domenica
Time
Scattering coefficient at 550 nm (2016)
hour
month
weekday
mean and 95% confidence interval in mean

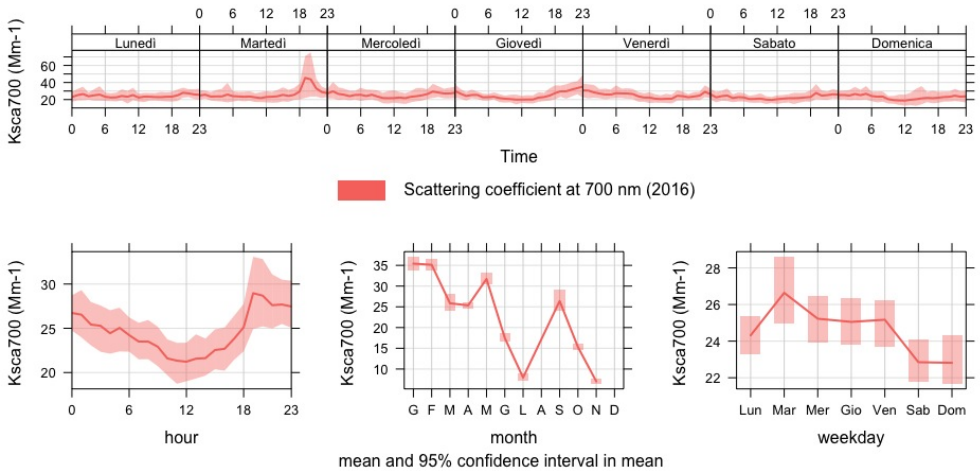
Ksca700 (Mm-1)
Lunedì
Martedì
Mercoledì
Giovedì
Venerdì
Sabato
Domenica
Time
Scattering coefficient at 700 nm (2016)
hour
month
weekday
mean and 95% confidence interval in mean

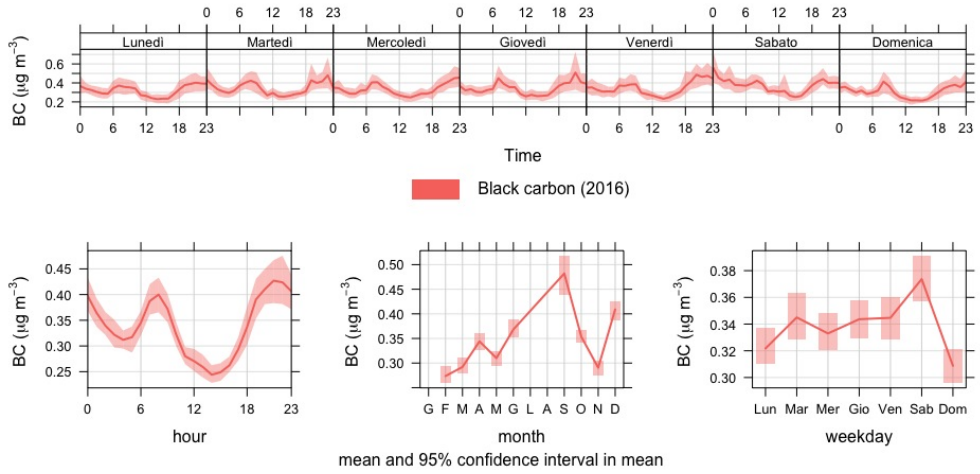
BC (µg m-3)
Lunedì
Martedì
Mercoledì
Giovedì
Venerdì
Sabato
Domenica
Time
Black carbon (2016)
hour
month
weekday
mean and 95% confidence interval in mean

APPENDIX 4: MODIS channels and data products and UN Land Cover Classification System

MODIS Channels (drawn from https://ladsweb.modaps.eosdis.nasa.gov/missions-and-measurements/modis/, revised)			
Primary Use	**Band**	**Bandwidth**	**Spectral Radiance**
Land/Cloud/Aerosols Boundaries	1	620 - 670	21.8
	2	841 - 876	24.7
Land/Cloud/Aerosols Properties	3	459 - 479	35.3
	4	545 - 565	29.0
	5	1230 - 1250	5.4
	6	1628 - 1652	7.3
	7	2105 - 2155	1.0
Ocean Color/Phytoplankton/Biogeochemistry	8	405 - 420	44.9
	9	438 - 448	41.9
	10	438 - 493	32.1
	11	526 - 536	27.9
	12	546 - 556	21.0
	13	662 - 672	9.5
	14	673 - 683	8.7
	15	743 - 753	10.2
	16	862 - 877	6.2
Atmospheric Water Vapor	17	890 - 920	10.0
	18	931 - 941	3.6

	19	915 - 965	15.0
Surface/Cloud Temperature	20	3.660 - 3.840	0.45 (300K)
	21	3.929 - 3.989	2.38 (335K)
	22	3.929 - 3.989	0.67 (300K)
	23	4.020 - 4.080	0.79 (300K)
Atmospheric Temperature	24	4.433 - 4.498	0.17 (250K)
	25	4.482 - 4.549	0.59 (275K)
Cirrus Clouds Water Vapor	26	1.360 - 1.390	6.00
	27	6.535 - 6.895	1.16 (240K)
	28	7.175 - 7.475	2.18 (250K)
Cloud Properties	29	8.400 - 8.700	9.58 (300K)
Ozone	30	9.580 - 9.880	3.69 (250K)
Surface/Cloud Temperature	31	10.780 - 11.280	9.55 (300K)
	32	11.770 - 12.270	8.94 (300K)
Cloud Top Altitude	33	13.185 - 13.485	4.52 (260K)
	34	13.485 - 13.785	3.76 (250K)
	35	13.785 - 14.085	3.11 (240K)
	36	14.085 - 14.385	2.08 (220K)

MODIS DATA PRODUCTS	
Level 1	MODIS Raw Radiances MODIS Calibrated Radiances MODIS Geolocation Fields
Atmosphere Products	MODIS Aerosol Product MODIS Total Precipitable Water MODIS Cloud Product MODIS Atmospheric Profiles MODIS Atmosphere Joint Product MODIS Atmosphere Gridded Product MODIS Cloud Mask
MODIS Land Products	MODIS Surface Reflectance MODIS Land Surface Temperature and Emissivity (MOD11) MODIS Land Surface Temperature and Emissivity (MOD21) MODIS Land Cover Products MODIS Vegetation Index Products (NDVI and EVI) MODIS Thermal Anomalies - Active Fires MODIS Fraction of Photosynthetically Active Radiation (FPAR) / Leaf Area Index (LAI) MODIS Evapotranspiration MODIS Gross Primary Productivity (GPP) / Net Primary Productivity (NPP) MODIS Bidirectional Reflectance Distribution Function (BRDF) / Albedo Parameter MODIS Vegetation Continuous Fields MODIS Water Mask MODIS Burned Area Product
MODIS Cryosphere Products	MODIS Snow Cover MODIS Sea Ice and Ice Surface Temperature

MODIS Ocean Products	MODIS Sea Surface Temperature MODIS Remote Sensing Reflectance MODIS Chlorophyll-a Concentration MODIS Diffuse Attenuation at 490 nm MODIS Particulate Organic Carbon MODIS Particulate Inorganic Carbon MODIS Normalized Fluorescence Line Height (FLH) MODIS Instantaneous Photosynthetically Available Radiation MODIS Daily Mean Photosynthetically Available Radiation

MODIS Thermal Anomalies / Fire products		
Product name	**Terra product ID**	**Aqua product ID**
Thermal Anomalies/Fire Daily L3 Global 1km	MOD14A1	MYD14A1
Thermal Anomalies/Fire 8-Day L3 Global 1km	MOD14A2	MYD14A2
Thermal Anomalies/Fire 5-Min L2 Swath 1km	MOD14	MYD14

MOD14/MYD14 fire mask pixel classes	
0	not processed (missing input data)
1	not processed (obsolete; not used since Collection 1)
2	not processed (other reason)
3	non-fire water pixel
4	cloud (land or water)
5	non-fire land pixel
6	unknown (land or water)
7	fire (low confidence, land or water)
8	fire (nominal confidence, land or water)
9	fire (high confidence, land or water)

UN Land Cover Classification System

0	No data
10	Cropland, rainfed
11	Herbaceous cover
12	Tree or shrub cover
20	Cropland, irrigated or post-flooding
30	Mosaic cropland (>50%) / natural vegetation (tree, shrub, herbaceous cover) (<50%)
40	Mosaic natural vegetation (tree, shrub, herbaceous cover) (>50%) / cropland (<50%)
50	Tree cover, broadleaved, evergreen, closed to open (>15%)
60	Tree cover, broadleaved, deciduous, closed to open (>15%)
61	Tree cover, broadleaved, deciduous, closed (>40%)
62	Tree cover, broadleaved, deciduous, open (15-40%)
70	Tree cover, needleleaved, evergreen, closed to open (>15%)
71	Tree cover, needleleaved, evergreen, closed (>40%)
72	Tree cover, needleleaved, evergreen, open (15-40%)
80	Tree cover, needleleaved, deciduous, closed to open (>15%)
81	Tree cover, needleleaved, deciduous, closed (>40%)
82	Tree cover, needleleaved, deciduous, open (15-40%)
90	Tree cover, mixed leaf type (broadleaved and needleleaved)
100	Mosaic tree and shrub (>50%) / herbaceous cover (<50%)
110	Mosaic herbaceous cover (>50%) / tree and shrub (<50%)
120	Shrubland
121	Shrubland evergreen
122	Shrubland deciduous
130	Grassland
140	Lichens and mosses
150	Sparse vegetation (tree, shrub, herbaceous cover) (<15%)
151	Sparse tree (<15%)
152	Sparse shrub (<15%)
153	Sparse herbaceous cover (<15%)
160	Tree cover, flooded, fresh or brakish water
170	Tree cover, flooded, saline water
180	Shrub or herbaceous cover, flooded, fresh/saline/brakish water
190	Urban areas
200	Bare areas
201	Consolidated bare areas
202	Unconsolidated bare areas
210	Water bodies
220	Permanent snow and ice

APPENDIX 5: Scatter Plots during BC events

Scatter Plots v/s BC during BC events

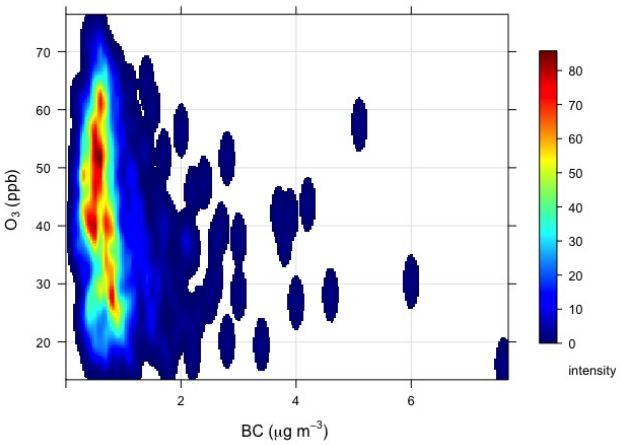

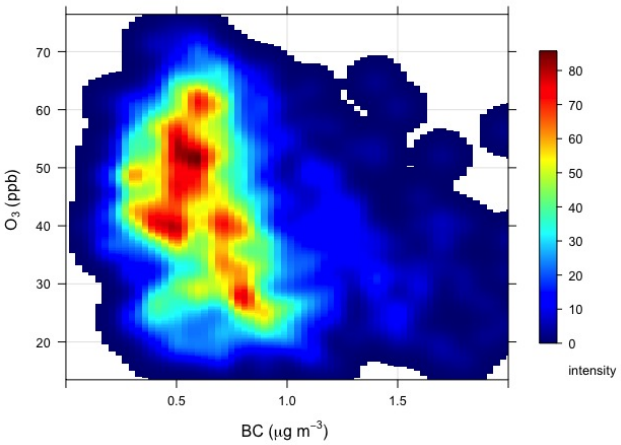

p = -0,2345

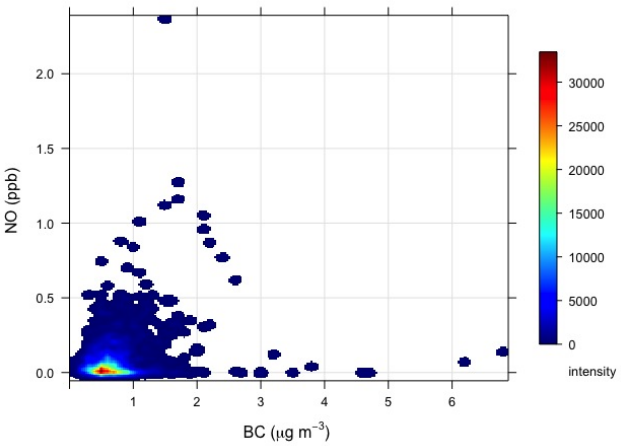

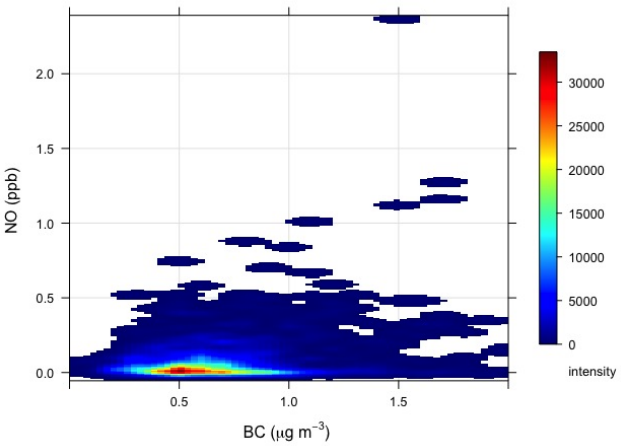

p = 0,2077

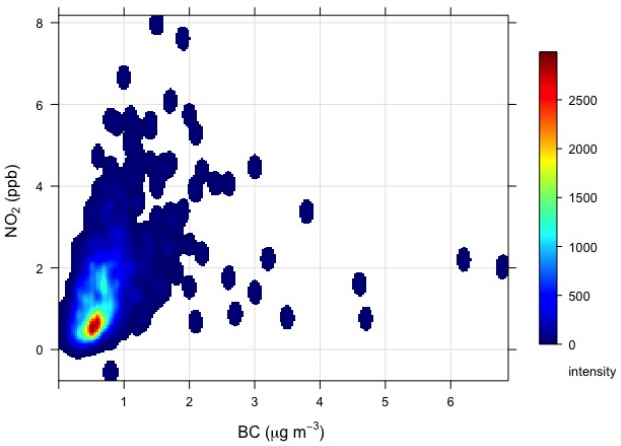

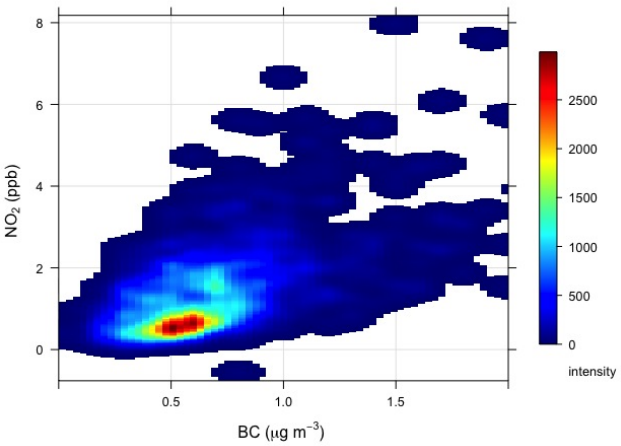

p = 0,4212

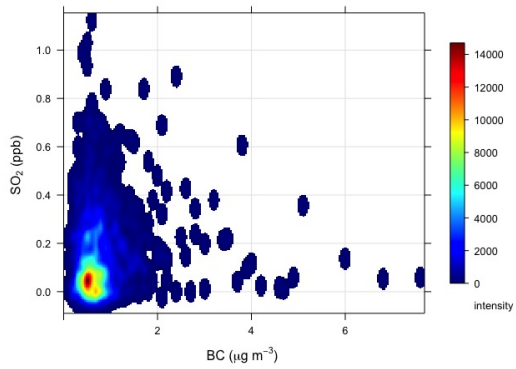

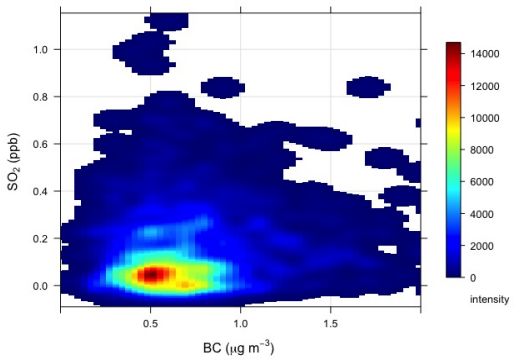

p=0,075

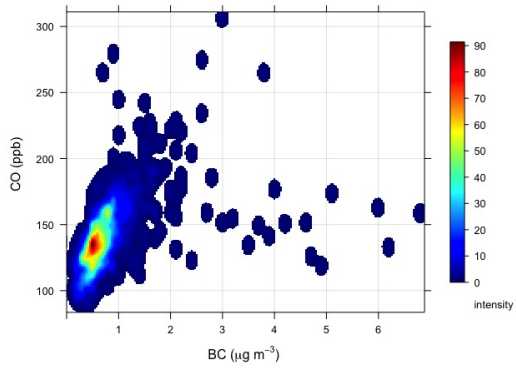

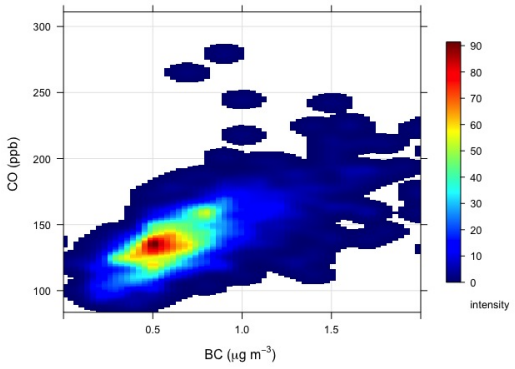

p=0,4924

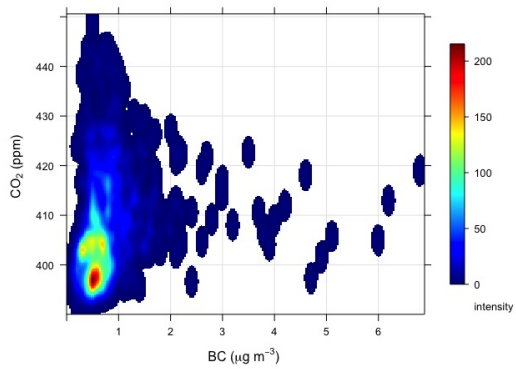

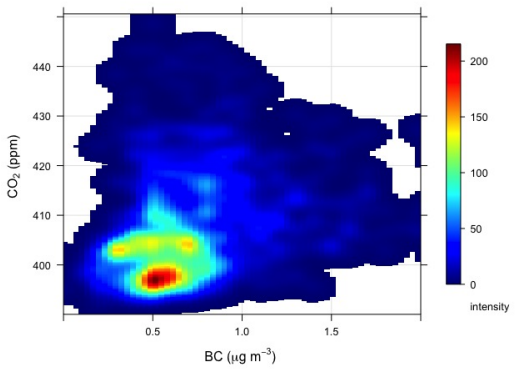

p=0,2087

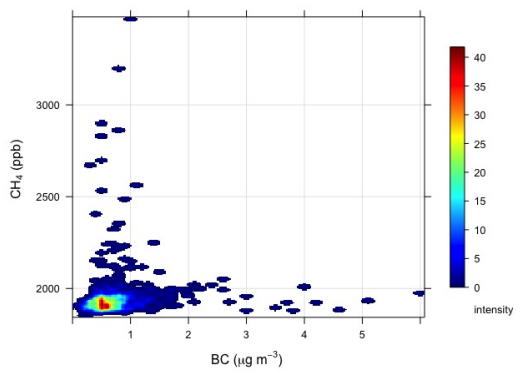

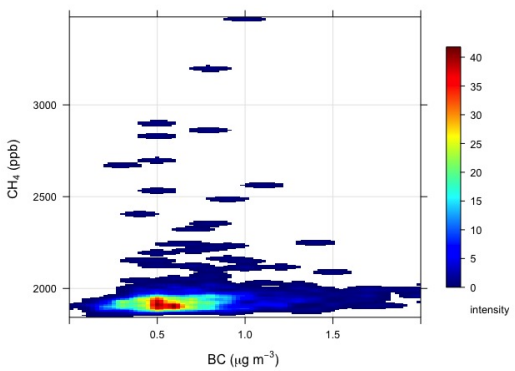

p=0,0760

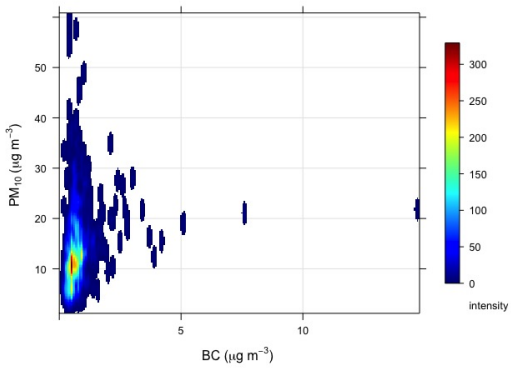

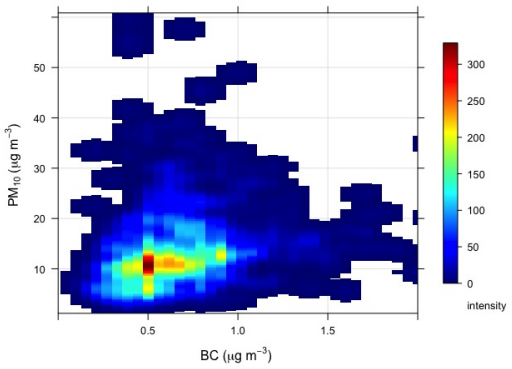

p=0,1653

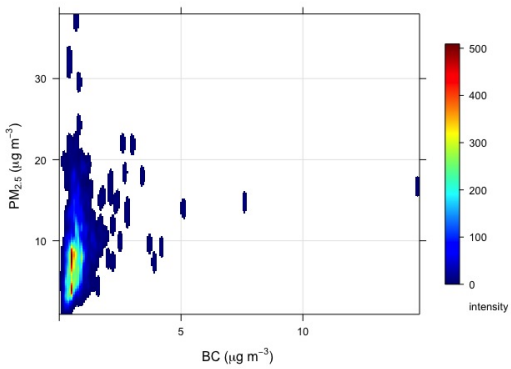

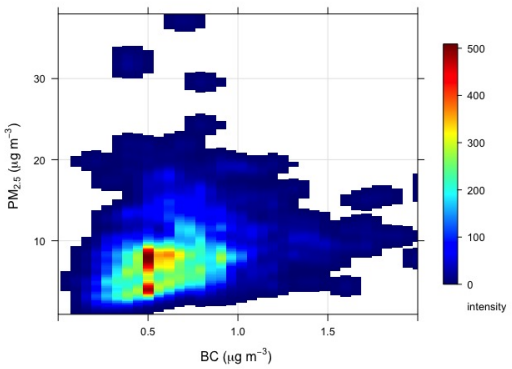

p=0,2268

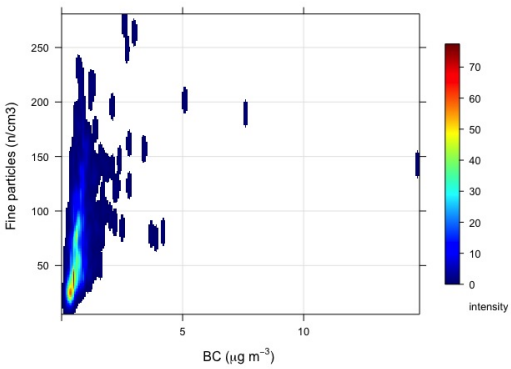

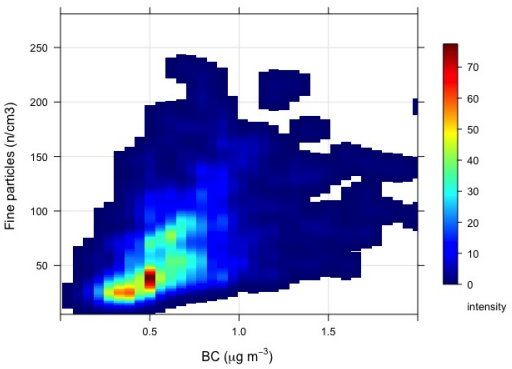

p=0,3828

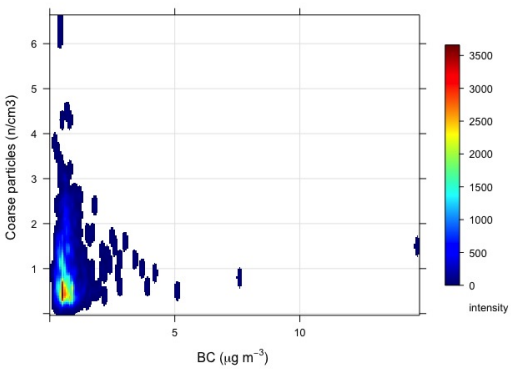

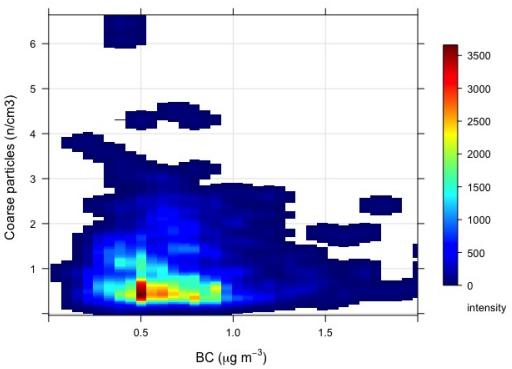

p=-0,0008

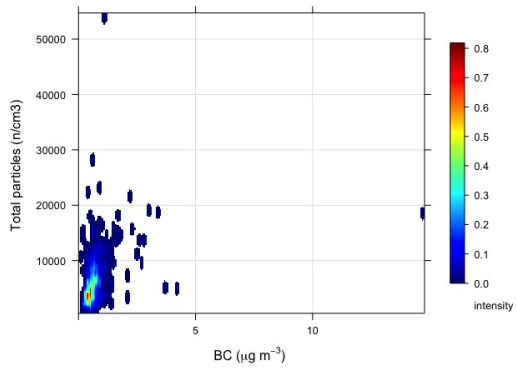

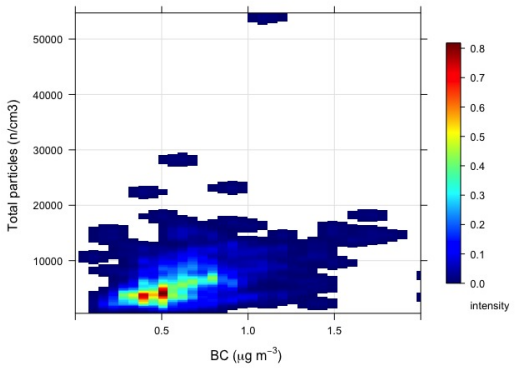

p=0,3387

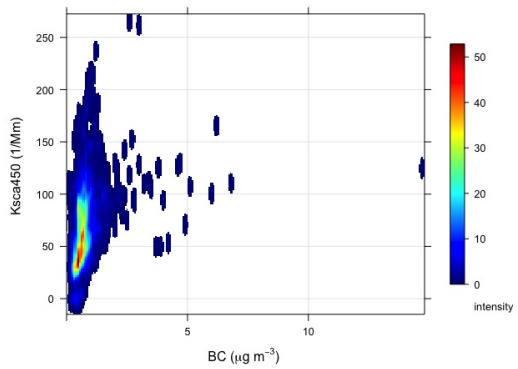

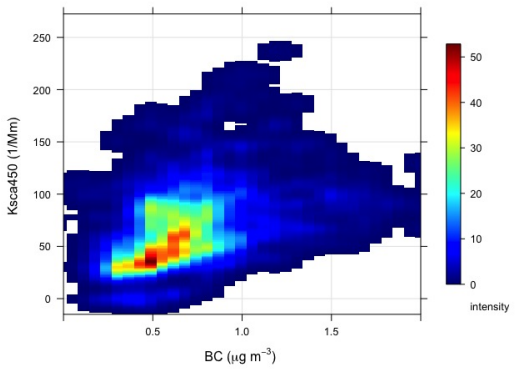

p=0,2929

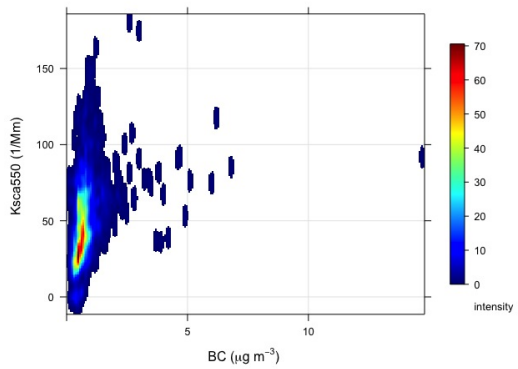

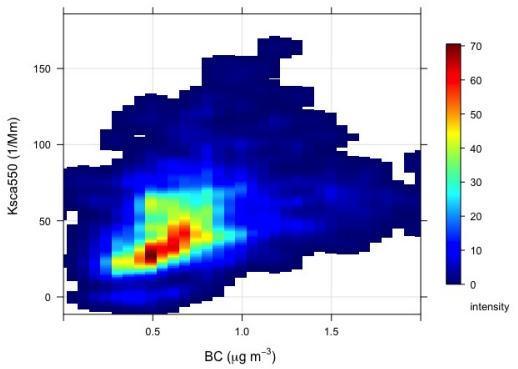

p=0,2893

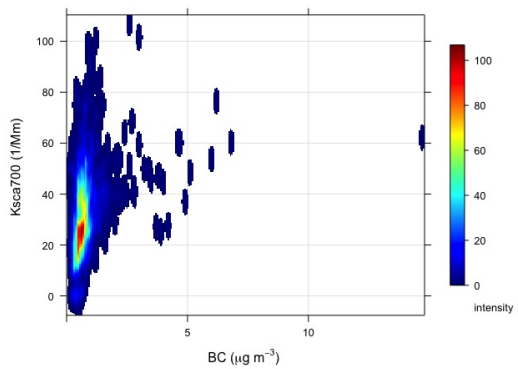

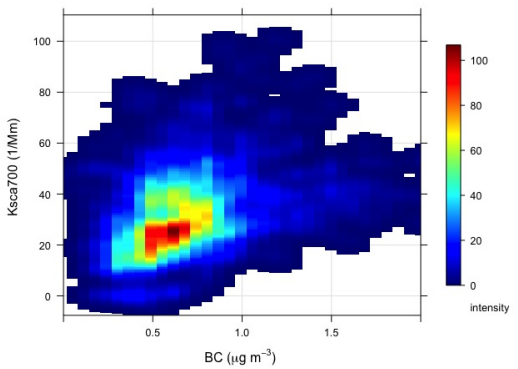

p=0,2654

Scatter Plot v/s CO during BC events

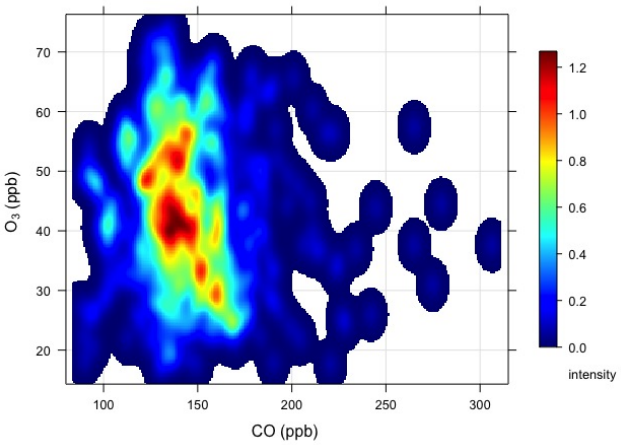

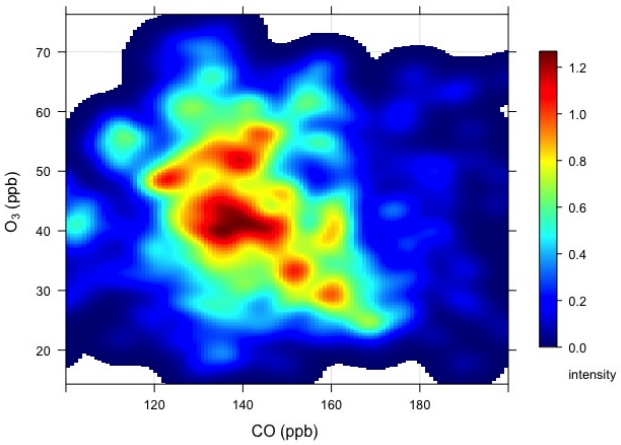

p = -0,1264

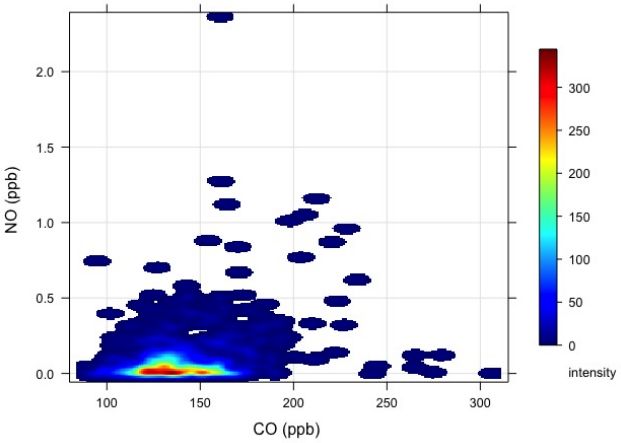

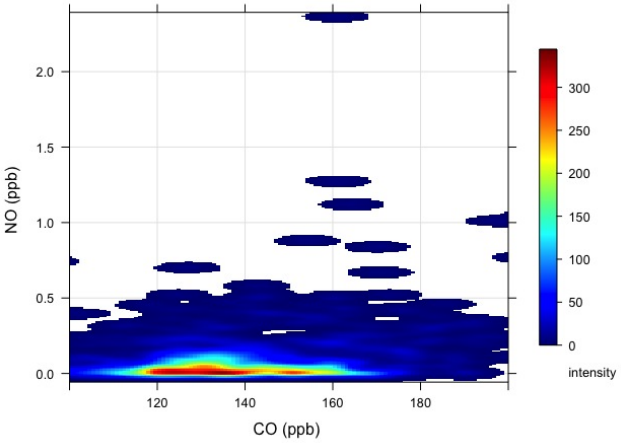

p = 0,2625

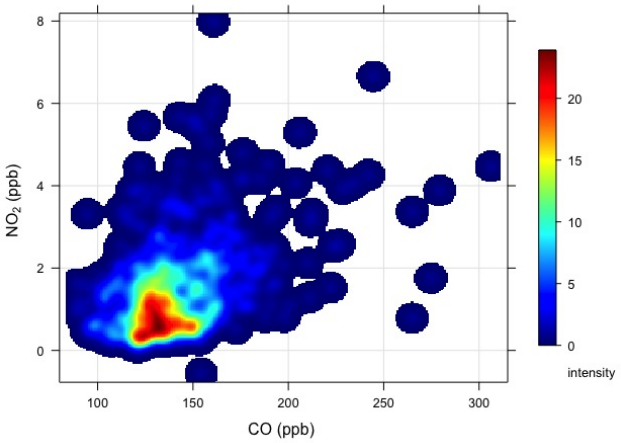

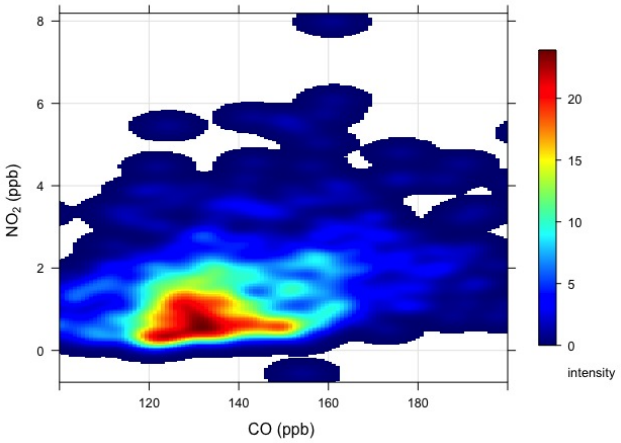

p = 0,3861

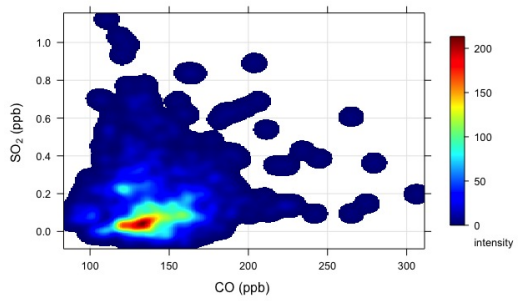

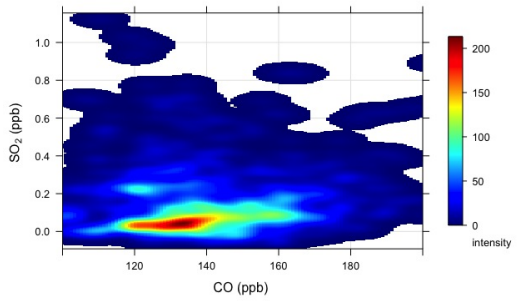

p=0,1008

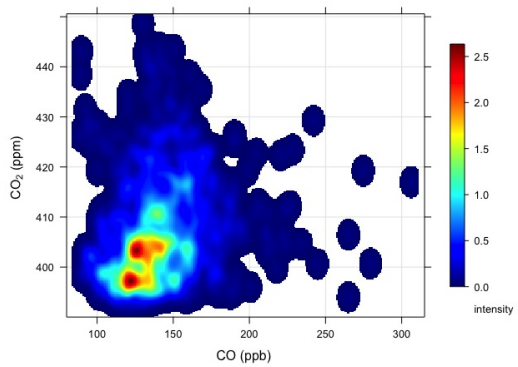

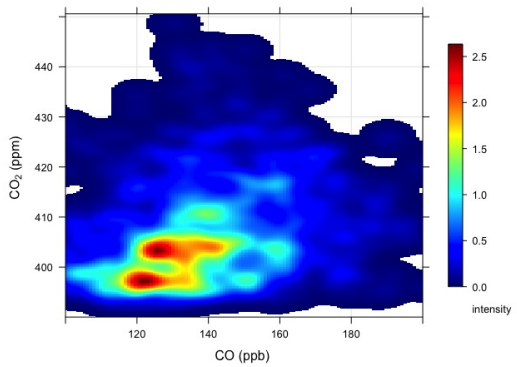

p=0,2088

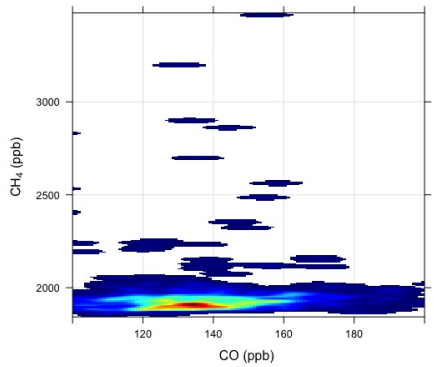

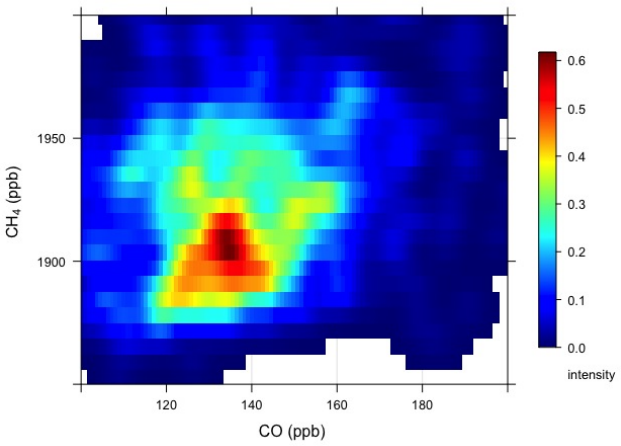

p = 0,0243

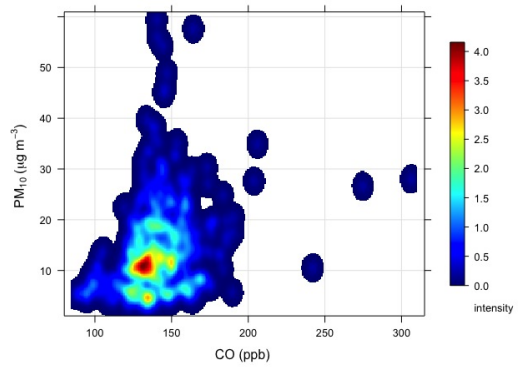

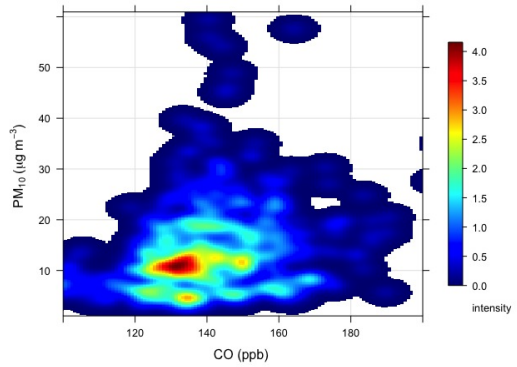

p=0,2622

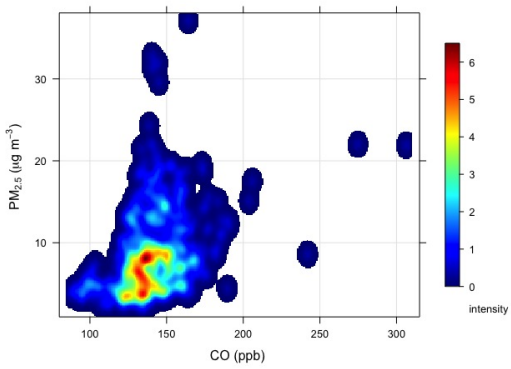

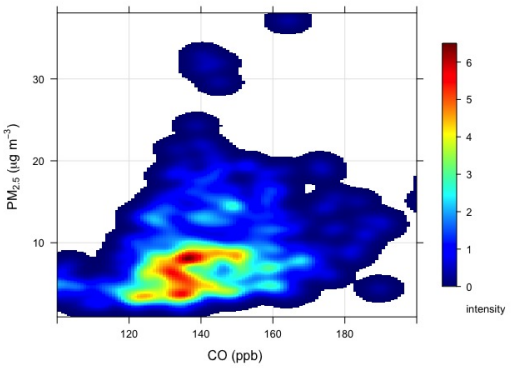

p=0,3468

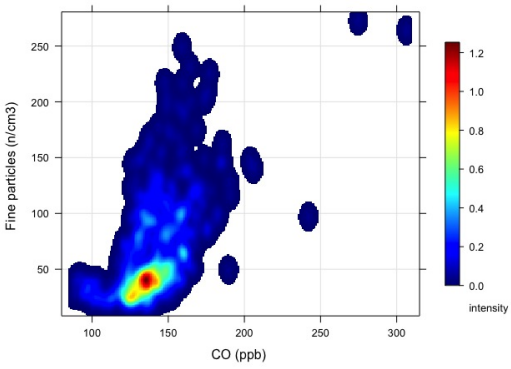

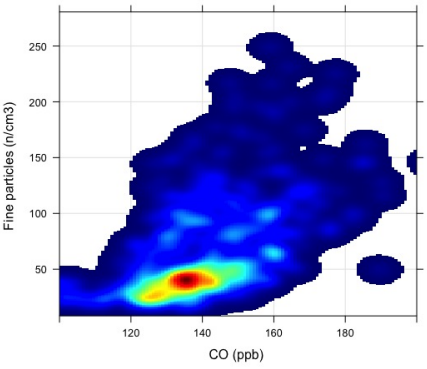

p=0,5740

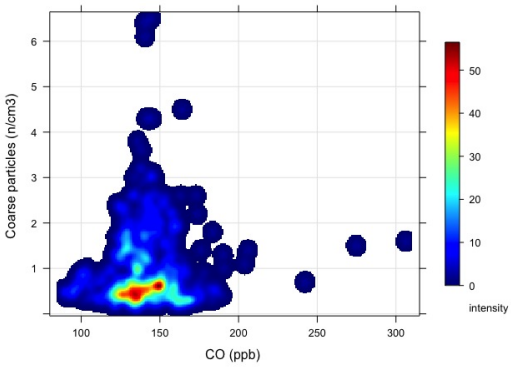

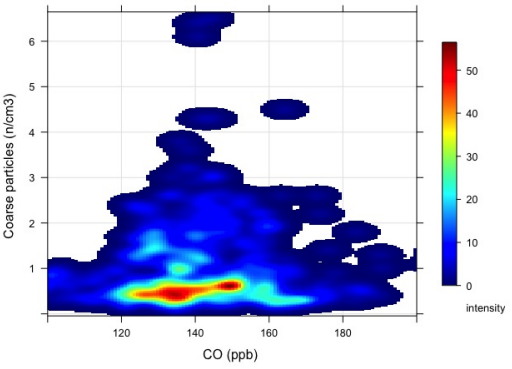

p=0,0623

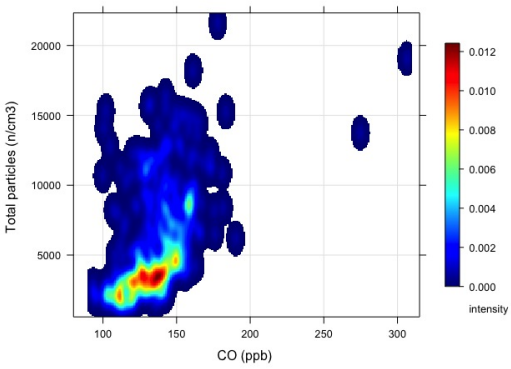

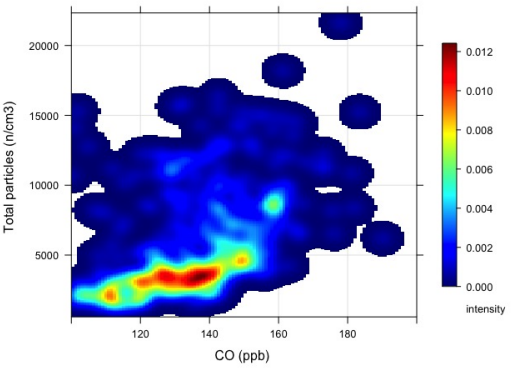

p=0,4981

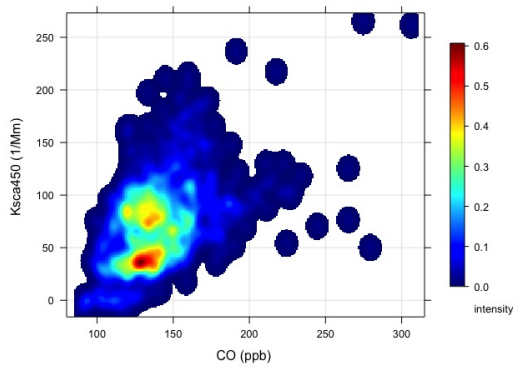

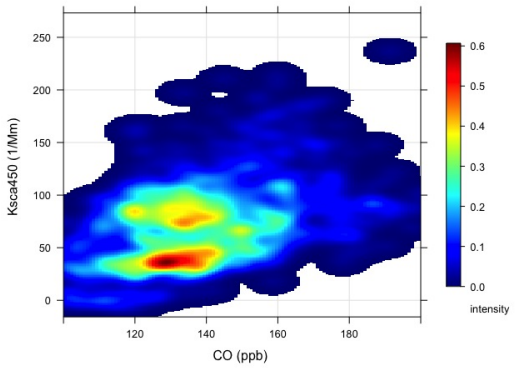

p=0,4578

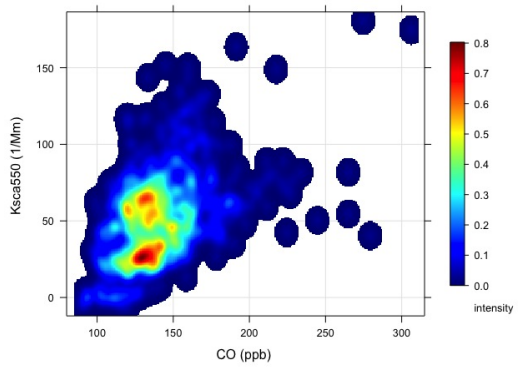

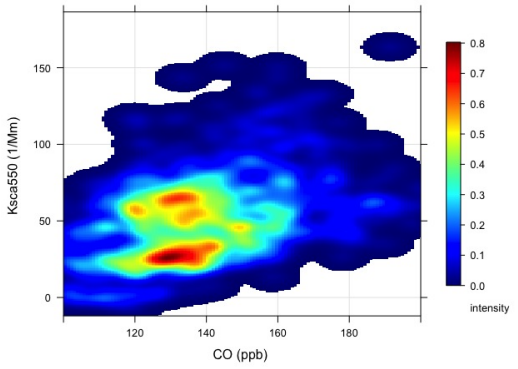

p=0,4415

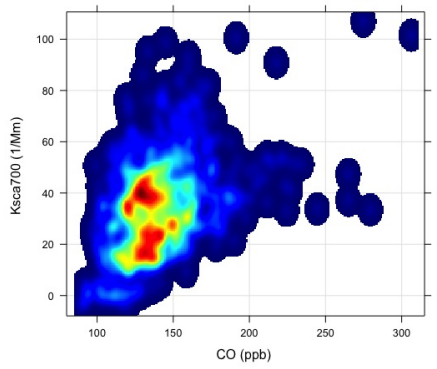

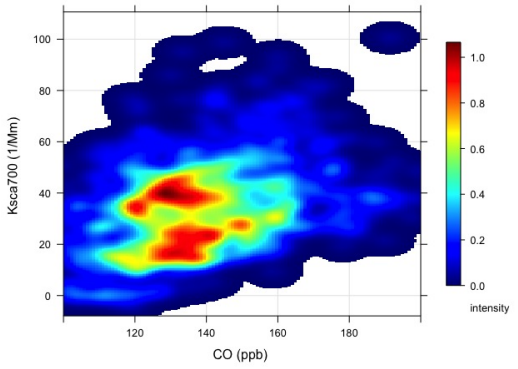

p=0,3991